THE BELL SYSTEM TECHNICAL JOURNAL

DEVOTED TO THE SCIENTIFIC AND ENGINEERING ASPECTS OF ELECTRICAL COMMUNICATION

Volume 58 October 1979 Number 8

Unbiased Spectral Estimation and System Identification Using Short-Time Spectral Analysis Methods

By J. B. ALLEN and L. R. RABINER

(Manuscript received March 16, 1979)

The methods of system identification and spectral analysis are well documented in the literature. In this paper, we attempt to merge the methods of least-square system identification and short-time Fourier transform spectral estimation. Starting from the least-squares normal equations for a linear system identification problem and expanding the signals in short-time Fourier transforms, we derive a Toeplitz system of equations, the solution of which approximates the original least-squares equation solution. We then bound the error norm between the two solution methods and show the properties of the error by numerical methods. The resulting "spectral" estimation method is shown to completely remove the bias normally associated with previously proposed spectral estimation procedures. The method appears to be particularly useful when one is interested in linear system identification of very large systems (long impulses response) or for system identification in the presence of nonstationary (e.g., burst) noise. Extensive numerical results are included.

I. INTRODUCTION

Although time-domain methods have been in use for system identification and modeling for at least 35 years, no simple, robust procedure has been proposed which uses short-time Fourier transform methods. Classical spectral analysis methods are generally inadequate for all but the simplest cases because of their unsatisfactory properties.

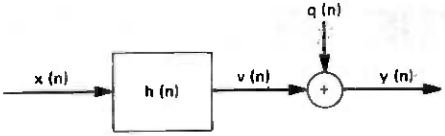

Fig. 1—Block diagram of the system identification model.

Recent results in the theory of short-time spectral analysis have suggested a framework for a new method of spectral estimation and system identification.[1-6] It is the purpose of this paper to describe the theory of this new algorithm and to compare and contrast it to three alternative procedures of system identification. In this paper we attempt to clear up many questions raised by an earlier related paper.[1]

Figure 1 is a block diagram of the general system identification model. The input signal $x(n)$ is assumed to be zero mean white noise having variance σ_x^2. The linear system $h(n)$ is assumed to be a finite impulse response (FIR) system of duration M samples,

$$h(n) = 0, \quad n < 0, n > M - 1. \tag{1}$$

At the output of the linear system, an independent white noise $q(n)$ (having zero mean and variance σ_q^2) is added to $v(n)$ to give the output signal $y(n)$. Thus

$$y(n) = x(n) * h(n) + q(n) \tag{2a}$$

$$= \sum_{m=0}^{M-1} h(m)x(n-m) + q(n). \tag{2b}$$

The signal-to-noise ratio (s/n) at the output of the system is defined as

$$\text{s/n} = 10 \log_{10}\left(\frac{\mathbf{E}(v^2(n))}{\mathbf{E}(q^2(n))}\right) = 10 \log_{10}\left(\frac{\sigma_v^2}{\sigma_q^2}\right), \tag{3}$$

where E is the expectation operation.

The system identification problem is one of finding an estimate $\hat{h}(n)$ of $h(n)$, given only N samples of the input $x(n)$ and the output $y(n)$. It is assumed that the duration of $\hat{h}(n)$ (call this $\hat{M}$) satisfies the relation

$$\hat{M} \geq M, \tag{4}$$

i.e., that we have knowledge of, or can accurately bound, the duration of the system impulse response. In general, we assume that $N \gg \hat{M}$. Assuming the constraint of eq. (4) is obeyed, one reasonable measure of system performance is the quantity

$$Q = 10 \log_{10} \left[\frac{\sum_{m=0}^{\hat{M}-1} [h(m) - \hat{h}(m)]^2}{\sum_{m=0}^{M-1} h^2(m)} \right]. \tag{5}$$

The quantity Q is called the "misadjustment" or "misalignment" between $h(n)$ and $\hat{h}(n)$.

Several classes of techniques are known in the time domain for solving the system identification problem, the most important of which is the classical least-squares analysis (LSA) method. In the frequency domain, however, only very simple, suboptimal techniques have been proposed for solving the system identification problem, and these techniques have not proven to be entirely adequate for any reasonable class of problems.[5,7] In this paper, we derive a new short-time Fourier transform domain approach to the system identification problem which alleviates many of the problems encountered using previously proposed frequency domain methods. High-quality frequency domain techniques are interesting for many reasons, but several notable ones are that (*i*) very large systems may be estimated ($\hat{M} \approx 10^3$ points), (*ii*) FFT methods are numerically very efficient, (*iii*) ill-conditioned problems are naturally identified, and (*iv*) the coherence function may be computed and used adaptively to dynamically modify the analysis procedures in a data-dependent way (a form of nonlinear analysis).[11] Furthermore, with the advent of high-speed array processors, algorithmic procedures which use FFTs are frequently easily implemented.

II. LEAST-SQUARES SOLUTION

Several basic results are necessary before we describe our frequency domain method. Since our approach is based on the method of least-squares analysis (LSA), we define that procedure first.

In the LSA method, one minimizes the quantity

$$I = \sum_{n=\hat{M}-1}^{N-1} (y(n) - \hat{y}(n))^2, \tag{6}$$

where

$$y(n) = \sum_{m=0}^{M-1} h(m)x(n-m) + q(n)$$

$$= h * x + q(n) \tag{7}$$

and

$$\hat{y}(n) = \sum_{m=0}^{\hat{M}-1} \hat{h}(m)x(n-m) = \hat{h} * x. \tag{8}$$

Taking partials of I with respect to $\tilde{h}(l)$, the unknowns, for $0 \leq l \leq \hat{M} - 1$ results in the set of equations

$$\sum_{n=\hat{M}-1}^{N-1} (y(n) - \hat{y}(n))x(n-l) = 0, \qquad 0 \leq l \leq \hat{M} - 1, \tag{9}$$

or in terms of x and y

$$\sum_{m=0}^{\hat{M}-1} \tilde{h}(m) \sum_{n} x(n-l)x(n-m) = \sum_{n} y(n)x(n-l), \; 0 \leq l \leq \hat{M} - 1, \tag{10}$$

where in all cases $\sum_n$ implies a sum from $\hat{M} - 1$ to $N - 1$, where N is the total number of data points required by the analysis. Our limits on n have been chosen so that the first and last required points of data are $x(0)$ and $x(N-1)$.

We now define

$$\phi(l, m) = \sum_{n} x(n-l)x(n-m) \tag{11}$$

$$r(l) = \sum_{n} y(n)x(n-l) \tag{12}$$

$$\boldsymbol{\phi} = [\phi(l, m)] \tag{13}$$

$$\mathbf{r} = [r(l)] \tag{14}$$

$$\tilde{\mathbf{h}} = [\tilde{h}(l)]. \tag{15}$$

Using this notation, eq. (10) becomes the matrix equation

$$\boldsymbol{\phi}\tilde{\mathbf{h}} = \mathbf{r}. \tag{16}$$

Our approach will be to approximate eq. (16) by a Toeplitz matrix equation which may be solved by one of the Toeplitz inversion methods[8,9] or approximately by DFT methods. In general, the solution of eq. (11) would be the optimal approach; however, when $\tilde{\mathbf{h}}$ is very large (i.e., $\hat{M} \approx 10^3$), the computation, storage, and solution of eq. (11) is totally impractical. Under these conditions, the methods of this paper might be useful.

III. OVERLAP-ADD EXPANSIONS

The key to our method is the overlap-add expansion of a signal based on the following identity:

$$\sum_{m=-\infty}^{\infty} w(mR - n) = (1/R) \sum_{p=0}^{R-1} W(e^{j(2\pi/R)p})e^{-j(2\pi/R)np}, \tag{17}$$

where $W(z)$ is the z transform of $w(n)$ and m, R, n, p are integers. Equation (17) is the discrete version of the Poisson sum formula.[2] If

we now assume that $w(n)$ is a time-limited lowpass function, such as a Hamming or Kaiser window, and R is chosen such that $e^{j2\pi/R}$ is greater than the cutoff frequency of $W(z)$, then the following approximate relation holds:

$$(R/W(e^{j0})) \sum_{m=-\infty}^{\infty} w(mR - n) = 1, \tag{18}$$

with an error determined by the out-of-band energy in the window $w(n)$. For any reasonable window, the error is negligible.[2] If we define $D = W(e^{j0})/R$ and multiply eq. (18) by any signal $x(n)$, we obtain the overlap-add expansion of $x(n)$:

$$x(n) = \sum_{m=-\infty}^{\infty} x_m(n), \tag{19}$$

where

$$x_m(n) = \frac{1}{D} w(mR - n)x(n). \tag{20}$$

The Fourier transform of $x_m(n)$ is called the "short-time" Fourier transform.[3,4] Expansions of ϕ and $\mathbf{r}$ by use of overlap-add expansions of $x(n)$ and $y(n)$ are possible through straightforward application of eqs. (19) and (11) and (12):

$$\phi(l, m) = \sum_n \sum_{k=-\infty}^{\infty} x_k(n - l) \sum_{p=-\infty}^{\infty} x_p(n - m)$$

$$= \sum_{p=-\infty}^{\infty} \sum_{k=-\infty}^{\infty} \phi_{pk}(l, m), \tag{21}$$

where we have defined

$$\phi_{pk}(l, m) = \sum_n x_k(n - l)x_p(n - m)$$

$$= \frac{1}{D^2} \sum_n x(n - l)w(kR + l - n)$$

$$\cdot x(n - m)w(pR + m - n) \tag{22}$$

and

$$r(l) = \sum_n y(n)x(n - l)$$

$$= \sum_n \sum_{p=-\infty}^{\infty} \sum_{k=-\infty}^{\infty} y_p(n)x_k(n - l)$$

$$= \sum_{p=-\infty}^{\infty} \sum_{k=-\infty}^{\infty} r_{pk}(l), \tag{23}$$

where

$$r_{pk}(l) = \sum_n y_p(n) x_k(n-l)$$

$$= \frac{1}{D^2} \sum_n y(n) w(pR - n) x(n-l) w(kR + l - n). \tag{24}$$

In Fig. 2 we show the relative window displacements for the term $\phi_{pk}(l, m)$ of eq. (22) assuming a window L points long. Due to the time truncation of the windows, the sum on n does not extend beyond the interval $N_A \leq n \leq N_B$, where

$$N_A = \max(kR + l, pR + m) + 1 - L$$

$$N_B = \min(kR + l, pR + m). \tag{25}$$

The situation is identical for the case of $r_{pk}(l)$ if m is set to zero in eq. (25).

When implementing the sums on p and k, it is frequently convenient to make a linear transformation of variables from k to q of the form $k = p + q$. In these variables, N_A and N_B may be written as

$$N_A(p, q) = pR - L + 1 + \max(m, qR + l) \tag{26}$$

$$N_B(p, q) = pR + \min(m, qR + l). \tag{27}$$

IV. SHORT-TIME SPECTRAL APPROACH TO SYSTEM IDENTIFICATION

In this section, we show how to split the LSA matrix equation $\phi \mathbf{h} = \mathbf{r}$ into the sum of a Toeplitz matrix and an error matrix. The Toeplitz matrix may be evaluated in the frequency domain and inverted by Toeplitz matrix inversion methods (or approximately by DFT methods). The error matrix will be shown to decrease (relative to the Toeplitz part) as $1/N$, where N is the number of data points. Thus as N increases, the error in the solution (relative to the LSA solution) will decrease at the rate of 6 dB per octave as the number of data points

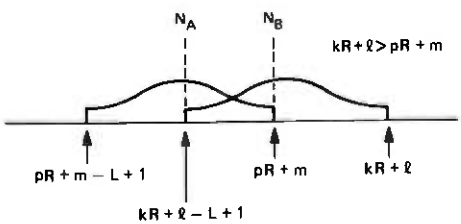

Fig. 2—Relative position of the windows for the matrix element ϕ_{pk}.

increases. Significant errors in $\bar{\mathbf{h}}$ due to the additive noise $q(n)$ are also present when the s/n is small, and these errors decrease at the rate of 3 dB per octave as N increases.[6] Thus, for large enough N, the truncation errors due to our approximation of the LSA matrix equation will be less than those due to the additive noise $q(n)$. Under these conditions, the Toeplitz estimate will be as accurate as the LSA result.

We split eq. (11) as follows

$$\begin{aligned} \boldsymbol{\phi} &= \hat{\boldsymbol{\phi}} + \boldsymbol{\epsilon} \\ \mathbf{r} &= \hat{\mathbf{r}} + \boldsymbol{\delta} \\ \bar{\mathbf{h}} &= \hat{\bar{\mathbf{h}}} + \boldsymbol{\Delta}, \end{aligned} \tag{28}$$

where $\boldsymbol{\epsilon}$ is the non-Toeplitz part of $\boldsymbol{\phi}$, $\hat{\boldsymbol{\phi}}$ is Toeplitz and symmetric (i.e., $\hat{\boldsymbol{\phi}} = [\hat{\phi}(l-m)] = [\hat{\phi}(m-l)]$), and $\hat{\bar{\mathbf{h}}}$ satisfies the equation

$$\hat{\boldsymbol{\phi}}\hat{\bar{\mathbf{h}}} = \hat{\mathbf{r}}. \tag{29}$$

$\boldsymbol{\Delta}$ is the error between the LSA solution and the Toeplitz solution eq. (29). By bounding the norm of $\boldsymbol{\Delta}$, $\|\boldsymbol{\Delta}\| = \|\bar{\mathbf{h}} - \hat{\bar{\mathbf{h}}}\|$, we can evaluate the error introduced by our procedure.

To obtain an expression for $\hat{\boldsymbol{\phi}}$, we observe the following: When N_A and N_B are inside the range of the sum on n, namely, $\hat{M} - 1 \leqslant n \leqslant N - 1$, the sum on n is limited by the windows rather than by the data. We define $\hat{\boldsymbol{\phi}}$ to be composed of all terms of $\phi_{pk}(l, m)$ of eq. (21) such that N_A and N_B lie inside the natural interval of the data independent of $l - m$ and $\boldsymbol{\epsilon}$ to include all the remaining terms of $\phi_{pk}(l, m)$. Thus

$$\hat{\phi}(l-m) = \sum_{p \in \mathbf{S}} \sum_{k \in \mathbf{S}} \phi_{pk}(l, m) \tag{30}$$

$$\hat{r}(l) = \sum_{p \in \mathbf{S}} \sum_{k \in \mathbf{S}} r_{pk}(l) \tag{31}$$

$$\epsilon(l, m) = \sum_{p \notin \mathbf{S}} \sum_{k \notin \mathbf{S}} \phi_{pk}(l, m) \tag{32}$$

$$\delta(l) = \sum_{p \notin \mathbf{S}} \sum_{k \notin \mathbf{S}} r_{pk}(l) \tag{33}$$

define the matrix elements of $\hat{\boldsymbol{\phi}}$, $\hat{\mathbf{r}}$, $\boldsymbol{\epsilon}$, and $\boldsymbol{\delta}$, respectively. For $\hat{\boldsymbol{\phi}}$ and $\hat{\mathbf{r}}$, the sums on p and k are over the set $\mathbf{S}(p, k)$, while $\boldsymbol{\epsilon}$ and $\boldsymbol{\delta}$ are summed over all k and p outside $\mathbf{S}$. The set $\mathbf{S}$ is defined by all integers p, k, as shown by the dots in Fig. 3, such that

$$\begin{aligned} N_A &\geqslant \hat{M} - 1 \\ N_B &\leqslant N - 1 \\ N_A &\leqslant N_B. \end{aligned} \tag{34}$$

Equation (34) is to be satisfied for all m and l in the range $[0, \hat{M} - 1]$. In the appendix we give an explicit formula for $\hat{\phi}(l - m)$. From Fig. 3

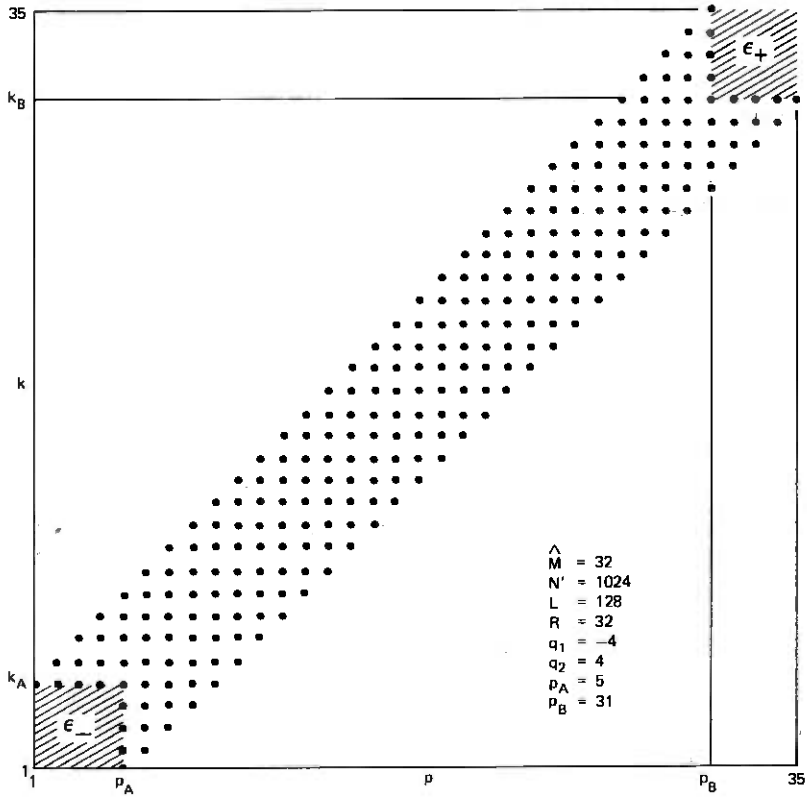

Fig. 3—Points comprising the set S in the (p, k) plane which are used in computing $\hat{\phi}$ and $\hat{r}$. Also shown are the regions which define ϵ (see the appendix).

we see that, in general, the set forms a strip which is missing small pieces at its ends. These small pieces are the set of $p, k \notin \mathbf{S}$ which may be used to compute ϵ and δ (see appendix).

Because of the definition of the set S, the sum on n in eqs. (22) and (24) may be extended to $\pm\infty$ since the windows naturally truncate the data to $N_A \leqslant n \leqslant N_B$. As a result of this definition, $\hat{\phi}$ is only a function of $l - m$ and is therefore Toeplitz. Such is not the case for $\epsilon(l, m)$, however, since most terms in this sum are truncated at either $n = \hat{M} - 1$ or $n = N - 1$. Finally, note that the expected value of elements of $\hat{\phi}$ or $\hat{\mathbf{r}}$ increases linearly in N (i.e., is of order N),

$$\mathbf{E}(\hat{\phi}) = O(N)$$

$$\mathbf{E}(\hat{r}) = O(N),$$

while the expected value of elements of ϵ and δ is of order 1 (i.e., independent of N)

$$\mathbf{E}(\delta) = O(1)$$

$$\mathbf{E}(\epsilon) = O(1).$$

Thus, as N approaches ∞, the solution of eq. (29) approaches that of eq. (16) at a rate of 6 dB per octave in N.

V. TRUNCATION ERROR ANALYSIS

A bound on the truncation errors may be obtained from eqs. (16), (28), and (29) in the following way. From eqs. (16) and (28),

$$(\hat{\boldsymbol{\phi}} + \boldsymbol{\epsilon})(\hat{\mathbf{h}} + \boldsymbol{\Delta}) = \hat{\mathbf{r}} + \boldsymbol{\delta} \tag{35}$$

or

$$\hat{\boldsymbol{\phi}}\hat{\mathbf{h}} + \hat{\boldsymbol{\phi}}\boldsymbol{\Delta} + \boldsymbol{\epsilon}\hat{\mathbf{h}} + \boldsymbol{\epsilon}\boldsymbol{\Delta} = \hat{\mathbf{r}} + \boldsymbol{\delta}. \tag{36}$$

As a result of eq. (29),

$$\hat{\boldsymbol{\phi}}\boldsymbol{\Delta} + \boldsymbol{\epsilon}\hat{\mathbf{h}} + \boldsymbol{\epsilon}\boldsymbol{\Delta} = \boldsymbol{\delta}. \tag{37}$$

Next we multiply by $\hat{\boldsymbol{\phi}}^{-1}$ and solve for $\boldsymbol{\Delta}$ as

$$\boldsymbol{\Delta} = \hat{\boldsymbol{\phi}}^{-1}(\boldsymbol{\delta} - \boldsymbol{\epsilon}\hat{\mathbf{h}}) - \hat{\boldsymbol{\phi}}^{-1}\boldsymbol{\epsilon}\boldsymbol{\Delta}. \tag{38}$$

Forming the norm of each side of eq. (38), we define a measure of error Q_Δ [eq. (5)] which, after some algebra, may be shown to be bounded by ($\|\cdot\|$ as defined here is the Euclidean norm of a vector)

$$Q_\Delta = 20 \log_{10}\left[\frac{\|\boldsymbol{\Delta}\|}{\|\hat{\mathbf{h}}\|}\right] \leqslant 20 \log_{10}\left[\frac{\|\hat{\boldsymbol{\phi}}^{-1}\| \cdot \|\boldsymbol{\delta} - \boldsymbol{\epsilon}\hat{\mathbf{h}}\|}{1 - \|\hat{\boldsymbol{\phi}}^{-1}\| \cdot \|\boldsymbol{\epsilon}\|}\right]. \tag{39}$$

If we let $\lambda_i(\mathbf{A})$ denote the ith eigenvalue of the matrix $\mathbf{A}$, then it can be shown that

$$\|\hat{\boldsymbol{\phi}}^{-1}\| = \{\min_i \lambda_i(\hat{\boldsymbol{\phi}}^t\hat{\boldsymbol{\phi}})\}^{-1/2}$$

$$\|\boldsymbol{\epsilon}\| = \{\max_i \lambda_i(\boldsymbol{\epsilon}^t\boldsymbol{\epsilon})\}^{1/2}$$

where, by definition,

$$\|\hat{\mathbf{h}}\| = \left(\sum_{l=0}^{\hat{M}-1} \hat{h}^2(l)\right)^{1/2}$$

$$\|\boldsymbol{\Delta}\| = \left(\sum_{l=0}^{\hat{M}-1} \Delta^2(l)\right)^{1/2}. \tag{40}$$

Useful bounds on these norms are easily obtained for $\boldsymbol{\epsilon}$ and $\hat{\boldsymbol{\phi}}^{-1}$. For the latter, if $\hat{\boldsymbol{\Phi}}(\omega_k)$ is the $2\hat{M} - 1$ point DFT of $[\hat{\phi}_0, \hat{\phi}_1, \cdots, \hat{\phi}_{\hat{M}-1}, \hat{\phi}_{1-\hat{M}}, \cdots, \hat{\phi}_{-1}]$, then

$$\|\hat{\phi}^{-1}\| \leq \min_{\omega_k} |\hat{\Phi}(\omega_k)|^{-1}. \tag{41}$$

In practice, $\hat{\Phi}(\omega_k)$ and the DFT of $\hat{r}$, $\hat{R}(\omega_k)$ are directly computed from the data $x(n)$ and $y(n)$. Q_Δ is only of theoretical interest and would generally not be computed in a real problem.

VI. IMPLEMENTATION OF THE SHORT-TIME SPECTRAL APPROACH TO SYSTEM IDENTIFICATION

As a result of the previous discussion, our method is implemented as follows:

(*i*) Form windowed data segments $y_p(n)$ and $x_k(n)$ for each p and k in S.

(*ii*) Compute the correlations $\hat{\phi}_{pk}(l-m)$ and $\hat{r}_{pk}(l)$ which may be done as follows (using fast correlation techniques):

$$\begin{aligned} X_k(\omega) &= \mathbf{F}\{x_k(n)\} \\ Y_p(\omega) &= \mathbf{F}\{y_p(n)\} \\ \hat{\Phi}_{pk}(\omega) &= X_k^*(\omega) X_p(\omega) \\ \hat{R}_{pk}(\omega) &= X_k^*(\omega)\, Y_p(\omega) \\ \hat{\phi}_{pk}(n) &= \mathbf{F}^{-1}[\hat{\Phi}_{pk}(\omega)] \\ \hat{r}_{pk}(n) &= \mathbf{F}^{-1}[\hat{R}_{pk}(\omega)]. \end{aligned} \tag{42}$$

$\mathbf{F}[\cdot]$ and $\mathbf{F}^{-1}[\cdot]$ are the Fourier transform operations and $()^*$ defines conjugation.

(*iii*) Form $\hat{\phi}(l)$ and $\hat{r}(l)$ by summing over all $p, k \in \mathrm{S}$ as discussed in the appendix. (In practice, this computation is done recursively. Furthermore, the sum is best done in the frequency domain.)

(*iv*) (Solution Method 1) Finally, solve the matrix equation

$$\hat{\boldsymbol{\phi}}\hat{\mathbf{h}} = \hat{\mathbf{r}}.$$

This equation may be solved by Toeplitz matrix inversion methods which require only $\hat{M}^2$ operations and $2\hat{M}$ storage locations.

(*iv'*) (Solution Method 2) Alternatively, under some conditions we may approximately find $\hat{H}(\omega)$ by Fourier transforms from

$$\hat{\Phi}(\omega) = \mathbf{F}\left[\sum_{p\in \mathrm{S}} \sum_{k\in \mathrm{S}} \hat{\phi}_{pk}(l)\right]$$

$$\hat{R}(\omega) = \mathbf{F}\left[\sum_{p\in \mathrm{S}} \sum_{k\in \mathrm{S}} \hat{r}_{pk}(l)\right]$$

$$\hat{H}(\omega) = \frac{\hat{R}(\omega)}{\hat{\Phi}(\omega)}.$$

$\hat{\Phi}(\omega)$ is the autospectral estimate and $\hat{R}(\omega)$ is the cross-spectral estimate. They sharply differ from the classical definitions of these quantities because the cross terms $p \neq k$ have been included. The inclusion of these cross terms is responsible for the removal of the bias in these estimates (see the next section). The DFT version of the above differs slightly in some of its details.

VII. BIAS AND THE CLASSICAL CASE OF SPECTRAL ESTIMATION

The most common method of spectral estimation is equivalent to forming the estimate

$$S_{xy}(\omega) = \sum_k Y_k(\omega) X_k^*(\omega), \tag{43}$$

where the sum on k is taken on nonoverlapping or slightly overlapping intervals (i.e., $R = L$ or $R = L/2$). There appear to be several flaws in this method. First, R should be less than L/Ω where Ω is the time-bandwidth product of the window, as is required by the Nyquist theorem.[2-4] For a Hamming window, Ω is 4. Second, because of the absence of cross terms, bias is present in the estimate as may be seen by inverse Fourier transforming $S_{xy}(\omega)$. For example, if in eqs. (29) to (31) we modify the sum on k to be $k = p + q$ with q a fixed integer, then eq. (29) becomes

$$\sum_{m=0}^{\hat{M}-1} \hat{h}(m) \sum_p \hat{\phi}_{p,p+q}(l-m) = \sum_p \hat{r}_{p,p+q}(l). \tag{44}$$

If we define the (decimated) autocorrelation of the window by

$$\psi_w(l) = \sum_p w(pR) w(pR + l), \tag{45}$$

then, for a white noise input (with variance σ_x^2) and for no additive noise ($\sigma_q^2 = 0$), if we assume ergodicity, i.e.,

$$\lim_{N\to\infty}\left[\frac{1}{N}\sum_{n=0}^{N-1} x(n)x(n+m)\right] = \sigma_x^2\delta(m) = \mathrm{E}[x(n)x(n+m)], \tag{46}$$

where $\delta(m)$ is one when $m = 0$ and zero otherwise, the term in the left-hand side of eq. (44) reduces to (as $N \to \infty$)

$$\lim_{N\to\infty}\left[\frac{1}{N}\sum_p \hat{\phi}_{p,p+q}(l-m)\right] = \lim_{N\to\infty}\left[\frac{1}{N}\sum_{n=0}^{N-1} x(n-m)x(n-l) \sum_p w(pR+m-n) \cdot w((p+q)R+1-n)\right] \tag{47}$$

$$= \sigma_x^2\delta(m-l)\psi_w(qR+l-m) \tag{48}$$

and the right-hand side of eq. (44) similarly reduces to

$$\lim_{N\to\infty}\left[\frac{1}{N}\sum_{p}\hat{r}_{p,p+q}(l)\right] = \lim_{N\to\infty}\left[\frac{1}{N}\sum_{n=0}^{N-1} y(n)x(n-l) \sum_{p} w(pR-n)w((p+q)R+l-n)\right] \quad (49)$$

$$= \sigma_x^2 h(l)\psi_w(qR+l). \quad (50)$$

From eqs. (44), (48), and (50), we get

$$\sigma_x^2\hat{h}(l)\psi_w(qR) = \sigma_x^2 h(l)\psi_w(qR+l) \quad (51)$$

or

$$\hat{h}(l) = h(l)\frac{\psi_w(qR+l)}{\psi_w(qR)}. \quad (52)$$

Equation (52) shows that the effect of the window is to modify the estimate of h by the quantity $\psi_w(qR+l)/\psi_w(qR)$. When $q=0$ [the classical case, eq. (43)], we have the result

$$\hat{h}(l) = h(l)\frac{\psi_w(l)}{\psi_w(0)}; \quad (53)$$

thus, $\hat{h}(l)$ is a biased version of $h(l)$. By summing over q [i.e., sum eq. (44) over q], the bias is removed since ψ_w is a lowpass function, satisfying the relation [see eq. (18)]

$$\sum_{q}\psi_w(qR+l) = \sum_{q}\psi_w(qR) = \text{constant} \quad (54)$$

and eq. (52) gives the desired result

$$\hat{h}(l) = h(l), \quad (55)$$

independent of the window.

VIII. EXPERIMENTAL RESULTS

In this section, we give some numerical results for a simulated system identification problem. Using the system of Fig. 1 as the model, a specific FIR system was chosen for $h(n)$ with impulse response duration $M=7$ samples. This is the simple system used in Refs. 1 and 6, and its impulse response is given by

n	0	1	2	3	4	5	6
$h(n)$	0.1	0.5	1.0	0.5	−0.5	−1.0	0.5

The input to the system $x(n)$ was a Gaussian noise with zero mean and variance σ_x^2. The additive noise $q(n)$ was an independent Gaussian

noise with zero mean and variance σ_q^2. In each of these examples, a Hamming window was used.

Figure 4 shows a plot of Q [eq. (5)] as a function of N for $\sigma_q^2 = 0$ (i.e., no additive noise) and for values of the parameter q_0, where q_0 is the number of off-diagonal cross terms used in estimating $\hat{\phi}$ and $\hat{\mathbf{r}}$, as expressed in the form

$$\hat{\phi}(l) = \sum_{q=-q_0}^{q_0} \sum_{p=p_1}^{p_2} \hat{\phi}_{p,p+q}(l) \tag{56}$$

$$\hat{r}(l) = \sum_{q=-q_0}^{q_0} \sum_{p=p_1}^{p_2} \hat{r}_{p,p+q}(l). \tag{57}$$

For this example, solution method 1 [Section VI, step (*iv*)] was used to solve the matrix equation. As q_0 gets larger (i.e., as more cross terms are included), the bias is removed as seen in Fig. 4. If $q_0 \geq q_{\max}$, where [see eq. (70) in the appendix]

$$q_{\max} = \left\lfloor \frac{M + L - 2}{R} \right\rfloor, \tag{58}$$

then no further changes occur in $\hat{\phi}(l)$, $\hat{r}(l)$ (or Q). In this example, $q_{\max} = 5$. The effects of the bias for $q_0 = 0$, 1, 2, and 3 are such that, for large values of N, Q is from 15 to 45 dB worse than for the unbiased estimates. For values of q_0 greater than 3, only small changes occur in Q. Thus there is a computational tradeoff—especially in cases where $q_{\max}$ is calculated using $\hat{M}$ and $\hat{M}$ is greater than M. When $\hat{M} \approx M$ and

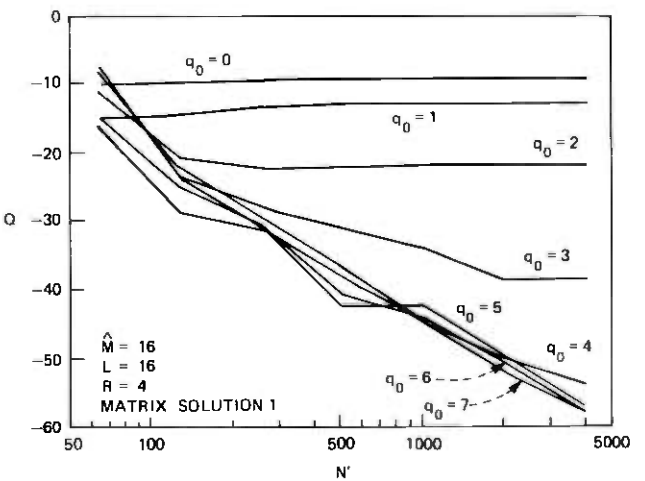

Fig. 4—Plots of Q versus N for $\hat{M} = 16$, $L = 16$, $R = 4$, s/n = ∞, and several values of q_0, using matrix solution method 1 [Section VI, step (*iv*)].

the impulse response of the system has large values near $n = \hat{M}$, then values of up to q_{max} are required for the best solutions.

Figure 5 shows plots of Q versus N for different Hamming window lengths L for the matrix solution method 1 (Fig. 5a) and for the FFT solution method 2 (Fig. 5b), for a fixed value of $\hat{M} = 8$ and for $\sigma_q^2 = 0$. (Comparable results were obtained for larger values of $\hat{M}$ up to $\hat{M} = 64$.) It can be seen by comparing the curves of Figs. 5a and 5b that the Q values obtained from the matrix solutions were from 10 to 20 dB better than those obtained from the FFT solution [Section VI, step (iv)] for small N (such that Q from the matrix solution was −30 dB or larger). For large N, the two methods of solution yielded essentially identical results.

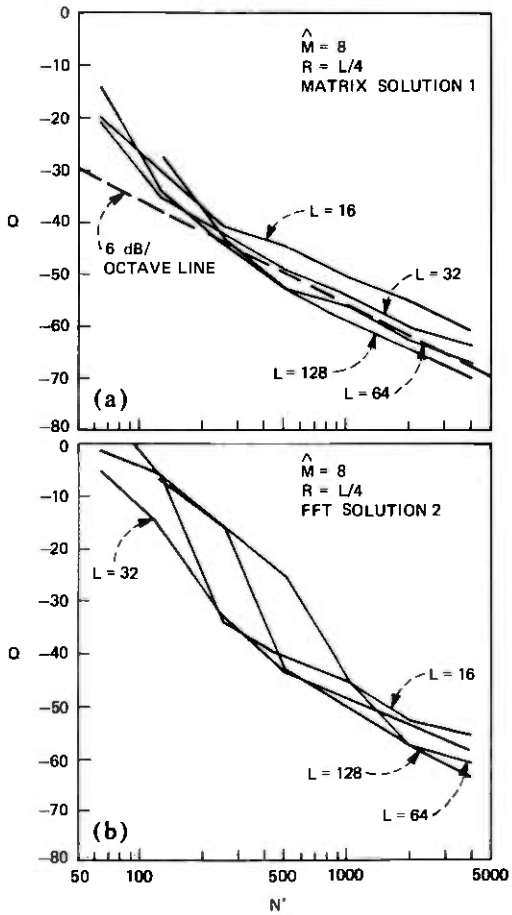

Fig. 5—Plots of Q versus N for $\hat{M} = 8$, $R = L/4$, s/n = ∞, and for several values of L for: (a) matrix method 1 and (b) FFT method 2 [Section VI, step (iv')].

From Figure 5a, two additional points are noted. First, we see that the asymptotic behavior of the curves of Q versus N is a 6-dB-per-octave slope as shown by the dotted line in this figure. For small N, the curves deviate from this slope. Second, we see small but consistent differences in the curve of Q versus N for different values of L. An exact explanation of this result is beyond the slope of this paper; however, eq. (39) shows that Q_Δ is directly proportional to the norm of $\boldsymbol{\delta} - \epsilon\hat{\mathbf{h}}$. It can be shown that $\|\boldsymbol{\delta} - \epsilon\hat{\mathbf{h}}\|$ gets smaller as L increases (since the error terms become more highly correlated), thus Q_Δ depends on L in a very complicated manner as illustrated in Fig. 5. A simple analysis of the effects of $\|\boldsymbol{\delta} - \epsilon\mathbf{h}\|$ on Q is as follows. If $\boldsymbol{\delta}$ and $\epsilon\mathbf{h}$ are not correlated, then

$$\|\boldsymbol{\delta} - \epsilon\mathbf{h}\| \approx \|\boldsymbol{\delta}\| + \|\epsilon\mathbf{h}\|. \tag{59}$$

When the two terms are correlated,

$$\|\boldsymbol{\delta} - \epsilon\mathbf{h}\| \ll \|\boldsymbol{\delta}\| + \|\epsilon\mathbf{h}\|. \tag{60}$$

Equation (59) implies that, if $\|\boldsymbol{\delta}\|$ is made zero, $\|\boldsymbol{\delta} - \epsilon\mathbf{h}\|$ decreases since one of two terms has been removed. Equation (60) implies that the error must greatly increase when $\|\boldsymbol{\delta}\| = 0$. Experimentally, $\boldsymbol{\delta}$ was set to 0 in our numerical simulations (by computing $\mathbf{r}$ exactly), and it was observed that the error Q increased by more than 20 dB. This showed that eq. (59) was a bad approximation because $\boldsymbol{\delta}$ and $\epsilon\mathbf{h}$ were highly correlated.

Figure 6 shows a direct comparison between the Q values obtained from the matrix solution method 1 (Section VI), the FFT solution method 2 (Section VI), and a third method which we call the classical Toeplitz case (solution method 3), for $\hat{M} = 8$ (Fig. 6a) and $\hat{M} = 64$ (Fig. 6b) and for $\sigma_q^2 = 0$. For the first two solution methods, a value of $L = 64$ was used for the window. Method 3, the classical Toeplitz case,[5] computes matrix elements $\hat{\phi}_T(l)$ and $\hat{\mathbf{r}}_T(l)$ directly from the data as

$$\hat{\phi}_T(l) = \sum_{n=\hat{M}-1}^{N-1-|l|} x(n)x(n+l)$$

$$\hat{r}_T(l) = \sum_{n=\hat{M}-1}^{N-1-|l|} x(n)y(n+l) \tag{61}$$

and determines $\hat{h}_T(n)$ as the solution of the matrix equation

$$\hat{\boldsymbol{\phi}}_T\hat{\mathbf{h}}_T = \hat{\mathbf{r}}_T. \tag{62}$$

By comparing the three solution methods, it is seen that the matrix solution method 1 gives the smallest Q values for almost the entire range of N, whereas the FFT method 2 gives smaller Q values than the

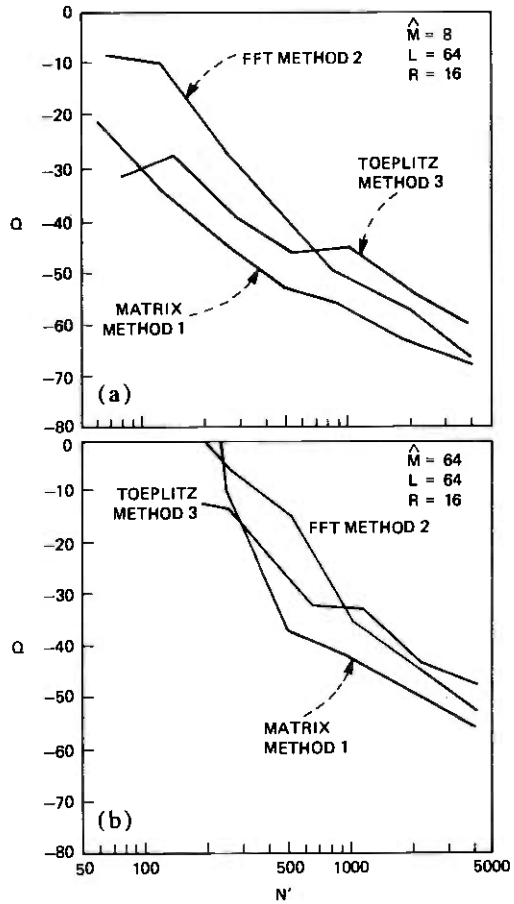

Fig. 6—Comparisons of the curves of Q versus N for $L = 64$, $R = 16$, s/n = ∞, for solution methods 1 to 3 for (a) $\hat{M} = 8$, and (b) $\hat{M} = 64$. Method 3 is defined in the text by eq. (62).

Toeplitz method 3 for large values of N, and larger Q values for small N. Analysis of the classical Toeplitz case shows that this method is identical to the matrix solution method 1 using a rectangular window with a shift of $R = L$ (i.e., an entire window shift). Figure 6 thus directly demonstrates that Hamming window results are better than rectangular window results.

Figure 7 shows a plot of Q versus $\hat{M}$ for a fixed value of $N = 1024$ and for several values of L. It can be seen that the curves of Q versus $\hat{M}$ have a slope of about 3 dB per octave in $\hat{M}$, as predicted based on the definition of eq. (5).[6] However, we also see the interesting effect that, for certain values of $\hat{M}$ and for different values of L, the value of Q makes a discrete jump and then jumps back to its previous level

(approximately). This effect is due to discrete changes in the limits q_1 and q_2 with L (see appendix) which is directly reflected in the curves of Q versus $\hat{M}$. The point of this figure is to show the effect of the positioning of the windows with respect to the data. Depending on the exact window placement, 3 dB of difference can be expected in a typical case.

As a final example, Fig. 8 shows a set of curves of Q vs N for s/n = 8 dB, $\hat{M} = 16$, and for several values of L. Also plotted in the figure is the theoretical curve[6] (dashed line) for the least-squares analysis $Q_{LSA} = 10 \log_{10}[\hat{M}/N] - \text{s/n}$. This curve drops at a rate of 3 dB per octave as N increases. It is seen that the measured Q curves from the matrix solution method 1 are quite close (within a few decibels) to the theoretical curve for values of N greater than about 100. In these cases, as N increases beyond about 100 points, the s/n-induced errors dominate the truncation (ϵ and δ induced) errors. Thus (for $N > 100$) there is no advantage in solving the LSA equation since the Toeplitz solution is equally accurate.

IX. DISCUSSION

The purpose of this paper has been to focus on the problems of system identification and spectral estimation and to investigate tech-

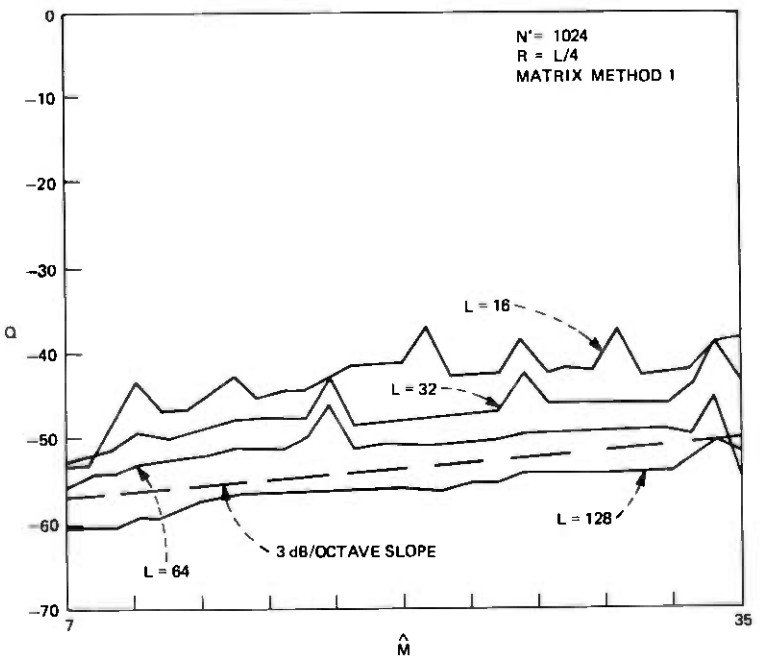

Fig. 7—Plots of Q versus $\hat{M}$ for $N = 1024$, $R = L/4$, s/n = ∞, and several values of L for matrix method 1. $\hat{M}$ is on a linear scale for this figure.

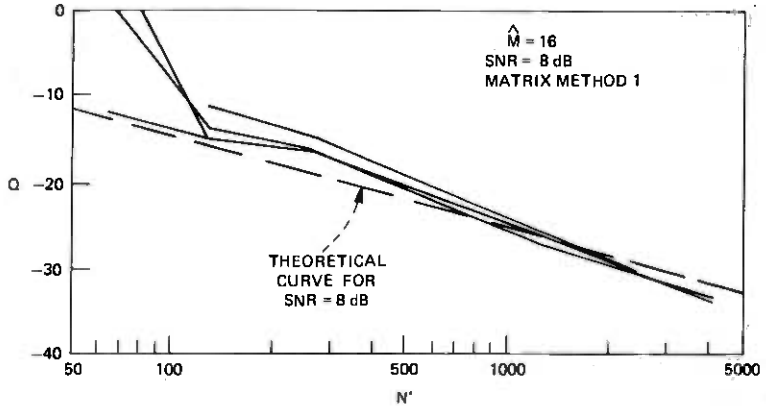

Fig. 8—Plots of Q versus N for $\hat{M} = 16$, s/n = 8 dB, and several values of L for matrix method 1. The dashed line is the theoretical LSA result for Q as derived in Ref. 6 (see text).

niques based on the short-time spectrum. We have shown that the problem of system identification can be solved by expanding each term of the least-squares solution in terms of short-time signals. By carefully examining and partitioning the terms entering into the computation, the system identification problem was approximately transformed from a general positive definite matrix inversion problem (the least-squares normal equations) to a Toeplitz matrix inversion problem with an error which was bounded and of order $1/N$. The terms which entered into the Toeplitz problem were identified as estimates of the power spectrum of the input and the cross power spectrum of the input and output. It was shown that the individual spectral estimates were unbiased—that is, they were independent of the window used to make the estimates.

Most of this paper has dealt with theoretical and numerical investigations of the properties of the resulting spectral estimates and their effect on the system identification solution. We have shown the following to be true:

(*i*) The spectral estimates $\mathbf{F}(\hat{\phi}(l))$ and $\mathbf{F}(\hat{r}(l))$ are unbiased.

(*ii*) The quality Q of the system identification estimate improves at a rate of 6 dB per octave as N increases for sufficiently large N and small additive noise (data-limited region).

(*iii*) The quality Q improves at a rate of 3 dB per octave as N increases for sufficiently large N and large additive noise (noise-limited region).

(*iv*) The resulting method approximates the least-squares normal equation by a Toeplitz equation, which is more accurate than the

standard Toeplitz approach which uses rectangular windows of duration equal to the total data length.

(*v*) The quality Q improves at a rate of 3 dB per octave as $\hat{M}$ decreases, if $\hat{M} \geq M$.

The key issue that remains to be discussed is the possible advantages and disadvantages of the short-time spectral approach [compared to alternative procedures such as the LSA or LMS (least-mean-squares[6] method)]. The main advantages of this method are:

(*i*) Implementation of the spectral estimates is straightforward and is readily performed using FFTs.

(*ii*) The resulting matrix equation can be solved directly using a Levinson[8] or Trench[9] inversion, or approximately via FFT methods.

(*iii*) The resulting solution has good asymptotic properties with respect to the variables N, $\hat{M}$, and s/n.

(*iv*) The method is easily amenable to adaptive procedures based on short-time spectral estimates. This property could be useful for systems where the additive noise is nonstationary—e.g., burst noise or corrupting speech.

(*v*) The method might potentially be applied to problems where $\hat{M}$ is on the order of 1000.

The disadvantages of the method are:

(*i*) The quality factor Q for the noiseless case for data lengths comparable to the impulse response duration ($N \approx M$) is significantly worse than that obtained from the LSA method.

(*ii*) A Toeplitz matrix equation must still be solved to obtain the highest accuracy solutions. However, it should be pointed out that the time required to invert a Toeplitz matrix is usually much less that the time required to compute it (i.e., when $N \gg \hat{M}$).

The final assessment of the utility of this, or any other spectral estimation or system identification method, is its applicability to a real world problem. One natural application for this method is the echo cancellation problem[10] where the impulse responses are long and possibly time-varying and additive nonstationary noise is present. We anticipate applying our technique to this problem as a more stringent test of its capabilities.

X. SUMMARY

In this paper, we have discussed a class of system identification and spectral estimation methods based on the short-time spectral representation of signals. We have discussed the properties of these methods and illustrated them with some simple examples. Our conclusion is that, for some applications, this new method provides a practical alternative to the classical least-squares analysis method. We would like to thank I. W. Sandberg for discussion on Section V.

APPENDIX

We derive here an explicit formula for $\hat{\phi}$ and ϵ. The constraints on N_A and N_B are

$$N_A \geq \hat{M} - 1 \tag{63}$$

$$N_B \leq N - 1 \tag{64}$$

$$N_A \leq N_B. \tag{65}$$

The equation for $\hat{\phi}(l - m)$ is

$$\hat{\phi}(l - m) = \sum_{q=q_1}^{q_2} \sum_{p=p_1}^{p_2} \phi_{p,pR+q}(l, m), \tag{66}$$

where $\phi_{p,pR+q}(l, m)$ is given by eq. (22) with $k = pR + q$. Constraint (63) gives p_1, (64) gives p_2, and (65) gives q_1 and q_2 as follows. From eqs. (63) and (26),

$$pR \geq \hat{M} + L - 2 - \max(m, qR + l).$$

Since we wish this to hold for all lags (m, l) on $[0, \hat{M} - 1]$, it must hold for $m = l = 0$, the values which give the greatest p value for which the inequality holds. Thus

$$p_1(q) = \left\lceil \frac{\hat{M} + L - 2}{R} \right\rceil - \max(0, q). \tag{67}$$

The functions $\lceil x \rceil$ and $\lfloor x \rfloor$ are called CEILING(x) and FLOOR(x). They are defined by truncation to the next integer above and below x, respectively. For example, $\lceil \pi \rceil = 4$, $\lfloor -\pi \rfloor = -4$, $\lceil 0.5 \rceil = 1$, etc. For any x, $\lceil x \rceil = -\lfloor -x \rfloor$, $\lfloor x + n \rfloor = \lfloor x \rfloor + n$, and $\lceil x + n \rceil = \lceil x \rceil + n$, where n is an integer.

Constraint (64) gives p_2 with $m = l = \hat{M} - 1$ as the worst case. Using eq. (27),

$$p_2(q) = \left\lfloor \frac{N - \hat{M}}{R} \right\rfloor - \min(0, q). \tag{68}$$

Finally from constraint (65) and eqs. (26) and (27),

$$q_1 = \left\lceil \frac{m - l - L + 1}{R} \right\rceil \tag{69}$$

$$q_2 = \left\lfloor \frac{m - l + L - 1}{R} \right\rfloor. \tag{70}$$

Since p_1 and p_2 are functions of q, the $p(q)$ sum must be done first as shown in (66). Thus (66) to (70) completely specify $\hat{\phi}$.

Next we give formulas for ϵ. ϵ has two components, as may be seen in Fig. 3, which we call ϵ_+ and ϵ_-. Then $\epsilon = \epsilon_+ + \epsilon_-$, where

$$\epsilon_-(l, m) = \sum_{p=p_3}^{p_4} \sum_{k=k_3}^{k_4} \phi_{pk}(l, m) \tag{71}$$

with

$$p_3 = \left\lceil \frac{\hat{M} - 1 - m}{R} \right\rceil \tag{72}$$

$$k_4 = p_4 = \left\lceil \frac{L + \hat{M} - 2}{R} \right\rceil - 1 \tag{73}$$

$$k_3 = \left\lceil \frac{\hat{M} - 1 - l}{R} \right\rceil \tag{74}$$

and

$$\epsilon_+(l, m) = \sum_{p=p_5}^{p_6} \sum_{k=k_5}^{k_6} \phi_{pk}(l, m) \tag{75}$$

$$k_5 = p_5 = \left\lfloor \frac{N - \hat{M}}{R} \right\rfloor + 1 \tag{76}$$

$$p_6 = \left\lfloor \frac{N - 2 + L - m}{R} \right\rfloor \tag{77}$$

$$k_6 = \left\lfloor \frac{N - 2 + L - l}{R} \right\rfloor. \tag{78}$$

REFERENCES

1. L. R. Rabiner and Jont B. Allen, "Short-Time Fourier Analysis Techniques for FIR System Identification and Power Spectrum Estimation," IEEE Trans. Acoustics, Speech, and Signal Processing, *ASSP-27*, No. 2 (April 1979), pp. 182–192.
2. Jont B. Allen and R. Yarlagadda, "The Digital Poisson Summation Formula and One Application," unpublished work.
3. Jont B. Allen, "Short-Term Spectral Analysis, Synthesis, and Modification by Discrete Fourier Transform," IEEE Trans. Acoustics, Speech, and Signal Processing, *ASSP-25*, No. 3 (June 1977), pp. 235–238.
4. Jont B. Allen and L. R. Rabiner, "A Unified Approach to Short-Time Fourier Analysis and Synthesis," Proc. IEEE, *65*, No. 11 (November 1977), pp. 1558–1564.
5. G. M. Jenkins and D. G. Watts, *Spectral Analysis and Its Applications*, San Francisco: Holden-Day, 1968.
6. L. R. Rabiner, R. E. Crochiere, and Jont B. Allen, "FIR System Modelling and Identification in the Presence of Noise and Bandlimited Inputs," IEEE Trans. on Acoustics, Speech, and Signal Processing, *ASSP-26*, No. 4 (August 1978), pp. 319–333.
7. P. Eykhoff, *System Identification*, New York: John Wiley, 1974.
8. E. A. Robinson, "Multichannel Time Series Analysis with Digital Computer Programs," 2nd ed., San Francisco: Holden-Day, 1976, p. 44.
9. S. Zohar "Toeplitz Matrix Inversion: The Algorithm of W. F. Trench," J. Assoc. Comput. Mach. *16* (1967), pp. 592–601.
10. M. M. Sondhi, "An Adaptive Echo Cancellor," B.S.T.J., *46*, No. 3 (March 1967), pp. 497–511.
11. J. B. Allen, D. A. Berkley, and J. Blauert, "Multimicrophone Signal-Processing Technique to Remove Room Reverberation from Speech Signals," J. Acoust. Soc. Amer., *62*, No. 4 (October 1977), pp. 912–915.

THE BELL SYSTEM TECHNICAL JOURNAL
Vol. 58, No. 8, October 1978
Printed in U.S.A.

On Concentrators, Superconcentrators, Generalizers, and Nonblocking Networks

By F. R. K. CHUNG

(Manuscript received November 9, 1978)

In this paper, we study various communication networks, such as concentrators, superconcentrators, generalizers, and rearrangeable and nonblocking networks. We improve bounds for the number of edges (which can be viewed as approximations of the cost) in some networks by combinatorial analysis.

I. INTRODUCTION

A communication network can be viewed as a collection of vertices and edges which provides connection between input vertices and output vertices by nonintersecting (vertex-disjoint) paths. Various types of communication networks, such as concentrators, superconcentrators, generalizers, and rearrangeable and nonblocking networks, have been extensively studied[1-8] and can be used to build efficient switching networks or to serve as useful tools for complexity theory for algorithms.[8]

An (n, m)-concentrator is a graph with n input vertices and m output vertices, $n \geq m$, having the property that, for any set of m or fewer inputs, a set of vertex-disjoint paths exists that join the given inputs in a one-to-one fashion to different outputs. If this graph is directed or acyclic, we call it a directed or acyclic (n, m)-concentrator, respectively. Pinsker[4] shows the existence of a directed acyclic (n, m)-concentrator with $29n$ edges. We show that there exist (n, m)-concentrators with $15n$ edges, there exist directed (n, m)-concentrators with about $25n$ edges, and there exist directed acyclic (n, m)-concentrators with $27n$ edges.

An n-superconcentrator is a graph with n inputs and n outputs having the property that, for any set of inputs and any equinumerous set of outputs, a set of vertex-disjoint paths exists that join the given inputs in a one-to-one fashion to the given outputs. Valiant[9] shows the existence of directed acyclic n-superconcentrators with $238n$ edges.

Pippenger[5] improved this bound by showing the existence of directed acyclic n-superconcentrator with about $39n$ edges. We show there exist n-superconcentrators with about $18.5n$ edges, there exist directed superconcentrators with about $36n$ edges, and there exist directed acyclic superconcentrators with about $38.5n$ edges.

An n-generalizer is a graph with n inputs and n outputs having the property that, for any given correspondence between inputs and nonnegative integers that sum to n, a set of vertex-disjoint trees exists that join each input to the corresponding number of distinct outputs. Pippenger[7] proves that directed acyclic n-generalizers exist with about $120n$ edges. We show that n-generalizers exist with about $61.5n$ edges.

An n-nonblocking graph is a graph with n inputs and n outputs having the property that, for any given sequence of one-to-one correspondences between inputs and outputs, we can establish vertex-disjoint paths to join inputs to the corresponding outputs sequentially without disturbing existing paths. Bassalygo and Pinsker[1] prove the existence of directed and acyclic n-nonblocking graphs with $67.26n \log_2 n$ edges. Pippenger improved the bound to $56.79n$ edges. In this paper we show that directed acyclic n-blocking graphs exist with about $55n$ edges.

II. PRELIMINARIES

We first prove some auxiliary lemmas that mainly follow the lines of Pinsker[4] and Pippenger.[5]

Lemma 1: *For integers n, a, b, x, $a \geq b \geq 2$ and a real number $\alpha < 1$, a bipartite graph exists with an inputs and bn outputs in which every input has degree bx and every output has degree ax and so that, for every set of $k \leq \alpha an$ inputs, a k-matching exists from the given inputs to some set of k outputs provided*

$$x > \frac{H(\alpha) + (b/a)H(a\alpha/b)}{bH(\alpha) - a\alpha H(b/a)}$$

and

$$\alpha < \frac{b(b-2)}{ab - a - b} \quad \text{and} \quad xb > 4,$$

where

$$H(z) = -z \log_2 z - (1-z)\log_2(1-z)$$

is the well-known entropy function and n is sufficiently large.

Proof: For a permutation p on $\{0, 1, \cdots, abxn - 1\}$, we consider a labeled bipartite graph B_p with an inputs and bn outputs in which every input y is adjacent to the outputs $\{z : z \equiv p(y') \pmod{bn}$ for some

$y' \equiv y \pmod{an}$}. The total number of such bipartite graphs is $(abxn)!$

Suppose B_p has the property that there are k inputs, $k \leq \alpha an$, such that there is no k-matching between these k inputs and some k outputs. From Hall's Theorem,[8,10] we know that there exist some k' inputs, $k' \leq k$, such that the total number of outputs adjacent to at least one of the k' inputs is less than k'. Thus the total number of B_p satisfying the above property does not exceed

$$A = \sum_{k \leq \alpha an} \binom{an}{k}\binom{bn}{k} \frac{(axk)!}{(axk - bxk)!} \cdot (abxn - bxk)!$$

Suppose $A < (abxn)!$ Then a bipartite graph B_p exists in which, for any k inputs, a k-matching exists between these given inputs and some k outputs. It suffices to show that $A < (abxn)!$ We let

$$f(k) = \binom{an}{k}\binom{bn}{k} \frac{(axk)!}{(axk - bxk)!} (abxn - bxk)!$$

For $k = \beta an$, we define

$$g(\beta) = \frac{f(k+1)}{f(k)}.$$

It is easily verified that

$$g(\beta) = (1 + o(1)) \cdot \frac{t^a}{(t-1)^{a-b}} \cdot \frac{(t^{-1} - \beta)\beta^{b-2}}{(1-\beta)^{b-1}},$$

where $t = a/b$ and $o(1)$ is arbitrarily small when n is sufficiently large. Let

$$p(\beta) = \frac{(t^{-1} - \beta)\beta^{b-2}}{(1-\beta)^{b-1}}.$$

By straightforward calculation, we have the first derivative $p'(\beta) > 0$ since

$$\beta < \alpha < \frac{b(b-2)}{ab - a - b}.$$

Let β_0, $0 < \beta_0 < \alpha$, be the real-number solution of

$$\frac{t^a}{(t-1)^{a-b}} \cdot p(\beta) = 1.$$

It follows immediately that, for n sufficiently large, we have

$$f(k+1) > f(k) \quad \text{if} \quad \beta = \frac{k}{an} > \beta_0 \quad \text{and}$$

$$f(k+1) < f(k) \quad \text{if} \quad \beta = \frac{k}{an} < \beta_0.$$

We consider the following two possibilities.

Case 1: $f(1) > f(\lfloor \alpha a n \rfloor)$.

From (1) we have

$$A \le \alpha a n f(1)$$

$$\le \alpha a^2 b n^3 \cdot \frac{(ax)!}{(ax - bx)!} (abxn - bx)!$$

$$< \frac{\alpha a^2 b n^3}{(bn - 1)^{bx}} \cdot (abxn)!$$

We have

$$A < (abxn)!$$

since $bx \ge 4$ and n is large.

Case 2: $f(\lfloor \alpha a n \rfloor) > f(1)$.

We use the following inequality for binomial coefficients (see Ref. 11).

$$((8np(1-p))^{-1/2})2^{nH(p)} \le \binom{n}{np} \le ((2\pi np(1-p))^{-1/2})2^{nH(p)}.$$

$$A \le \alpha a n f(\lfloor \alpha a n \rfloor)$$

$$\le \frac{\alpha a n \binom{an}{\alpha a n}\binom{bn}{\alpha a n}\binom{\alpha a^2 xn}{\alpha abxn}}{\binom{abxn}{\alpha abxn}} (abxn)!$$

$$< \frac{1}{\pi\sqrt{(1-(a\alpha)/b)(1-(b/a))}} 2^{\alpha n H(a)} + bnH\left(\frac{a\alpha}{b}\right)$$

$$+ a^2 \alpha n x H\left(\frac{b}{a}\right) - abxnH(\alpha)(abxn)!$$

$$< (abxn)! \quad \text{for} \quad n \quad \text{sufficiently large.}$$

This completes the proof of Lemma 1.

The bipartite graphs in Lemma 1 will be denoted by $B(n, a, b, \alpha)$. We also let $\bar{B}(n, a, b, \alpha)$ denote the same bipartite graph except that the set of inputs and outputs are interchanged.

Lemma 2: *For any integers n and t and real numbers α, β, $0 < \alpha < \beta < 1$, a bipartite graph exists with n inputs and tn outputs in which*

every input has degree tx and every output has degree x and every set of k inputs, $k = \alpha\theta n < \alpha n$, are adjacent to at least $\beta\theta tn$ different outputs provided

$$x > \frac{H(\alpha) + tH(\beta)}{t(H(\alpha) - \beta H(\alpha/\beta))}$$

and

$$xt > \frac{2 + \beta/\alpha + 3\alpha\beta}{1 - \beta}.$$

Proof: For a permutation p on $\{0, 1, \cdots, xtn - 1\}$, we consider a labeled bipartite graph B_p with n inputs and tn outputs in which every input y is adjacent to outputs $\{z : z \equiv p(y') \pmod{tn}$ for some $y' \equiv y \pmod{n}\}$. The total number of such bipartite graphs is $(xtn)!$

The number of B_p having the property that some k, $k = \alpha\theta n < \alpha n$, inputs are connected to less than $\beta\theta tn$ different outputs is bounded above by

$$A' = \sum_{k=\alpha\theta n<\alpha n} \binom{n}{\alpha\theta n}\binom{tn}{\beta\theta tn} \frac{(x\beta\theta tn)!(xtn - \alpha\theta xtn)!}{(x\beta\theta tn - x\alpha\theta tn)!}.$$

By an argument similar to that in the proof of Lemma 1, we can prove that

$$A' < (xtn)!$$

since

$$xt > \frac{2 + \beta/\alpha + 3\alpha\beta}{1 - \beta}$$

and

$$H(\alpha) + tH(\beta) + x\beta H\left(\frac{\alpha}{\beta}\right) - xtH(\alpha) < 0.$$

Therefore a bipartite graph B_p exists having the property that every set of k inputs, $k = \alpha\theta n < \alpha n$, are adjacent to at least $\beta\theta tn$ different outputs.

The bipartite graph mentioned in Lemma 2 will be denoted by $B'(n, t, \alpha, \beta)$.

III. SUPERCONCENTRATORS

A one-sided n-superconcentrator is a graph with n terminal vertices such that, for any two sets of equinumerous terminal vertices, we can find vertex-disjoint paths connecting vertices of one set to the vertices of the other.

Theorem 1: *There exist one-sided n-superconcentrators* $S_0(n)$ *with* $17.5n + O(\log n)$ *edges.*

Proof: Figure 1 illustrates the recursive construction for $S_0(n)$, where B is a subgraph of $B(\lceil n/7 \rceil, 7, 5, \frac{1}{2})$ in Lemma 1.

For any two sets of k terminal vertices, say, X and Y, we want to find vertex disjoint paths connecting vertices in X to vertices in Y. Let $X' = X - Y$, $Y' = Y - X$. It suffices to find vertex-disjoint paths connecting vertices in X' to vertices in Y'. We note that the number k' of vertices in X' does not exceed $n/2$. From Lemma 1, we know that a matching exists between X' and some set X'' of k' output vertices of B. Similarly, a matching exists between Y' and some set Y'' of k' output vertices of B. Vertices in X'' and Y'' can be connected by vertex-disjoint paths in $S_0(5\lceil n/7 \rceil)$. Therefore, $S_0(n)$ is indeed a superconcentrator.

The number of edges in B is $5n$. The number of edges in $S_0(n)$ is bounded above by

$$5n + 17.5\left(5\left\lceil \frac{n}{7} \right\rceil\right) + 80\left(\log 5\left\lceil \frac{n}{7} \right\rceil\right) \leq 17.5n + 80(\log n).$$

Theorem 1 is proved.

Theorem 2: *There exists n-superconcentrator* $S(n)$ *with* $18.5n + O(\log n)$ *edges.*

Proof: The construction for $S(n)$ is shown in Fig. 2.

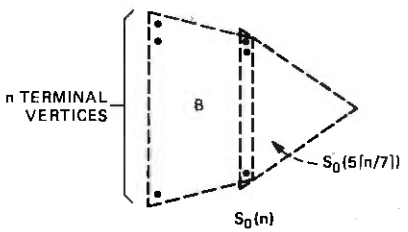

Fig. 1—A recursive construction for $S_0(n)$.

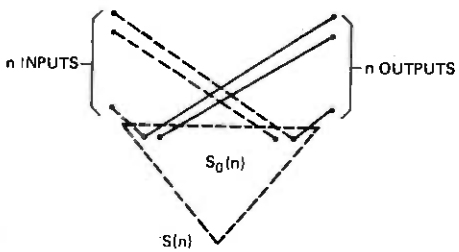

Fig. 2—A construction for $S(n)$.

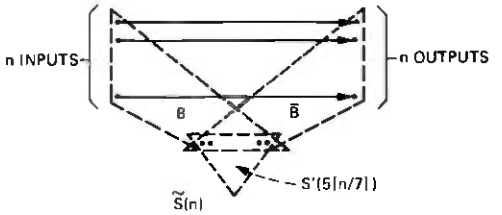

Fig. 3—A construction for $\tilde{S}(n)$.

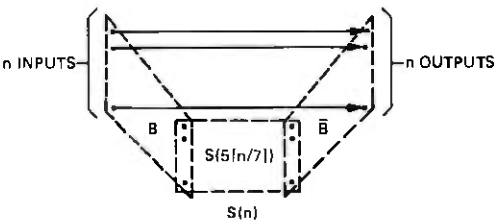

Fig. 4—A construction for $\mathbf{S}(n)$.

It is easily seen that $S(n)$ is a superconcentrator and has $18.5n + O(\log n)$ edges.

Theorem 3: *There exists directed superconcentrators* $\tilde{S}(n)$ *with* $36n + O(\log n)$ *edges.*

Proof: The construction of $\tilde{S}(n)$ is shown in Fig. 3, where $S'(n)$ is a directed graph obtained by replacing each edge in $S_0(n)$ by two directed edges of different directions.

It is easily seen that $\tilde{S}(n)$ has $36n + O(\log n)$ edges.

Theorem 4: *There exist directed acyclic superconcentrators* $\mathbf{S}(n)$ *with* $38.5n + O(\log n)$ *edges.*

Proof: $\mathbf{S}(n)$ is constructed similar to that in Ref. 4 except that the parameters are different (see Fig. 4).

It can be easily seen that $\mathbf{S}(n)$ has $38.5n + O(\log n)$ edges.

IV. CONCENTRATORS

An (n, m)-concentrator can be constructed as follows:

Case 1: $m < \frac{n}{3}$.

We construct $C(n, m)$ as shown in Fig. 5. For $1 \leq i \leq m$, input i is connected to output i by an edge. The connection between the inputs i, $i > m$, and the outputs can be viewed as a "composition" of two bipartite graphs, i.e., the outputs of the first bipartite graph are inputs of the second bipartite graph. The first bipartite graph is a subgraph B of $B(\lceil n/6 \rceil, 4, 3, 1/3)$ with $n - m$ inputs and $n/2$ outputs. From

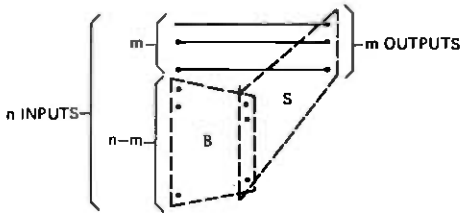

Fig. 5—A construction of $C(n, m)$ for $m < (n/3)$.

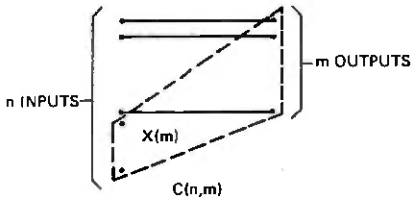

Fig. 6—A construction of $C(n, m)$ for $(n/3) < m \leq (2/3)n$.

Lemma 1, we know that the first bipartite graph contains at most $4n$ edges. The second bipartite graph is a subgraph S of $S_0(\lceil n/2 \rceil)$ with $n/2$ inputs and m outputs.

To show that $C(n, m)$ in Fig. 5 is a concentrator, we let W denote a set of k inputs.

Suppose input i is in W and $i \leq m$. We join input i to output i. Let W' be the set of inputs i, $i > m$, in W. From Lemma 1, we know that a matching exists between W' and some outputs in B, which will then be joined to specified distinct outputs since S is a subgraph of $S_0(\lceil n/2 \rceil)$. Therefore, $C(n, m)$ in Fig. 5 is a concentrator.

Case 2: $n/3 < m \leq 2/3\ n$.

If we take $X(m)$ in Fig. 6 to be a subgraph of $2/3\ n$-superconcentrator with n-m inputs and m outputs, it is easily checked that $C(n, m)$ is a concentrator.

Case 3: $m > 2/3\ n$.

We choose B in Fig. 7 to be a subgraph of $\bar{B}(\lceil n/4 \rceil, 3, 2, 1/3)$ if $3/4\ n \geq m > 2/3\ n$, to be a subgraph of $\bar{B}(\lceil n/8 \rceil, 7, 4, 1/4)$ if $7/8\ n \geq m > 3/4\ n$, and to be a subgraph of $\bar{B}(n, 2, 1, 1/8)$ if $n \geq m > 7/8\ n$. In any of the three cases, the number of edges in B does not exceed $4n + 7$.

To see that $C(n, m)$ is a concentrator, we consider the case $7/8\ n > m \geq 3/8\ n$. The other two cases can be verified similarly. Now let A denote a set of $k \leq m$ inputs. We want to show that a set of vertex-disjoint paths exists connecting vertices in A to some k output vertices. For any number x, $0 \leq x < n - m$, we consider the set of inputs $I_x = \{y : y \equiv x (\text{mod } n - m)\}$ and the set of outputs $O_x = \{z : z \equiv x (\text{mod } n -$

$m)\}$. We note that $|I_x| \geq |O_x| \geq |I_x| - 1$. Suppose $|I_x \cap A| < |O_x|$. We can join vertices in $I_x \cap A$ to O_x by a matching. Thus we only have to consider the case that $|I_x \cap A| = |I_x| = |O_x| + 1$. The first $|O_x|$ vertices in $|I_x \cap A|$ can be connected to vertices in 0_x by a matching. Thus at least $3/4\ m$ vertices in A can be connected to output vertices by vertex-disjoint edges. The remaining $\lfloor m/4 \rfloor$ vertices in A will then be connected through $S_0(\lceil n/2 \rceil)$. To see this, we note that B is a subgraph of $\bar{B}(\lceil n/8 \rceil, 7, 4, 1/4)$. For any set of $m/4$ output vertices of B, a matching exists between the given output vertices and some input vertices of B. Thus these vertices will be connected to the vertices in A through $S_0(\lceil n/2 \rceil)$.

Theorem 5: *There exist* (n, m)*-concentrators with* $14.75n + O(\log n)$ *edges.*

Proof: By the construction mentioned above, we note that in Case 2 we have

$$|C(n, m)| \leq m + |S(\lceil 2/3\ n \rceil)| \leq 13n + O(\log n).$$

In Case 1 and 3, we have

$$|C(n, m)| \leq n + 5n + |S_0(\lceil n/2 \rceil)| + O(\log n) \leq 14.75n + O(\log n).$$

Theorem 6: *There exist directed* (n, m)*-concentrators* $\bar{C}(n, m)$ *with* $24.67n + O(\log n)$ *edges.*

Proof: By taking $X(n)$ to be $S'(m)$, we have

$$\bar{C}(n, m) \leq 24.67n + O(\log n).$$

Theorem 7: *There exist directed acyclic* (n, m)*-concentrators* $C(n, m)$ *with* $27n + O(\log n)$ *edges.*

Proof: By taking $X(m)$ to be the directed acyclic superconcentrator, we have $|C(n, m)| \leq 27n + O(\log n)$.

Theorem 8: *There exists undirected, directed, acyclic directed* $(n, n/2)$*-concentrators with* $9.75n + O(\log n)$, $18.5n + O(\log n)$, $19.75n + O(\log n)$ *edges, respectively.*

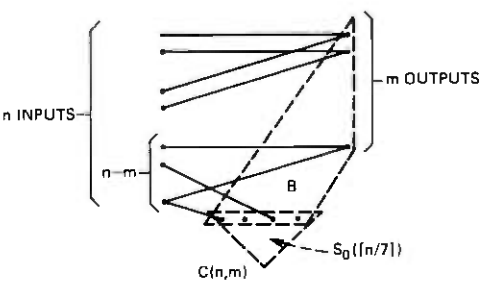

Fig. 7—A construction for $C(n, m)$ for $m > (2/3)n$.

Proof: We can construct undirected, directed, acyclic directed $(n, n/2)$-concentrator by taking S'' in Fig. 8 to be $S(\lceil n/2 \rceil)$, $\vec{S}(\lceil n/2 \rceil)$ and $\mathbf{S}(\lceil n/2 \rceil)$, respectively. We can then obtain the desired bounds.

V. GENERALIZERS

An n generalizer can be constructed as follows (see Ref. 6 and Fig. 9):

$$|G(n)| \leq 3/2\, n + |G(n/2)| + |S(n)| + |S(\lceil n/2 \rceil)|.$$

Using Theorems 1 to 4, we have the following:

Theorem 9: *There exist n-generalizers with* $61.5n + O(\log n)$ *edges.*

Theorem 10: *There exist directed n-generalizers with* $111n + O(\log n)$ *edges.*

Theorem 11: *There exist directed acyclic n-generalizers with*

$$118.5n + O(\log n) \text{ edges.}$$

VI. NONBLOCKING GRAPHS

A k-access graph $G(n, m, k)$ is a graph with n inputs, m outputs having the property that, for any given set S of vertex-disjoint paths connecting inputs to outputs, an input vertex which is not in S can be

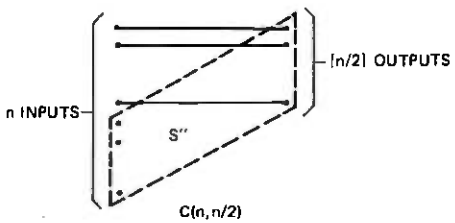

Fig. 8—A construction for $C(n, n/2)$.

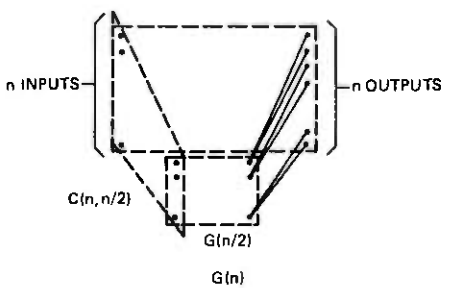

Fig. 9. A construction for $G(n)$.

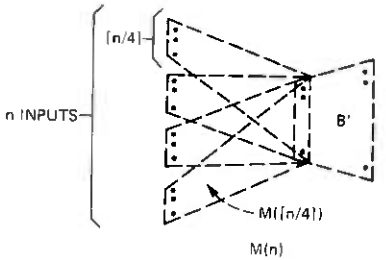

Fig. 10. A construction for $M(n)$.

connected to k different outputs by paths not containing any vertex in S. If k is greater than or equal to $m/2$, a k-access graph is also called a major-access graph. A nonblocking graph with n inputs and n outputs can be built by combining a major-access graph $G(n, m, k)$ and its mirror image.

We now construct a major access graph by using the $B'(n, t, \alpha, \beta)$ in Lemma 2 by a method similar to that in Ref. 6.

Let $M(n)$ denote a major access graph with n inputs, at most $f(n) = 11n + 17 \log_2 n$ outputs, constructed as shown in Fig. 10.

$M(n)$ will be a $2/3\, f(n)$-access graph if we take B' to be $B'(f(\lceil n/4 \rceil), 4, 13/33, 25/33)$. We note that B' has $20f(\lceil n/4 \rceil)$ edges. The total number of edges in $M(n)$ is

$$|M(n)| \leq |4M(\lceil n/4 \rceil)| + 220\lceil n/4 \rceil + 340 \log_2 n/4$$
$$\leq 27.4n \log_2 n + O((\log n)^2).$$

We will prove by induction on n that $M(n)$ is a $2/3\ f(n)$-access graph. For any given set S of vertex-disjoint paths connecting inputs to outputs in $M(n)$, let x denote an input vertex not in S. Suppose x is an input of M' which is a copy of $M(\lceil n/4 \rceil)$. We can connect x to $2/3\ f(\lceil n/4 \rceil)$ output vertices of $M(\lceil n/4 \rceil)$ by paths not containing any vertex in a path in S, which join a vertex of M' to some output of M'. Thus x is connected to about 13/33 of the total number of inputs of B' which are not in S. Thus x is connected to 25/33 of the number of outputs of B' of which at most n vertices can be in S. Therefore x is connected to 2/3 of the number of outputs of B' by paths not containing vertices in S. Therefore $M(n)$ is a $(2/3)\ f(n)$-access graph and we note that $M(n)$ is, in fact, a one-sided nonblocking graph. We have the following:

Theorem 12: *There exist one-sided nonblocking graphs with* $27.5n \log_2 n + O((\log n)^2)$ *edges.*

Theorem 13: *There exist directed acyclic nonblocking graphs* $N(n)$ *with* $55n \log_2 n + O((\log n)^2)$ *edges.*

Proof: The proof follows immediately from

$$|N(n)| \leq |2M(n)|.$$

We note that, if we choose the size of $M(n)$ more carefully, say, $M(n)$ having $10.9n + O(\log n)$ outputs, we can, in fact, show that $|N(n)| \leq 54.5n \log_2 n$.

VII. REMARKS

In this paper we prove the existence of various graphs by nonconstructive combinatorial probabilistic arguments. Margulis[3] gives an explicit construction for a sequence of bipartite graphs in which one bipartite graph satisfies the property required in Lemma 1 for given n, a, b, α, or in Lemma 2 for given n, α, β, t. However, he could not determine which one in the sequence is the bipartite graphs we need.

We remark that the bounds in Theorems 1 to 4 are the best possible under the conditions proven in Lemma 1 (by choosing $a = 7$, $b = 5$). We also note that all the bounds would be improved if we can improve the bound on x in Lemma 1 or 2.

In this paper, we deal with various graphs which represent corresponding switching networks. In the graph representation of a switching network, a point corresponds to a "line" and an edge corresponds to a "crosspoint." (The reader is referred to Ref. 2 for detail.) Therefore, the number of edges in the graph corresponds to the number of crosspoints which is a major part of the cost for a switching network. For example, the bounds we proved in Theorem 12 provide an estimate for the number of crosspoints of a nonblocking network. We summarize our results in Table I.

We remark that Ofer Gabber and Zvi Galil have recently found explicit constructions of linear size concentrators and superconcentrators. They proved the existence of an n-superconcentrator with $273n$ edges constructively by a complicated analytical argument. In fact, the constant 273 can be lowered to 262.

Table I

Graph \ Type (No. of Edges)	Undirected	Directed	Acyclic directed
One-sided superconcentrator	$17.5n + O(\log n)$	$35n + O(\log n)$	
Superconcentrator	$18.5n + O(\log n)$	$36n + O(\log n)$	$38.5n + O(\log n)$
Concentrator	$14.75n + O(\log n)$	$24.67n + O(\log n)$	$27n + O(\log n)$
$(n, n/2)$-concentrator	$9.75n + O(\log n)$	$18.5n + O(\log n)$	$19.5n + O(\log n)$
Generalizer	$61.5n + O(\log n)$	$111n + O(\log n)$	$118.5n + O(\log n)$
One-sided nonblocking graph	$27.25n \log_2 n$	$54.5n \log_2 n$	
Nonblocking graph	$54.5\ n \log_2 n$	$54.5n \log_2 n$	$54.5n \log_2 n$

REFERENCES

1. L. A. Bassalygo and M. S. Pinsker, "Complexity of an Optimum Non-Blocking Switching Network Without Reconnections," Problemy Peredachi Informatsii, *9*, No. 1 (1973), pp. 84–87; translated into English in Problems of Info. Trans., *9*, No. 1 (1974), pp. 64–66.
2. F. R. K. Chung, "Optimal Rearrangeable Graphs," B.S.T.J., *54*, No. 9 (November 1975), pp. 1647–1661.
3. G. A. Margulis, "Explicit Construction of Concentrators," Problemy Peredachi Informatsii, *9*, No. 4 (1973), pp. 71–80, translated into English in Problems of Info. Trans., *9*, No. 4 (1973), pp. 325–332.
4. M. S. Pinsker, "On the Complexity of a Concentrator," Proc. 7th International Teletraffic Conference, Stockholm (1973), pp. 318/1–318/4.
5. N. Pippenger, "Superconcentrators," SIAM J. Comput., *6*, No. 2 (1977), pp. 298–304.
6. N. Pippenger, "On Rearrangeable and Non-blocking Switching," (to appear in Networks).
7. N. Pippenger, "Generalized Connectors," SIAM J. Comput., *7*, No. 4 (1978), pp. 510–514.
8. H. J. Ryser, "Combinatorial Mathematics," The Carus Mathematical Monographs, No. 14, New York: Math. Assoc. of America, 1963.
9. L. G. Valiant, "On Nonlinear Lower Bounds in Computational Complexity," Proc. 7th Annual ACM Symposium on Theory of Computing, Albuquerque (1975), pp. 45–53.
10. P. Hall, "On Representatives of Subsets," J. London Math. Soc., *10* (1935), pp. 26–30.
11. R. Ash, *Information Theory*, New York: Interscience Publishers, 1965, p. 113.

THE BELL SYSTEM TECHNICAL JOURNAL
Vol. 58, No. 8, October 1979
Printed in U.S.A.

Transmission Unavailability of Frequency-Diversity Protected Microwave FM Radio Systems Caused by Multipath Fading

By A. VIGANTS and M. V. PURSLEY

(Manuscript received April 2, 1979)

Estimates of transmission unavailability caused by multipath fading are needed to determine the adequacy of diversity protection arrangements. A computer program producing such estimates was made available for general Bell System use in 1977. In this paper, we summarize the underlying mathematical model of frequency diversity operation and atmospheric multipath fading and use it to study frequency diversity behavior.

I. INTRODUCTION

Microwave FM radio systems utilized in the Bell System provide protected broadband communications channels that generally have a capacity, depending on the frequency band and on the type of equipment, of 1200 to 2400 message circuits per channel. The protected channels, with protection provided by radio switching systems, are referred to as "working" channels, to distinguish these from the actual radio channels, which are assigned as either "regular" or "protection" channels. The number of regular channels in a radio system equals the number of working channels. Equipment failures, atmospheric fading, or other impairments in a regular channel cause temporary transfers of the communications traffic to a protection channel at a different radio frequency, if an unoccupied and unimpaired protection channel is available. In the case of fading, such frequency-diversity protection switching capitalizes on the frequency selectivity of the multipath fading process, where, at an instant in time, the strength of the received signal is a function of frequency. The Bell System long-haul microwave FM radio network contains approximately 1600 one-way frequency-diversity switching sections (800 route segments) with an average of three radio hops per switching section.

The communications traffic in a working channel can be temporarily subjected to high noise when, in a switching section, the number of impaired radio channels exceeds the number of protection channels. Bell System practice is to describe this in terms of the amount of time during which the noise in a working channel exceeds 55 dBrnc0 in a message circuit at the top frequency assignment in the baseband.[1] In this paper, this time is referred to as "service failure time" in accordance with designations on protection switching equipment and terminology used in the operation of the plant. The terms "service failure" and "outage" are frequently synonymous,[1] but use of the latter term can sometimes result in semantic difficulties, since some service failures may not result in outages as perceived or defined by some communications users.

In modern microwave radio systems, protection requirements are frequently governed by the presence of multipath fading,[2-13] as opposed to causes associated with equipment or human intervention.[1] Estimates of service failure time due to multipath fading are therefore needed to determine the adequacy of diversity protection arrangements when new routes are planned, when transmission parameters of existing routes are changed, or when alternate protection strategies are considered for future use. In 1977, a computer program producing such estimates was made available for general Bell System application. It is extensively used to treat everyday design and planning tasks on an individualized basis for microwave FM radio routes equipped with frequency-diversity and space-diversity[9] protection.

A mathematical model of frequency-diversity operation and multipath fading is central to the computer program. In this paper, the model is summarized and utilized to study representative radio systems on fully and partially developed routes. The effect of radio channels with reduced fade margins, the service failure time of individual channels, and parameters that can be used to characterize frequency-diversity systems are treated. A discussion is included of the addition of space-diversity protection to frequency-diversity protection, often necessary to reduce service failure time.

The numerical results presented in this paper should be considered in the context of transmission performance objectives. A proposed design or modification of a frequency-diversity protection switching section containing S radio hops is satisfactory when

$$\sum_{h=1}^{S} T_h \leq T_{\text{obj}}, \tag{1}$$

where T_h is the estimated service failure time of an average radio channel due to multipath fading on a particular radio hop. The service failure time due to simultaneous deep fading on different hops is much

smaller and is therefore neglected in the above expression. The design-objective time T_{obj} is obtained from the reliability objectives for microwave FM radio, which specify an annual outage of 0.02 percent or less due to all causes for a two-way circuit on a 4000-mile long-haul or a 250-mile short-haul route.[1] In practice, this objective is prorated to the actual distance and applied to the service failure time. One-half the objective is allocated to multipath fading, and the other half to equipment, maintenance, and other causes.[9] For multipath fading, one-half the 0.01-percent two-way allocation is applied to each direction of transmission. This accommodates customers that may transmit in only one direction and conforms to the structure of the plant, where independent protection switching systems and different radio frequencies are used in the two directions of transmission. Furthermore, the service failure time associated with a single protection switching system can be expected to be substantially larger than the service failure time occurring simultaneously in the two directions, since the latter kind of failure requires simultaneous deep fading on a larger number of radio channels. Consequently, the one-way multipath-fading service failure time objective for a section of a route containing S hops is, in seconds per year,

$$T_{obj} = (1600/D_{ref}) \sum_{h=1}^{S} D_h, \tag{2}$$

where D_{ref} is 4000 miles for long-haul and 250 miles for short-haul radio, and D_h is the hop length in miles. In the case of a frequency-diversity switching section containing a single 25-mile hop, the values of T_{obj} are 10 seconds per year for long-haul and 160 seconds per year for short-haul radio. In the past, it was often assumed that only half the hops on a long route would experience significant fading.[1,9] This assumption is no longer necessary, since fading estimates can now be made for every hop on a route.[5,9]

II. THE MATHEMATICAL MODEL

The service failure time of an average working channel, caused by multipath fading on a particular radio hop, can be expressed as

$$T_h = N^{-1} Z_h, \tag{3}$$

where N is the number of working channels and Z_h, referred to as the facility service failure time, is the sum of the service failure times of the working channels. The facility service failure time can be expressed as

$$Z_h = \sum_{i=1}^{N} iT''(i), \tag{4}$$

where $T''(i)$ is the accumulated time during which exactly i of the N working channels experience service failure. The terms in this sum are associated with simultaneous fading of radio channels. For a frequency-diversity protection switching section with M radio channels of which u are protection channels,

$$M = u + N, \tag{5}$$

eq. (4) becomes

$$Z_h = \sum_{i=1}^{N} iT'(u + i), \tag{6}$$

where $T'(u + i)$ is the accumulated time during which exactly $u + i$ of the M radio channels have failed simultaneously. A failure in this context is an exceedance of the 55-dBrnc0 noise value.

The simultaneous fading of radio channels is normally described in terms of the amount of time during which particular sets of $u + i$ channels have failed, with the status of the other $M - u - i$ channels not specified. With such a time denoted by $T_k(u + i)$, the expression for Z_h becomes an alternating series

$$Z_h = \sum_{i=1}^{N} \sum_{k=1}^{J(u+i)} (-1)^{i-1} C_{u-1}^{u+i-2}\, T_k(u + i), \tag{7}$$

where $J(u + i)$ is the binomial coefficient C_{u+i}^{M}, and where the subscript k enumerates the sets of $u + i$ channels obtainable from the M channels. This expression has been used by other authors,[1] but its general mathematical equivalence to the definition in eq. (6) has not been demonstrated; a proof of this equivalence is supplied in Appendix A.

The expressions for the simultaneous failure time of a number of radio channels, denoted by $T_k(u + i)$, are based on a generalized model of simultaneous multipath fading in an arbitrary number of radio channels obtained empirically from experimental data. The estimation of the amount of fading and the calculation of $T_k(u + i)$ are summarized in Appendix B. A simplified form of $T_k(u + i)$, without path length dependence and without accommodation of fade margin differences between radio channels, has been utilized previously to demonstrate the feasibility of joint frequency-diversity protection for radio systems in the 4-GHz and 6-GHz bands.[1]

Numerical evaluation of Z_h from the alternating series requires a computer program that efficiently selects and classifies radio channel combinations from a particular frequency plan and calculates the corresponding values of $T_k(u + i)$, since the number of terms can be large. For example, there are 184,756 ten-channel combinations when all radio channels in the 4-GHz and 6-GHz bands are used (400A

protection system with 2 protection and 18 regular channels). The computation of the combinations is discussed in Appendix C.

III. REPRESENTATIVE RESULTS FOR FULLY DEVELOPED ROUTES

A fully developed 4-GHz route contains a total of 12 radio channels consisting of one protection channel and 11 regular channels. The notation 1 × 11 is used to describe this. On fully developed 6-GHz routes, the total number of radio channels is 8 and the protection scheme is 1 × 7. When both bands are utilized, the two protection channels can be placed in the 6-GHz band, which results in 2 × 18 protection.

Representative estimated values of service failure times for these protection schemes can be obtained from calculations for a switching section containing one 25-mile hop with average terrain and climate. Without diversity protection, the service failure time of an average channel in the 4-GHz band is 269 seconds per year for a fade margin of 37 dB. In the 6-GHz band, the corresponding service failure time is 208 seconds per year for a fade margin of 40 dB.

When 2 × 18 protection is applied, the calculated service failure time is 6 seconds per year, which meets the long-haul objective of 10 seconds per year. Use of one of the protection channels for temporary service in the fading season increases the service failure time to 15 seconds per year as a result of the 1 × 19 configuration. The fade margin affects the service failure time. With diversity protection applied, a 5-dB fade margin decrease in all channels increases the service failure time by a factor of ten (Fig. 1).

For 1 × 11 and 1 × 7 protection, the calculated service failure times are about 15 seconds per year (Fig. 1). Prior to a conversion to one protection channel per band, required by spectrum conservation measures, the service failure times for 2 × 10 and 2 × 6 protection would have been about 6 seconds per year, meeting the long-haul objective.

The relative positions of the curves in Fig. 1 are significant. For example, the service failure time of an average channel in the 2 × 18 scheme is between those for average channels in the 2 × 10 and 2 × 6 schemes. This suggests that, because of decorrelation of fading between the 4-GHz and 6-GHz bands, the 2 × 18 functions part of the time as a 2 × 12 and part of the time as a 2 × 6.

The frequency-diversity parameters that can be used to scale the results to other path lengths and climatic conditions are discussed in Appendix D.

IV. PARTIALLY DEVELOPED ROUTES

On partially developed routes where only a part of all available frequency assignments is utilized, the service failure time is a function

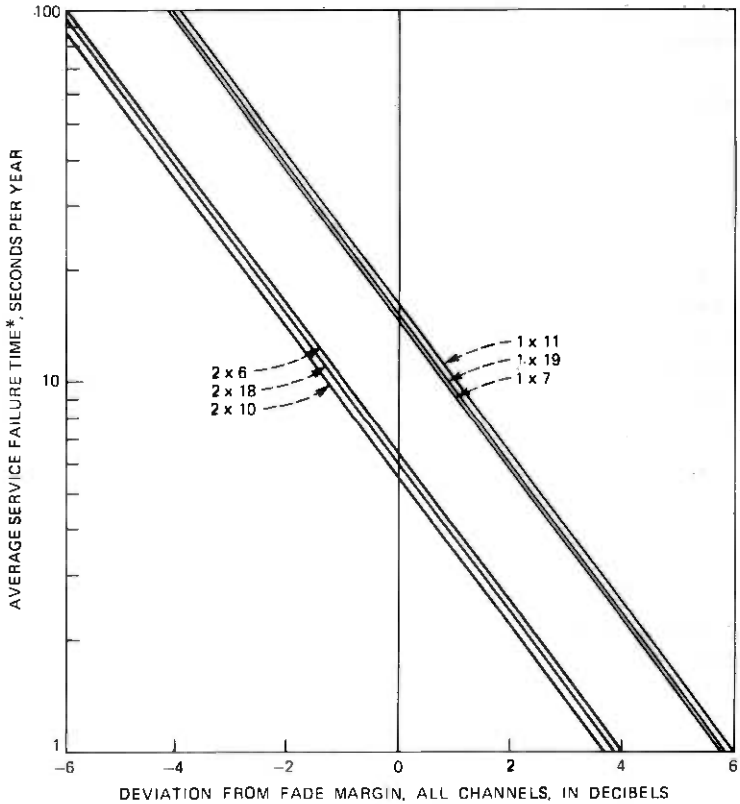

Fig. 1—Service failure time of average working channel due to multipath fading on a 25-mile hop with average climate and terrain. Fade margin = 37 dB, 4-GHz band; fade margin = 40 dB, 6-GHz band; average annual temperature = 55°F; terrain roughness = 50 ft.

* Average service failure time and service failure time of average working channel are synonymous in the context of this work.

of the frequency arrangement of the radio channels. A "best-case" arrangement is one where the frequency separation of adjacent channels is maximized. In a "worst-case" arrangement, the channels are crowded into the high end of the frequency band. Such arrangements do not necessarily correspond to actual or permitted growth strategies, but they do provide bounds for the variation of service failure time on partially developed routes.

In continuation of the example in Fig. 1, calculated results for the best and worst cases are shown in Fig. 2 as a function of the number of working channels. The best-case results for the 4-GHz band show that the 10 seconds-per-year long-haul objective cannot be met by

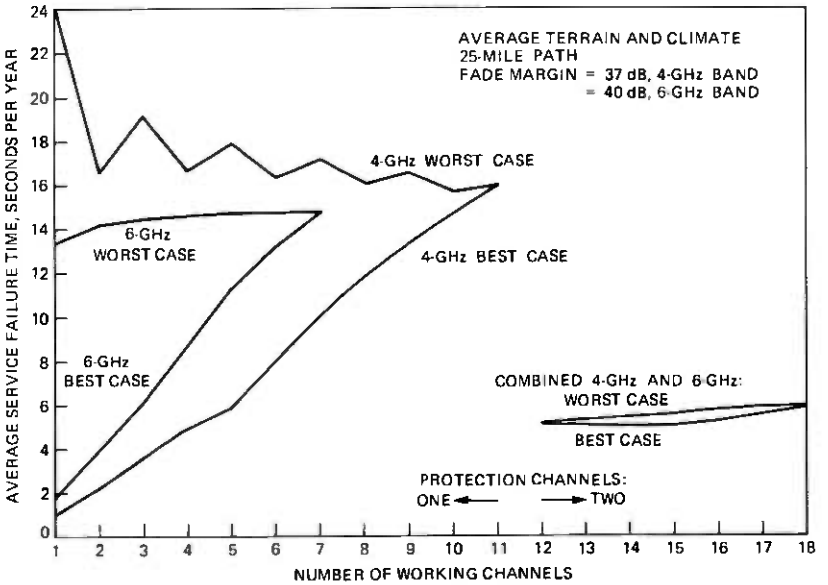

Fig. 2—Bounding cases for service failure time of average working channels. Frequency assignments are listed in Appendix E.

frequency diversity alone when the number of working channels is larger than seven. The ripple in the worst case is caused by the alternating 20-MHz and 60-MHz increments as channels are added.

In the 6-GHz band, the long-haul objective cannot be met by frequency diversity alone when the number of working channels is larger than four. The 6-GHz worst case is better than the 4-GHz worst case because the 6-GHz fade margin is larger than the 4-GHz fade margin in this example.

In a combined protection system for the two frequency bands, introduced after the 4-GHz band is fully developed, the arrangement of the channels in the 6-GHz band has only a small effect on the service failure time of an average channel, which varies between 5 and 6 seconds per year.

V. EFFECT OF CHANNELS WITH REDUCED FADE MARGINS

A radio channel with a substandard fade margin experiences a failure time that is larger than normal. The presence of such a channel increases protection unavailability, which results in increased service failure times for all working channels. The increase in the service failure time of an average working channel, caused by the presence of one or two substandard radio channels on a fully developed route, is shown in Fig. 3 as a function of the reduction of the fade margin from

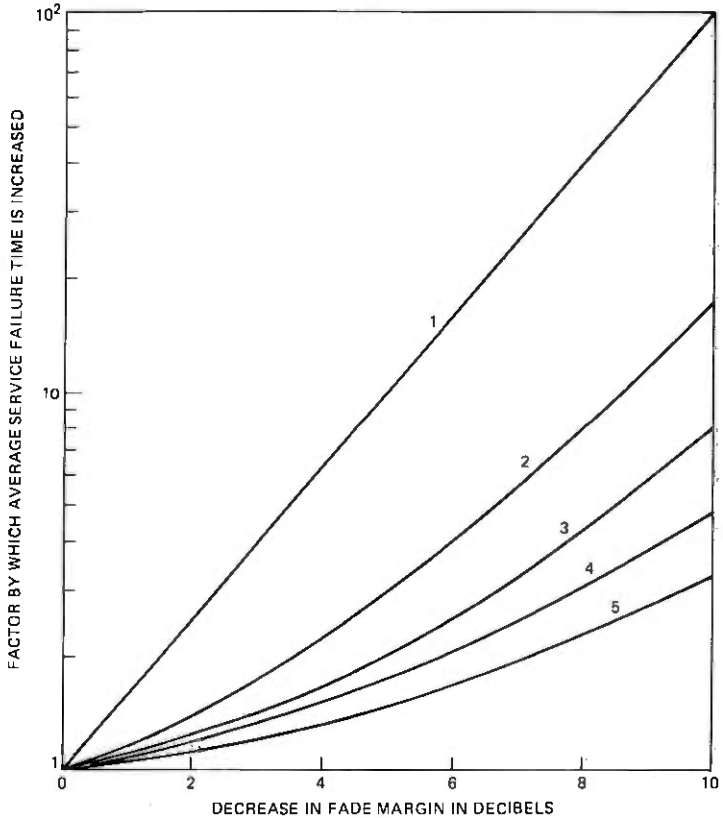

Fig. 3—Increase in service failure time of average working channel when fade margins are reduced for: (1) all radio channels; (2) two midband channels in 1 × 7 system, 6 GHz; (3) two midband channels in 1 × 11 system, 4 GHz; (4) one midband channel in 1 × 7 system, 6 GHz; (5) one midband channel in 1 × 11 system, 4 GHz.

its normal value. As an example, the service failure time of an average working channel in a 1 × 11 system is doubled when the fade margin of one midband radio channel is degraded by 7 dB; this is equivalent to a 1.5-dB degradation of the fade margins of all channels.

The service failure time indicated by a protection switching monitor actuated by the protection switching equipment can be larger than the actual service failure time if adjustments in the protection switching system are incorrect so that, for a particular channel, a transfer to protection occurs early, at a noise value smaller than 55 dBrnc0. The actual service failure time, while smaller than that indicated (Fig. 4), is larger than normal because occupancy of the protection channel has been increased.

Transfers to protection are normally permitted only when the amount of noise after the transfer is at least a few decibels smaller

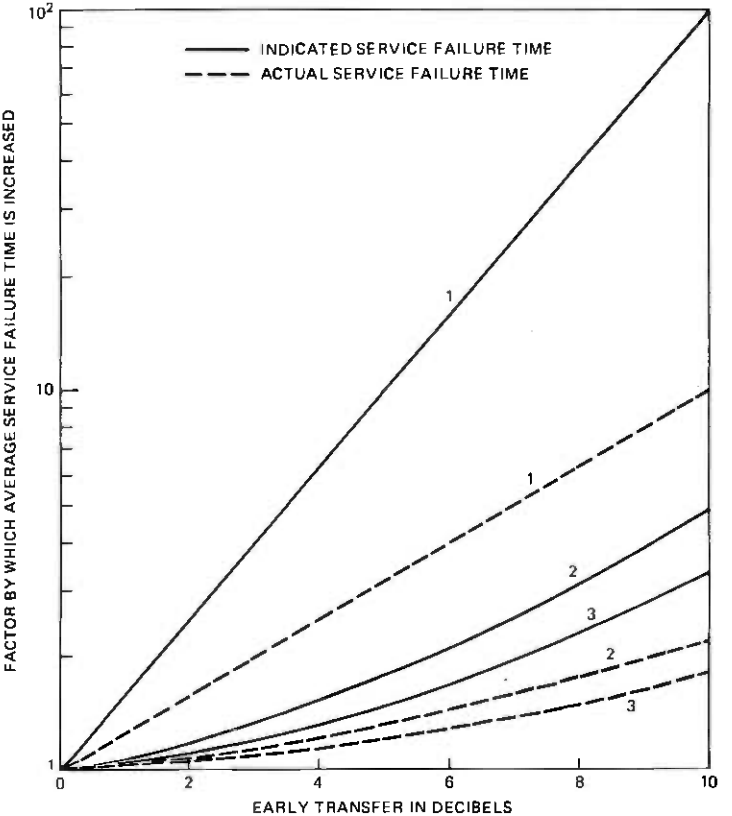

Fig. 4—Increase in service failure time of average working channel when transfer to protection occurs early for: (1) all channels; (2) one midband channel in 1 × 7 system, 6 GHz; (3) one midband channel in 1 × 11 system, 4 GHz.

than 55 dBrnc0. The increase in service failure time due to a 3-dB difference of this kind is very roughly the same as that due to transfers to protection that occur 3 dB early. From Fig. 4, this is equivalent to a fraction of a decibel decrease in the fade margins of all channels. Consequently, such differences associated with the protection channels are not included in the mathematical model presented in this paper, since their relatively small effects do not justify the added analytical and computational complexity.

VI. SERVICE FAILURE TIME OF INDIVIDUAL CHANNELS

In addition to the service failure time of an average channel utilized in engineering applications, the mathematical model developed in this work can provide other information about the operation of frequency-diversity protection. In particular, the service failure times of individ-

ual working channels can be obtained from a decomposition of the facility service failure time.

As an example, consider a 1 × 3 protection system in the 4-GHz band with parameters as in Fig. 2, utilizing channels 2, 4, 6 and 8 (80-MHz separation of adjacent channels). The simultaneous failure times for particular sets of exactly $u + i$ channels are needed in the decomposition. These times, denoted by $T'_k(u + i)$ and listed in Table I, are summations [as specified in eq. (14)] of the failure times $T_k(u + i)$ calculated as outlined in Appendix B. The numerical values illustrate the frequency selectivity and frequency dependence of multipath fading. For example, the failure time of channels 2 and 4, but not 6 and 8, which can be caused by a slope in the frequency response, is 2.58 seconds. The failure time of channels 6 and 8, but not 2 and 4, is 3.07 seconds. This is larger than the 2.58 seconds because the amount of fading increases with frequency. The failure time of channels 4 and 6, but not 2 and 8, is 2.22 seconds. This is smaller than either the 2.58 seconds or the 3.07 seconds because this failure results from a minimum in the frequency response. The facility service failure time for this example is, from eq. (6),

$$\begin{aligned} Z_h &= \sum_{k=1}^{6} T'_k(2) + 2 \sum_{k=1}^{4} T'_k(3) + 3\, T'_1(4) \\ &= 8.81 + 2 \times 2.12 + 3 \times 1.00 \\ &= 16.05 \text{ channel-seconds per year.} \end{aligned} \tag{8}$$

The corresponding service failure time of an average channel is, from eq. (3), one-third of this

$$T_h = 5.35 \text{ seconds per year.} \tag{9}$$

About 45 percent of this time occurs when 3 or all 4 of the radio channels have failed simultaneously.

The expressions for the service failure time of individual channels are obtained by inspection from Table I. In the case where channel 2 is used for protection, the service failure time of the working channel assigned to channel 4 is

$$\begin{aligned} T_{h,4} &= T'_1(2) + (\tfrac{1}{2})\, T'_4(2) + (\tfrac{1}{2})\, T'_5(2) \\ &\quad + T'_1(3) + T'_2(3) + (\tfrac{2}{3})\, T'_4(3) + T'_1(4) \\ &= 6.484 \text{ seconds per year,} \end{aligned} \tag{10}$$

where the fractions are based on statistically equal protection occupancy in cases of simultaneous failures.

The results of such calculations (summarized in Table II) show that the location of the protection channel affects the spread of the individ-

Table I—Simultaneous failures of exactly $u + i$ radio channels. Channel numbers: 2, 4, 6, 8; frequencies, GHz: 3.73, 3.81, 3.89, 3.97.

$u + i$	k	Channels	$T_k'(u + i)$, sec/year
2	1	2, 4	2.58
2	2	2, 6	0.37
2	3	2, 8	0.17
2	4	4, 6	2.22
2	5	4, 8	0.40
2	6	6, 8	3.07
3	1	2, 4, 6	0.77
3	2	2, 4, 8	0.23
3	3	2, 6, 8	0.23
3	4	4, 6, 8	0.89
4	1	2, 4, 6, 8	1.00

Table II—Service failure time of individual working channels for a 1 × 3 system in the 4-GHz band. Channel numbers: 2, 4, 6, 8; frequencies, GHz: 3.73, 3.81, 3.89, 3.97.

Working Channel*	Service Failure Time, Seconds/Year (percent of average in parentheses)			
	Protection channel assignment			
	2	4	6	8
2	—	5.003 (94)	3.898 (73)	3.618 (68)
4	6.484 (121)	—	6.524 (122)	5.434 (101)
6	5.608 (105)	6.753 (126)	—	6.998 (131)
8	3.958 (74)	4.294 (80)	5.628 (105)	—
Total seconds	16.05	16.05	16.05	16.05
Range of percent:				
Minimum	74	80	73	68
Maximum	121	126	122	131

* Working channels in this table are identified by the number of the corresponding regular radio channel.

ual service failure times. The facility service failure time and, therefore, the service failure time of an average channel are not affected by the location of the protection channel. The largest spread of the individual service failure times (68 to 131 percent of average) occurs when the channel at the highest frequency (channel 8) is used for protection.

Protection channel assignments could be optimized based on results such as those presented in Table II. However, a general treatment of this is beyond the current scope of this study.

VII. ADDITION OF SPACE DIVERSITY TO FREQUENCY DIVERSITY

Space-diversity protective switching capitalizes on the spatial selectivity of the multipath fading process, where, at an instant in time and at a given radio frequency, the strength of the received signal is a random function of location along the height of the receiving tower.[6,7,9] For FM radio carrying analog message traffic, space-diversity in most cases in the Bell System consists of two vertically separated receiving antennas and, for each radio channel, a waveguide switch that connects a receiver to either of the two antennas. The switch is activated when the receiver input decreases below a threshold.

The presence of digital traffic in the FM radio network affects the choice of timing in the switch. The number of antenna-to-antenna transfers should be as small as possible, since these can cause errors in digital transmission. For thresholds corresponding to fades deeper than about 35 dB, this is accomplished when, in the case of simultaneous fading on the two antennas, the interval between repeated transfers is 10 seconds. Intervals longer than this cause significant increases in the service failure time of analog message circuits.

When added to frequency-diversity to reduce service failure time, space-diversity is activated before frequency-diversity to avoid undesirable interactions of the two protection systems. Currently, frequency-diversity is activated at a noise threshold of 55 dBrnc0, and 52 dBrnc0 is the desired threshold value for space-diversity activation when it is added to frequency-diversity. Such an arrangement has assured orderly evolution and uniform maintenance procedures of protection switching systems. In the future, because of increased use of space-diversity, changed threshold values may be desirable, ideally 58 dBrnc0 for frequency-diversity and 55 dBrnc0 for space-diversity, to further reduce service impairments.

The reduced service failure time resulting from an addition of space diversity in the manner described above can be calculated from eq. (7) with the values of $T_k(u + i)$ divided by the appropriate improvement value for threshold-switched space-diversity.[9] Such calculations, which can be readily incorporated in a computer program, will not be pursued in this paper where the emphasis is on an exploration of frequency-diversity behavior.

VIII. ACKNOWLEDGMENTS

We wish to express our appreciation to W. T. Barnett, whose model of simultaneous fading we utilize, and to H. Adams, who helped to develop the computer program.

APPENDIX A

Derivation of the Alternating Series

Generally, we prefer to describe fading in terms of time rather than in terms of probability, since the latter description can lead to inadvertent confusion because of the nonstationarity of the fading process. However, for the purposes of combinatorial manipulation, T_h can be converted to a fraction designating a probability

$$P_h = T_h/T_b, \tag{11}$$

where T_b is an observation period (time base) such as a year. From eqs. (3) and (6),

$$P_h = N^{-1} \sum_{i=1}^{N} iP'(u+i), \tag{12}$$

where

$$P'(u+i) = T'(u+i)/T_b. \tag{13}$$

To derive the alternating series from eq. (12), we apply a theorem from probability theory (page 77 in Ref. 14). According to it, the probability that exactly $u+i$ out of M channels fail simultaneously is

$$P'(u+i) = \sum_{r=u+i}^{M} (-1)^{r-u-i} C_{u+i}^{r} S(r), \tag{14}$$

where

$$S(r) = \sum_{k=1}^{J(r)} P_k(r) \tag{15}$$

in which $J(r)$ is the binomial coefficient C_r^M, and where, in the context of this work,

$$P_k(r) = T_k(r)/T_b. \tag{16}$$

After substitution into eq. (12), and collection of like terms,

$$P_h = N^{-1} \sum_{i=1}^{N} \sum_{p=1}^{i} (-1)^{i+p} p C_{u+p}^{u+i} S(u+i). \tag{17}$$

Application of the recursion relationship

$$C_n^m = C_{n-2}^{m-2} + 2C_{n-1}^{m-2} + C_n^{m-2} \tag{18}$$

reveals that, because of cancellation of terms,

$$\sum_{p=1}^{i} (-1)^{p+1} p C_{u+p}^{u+i} = C_{u-1}^{u+i-2}. \tag{19}$$

Therefore

$$P_h = N^{-1} \sum_{i=1}^{N} (-1)^{i-1} C_{u-1}^{u+i-2} S(u+i). \tag{20}$$

After multiplication by NT_b, this becomes the alternating series expression for Z_h in eq (7).

APPENDIX B

Simultaneous Failure of Radio Channels

In the case of a single radio channel, the annual amount of time during which the received signal is below a level, as a result of multipath fading, is[5,9]

$$T = rT_0L^2, \qquad L < 0.1, \tag{21}$$

where L describes a normalized voltage such that the level in decibels relative to a nonfaded received signal is 20 log L. For a fade margin of F dB, where F is a positive number, the corresponding voltage level is

$$L_0 = 10^{-(F/20)}. \tag{22}$$

When L_0 is used as value of L in eq. (21), T becomes the time during which the channel has failed, where failure is defined as noise in excess of 55 dBrnc0. The quantity T_0 is a time interval related to the length of the fading season [eq. (20) in Ref. 9]. The fade occurrence factor is[5,9]

$$r = c(f/4)D^3 10^{-5}, \tag{23}$$

where D is the path length in miles, f is the carrier frequency in gigahertz, and c describes the climate and terrain (eqs. (4) and (5) in Ref. 9). The value of c is unity when the climate and terrain are average.

Empirical expressions for simultaneous fading of radio channels have been obtained by W. T. Barnett from experimental data. From these, expressed in a form similar to that for a single channel, the time during which $u + i$ radio channels have failed simultaneously is

$$T_k(u+i) = r_k(u+i)T_0L_0^4, \tag{24}$$

where the subscript k is used to identify various sets of $u + i$ channels. This expression is valid when $T_k(u + i)$ is smaller than the values of T for the channels in question. The simultaneous failure time varies with fade margin more than the single channel failure time (L_0^4 versus L_0^2 variation). The quantity L_0 describes the actual fade margin when it is the same for all channels. In the case of channels with differing fade margins, L_0 describes a nominal fade margin, and the description of differences from it is contained in $r_k(u + i)$. The occurrence factor is

$$r_k(u+i) = (cD^4 10^{-5}/400) f_k(u+i), \tag{25}$$

where

$$f_k(u+i) = (u+i) \Big/ \sum_{p=1}^{I(u+i)} (L_0/L_{1p})^2 (L_0/L_{2p})^2 (\delta_p/f_p^2). \tag{26}$$

The quantities in this expression are associated with pairs of channels formed from the $u + i$ channels. The number of such pairs is

$$I(u+i) = C_2^{u+i}. \tag{27}$$

The subscript p identifies the pairs. The fade margins of the channels in a pair are described by L_{1p} and L_{2p}. The corresponding carrier frequencies f_{1p} and f_{2p} are expressed in gigahertz ($f_{1p} < f_{2p}$). The average frequency for a pair is

$$f_p = (f_{1p} + f_{2p})/2 \tag{28}$$

and the fractional frequency difference is

$$\delta_p = (f_{2p} - f_{1p})/f_p. \tag{29}$$

A value of 0.05 is used for δ_p when one of the channels is in the 4-GHz band and the other in the 6-GHz band.

APPENDIX C

Computation of Combinations of Channels

The evaluation of Z_h in eq. (7) requires identification of the combinations of r frequencies that can be formed from the M carrier frequencies of the radio channels. If the frequencies are tagged using the integers 1 through M, then the combinations required are subsets of the set $\{1, 2, \cdots, M\}$. The integers appearing in the subsets serve as pointers (used pairwise) to precalculated values of δ_p/f_p^2 for frequency pairs in a subset [eqs. (28) and (29)].

Given M and r, the computation is initialized by defining (for $i = 1, 2, \cdots, r$)

$$\alpha_i = i, \qquad i \neq r \tag{30}$$

$$\alpha_i = (r-1), \qquad i = r \tag{31}$$

$$\beta_i = M - r + i. \tag{32}$$

The subsets are then generated as follows:

(*i*) Starting with $j = r$, find the first j such that $\alpha_j < \beta_j$.

(*ii*) Replace α_j with $\alpha_j + 1$.

(*iii*) For $k = (j+1), (j+2), \cdots, r$ replace α_k with $\alpha_{k-1} + 1$.

In this procedure, elements of subsets are incremented to form new subsets, and the elements of each subset are ordered within the vector α such that $\alpha_j < \alpha_{j+1}$. Repeated generation of the same combination of

frequencies is thereby avoided. The first iteration after initialization produces the subset $\{1, 2, \cdots, r\}$. The iteration is continued until execution of step (i) fails, when all the required C_r^M combinations have been produced. The potentially large number of combinations necessitates double precision computation in summations over the subsets.

APPENDIX D

Frequency-Diversity Parameters

The service failure time of an average channel can be expressed as

$$T_h = T_{uh}/I_h, \tag{33}$$

where T_{uh} is the unprotected service failure time for the hop in question obtained from eq. (21) after substitution of L_0 from eq. (22). The improvement resulting from the use of frequency-diversity protection is

$$I_h = qL_0^{-2}, \tag{34}$$

where

$$q = 100\, f_0/DG, \tag{35}$$

in which D is the path length in miles and f_0 is the frequency in gigahertz at which T_{uh} is calculated. An average of the carrier frequencies of the radio channels is a suitable value for the reference frequency f_0. Alternatively, f_0 can be the center frequency of a band, which facilitates band identification when the calculations are performed for frequency plans formulated by the International Radio Consultative Committee (CCIR). The parameter G is determined by the carrier frequencies of the radio channels and by the channel-to-channel variations of fade margins

$$G = N^{-1} \sum_{i=1}^{N} \sum_{k=1}^{J(u+i)} (-1)^{i-1} C_{u-1}^{u+i-2} f_k(u+i), \tag{36}$$

where $f_k(u+i)$ and the summation are defined in Appendix B. In the simple case of 1×1 frequency diversity with the same fade margin for both channels,

$$G = 2f_p^3/\Delta f, \tag{37}$$

where f_p is the average and Δf is the difference of the two carrier frequencies, expressed in GHz. The corresponding value of q in this 1×1 case,

$$q = (f_0/f_p)(50/f_p D)(\Delta f/f_p) \tag{38}$$

has been used previously with the factor f_0/f_p approximated by unity.[9]

When the fade margins of all radio channels are identical, the

Table III—Values of G for fully developed routes. Fade margins are identical for all radio channels in a given protection scheme.

Frequency Band, GHz	Protection Scheme	Value of G
4	2 × 10	1597
4	1 × 11	4682
6	2 × 6	7380
6	1 × 7	17059

Frequencies in the 4-GHz band:
$3.670 + 0.040\ i$, $i = 1, 3, 5, \cdots 11$
$3.650 + 0.040\ i$, $i = 2, 4, 6, \cdots 12$
Frequencies in the 6-GHz band:
5.9452, 5.9748, 6.0045, 6.0342, 6.0638, 6.0935, 6.1231, 6.1528

parameter G depends only on the frequency arrangement of the channels. Tabulated values of G, such as shown in Table III for fully developed routes, can therefore be used in eq. (33) to calculate the service failure time for common frequency arrangements.

In the 2 × 18 case in Fig. 1, the choice of reference fade margin ($-20 \log L_0$) becomes arbitrary because there are two fade margins (37 and 40 dB, in the 4- and 6-GHz bands, respectively). The choice has no effect on T_h, but it does affect the various factors in T_h such as G. When T_{uh} and f_0 are the averages for the 20 radio channels, the reference fade margin is 38.27 dB [obtained from eq. (21)]. The value of G is 3129 for this choice of reference values.

APPENDIX E

Frequency Assignments in Figure 2

To simplify presentation, the radio channels in this work are numbered 1 to 20 in order of increasing frequency. The frequencies range from 3.71 to 6.1528 GHz as listed in Table III.

In the 4-GHz worst case, channels 12 and 11 are utilized in the 1 × 1 protection scheme, and the sequence in which additional working channels are assigned is 10, 9, 8, $\cdots$, 1. In the best case, channels 2 and 12 (same polarization) are used for the 1 × 1 scheme, and then channel 6 is added to form a 1 × 2 scheme. Channels 2, 4, 8, and 12 are utilized in the 1 × 3 scheme, and the sequence in which additional working channels are assigned is 6, 10, 1, 3, 5, 7, 9, and 11.

In the 6-GHz worst case, channels 20 and 19 are utilized in the 1 × 1 scheme, and the sequence in which additional working channels are assigned is 18, 17, $\cdots$, 13. In the best case, the channel utilization is

$1 \times 1 - 13, 20$
$1 \times 2 - 13, 16, 20$
$1 \times 3 - 13, 15, 17, 20$
$1 \times 4 - 13, 14, 16, 18, 20$
$1 \times 5 - 13, 14, 15, 17, 19, 20$
$1 \times 6 - 13, 14, 15, 16, 18, 19, 20$
$1 \times 7 - 13, 14, 15, 16, 17, 18, 19, 20$

In the combined protection system for the 4-GHz and 6-GHz bands, all 4-GHz channels and channels 20 and 19 are used in the worst-case 2×12 scheme. The sequence in which additional working channels are assigned is 18, 17, 16, $\cdots$, 13. In the best-case 2×12 scheme, all 4-GHz channels are also used, but the 6-GHz channels are 13 and 20. The pattern for the utilization of additional channels is the same as that in the 6-GHz best case.

REFERENCES

1. W. Y. S. Chen, "Estimated Outage in Long-Haul Radio Relay Systems with Protection Switching," B.S.T.J., *50*, No. 4 (April 1971), pp. 1455–1485.
2. A. B. Crawford and W. C. Jakes, Jr., "Selective Fading of Microwaves," B.S.T.J., *31*, No. 1 (January 1952), pp. 68–90.
3. R. L. Kaylor, "A Statistical Study of Selective Fading of Super-High Frequency Radio Signals," B.S.T.J., *32*, No. 5 (September 1953), pp. 1187–1202.
4. W. T. Barnett, "Microwave Line-of-Sight Propagation With and Without Frequency Diversity," B.S.T.J., *49*, No. 8 (October 1970), pp. 1827–1871.
5. W. T. Barnett, "Multipath Propagation at 4, 6, and 11 GHz," B.S.T.J., *51*, No. 2 (February 1972), pp. 321–361.
6. A. Vigants, "Space-Diversity Performance as a Function of Antenna Separation," IEEE Trans. Commun. Tech., *COM-16*, No. 6 (December 1968), pp. 831–836.
7. A. Vigants, "The Number of Fades in Space-Diversity Reception," B.S.T.J., *49*, No. 7 (September 1970), pp. 1513–1530.
8. A. Vigants, "Number and Duration of Fades at 6 and 4 GHz," B.S.T.J., *50*, No. 3 (March 1971), pp. 815–841.
9. A. Vigants, "Space-Diversity Engineering," B.S.T.J., 54, No. 1 (January 1975), pp. 103–142.
10. S. H. Lin, "Statistical Behavior of a Fading Signal," B.S.T.J., *50*, No. 10 (December 1971), pp. 3211–3270.
11. S. H. Lin, "Statistical Behavior of Deep Fades of Diversity Signals," IEEE Trans. Commun., *COM-20*, No. 6 (December 1972), pp. 1100–1107.
12. G. M. Babler, "A Study of Frequency Selective Fading for a Microwave Line-of-Sight Narrowband Radio Channel," B.S.T.J., *51*, No. 3 (March 1972), pp. 731–757.
13. G. M. Babler, "Selectively Faded Nondiversity and Space Diversity Narrowband Microwave Radio Channels," B.S.T.J., *52*, No. 2 (February 1973), pp. 239–261.
14. E. Parzen, *Modern Probability Theory and Its Applications*, New York: John Wiley and Sons, 1960, Chapter 2, Section 6.

THE BELL SYSTEM TECHNICAL JOURNAL
Vol. 58, No. 8, October 1979
Printed in U.S.A.

Automatic Recognition of Spoken Spelled Names for Obtaining Directory Listings

By A. E. ROSENBERG and C. E. SCHMIDT

(Manuscript received June 9, 1978)

An automatic speaker-dependent word recognizer is used to accept strings of spelled letters spoken in isolation. The output of the recognizer is a set of best-candidate letters for each letter spoken in the string. Candidate strings forming spelled last names and initials are compared to name strings obtained from a telephone directory stored in a disk file. A systematic search is carried out to find matching entries in the directory. An evaluation has been carried out with ten talkers spelling lists of names extracted from an 18,000-entry telephone directory. Although the median acoustic error rate per spelled letter is approximately 20 percent, the median error rate in furnishing the requested directory entry is approximately 4 percent.

I. INTRODUCTION

Since July 1976, an automatic directory assistance system has been available at Bell Laboratories via a dialed-up connection which provides Bell Laboratories telephone directory information in response to *TOUCH-TONE*® dial inquiries.[1,2] The system has been implemented on a Data General Nova 800 laboratory computer and makes use of an ADPCM (adaptive differential pulse-code modulation) voice-response system,[3] which is interfaced to the computer, to provide instructions and the desired directory information to the calling customer. To use the system, the caller dials the appropriate telephone number and then, following a voice-response prompt, spells out on the *TOUCH-TONE* dial the last name and initials of the individual for whom directory information is desired. A caller's spelled inquiry on the *TOUCH-TONE* dial can be compared directly with the names in a *TOUCH-TONE* version of the telephone directory and a list of possible matches compiled. In approximately 75 percent of all inquiries for which matches are obtained, matches are unique. For the remaining 25 percent, multiple matches are obtained due to individuals whose

names are spelled identically (at least with respect to those letters supplied in the inquiry) as well as spelling ambiguities arising from the fact that 3 or more letters are assigned to each dial button. Inquiries resulting in multiple matches are followed up by requests to the customer to supply additional information which can often resolve the ambiguity.

The *TOUCH-TONE* system has been demonstrated to have practical potential for automating customer inquiries to directory assistance. Nevertheless, mechanical intervention in the form of actuating the proper sequence of pushbuttons is required of the customer. Any such process mediating the customer's inquiry is likely to be accompanied by error. Moreover, spelling ambiguities arising from multiple letter assignments on the buttons result in a significant number of multiple matches. Although such matches are handled in a clever way, they require additional information to be extracted from the customer and prolong the inquiry.

Obviously the most direct and attractive mode for directory assistance inquiries is spoken utterances. It is also the most elusive for automation, since an automatic speech recognizer that could handle spoken inquiries in the most accommodating and efficient manner has yet to be devised. Moreover, any such device would have to be enormously complex compared with *TOUCH-TONE* inquiry systems. Nevertheless, practical systems for automatic speech recognition are currently available if enough restrictions are imposed. It is the purpose of this paper to demonstrate how such an existing speech recognizer might be incorporated into a system for voice-actuated directory assistance. The system does not represent the ultimate answer for voice-actuated inquiries; rather, it points towards a practical means given the current abilities of automatic speech recognizers.

Typically, the restrictions on contemporary automatic speech recognizers include utterances spoken in isolation by designated speakers from a limited vocabulary. Such a system has been implemented and evaluated at Bell Laboratories.[4,5] A block diagram of the system is shown in Fig. 1. The acoustic input signal is parameterized in terms of an eighth-order linear predictor coefficient (LPC) analysis. A description of the system operation is given in the next section.

Given the limited vocabulary restriction of contemporary word recognizers, it would not be possible to design a practical, automatic, directory assistance system in which spoken names are used to make requests for information. However, a vocabulary consisting of spelled letters has a manageable size, and spelling names to request directory information is a natural means of making such inquiries. In fact, requests to human directory-assistance operators often include spellings. One drawback, however, is that the spoken spelled alphabet is a

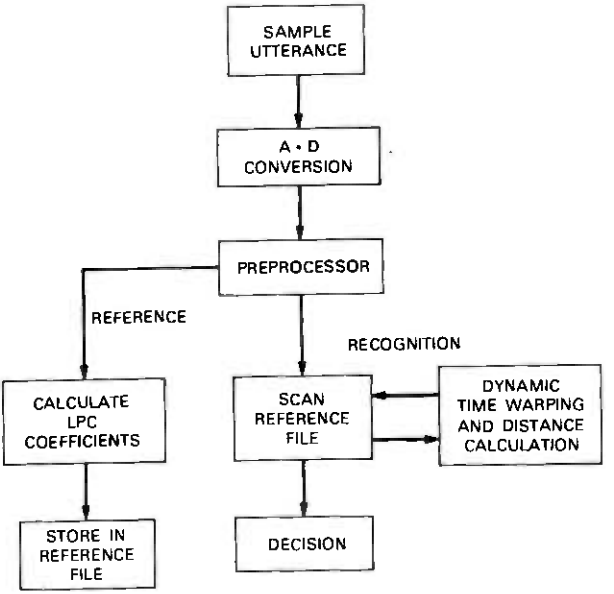

Fig. 1—Automatic word recognizer block diagram.

notoriously poor vocabulary for a word recognizer. This is because large groups of utterances within the vocabulary are easily confused because they have minimal acoustic distinctions. This difficulty can be alleviated by adopting modified recognition techniques. For example, the Itakura recognizer is essentially a template matcher and provides an overall distance or figure of merit for every template or reference pattern to which a sample pattern is compared. It is therefore possible to generalize the notion of recognition from a unique match to a set of possible matching candidates ordered by the overall distances provided by the recognizer. Even though there may be a significant probability that the correct word template is not the best matching candidate, the probability may be quite low that the correct word template is *not* found among, say, the five best matching candidates. Therefore, given a string of spoken letters as input to a recognizer, there is a high probability that the correct string of letters can be found among the candidates for recognition even though the recognizer is imperfect.

To find the correct matching string, the directory must be searched by systematically presenting to it candidate strings, starting with the most probable string as prescribed by the recognizer. In order for this kind of search to have a reasonable chance of obtaining the correct string, an additional condition must be satisfied—namely, the distribution of letter strings listed in the directory must be sparse compared

with all possible letter strings. For example, these are 26^8 or approximately 2×10^{11} possible strings of length 8, but only a small fraction of these will be found in a telephone directory. The evaluation described in Section III shows that the conditions are, in fact, satisfied by the kind of combination of recognizer and directory search to be described. The constraints imposed by the distribution of directory strings are such that it is possible to relax conditions even further by ignoring one or more positions in the string and still find the correct matching string in the directory. This situation arises when the acoustic recognizer fails to find any letter candidate in a given position in the string.

II. DETAILS OF OPERATION

The operation of the Itakura automatic speaker-dependent word recognizer is outlined in the block diagram of Fig. 1. The input acoustic signal is digitized at a 6.667-kHz rate and processed through an endpoint detector to locate the beginning and end of the utterance. The preprocessing consists of an eighth-order autocorrelation analysis over a 45-ms Hamming window every 15 ms through the utterance. For reference patterns, the autocorrelation coefficients are converted frame-by-frame to LPC coefficients. Recognition consists of a matching process in which a sample input pattern of autocorrelation coefficients is compared with an ensemble of stored reference patterns previously established by the designated speaker. The comparison consists of a frame-by-frame scan of the sample patterns against each reference pattern. A distance metric (or measure of dissimilarity) is calculated and accumulated by a dynamic programming technique as the scan proceeds. An accumulated distance rejection threshold function is imposed such that, if the accumulated distance exceeds the threshold at any point during the scan against a particular reference pattern, the scan is aborted and restarted against a new reference pattern. The vocabulary item corresponding to the reference pattern with the lowest accumulated distance is designated as the recognized item. If every reference pattern is rejected, the result is said to be a rejection. For the purposes of the present system, the output of the recognizer is considered to be a *set* of candidates for recognition ordered by their associated accumulated distances. Since the set does not include rejected items, the number of candidates for each trial may vary from zero to the size of the vocabulary.

The vocabulary for the present system is shown in Table I. It consists of the spoken representations for each letter in the alphabet, the set of digits zero through nine, and three commands. Spoken digits are needed when additional information must be solicited from the customer to resolve ambiguities resulting from similar entries in the

Table I—Vocabulary

1. A	14. N	27. Stop
2. B	15. O	28. Error
3. C	16. P	29. Repeat
4. D	17. Q	30. Zero
5. E	18. R	31. One
6. F	19. S	32. Two
7. G	20. T	33. Three
8. H	21. U	34. Four
9. I	22. V	35. Five
10. J	23. W	36. Six
11. K	24. X	37. Seven
12. L	25. Y	38. Eight
13. M	26. Z	39. Nine

directory. Such information may be in the form of numerical information such as organization numbers in the Bell Laboratories directory or street addresses in a public directory. The "stop" command, analogous to the "*" button in the *TOUCH-TONE* system, is used to terminate strings of utterances. The "error" and "repeat" commands are used to correct input errors.

In its present configuration, the data base for the system is the approximately 18000-entry Bell Laboratories directory. Many of the directory access routines for this system have been modified from the *TOUCH-TONE* directory assistance system.[1,2]

The system is accessed using an ordinary telephone handset via a dialed-up connection through the PBX at Bell Laboratories in Murray Hill, N.J. Upon receipt of an audible cue, the customer spells out the name of the individual for whom directory information is required. The letters must be spoken distinctly, separated by intervals of at least 100 ms. As in the *TOUCH-TONE* system, the letters of the last name are spelled first, followed by a "stop" command, followed by the initials and a final "stop" command. The requirements for the number of last-name letters and initials are also the same as in the *TOUCH-TONE* system. The entire string of spelled letters is uttered at once with the frame-by-frame calculation and storage of autocorrelation coefficients accomplished in real time. Off-line, the utterances are segmented using the end-point detector. The comparison and matching process, which in the present configuration takes approximately six seconds per utterance, provides a maximum of five candidate letters for each spoken letter.*

The overall operation of the system is shown in a simplified flow chart in Fig. 2. The directory search starts with the construction of an

* The maximum figure of five candidates is chosen somewhat arbitrarily. If the maximum is set low, the likelihood of excluding the correct letter increases. If it is set high, the number of candidate strings and, hence, the search time increases. In an informal evaluation, five seemed to represent a reasonable compromise.

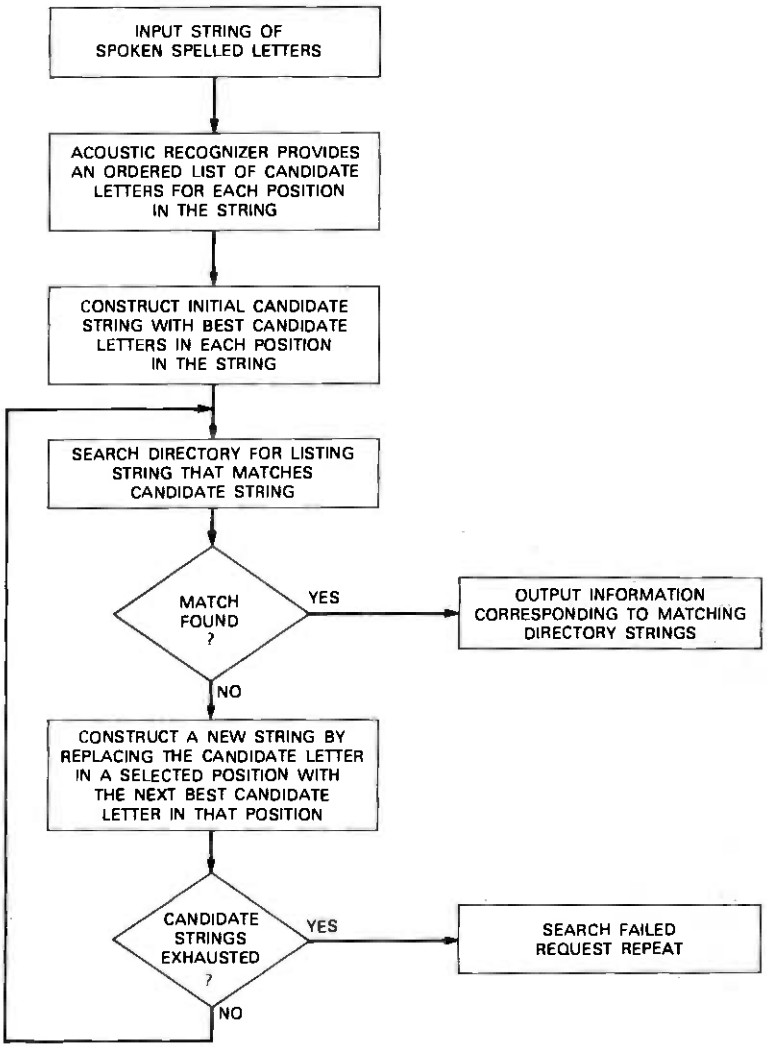

Fig. 2—Simplified flow chart of the overall system.

initial candidate string. The string is composed of the best candidate letters supplied by the acoustic recognizer for each letter position in the string of last-name letters and initials.* If one or more matching directory listing strings are found, the directory information for these

* In order to simplify the system description, it is assumed that there is no distinction between last-name letters and initials for candidate and listing strings. In actual practice, initials are handled somewhat differently than last-name letters. It is also assumed that the "stop" command is recognized without error, which is very nearly true in practice.

listings are output to the customer. If no match is found, a new candidate string is constructed by replacing the candidate letter in a selected position by the next best candidate letter in that position. The directory search is then restarted. If all candidate strings are exhausted, the search has failed and the request must be repeated.

The process of searching for a directory entry which matches an input string using the array of candidate letters provided by the recognizer can be separated into two operations. First, a suitable sequence of candidate strings must be constructed. Second, the directory must be probed for the existence of a match to each such candidate string. The first operation is more interesting and critical in the context of this investigation than the second. An efficient search technique serves to speed up the process and assumes greater importance as the size of the directory increases. But the technique used to construct sequences of candidate strings significantly affects both the accuracy and the efficiency of the overall process.

The search technique can be described very simply. Advantage is taken of the linear, alphabetical arrangement of the directory, grouping the listings into "buckets"[6] containing 128 consecutive listings each. A table stored in memory indexes each 128th listing in the directory by its first three letters. To probe a given candidate string, a search range consisting of one or more "buckets" is selected keyed to the string in the index table closest to the candidate string. The range is chosen to ensure that a matching directory string, if it exists, is included within the range. The candidate string is compared with each directory string within the selected range.

The more critical operation, as indicated above, is the technique used to construct a sequence of candidate strings. It is useful to introduce the technique which is actually used in this study with a discussion of a general approach. As shown in Fig. 3, we can model the entire process as follows. The directory can be represented as a finite-state Markov process generating strings of letters forming names which are spelled by the speaker and processed by the recognizer. The speaker and recognizer together are considered a discrete memoryless channel. A directory entry is a sequence of characters $\cdots *, *, u_1, u_2, \cdots, u_N, *, *, \cdots$, where * represents a blank or space and u_k represents a character $A, B, C, \cdots, Z$ or *. The output of the directory model at position k in the string is taken to be

$$x_k = (u_k, u_{k-1}, \cdots u_{k-\nu}), \tag{1}$$

where it is supposed that the present state of the directory x_k is a function of the present and ν preceding characters. The observed output of the recognizer is a series of measurements $z_1, z_2, \cdots z_k, \cdots z_N$. We suppose that the directory is represented by state transition

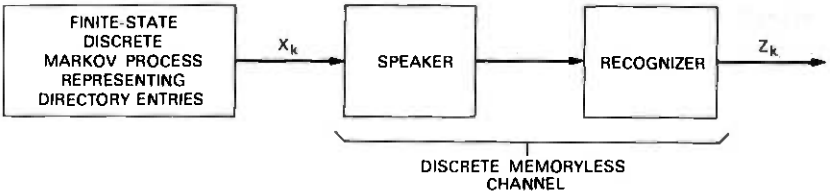

Fig. 3—Overall system model as a Markov process—memoryless channel.

probabilities $P(x_k/x_{k-1})$ and the speaker-recognizer combination by conditional probabilities $P(z_k/x_k)$. Since the speaker-recognizer combination is considered memoryless, we have

$$P(z_k/x_k) = P(z_k/u_k). \tag{2}$$

Given an observed sequence $\{z\}$, the problem is to reconstruct the input sequence $\{u\}$. This problem has been considered in many different forms, especially in coding theory studies.[7-9] A solution can be obtained by a maximum *a posteriori* probability estimation of $\{x\}$ or, equivalently, $\{u\}$, given $\{z\}$. It can be shown that solving the problem is equivalent to finding the shortest path through a graph which can be obtained by a dynamic programming technique.[7,9] The solution is provided by the Viterbi algorithm[3,10] stated as follows. Let

$$\lambda(x_k, x_{k-1}) = -\ln P(x_k/x_{k-1}) - \ln P(z_k/u_k). \tag{3}$$

For each k, compute

$$\Gamma(x_k, x_{k-1}) = \Gamma(x_{k-1}) + \lambda(x_k, x_{k-1}), \tag{4}$$

where

$$\Gamma(x_k) = \min_{x_{k-1}} \Gamma(x_k, x_{k-1}) \tag{5}$$

and

$$\Gamma(x_0) = 0. \tag{6}$$

Each time $\Gamma(x_k)$ is obtained, the value of x_{k-1} associated with the minimization is stored, so that upon reaching the final state x_{N+1}, where $u_{N+1} = *$, it is possible to trace a complete path back from $k = N$ to $k = 1$. Under reasonable assumptions, it is possible to substitute for $-\ln P(z_k/u_k)$ the set of recognizer distances $d(u_k/z_k)$. The choice of ν determines the degree of letter-by-letter statistical dependence by which the directory is characterized. For example, for $\nu = 0$, $P(x_k/x_{k-1}) = P(u_k/u_{k-1})$ and, in effect, the directory is characterized by position-dependent diagrams. Note that for small values of ν it is possible to find as a solution a sequence which is not actually found in the directory. However, if ν is specified to be longer than the longest string

in the directory, this outcome is excluded. In this case,

$$P(x_k/x_{k-1}) = P(x_k, x_{k-1})/P(x_{k-1}) = P(x_k)/P(x_{k-1}), \tag{7}$$

since, for ν large enough, x_k completely specifies x_{k-1}. $P(x_k)/P(x_{k-1})$ can be estimated by $N(x_k)/N(x_{k-1})$, where $N(x_k)$ is the number of occurrences of the sequence x_k in the directory. Substituting into eq. (4), we obtain

$$\Gamma(x_k, x_{k-1}) = \Gamma(x_{k-1}) + d(u_k/z_k) - \ln N(x_k)/N(x_{k-1}). \tag{8}$$

Note the important result that

$$\Gamma(x_k) = \Gamma(x_k, x_{k-1}) \tag{9}$$

since under the assumption for ν there is only one possible antecedent x_{k-1} to x_k.

A further modification which leads to an intuitively appealing result is obtained by replacing $-\ln N(x_k)/N(x_{k-1})$ by $\delta(x_k)$, where

$$\delta(x_k) = \begin{cases} 0 & \text{for } N(x_k) > 0 \\ \infty & \text{for } N(x_k) = 0. \end{cases} \tag{10}$$

The result of the iteration expressed by eq. (8) is then

$$x_N = \sum_{k=1}^{N} d(u_k/z_k) \tag{11}$$

for each x_N found in the directory. The solution then becomes that x_N for which $\Gamma(x_N)$, the accumulated sum of recognizer distances, is minimum.

This simplified procedure is illustrated by an example. A speaker has spelled the string "BERKLED", seeking a directory listing for D. Berkley. The last name has been truncated to six characters, and there is no separation between the letters of the last name and the initial. The recognizer distances $d(u_k/z_k)$ are shown in Table II. Figure 4 is a trellis diagram showing the search procedure for this string. Only those states are shown for which the transition distances $\lambda(x_k, x_{k-1})$ are finite. Over each transition arrow is the accumulated recognizer dis-

Table II—Example of letter candidates and corresponding recognizer distances for spelled input string "BERKLED"

Position	1	2	3	4	5	6	7
Spelled	B	E	R	K	L	E	D
	Candidate Letters and Distances						
	B 0.064	E 0.0183	I 0.160	K 0.101	L 0.114	E 0.059	P 0.089
	P 0.081	P 0.107	R 0.176	J 0.215		P 0.089	T 0.101
	E 0.091	B 0.112	O 0.189			B 0.090	D 0.111
	D 0.148					D 0.139	B 0.150
	G 0.154					G 0.144	Z 0.161

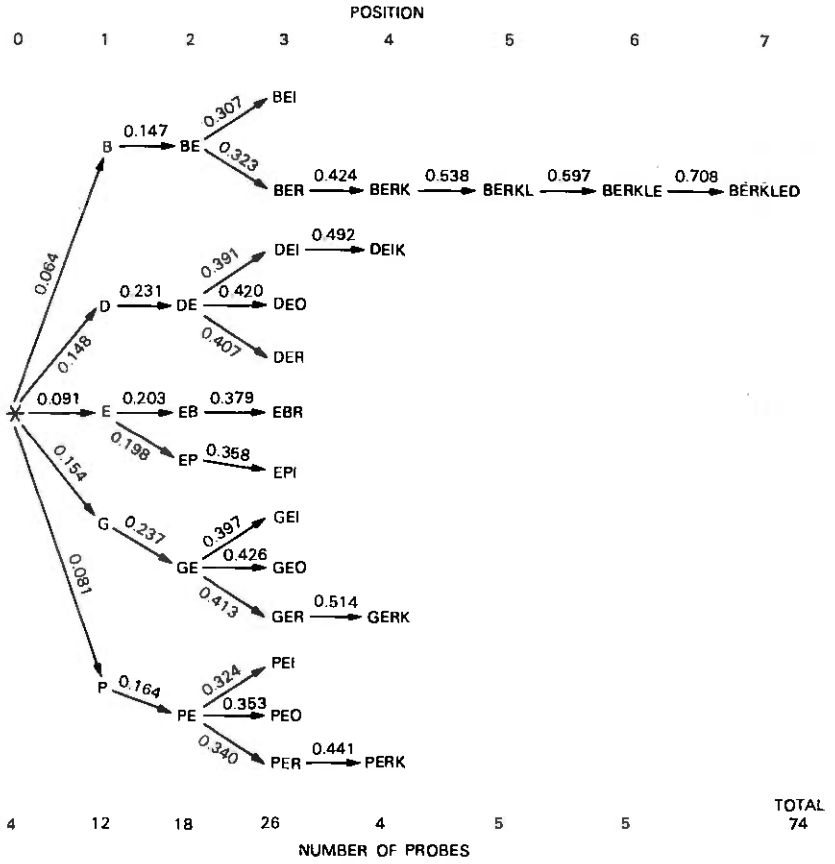

Fig. 4—Trellis diagram for the Viterbi search procedure corresponding to the example specified in Table II.

tance leading to the state on the right. In contrast to a trellis diagram for a general Viterbi algorithm procedure, there is just one incoming branch for each node. The only possible exception is the final accepting state, in which case, as already mentioned, the string with the least accumulated distance is taken as the solution.

For each u_k, there is a probe of the directory for every possible string prefix x_k to determine whether $N(x_k) > 0$, that is, whether one or more strings are listed in the directory with the prefix x_k. The number of probes for each k and the total is shown along the base of the figure for the example.

This procedure is exhaustive and has the optimum properties associated with Viterbi algorithm procedures. Nevertheless, it lacks some efficiencies. For example, suppose the best candidate letters provided by the recognizer form the actual intended string. With the Viterbi

algorithm approach, it is necessary to probe the directory for each string prefix prescribed by the candidate letters before a decision can be made. Since the candidate string formed from the best candidate letters is the most likely match according to the recognizer, it seems natural to probe the directory directly and immediately for this string.

Potentially more efficient strategies than the Viterbi algorithm do exist for determining best paths through trellis-type structures. Two such procedures, which were first investigated in the problem area of decoding convolutional codes, are the Fano algorithm[10] and the Zigangirov-Jelinek stack algorithm.[11,12] These procedures are included in the general class of procedures known as "backtrack" techniques.[13–15] They have the common property that the better, more probable branches in the trellis are probed first in the search for the best complete path.

An empirical backtrack technique is the actual procedure used in this study for finding matching directory strings. Outlined in the flow chart in Fig. 5, it is an iterative procedure in which each trial is an attempt to match a complete candidate string to a directory string. If no match is obtained, a new candidate string is constructed by replacing the candidate letter in the first position of mismatch. The first position of mismatch is the leftmost mismatch position of the best matching directory string scanning from left to right. The substitution replaces the existing candidate letter with the next best candidate letter provided by the recognizer in that position. If there are no more candidate letters available in the mismatch position, the selected position is "backtracked" to the preceding position.

Thus two salient points are associated with this procedure. First, candidate letters are replaced in the order of merit provided by the recognizer under the assumption that the most likely string matches are to be affected by the better candidate letters. Second, the backtrack procedure provides a systematic and efficient strategy for constructing candidate strings and probing the directory. It has a property, common also to the Viterbi procedure, in that, once a string prefix is found to result in a mismatch, it never appears again as the prefix of subsequent candidate strings. The backtrack procedure is also potentially exhaustive. However, we choose to terminate the procedure prior to exhaustion once one or more matching directory strings have been found. The assumption here is that the first match is likely to be the correct match so that there is little justification to driving the procedure to exhaustion. An example illustrating the backtrack procedure is shown in Fig. 6 with the same recognizer candidates used in the previous example. What is shown is the sequence of candidate and corresponding best matching directory strings which occurs until a complete match is found. The mismatch position is indicated by a square drawn around the corresponding letter in the candidate string. Note that the

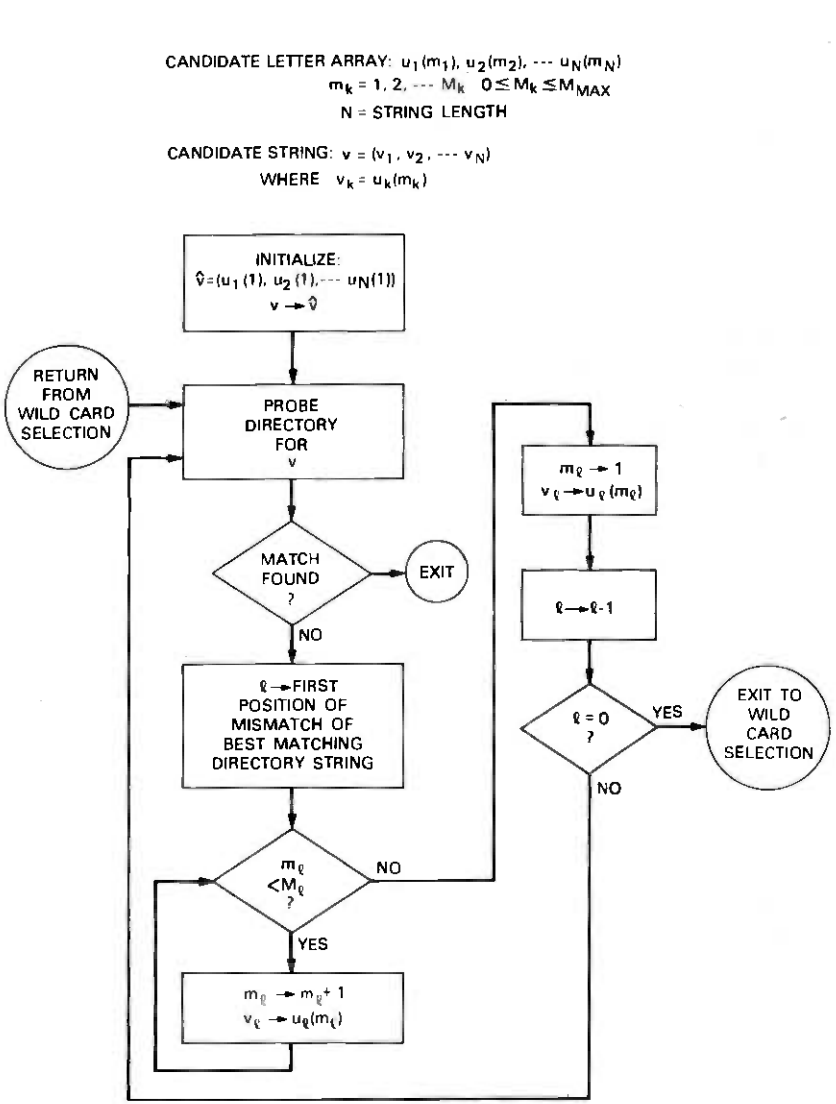

Fig. 5—Flow chart showing backtrack procedure for constructing candidate strings.

correct match is found after five probes of the directory compared with 74 probes required for the Viterbi procedure.

The efficiency and accuracy of this type of search is related to the ordering of the candidate letters in each position. The greater the number of correct letters found among the top candidates, the faster the search converges. In addition, since the search proceeds from left to right in the string, it proceeds faster if the correct letters are distributed among the high ranking candidates in the earlier positions rather than the later positions. In the example, if *B* were not the best

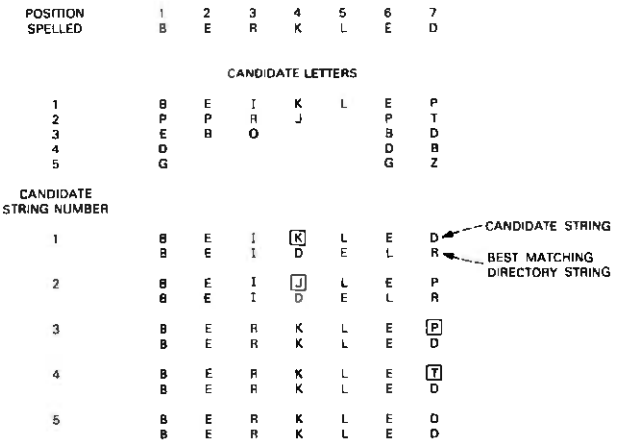

Fig. 6—Backtrack search corresponding to the example specified in Table II.

candidate letter in position 1, many more probes might be required before a match is found.

On the average, 160 directory strings are accessed and compared for each candidate string. In the present implementation, this consumes approximately 1 s, or approximately 6.25 ms per comparison. In the evaluation to be described later, it has been found that the median number of candidate strings searched per trial is 3.5, corresponding to a total search time of 3.5 s.

As previously mentioned, it is possible for no candidate letters to be available in one or more positions in the string. In this instance, these positions are simply ignored, and a match is possible with any letter in these positions. Of course, the greater the number of letter positions which are ignored in a search, the greater the likelihood of an error. Somewhat arbitrarily, no more than three no-candidate positions are allowed in the present implementation. The directory range must include every listing which includes the letters A to Z in the no-candidate positions. Hence, no-candidate positions also cause an increase in the directory search range and consequently the search time. Since the directory is ordered alphabetically by string position from left to right, this effect is greater for no-candidate positions in the initial part of the string and critical when there are no candidates in the first position. Since the absence of a candidate in the first position would require searching the directory from beginning to end, which would not be practical, an alternate scheme has been devised. A secondary directory table is available which contains an alphabetically ordered list of listing fragments comprising positions 2, 3, and 4. For each entry in this table, a set of addresses locates listings in the main directory containing the specified listing fragment. Thus, whenever a

candidate string with no candidate letters in the first position is presented, the secondary table is searched first for matching fragments which point to complete listings in the main directory. The resulting search time is negligibly greater than a search involving only the main directory.

The flow chart in Fig. 2 indicates that the search fails with no matching directory listings found after all candidate strings have been exhausted. However, the "search fails" result does not occur after all candidate strings composed of candidate letters supplied by the acoustic recognizer have been exhausted. At this point, the composition of candidate strings is relaxed by *imposing* a "no candidate" or "ignore" condition on a selected position and the search is restarted. The reasoning behind this "wild card" procedure is as follows. Assuming that a directory listing actually exists corresponding to the customer's request, the exhaustion of candidate strings constructed from the array of candidate letters indicates that the candidates supplied by the recognizer in one or more positions are all incorrect. Suppose that the probability of the correct letter not appearing as a candidate in a given position is approximately 0.05.* A simple calculation shows that, given this probability, the probability of only incorrect candidates being found in more than one position of a string of length 8 is approximately 0.06.† Thus, for the most part, when a search fails to find a matching listing with candidate letters supplied by the recognizer, it would suffice to impose an "ignore" or "wild card" condition at just one position. The position in which the "wild card" is most likely to effect a match is the maximum (rightmost) mismatch position over all previous searches. The most likely candidate string is the one containing the prefix which generated this mismatch position.

The "wild card" procedure is illustrated by another example shown in Fig. 7. This example is a modification of Example 1 in which the correct candidate letter "R" is not present among the candidates in position 3. In addition, the number of candidate letters in positions 1, 6, and 7 has been reduced to simplify the example. At candidate string number 11 "PBIKLEP", all candidate strings comprising supplied candidate letters have been exhausted. The best mismatching strings among all the candidate strings are strings numbers 1, 2, 6, 7, 8, and 9, in all of which the mismatch position is 4. The "wild card" flow chart shown in Fig. 8 indicates that the initial "wild card" candidate string is constructed by imposing a "wild card" on the first best mismatching candidate string, which is string number 1 in the example. The resulting

---

* This value conforms with the results of the evaluation to be described.

† This figure results from evaluating:

$$P = 1 - [p^n + np^{n-1}(1-p)], \text{ where } 1 - p = 0.05 \text{ and } n = 8.$$

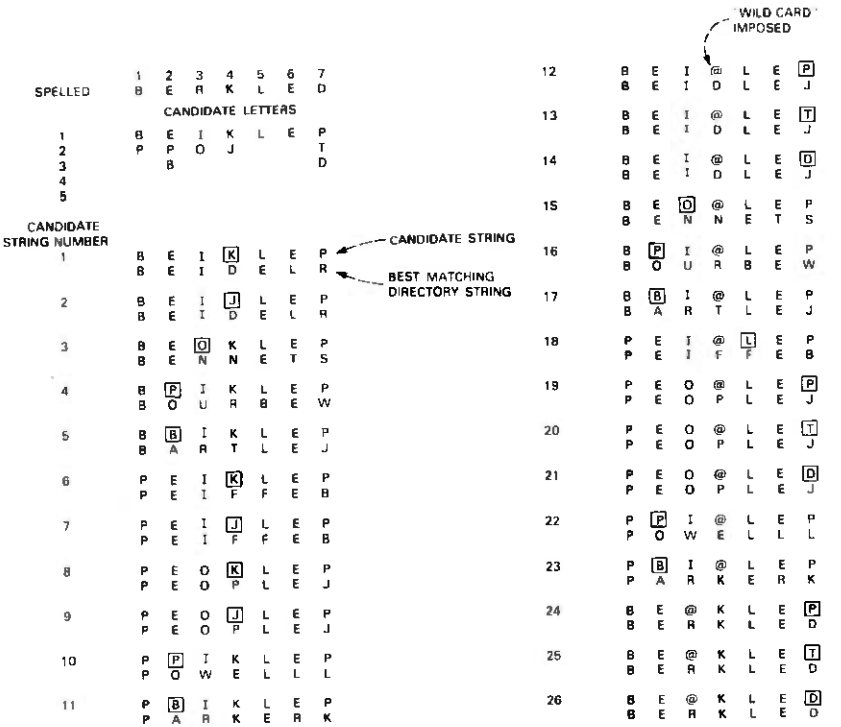

Fig. 7—Backtrack search example with imposed "wild card."

candidate string yields a mismatch in position 7 which is not resolved by the remaining candidate letters in that position (strings 13 and 14). The generation of candidate strings proceeds until all candidate strings are exhausted once more at candidate string number 23. The wild card is then backtracked to position 3, resulting in a match with candidate string number 26. A search results in a complete failure only when all candidate strings have been exhausted with the wild card backtracked to position 1.

III. EVALUATION

An evaluation was carried out to assess the performance of the system for a small sample of talkers. Ten adult talkers, six male and four female, participated in the experiment. Access to system was via an ordinary telephone handset over dialed-up lines through the local PBX. The system resides in a Data General Nova 840 laboratory computer interfaced to the telephone network through a Western Electric 407A data set. For each talker, two reference patterns were obtained for each of the 39 vocabulary items shown in Table I. These were obtained in two sessions of approximately 10 minutes each,

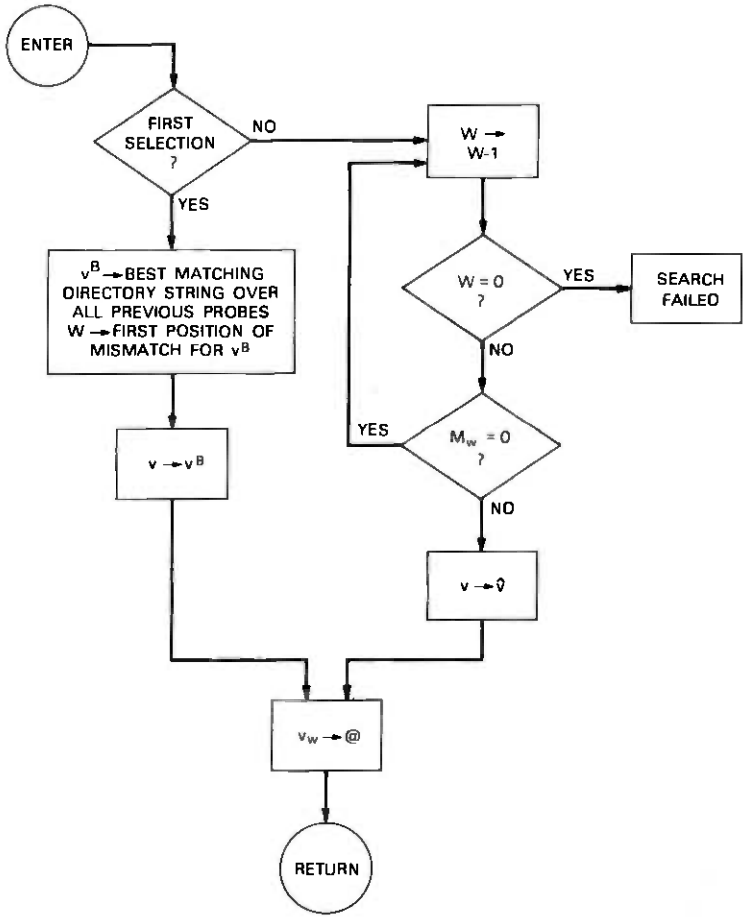

Fig. 8—Flow chart showing "wild card" position selection procedure.

separated by at least one day. The talkers were seated at the computer display terminal and received visual and audible cues for recording utterances. Following the reference sessions, one or more test sessions took place for each talker in which the list of 50 names shown in Table III were spelled out. These names were randomly selected from the Bell Laboratories telephone directory. For spelled input, the last names are truncated to six letters. The remaining letters are enclosed in parentheses. There is a grand total of 364 spelled letters in the list, the distribution of which is shown in Fig. 9. Upon receipt of a cue, with the truncated spelling of the name displayed, a spelled name was recorded in the manner described in Section II. The acoustic analysis data for each spelled name were recorded on digital tape for subsequent off-line recognition and directory search. Two rejection threshold condi-

Table III—Test list of 50 names. For input, last names are truncated to 6 letters

1. ZBOYAN A M	26. TINLEY M A
2. KRIEGE(R) G E	27. SHAEFF(ER) P A
3. ROHM B J	28. LIND G R
4. EPWORTH(H) R	29. SHIPLE(Y) J W
5. LINDHA(RD) E A	30. CUCCO J A
6. BURNS J F	31. HOFER F R
7. RUDDOC(K) B	32. DUNBAR J J
8. SCHILL(O) R F	33. DUKE S D
9. GOOZH J L	34. WASSON R D
10. VIROST(EK) A M	35. HOOD A A
11. LENNON F W	36. MENGEL M R
12. VASHIS(HTA) P	37. RAVER D F
13. DUFFY G L	38. FULTZ K E
14. YAEGER J C	39. CADWEL(L) K
15. CRAWFO(RD) C D	40. YOUHAS J M
16. WEEKS C G	41. VANBEN(THEM) J
17. AVEYAR(D) R L	42. DUNCAN(SON) J P
18. GRECO T J	43. SUMNER EE
19. MODARR(ESSI) A R	44. LAWREN(Z) D A
20. ERWIN W J	45. BLY J
21. LUM P S	46. NEWELL J A
22. SOOS N A	47. STAUBA(CH) W E
23. SKARIN R H	48. TATE B A
24. TENEYC(K) J H	49. ONDER J J
25. SACCO G A	50. SOLOMI(TA) K S

tions were observed for the recognition phase. The effect of relaxing the rejection threshold is to admit more candidates, which in turn increases the number of candidate strings and the time required for the directory search. For three of the 10 talkers, performance improved under a more relaxed threshold condition. For simplicity, the results are presented combining the two threshold conditions by including the results from the threshold condition that was best for each talker.

Word error rate, that is, acoustic error rate per spoken letter, is shown plotted as a function of number of best candidates in Fig. 10. The median across the 10 talkers is shown bracketed by the greatest and smallest individual error rates. This figure shows the rates for which the correct letter is not the best candidate, the best two candidates, etc. Thus the median rate at which the correct letter is not the best candidate is 20.5 percent, while the median rate at which the correct letter is not among the best five candidates is 4 percent. Improvement in performance diminishes rapidly as a function of the number of best candidates. Thus, there is likely to be only a negligible gain in performance if more than five best candidates are admitted.

Individual string error rates are shown as a function of individual word error rates—five best candidates in Fig. 11. String error rate is defined as the sum of string mismatch and no match rates. A mismatch is defined as obtaining an incorrect entry from the directory while no match is defined as finding no entry at all, a search failure. The median string error rate over all talkers, indicated by the arrow in the figure,

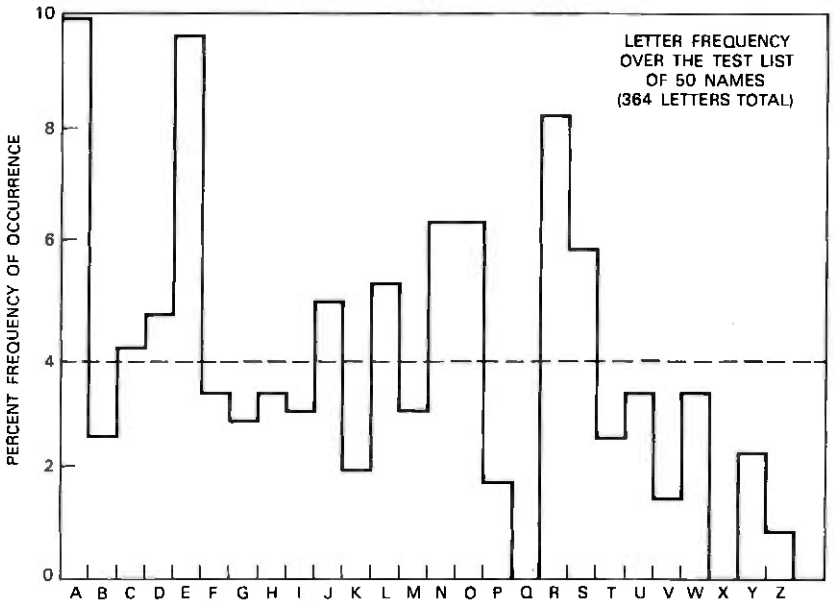

Fig. 9—Distribution of letters over the test list of 50 names.

is 4 percent, representing two errors over the 50-name list. The average mismatch rate is approximately four times greater than the average no-match rate.

A regression line has been fit among the individual points for string error rate plotted against word error rate (five best candidates). The coefficient of fit* is 0.78 indicating that word error rate (five best candidates) is a good predictor for string error rate. (This result is similar to the one obtained in Levinson et al.[16]) Attempts to fit a regression line among individual points of string error rate versus word error rate (less than five candidates) were not successful. This result is natural, since a correct directory match is highly dependent on the presence of the correct letter for each position among all the candidates presented for the search.

An important attendant result of this experiment is a tabulation of confusions made by the recognizer among the spoken letters. A confusion matrix is shown in Table IV. It provides the frequency of recognition for a given specified letter over all the trials of all the talkers. For the purpose of this tabulation, a letter is said to be recognized if it is ranked equal to or higher than the specified letter. In other words, an incorrect letter is counted each time it is a better candidate than the specified letter, while the specified letter is counted

* Estimate of the square of the correlation coefficient.

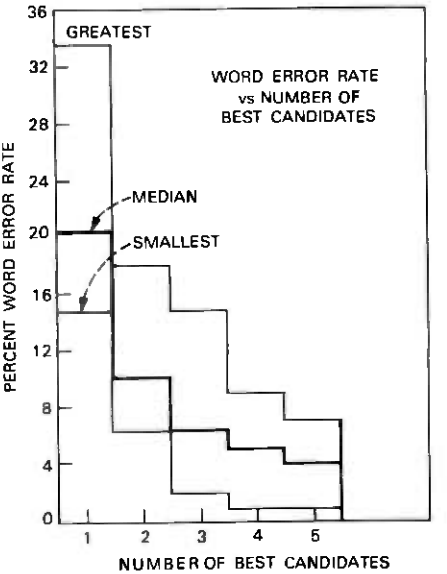

Fig. 10—Word error rate as a function of number of best candidates showing the median over the talker set as well as the greatest and smallest individual talker rates.

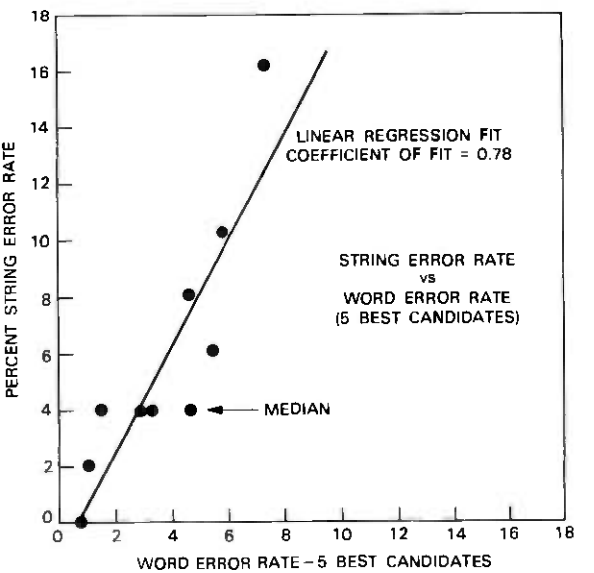

Fig. 11—Individual string error rates as a function of word error rate—5 best candidates.

Table IV—Confusion matrix showing frequency of recognition as a function of specified letter

Specified as	Percent Recognized as																	
	B	D	E	G	P	T	V	Z	C	A	J	K	I	Y	F	S	M	N
B (2.47)	36	21	9	0	9	5	11	0	0									
D (4.67)	9	42	7	7	12	8	10	0	0									
E (9.62)	9	7	44	0	16	11	7	0	0									
G (2.75)	0	5	0	65	0	8	0	5	0									
P (1.65)	6	6	0	0	56	14	9	5	0									
T (2.47)	0	9	0	5	16	55	6	0	5									
V (1.37)	7	10	0	8	9	6	49	0	5									
Z (0.82)	0	5	0	0	7	5	23	45	10									
C (4.12)	0	0	0	5	5	7	11	16	52									
A (9.89)									0	74	7	7						
J (4.94)									0	0	85	13						
K (1.92)									7	0	9	73						
I (3.02)													80	12				
Y (2.20)													0	96				
F (3.30)															90	10		
S (5.77)															8	89		
M (3.02)																	80	13
N (6.32)																	6	89

each time it appears in the list of candidates. Confusions less than 5 percent are ignored to simplify the matrix. The frequency of specification, from Fig. 9, is given in parentheses with each specified letter. There are 18 letters for which significant confusions are found. These letters are arranged into five groups with almost no interaction between the groups. The largest group, as expected, is the "BDE ..." family. Note that the confusions are rarely symmetric. For example, "B" is recognized as "D" 21 percent of the time, but "D" is recognized as "B" only 9 percent; "Z" is recognized as "V" 23 percent, but there is no significant confusion vice versa.

A different viewpoint is obtained by tabulating frequency of specification as a function of recognized letter. This tabulation, shown in Table V, specifically includes the *a priori* distribution of letters among the spelled names in the list. The relation between this frequency and the frequency of recognition as a function of specification is entirely analogous to the relation between *a posteriori* probability and channel probability in the specification of an information channel in information theory. Let $f(j_r/i_s)$ be the frequency of recognition of letter j_r given the specification of letter i_s. This frequency is analogous to channel probability and is an intrinsic property of the recognizer. According to Bayes' Law, $f(i_s/j_r)$, the frequency of specification of letter i_s given recognition of letter j_r (analogous to *a posteriori* probability), is given by

$$f(i_s/j_r) = \frac{f(j_r/i_s)f(i_s)}{\sum_{i_s} f(j_r/i_s)f(i_s)},$$

where $f(i_s)$ is the *a priori* frequency of letter i_s, and the summation in the denominator is carried out over all specified letters. Only for the special case when $f(i_s)$ is uniformly distributed, that, is equal to a constant, is $f(i_s/j_r)$ a function only of recognizer probabilities. It can then be appreciated that, since in the present situation the *a priori* distribution of letters is quite nonuniform, the effect on the *a posteriori* frequency of specification is highly significant. For example, when "P" is recognized, the specified letter is twice as likely to be an "E" than a "P." This makes some sense when it is realized that there are approximately six times as many E's in the list as P's.

The efficiency of the system is a function of the number of candidate strings searched until a match is obtained. The median number of candidate strings searched per spelled name for each individual talker is shown plotted as a function of string error rate. The median over the individual medians is 3.5. There is a fair correlation between number of strings searched and string error rate.

The percentage of trials for each talker which ended up as "wild card" searches is also shown plotted as a function of string-error rate

Table V—Confusion matrix showing frequency of specification as a function of recognized letter

	Percent Specified as																	
Recognized as	(2.47) B	(4.67) D	(9.66) E	(2.75) G	(1.65) P	(2.47) T	(1.37) V	(0.82) Z	(4.12) C	(9.89) A	(4.94) J	(1.92) K	(3.02) I	(2.20) Y	(3.30) F	(5.77) S	(3.02) M	(6.32) N
B	39	17	32	0	0	0	0	0	0									
D	15	50	16	0	0	5	0	0	0									
E	5	7	83	0	0	0	0	0	0									
G	5	14	10	49	0	0	0	0	8									
P	5	14	38	0	19	0	0	0	0									
T	0	11	29	0	5	33	0	0	7									
V	11	16	22	0	0	0	18	6	13									
Z	0	10	10	7	0	0	0	22	35									
C	0	0	0	0	0	0	0	0	75									
A										98	0	0						
J										15	81	0						
K										26	19	50						
I													96	0				
Y													17	82				
F															85	13		
S															6	93		
M																	86	12
N																	7	92

for individual talkers in Fig. 12. The rate of "wild card" searches also seems to correlate fairly well with string error rate. The median number of probes for a "wild card" search is approximately 50, more than 10 times the median for all searches. The string error rate for "wild card" searches is also very much higher than the overall string error rate, the median being approximately 19 percent.

An important fact which bears on the number of "wild card" searches and the "wild card" error rate is that a search cannot succeed if more than one position in the string has only incorrect candidates. There were nine such trials in the evaluation, contributing to nearly 50 percent of the "wild card" error rate.

IV. DISCUSSION

The most important feature of this system, borne out by the evaluation, is the powerful correcting influence of the context of spelled names as listed in a telephone directory on the recognition of spoken spelled letters. Given a median word error rate of approximately 20 percent on spoken spelled letters, the median string error rate is 4 percent. This result is entirely similar to the result observed by Levinson et al.[16] in which syntax constraints were seen to have a powerful correcting influence on the same automatic word recognizer

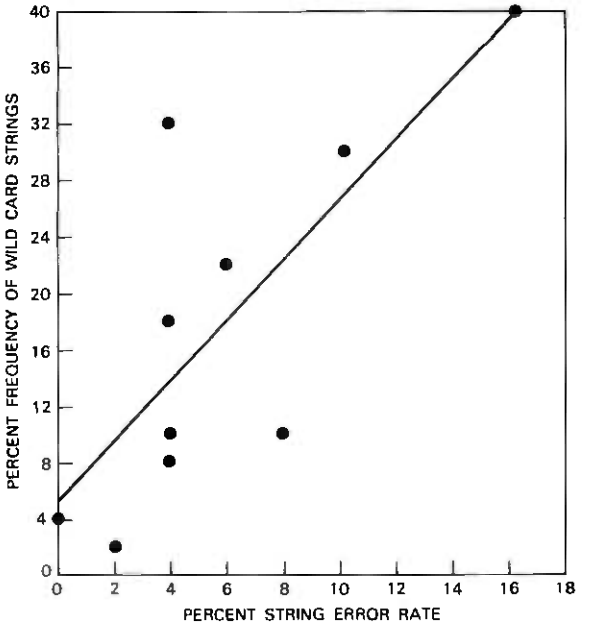

Fig. 12—Individual frequencies of "wild card" string searches as a function of string error rate.

for a 127-word flight information vocabulary. The error rate for parsed sentences was approximately 4 percent, while the acoustic word error was approximately 11 percent.

It has been noted previously that the vocabulary of spelled letters is a particularly difficult vocabulary for an automatic word recognizer due to the large number of minimal distinctions between words. This may account for the large difference in word error rates between the airline and spelled letter vocabularies. It should be noted that Itakura[1] obtained an 11.4 percent word error rate for the vocabulary of spelled letters plus digits. This is lower than the lowest individual error rate obtained in the present experiment (Fig. 10). However, the results are not directly comparable, since digits are much easier to recognize than spelled letters.

It is of interest to examine in some detail the kinds of errors obtained in the evaluation. First of all, recall from the discussion in Section II that if only incorrect candidate letters are found in more than one position the search is guaranteed to fail. This is because the "wild card" procedure imposes an "ignore" condition on just one letter position at a time. It was noted that for strings of length 8 and a word error rate (five best candidates) of 5 percent, the estimated rate at which only incorrect letters are found in more than one position is 6 percent. This, then, is the estimated rate of guaranteed failures. The situation deteriorates rapidly with increasing word error rate. If word error rate (five best candidates) increases to 8 percent, the rate of guaranteed failures can be expected to increase to 13 percent. The two talkers with the worst word error rate (five best candidates) performances of 7.4 and 5.9 percent generate guaranteed failures at rates of 6 and 8 percent, respectively. These figures, while not as bad as the predicted 13 percent for an 8-percent word error rate, represent a serious weakness in the system. There were just two guaranteed failures among all the remaining talkers.

After excluding errors associated with imposed "wild cards," the remaining string errors occur because of the existence in the directory of incorrect strings whose letters match candidate letters ranking higher than those corresponding to the correct string. Out of all the trials over all the talkers in the evaluation, there were six trials, or approximately 1 percent of the total, for which the above condition was true and for which errors were obtained. One particularly persistent example, accounting for four of the six errors, involved the test string "VANBEN*J*". In each case, in the fourth position "D" was a better candidate than the specified letter "B," resulting in the incorrect matching string "VANDEN*J*". This situation is associated with the conjunction of two adverse conditions. These are acoustic letter confusions of high probability and directory entries with highly similar name strings.

A similar situation which might have been expected to produce more mismatches than it did in the evaluation is mismatching initials even though last-name strings are correctly matched.* A string of initials of length 1 or 2 is a far weaker constraint on acoustic errors than the last-name string, which is generally length 6. For the most common last names, where there are many entries differing only in initials, such mismatches may be serious. (As presently implemented, this condition can actually produce worse results since matches are allowed even if second initials are not supplied by the talker or do not match the second initial in the listing string.)

A possible way to resolve the kinds of mismatches described here is to request the talker to specify additional information.† For example, if an additional last name character is requested for the example cited, there is little chance of mismatch between "VANBENT*J*" and "VANDENB*J*".

Although there were 88 "wild card" searches out of 500, there were only 34 searches in which one or more string positions had no candidates at all. Of these, only one string had more than one such position, and only one string generated an error. This low incidence of no-candidate positions is a consequence of the relaxed threshold conditions that were imposed. Preliminary experimentation had indicated a preference for admitting more rather than less candidates, with a greater likelihood for the correct letter to be among them.

Finally, inspection of Table V suggests a possible revision to the system. The table indicates which letters are likely to have been specified when a given letter is recognized, and accordingly accounts for both the *a priori* distribution of letters and the characteristics of the acoustic recognizer. Improved performance might be obtained if letters are included as candidates when the table indicates they are likely candidates, whether or not they are included as candidates by the recognizer on a given trial. With respect to the example cited in the results, it seems reasonable always to include "E" as a candidate when "P" is recognized, since the table indicates that "E" is twice as likely to have been the specified candidate.

Other possible modifications to the system come to mind. As has been emphasized, the present system is guaranteed to fail if there are only incorrect candidates in more than one position. The "wild card" process imposing the "wild card" position one at a time is the limiting factor. An additional "wild card" process can be designed which allows for two such positions. However, the process would likely be cumbersome and protracted. Moreover, it could well be self-defeating by the

* Only four mismatches were obtained.

† As mentioned previously, listing ambiguities are resolved by requesting the talker to specify location codes or organization numbers.

admission of more false or unintended matches rather than achieving better compensation for acoustical errors.

A worthwhile endeavor which would help resolve many of the uncertainties encountered in this study would be to determine quantitatively what statistical characteristics both the directory and the recognizer should have to attain a specified string error rate.

V. CONCLUSION

A means for obtaining voice-actuated directory assistance has been proposed, implemented, and evaluated. Requests made in the form of spoken spelled names can be executed reasonably reliably despite imperfect acoustic recognition. This is accomplished by offering alternate spellings of the name string to be searched in the directory, relying on the spelled context of the correct name to restrict matches to the entries that have been requested. Reliability as well as efficiency also results from the rank-ordering of possible spellings as prescribed by the recognizer combined with the systematic (alphabetic) organization of the directory. Such a system, of course, is not restricted to furnishing directory information but may be applied to any dictionary-like store in which the spelled context provides reasonable constraints.

The 4-percent string error rate obtained in the evaluation, while most encouraging in comparison with the 20-percent acoustic word error rate, does not seem adequate for actual directory assistance service. An immediate goal is improvement of the acoustic recognizer to provide word error rates in the range of 10 percent to provide, in turn, string error rates in the order of 1 to 2 percent.

VI. ACKNOWLEDGMENT

The authors wish to express their appreciation to M. E. Lesk for providing the *TOUCH-TONE* system directory access program and to J. F. Gimpel and N. F. Maxemchuk for helpful discussions on backtrack procedures and decoding techniques.

REFERENCES

1. M. E. Lesk and C. A. McGonegal, "User-Operated Directory Assistance," unpublished work.
2. L. R. Rabiner and R. W. Schafer, "Digital Techniques for Computer Voice Response: Implementations and Applications," Proc. IEEE, *64* (1976), pp. 401–576.
3. L. H. Rosenthal, et al., "A Multiline Computer Voice Response System Using ADPCM Coded Speech," IEEE Trans. Acoustics, Speech and Signal Proc., *ASSP-22* (1974), pp. 339–352.
4. F. Itakura, "Minimum Prediction Residual Principle Applied to Speech Recognition," IEEE Trans. Acoustics, Speech and Signal Proc., *ASSP-23* (1975), pp. 67–72.
5. A. E. Rosenberg and F. Itakura, "Evaluation of an Automatic Word Recognition System over Dialed-Up Telephone Lines," J. Acoust. Soc. Am., *60,* Suppl. No. 1 (1976), p. 512.
6. D. E. Knuth, "The Art of Computer Programming," Vol. 3, *Searching and Sorting,* New York: Addison-Wesley, 1973.

7. G. D. Forney, "The Viterbi Algorithm, Proc. IEEE, *61* (1973), pp. 268–278.
8. D. L. Neuhoff, "The Viterbi Algorithm as an Aid in Text Recognition," IEEE Trans. Inform. Theory, *IT-21* (1975), pp. 222–226.
9. C. J. Viterbi, "Error Bounds for Convolutional Codes and an Asymptotically Optimum Decoding Algorithm," IEEE Trans. Inform. Theory, *IT-13* (1967), pp. 260–269.
10. R. M. Fano, "A Heuristic Discussion of Probabilistic Decoding," IEEE Trans. Inform Theory, *IT-9* (1963), pp. 64–74.
11. K. Sh. Zigangirov, "Some Sequential Decoding Procedures," Problemi Peredachi Informatsii, *2* (1966), pp. 13–25.
12. F. Jelinek, "A Fast Sequential Decoding Algorithm Using a Stack," IBM J. Research and Development, *13* (1969), pp. 675–685.
13. S. W. Golomb and L. D. Baumert, "Backtrack Programming," J. ACM, *12* (1965), pp. 516–524.
14. A. Nijenhuis and H. S. Wilf, *Combinatorial Algorithms*, New York: Academic Press, 1978.
15. E. G. Whitehead, "Combinatorial Algorithms," Lecture notes published by Courant Institute of Mathematics, New York University, 1973.
16. S. E. Levinson, A. E. Rosenberg and J. L. Flanagan, "Evaluation of a Word Recognition System using Syntax Analysis," B.S.T.J., *57*, No. 5 (May–June 1978), pp. 1619–1626.

THE BELL SYSTEM TECHNICAL JOURNAL
Vol. 58, No. 8, October 1979
Printed in U.S.A.

A Vacuum-Assisted Plastic Repair Splice for Joining Optical Fiber Ribbons

BY A. H. CHERIN, P. J. RICH, C. J. ALOISIO, and R. R. CAMMONS

(Manuscript received May 11, 1979)

A vacuum-assisted, injection-molded, repair splice has been developed for joining linear arrays of optical fibers (fiber ribbons). We describe the assembly tool and procedure followed to fabricate an optical fiber ribbon repair splice. The use of vacuum assist in the connector itself during the assembly process allows one to easily hold the fibers in their grooves and greatly simplifies the assembly tools and procedures required to fabricate a splice. Numerous ribbon splices were made both in the laboratory and in a manhole test facility in an effort to evaluate the quality of the splices obtained using this splicing method. The average splice loss was 0.2 dB with 95 percent of the splice joints having losses less than 0.7 dB.

I. INTRODUCTION

A vacuum-assisted, injection-molded plastic splice has been developed for repairing optical fiber ribbons. In this paper, the molded plastic parts and the molding procedure used to fabricate them are described, the splice assembly process is discussed, and the loss characteristics of the completed splice are evaluated.

The problem of developing a field-adaptable repair splicing technique for joining groups of optical fibers in the form of linear arrays has been addressed by a number of different investigators.[1-5] The general approach followed by all these investigators has been similar and is described below.

To prepare a linear array of optical fibers (a ribbon) for repair splicing, the plastic material is removed from around the fibers and the ends prepared using a controlled fracturing technique.[6,2] The fibers are then inserted into a grooved substrate, which is used to align the fibers, to form a butt joint. The splice is completed by attaching a cover to the substrate and adding an index-matching material to the joint. Variations in the basic technique differ in the way the substrate

is made, in the complexity of the assembly procedure followed, and in the tools used to fabricate the splice. For a repair-splicing technique to be field adaptable, the assembly procedure must be accomplished in a routine fashion by craftspeople of average skill level. The fabrication tools must be relatively simple and adaptable to a hostile field environment. In addition, the splice hardware must meet tight tolerances, be mass-producible, and be inexpensive. In the past, no splicing technique has met all the above requirements. Using injection-molded plastic parts,[2] splice hardware can be mass-produced inexpensively and meet the required tolerances. The problem to date has been to develop simple assembly tools and procedures to fabricate a splice. The vacuum-assisted plastic splice described in this paper was designed with this problem in mind. The use of vacuum assist in the connector itself allows one to easily hold the fibers in their respective grooves during the assembly process. This is an evolutionary improvement of past splicing techniques using injection-molded parts that greatly simplifies the assembly tools and procedures required to fabricate a splice.

II. DESCRIPTION OF VACUUM-ASSISTED SPLICE

The vacuum-assisted splice as shown in Fig. 1 and 2 consists of an injection-molded plastic (polycarbonate) coverplate and grooved substrate. Both the substrate and coverplate have six vacuum slots, transverse to the direction of the grooves, to facilitate assembly of a

Fig. 1—Coverplate and substrate of injection molded splice.

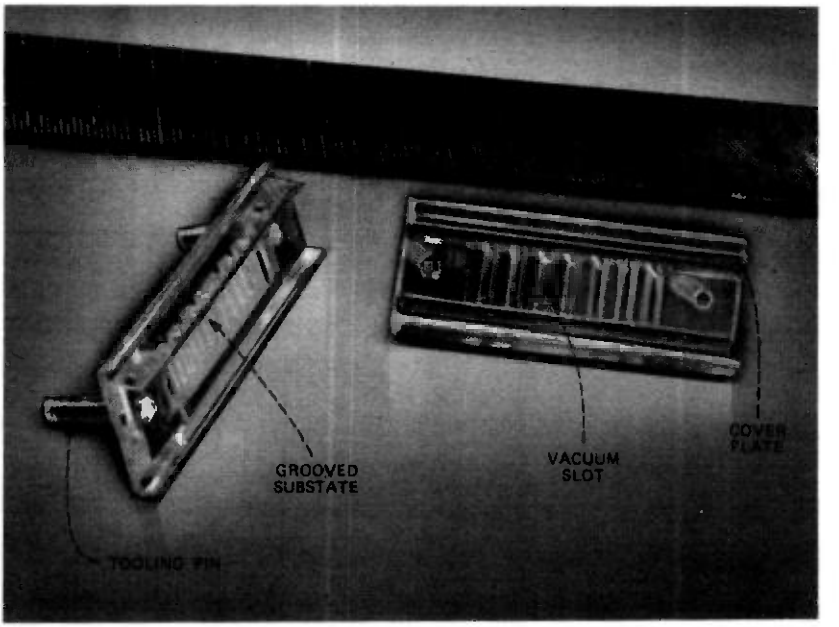

Fig. 2—Completed ribbon splice.

ribbon splice. A seventh slot is located in the center of the coverplate to allow injection of index-matching material into the completed splice. Tooling pins are molded onto both the coverplate and substrate to allow these parts to be easily mounted and aligned in the assembly tool. Injection-molded parts can be designed with a total assembly concept in mind. This allows a designer to build simplified assembly tools which take advantage of alignment features in the connector. After the ribbon splice has been assembled and removed from the assembly tool, the tooling pins are cut off to produce the completed splice shown in Fig. 1.

A cross section of the connector shown in Fig. 3 illustrates the grooves that house the fibers. The deviation of the critical width dimensions of the grooves in the plastic part compared to the master used in the mold was less than 1.0 μm.[2,3]

Figure 3 also shows the troughs which contain the adhesive needed to secure the coverplate to the substrate during the splice closure process.

III. MOLDING AND MATERIALS

The plastic parts were molded on an Arburg 200S Allrounder screw injection molding machine. The parts described in this paper have been molded from either polycarbonate (PC) or polymethylmethacry-

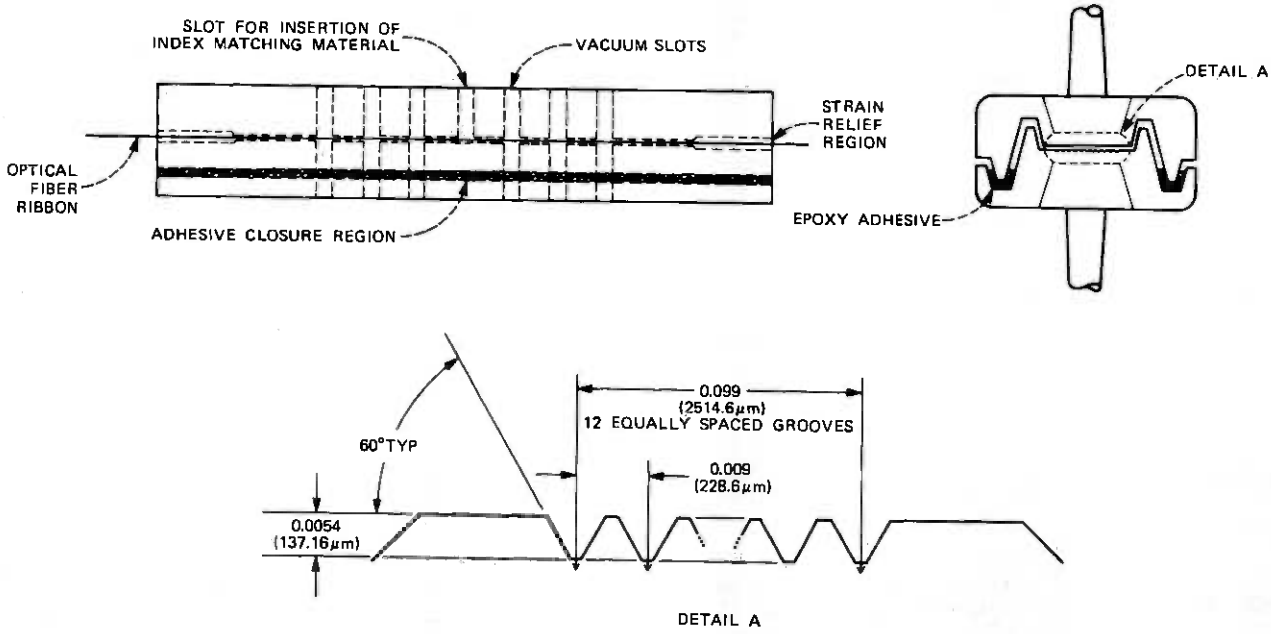

Fig. 3—Section through splice showing grooves and closure method.

late (PMMA). The reasons for these selections are discussed subsequently. Preliminary experiments with gate location indicated no significant differences in groove dimensions between the side and end gating. End gating, used in a feasibility plastic splice,[7] introduces the plastic into the mold cavity parallel to the grooves. In the vacuum-assisted repair splice geometries, this was not found to be necessary but may be required on more complex splice geometries.

It is important to remember that the plastic entering the mold cavity through the gate is *not* a simple liquid melt, but a rubbery solid exhibiting modulus values between 15 and 150 psi, depending upon the time scale of the deformation. If, for example, the gate cross-sectional area is not sufficiently large relative to that of the part to be molded, plastic will "jet" into the part producing undesirable features on the part surface. The gate for the plastic splice was designed to produce a uniform radial flow front.

Once the part has been filled, pressure must be maintained as the plastic is cooling to obtain precise reproduction of mold dimensions. This requires that the gate remain rubbery and thus capable of transmitting pressure until the part has cooled sufficiently to retain its dimensions. The 1-μm deviation out of the 228.6-μm groove width represents less than 0.5 percent shrinkage, well within the 1 percent claimed for amorphous plastics such as polycarbonate. It is instructive to calculate the maximum deviation to be expected from consideration of thermal expansion effects only. The plastic enters the mold at 300°C pushed by a pressure of 13,000 psi. The material is 150°C above the transition temperature, Tg, at which it will change to a glassy consistency common to many amorphous plastics, and it exhibits a modulus in the order of 200,000 psi. Above Tg, the linear thermal expansion coefficient is 1.35×10^{-4}°C^{-1}, approximately twice the value below Tg, 6.75×10^{-5}°C^{-1}. If the part were permitted to cool unconstrained by the pressure, a maximum deviation of 3 percent is calculated; that is, a 6-μm deviation for the groove width. Of course, in extreme cases where the pressure retention is not adequate to initially force the rubbery plastic into the mold details, greater deviations could be expected.[7]

In earlier designs, glass fibers were slid along the grooves during splice assembly. PMMA was selected because of its greater scratch resistance.[7] As information was obtained on environmental characteristics, it was determined that the Tg of PMMA at 115°C was too low. Distortion due to molded effects were observed at temperatures as low as 60°C. Since the vacuum-assist negated the need for scratch resistance, PC, with its Tg of 150°C, was selected. Higher temperature plastics such as polysulfone and polyphenylene sulfide are under study to further improve environment performance.

IV. A BRIEF DESCRIPTION OF THE ASSEMBLY PROCESS AND TOOLS

To prepare a linear array of optical fibers (a ribbon) for repair splicing, the plastic material is removed from around the fibers and the ends prepared using a controlled fracturing technique.[6] Figures 4a and 4b show the fracturing tool used to prepare the two ribbon ends. The resulting 12 uncoated fibers, on 9-mil centers, extend 0.40 inch beyond the plastic coated ribbon. After a substrate is placed into the assembly tool, the prepared fiber ends are inserted into the fiber-aligning grooves forming a butt joint in the substrate of the splice. Because of the vacuum-assist provided by the assembly tool (Fig. 5), the fibers are easily inserted into the aligning grooves and held in place during the remaining steps of the splice fabrication process. Adhesive (AP8004 epoxy, manufactured by Fenwal Inc.) is injected into the troughs of the substrate and, using the coverplate applique of the assembly tool, the coverplate is attached to the substrate. After the adhesive has cured (approximately 9 to 15 minutes), the coverplate applique is removed and index-matching gel is injected through the center slot of the coverplate. When the splice is removed from the assembly tool and the tooling pins cut off, the resulting completed splice is shown in Fig. 1.

The vacuum-assisted repair splice assembly procedure was analyzed to determine the amount of time required to assemble a ribbon splice. Table I provides a breakdown of the time needed for each of the assembly steps in the splicing process for two different epoxy curing times.

The manufacturer of the AP8004 epoxy claims a five-minute working time. To assure that the epoxy hardened properly, 15 minutes was allowed in this study. With insertion heaters in the assembly tool, this curing time could be easily reduced to 9 minutes. These realistic curing times result in a 19- to 25-minute assembly time for a one-ribbon splice. If 12 ribbons were spliced, the assembly time would be approximately 2¼ to 3¼ hours using current assembly tools and procedures.

V. LOSS CHARACTERISTICS OF SPLICE

Numerous ribbon splices were made both in the laboratory and in a manhole test facility (see Fig. 6 for an example of a manhole splicing environment), in an effort to evaluate the quality of the splices obtained using this splicing method. The 12 fiber ribbons that were used contained 110-μm O.D. graded-index fibers with 55-μm core diameters. To simulate the characteristics of a vacuum-assisted splice in a realistic communications system, the ribbon splices were used to join two 340-meter sections of optical fiber ribbon. The splices were measured in the configuration shown in Fig. 7. Insertion loss measurements were made using an optimized loose tube splice substitution technique.[8] To

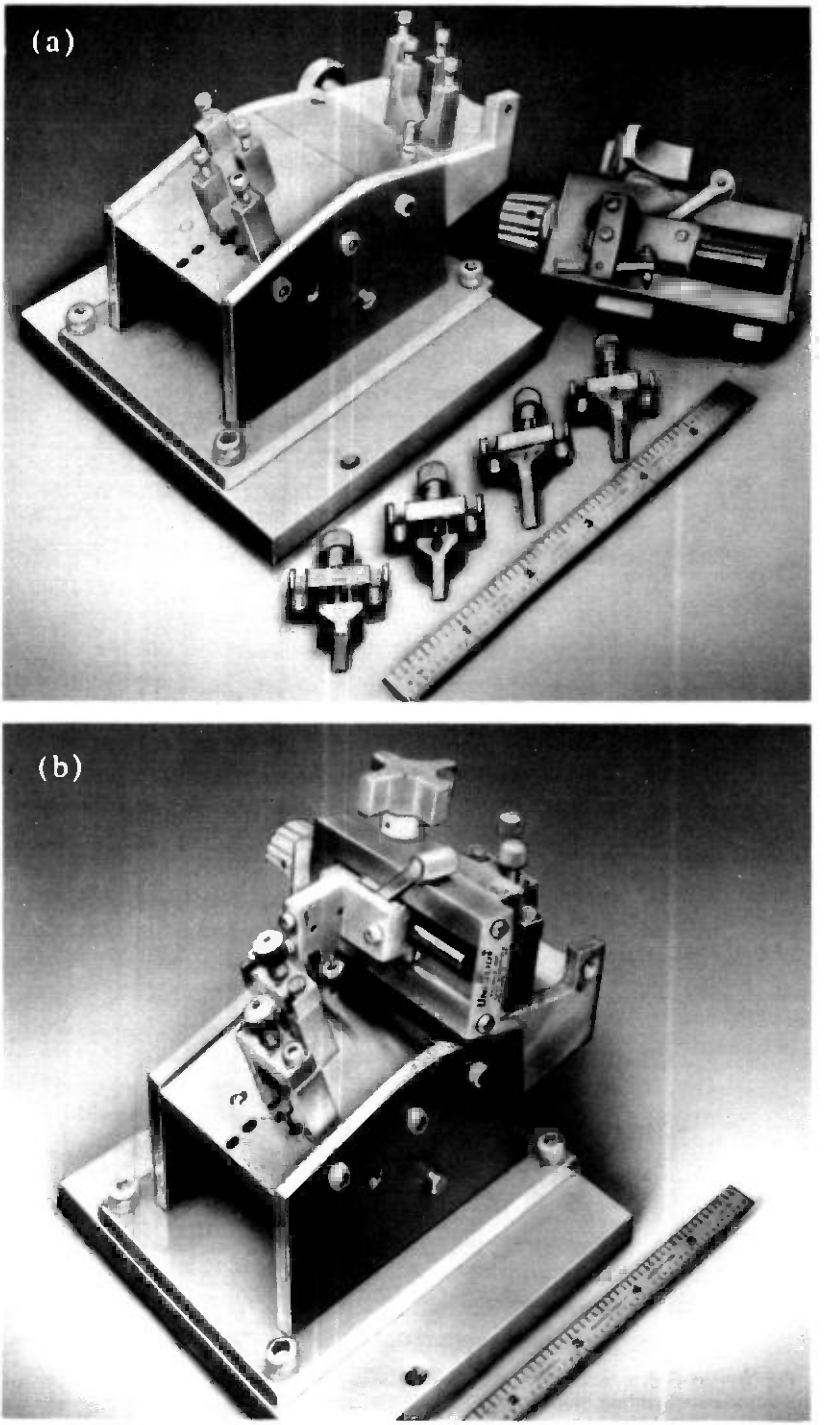

Fig. 4—(a) Component parts of fiber end preparation tool. (b) Assembled end preparation tool.

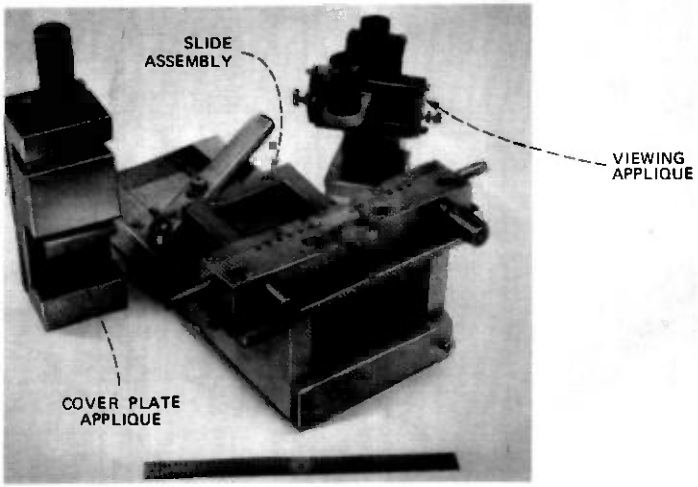

(a)

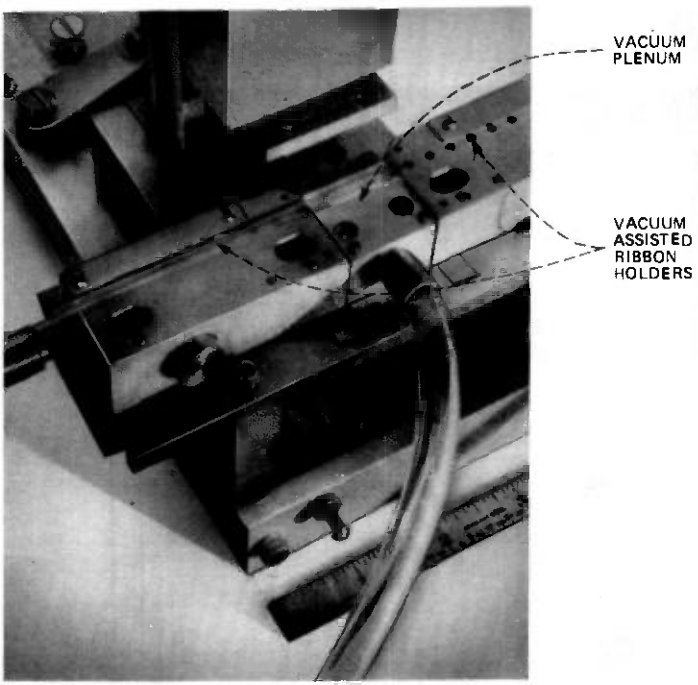

(b)

Fig. 5—(a) Splice assembly tool. (b) Splicing tool showing vacuum plenum and vacuum-assisted ribbon holders.

Table I

Procedure	Current Epoxy Cure Time	Accelerated Epoxy Cure Time
Ribbon stripping and end preparation	6 minutes	6 minutes
Splice fabrication	4 minutes	4 minutes
Epoxy cure	15 minutes	9 minutes
Assembly time for one ribbon splice	25 minutes	19 minutes
Assembly time for 12 ribbon splices	3.17 hours*	2.18 hours†

* Assembly procedure limited by epoxy cure time.
† Assembly time is operations limited.

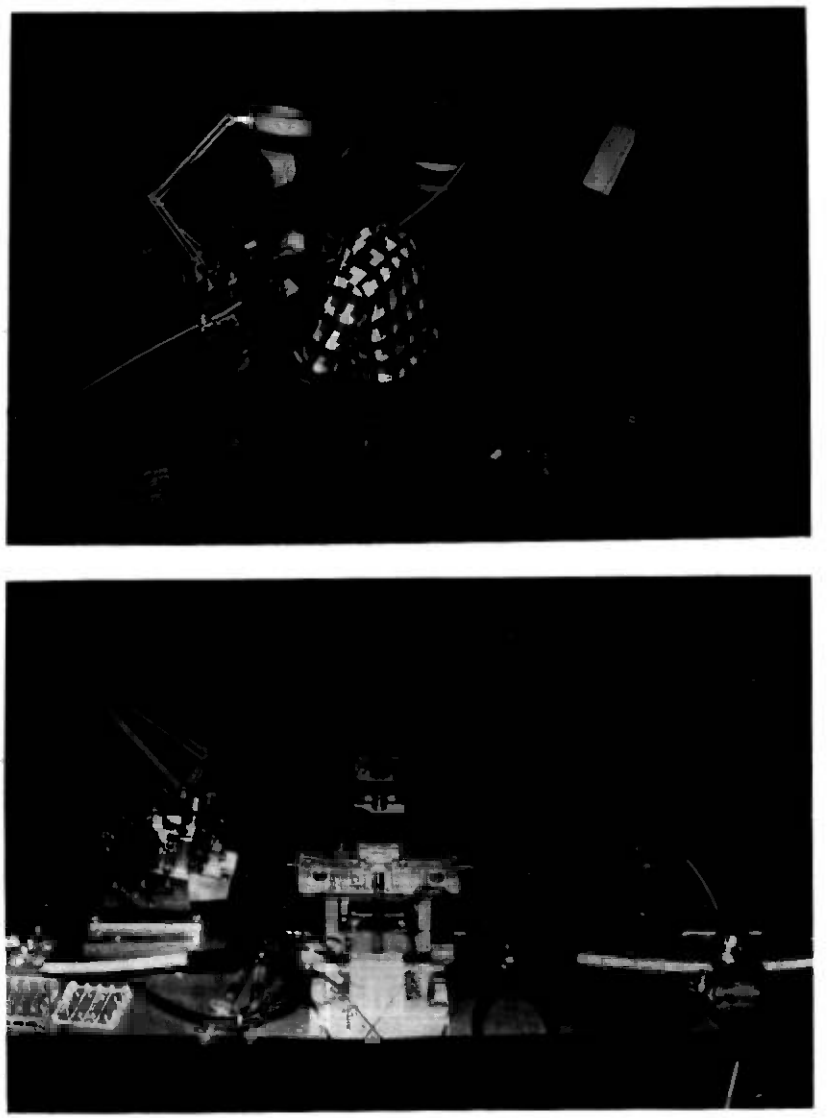

Fig. 6—Splice assembly tool in manhole environment.

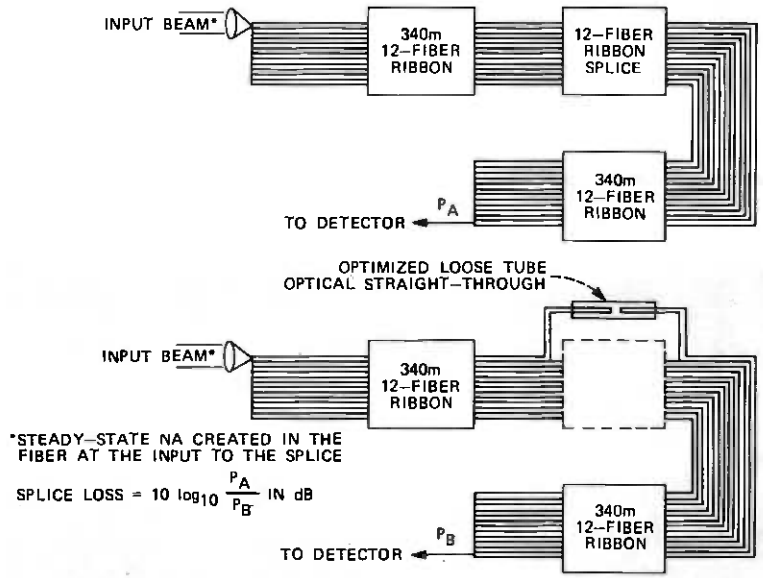

Fig. 7—Measurement procedure to obtain loss statistics of ribbon splice.

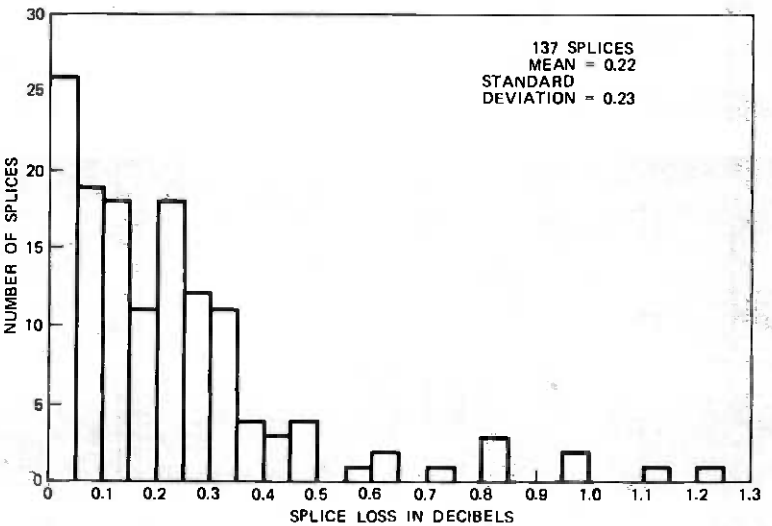

Fig. 8—Complete splice loss data.

understand this technique, consider fiber 1 in the 12-fiber-ribbon splice. To obtain splice loss, the system was tuned to obtain maximum output power P_A through the transmission path containing fiber 1. The splice containing fiber 1 was then cut out of the system and an optimized

loose tube optical straight-through was substituted in its place. The system is then tuned to obtained maximum output power P_B. P_A and P_B are used to calculate the splice loss in decibels. The loss of the optimized loose tube straight-through was less than 0.03 dB.

The loss statistics for the vacuum-assisted repair splice, obtained

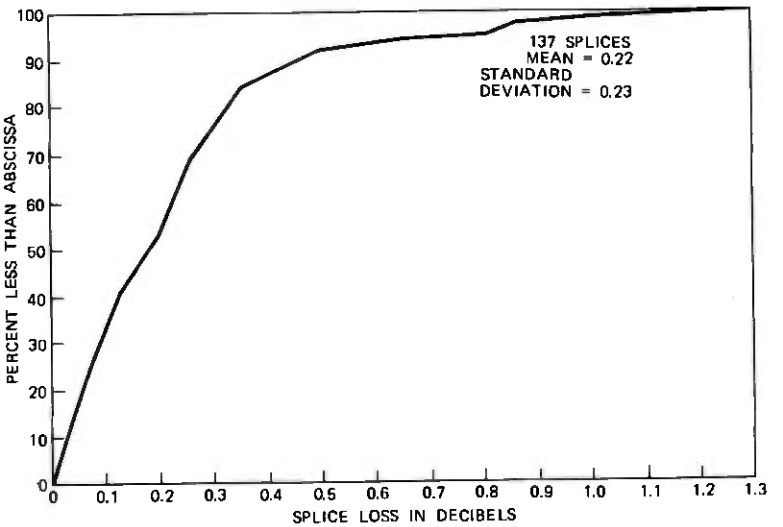

Fig. 9—Cumulative distribution function of complete splice loss data.

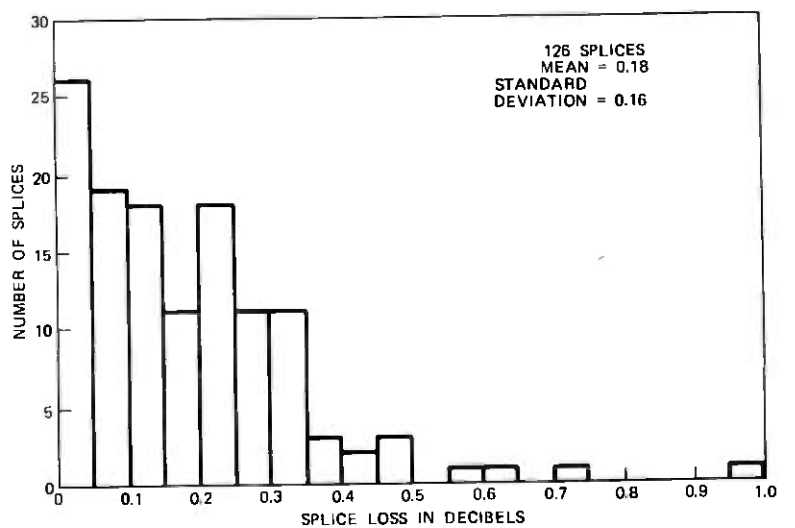

Fig. 10—Splice loss data.

from measuring 13 ribbon splices, are shown in Figs. 8 and 9. The average loss of the splices measured was 0.22 dB with a standard deviation of 0.23 dB. The data base for these statistics consisted of 137 splices. Only 11 fibers existed in a portion of the input ribbon preceding the splice. Therefore, one could only evaluate 11 of the 12 fiber splices in a ribbon splice. In addition, six fiber breaks occurred in the ribbon during the assembly and measurement processes. After the majority of the ribbon splices were made and measured analysis of the data showed that most of the outliers (splices with loss greater than 0.5 dB) occurred in one of the edge grooves of the ribbon splice. Modification of the coverplate applique reduced the number of subsequent outliers occurring in this groove. Elimination of this groove's loss data from the total data base results in the statistics shown in Figs. 10 and 11.

The average loss of the 126 remaining splices was 0.18 dB with a standard deviation of 0.16 dB. If one views the statistics shown in Fig. 10 as an optimistic assessment of the repair splice capability and those shown in Fig. 7 as a pessimistic assessment, bounds on the nature of the outliers produced by this splicing method can be obtained. A realistic appraisal of the loss statistics of the vacuum-assisted plastic repair splice would yield an average loss of 0.2 dB and outliers in the loss data that fall within the bounds shown in Fig. 12. It is of interest to note that no difference in the loss statistics was observed between splices made in the laboratory and those made in the manhole test facility.

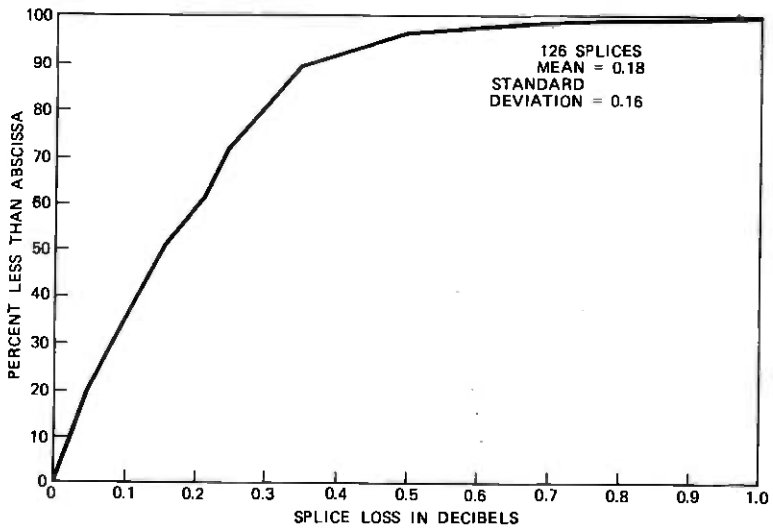

Fig. 11—Cumulative distribution function of splice loss data.

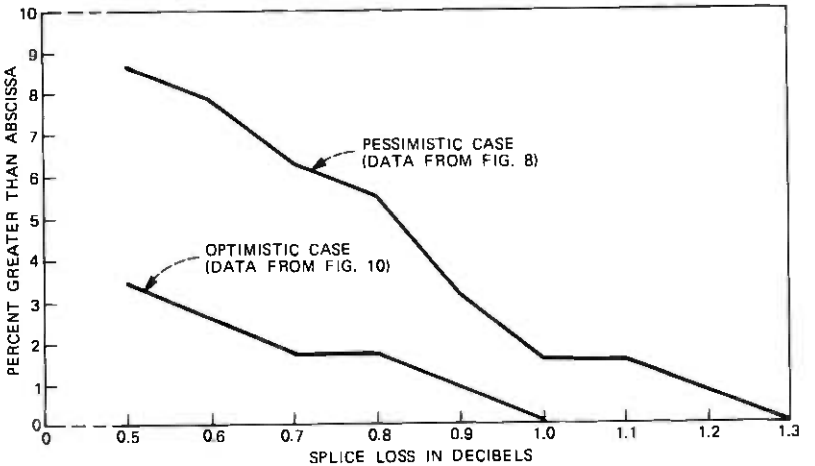

Fig. 12—Outlier cumulative distribution function bounds.

VI. FINAL COMMENTS

A field repair splicing method has been developed for joining 12-fiber optical fiber ribbons. This splicing method produces splices with an average loss of 0.2 dB in 20 to 25 minutes. The injection molded plastic hardware used is mass-producible and inexpensive. The use of vacuum assist during the assembly process allows one to easily hold the fibers in their aligning grooves and greatly simplifies the procedures required to fabricate a splice. The fabrication tools are relatively simple and, with proper redesign, adaptable to a field environment. Future work will be concentrated on determining the environmental characteristics of this splice. Preliminary data for polycarbonate plastic splices indicate that the temperature coefficient of the splice is approximately 0.007 dB/°C for the temperature range $-40°C \leq T \leq 5°C$, $35°C \leq T \leq 80°C$. This temperature coefficient can be decreased by proper materials considerations. Studies in this area are now in progress and will be reported in a future paper.[9]

VII. ACKNOWLEDGMENTS

The authors wish to thank D. M. Petrowski and A. Osborne for their assistance in the design and fabrication of the mold and assembly tool used in this work.

REFERENCES

1. A. H. Cherin and P. J. Rich, "An Injection Molded Splice Connector with Silicon Chip Insert for Joining Optical Fiber Ribbons," Topical Meeting on Optical Fiber Transmission II, OSA, Williamsburg, Va., February 22-24, 1977.

2. A. H. Cherin and P. J. Rich, "An Injection-Molded Plastic Connector for Splicing Optical Cable," B.S.T.J., *55*, No. 8 (October 1976), pp. 1057–1067.
3. E. L. Chinnock, D. Gloge, P. W. Smith, D. L. Bisbee, "Preparation of Optical Fiber Ends for Low-Loss Tape Splices," B.S.T.J., *54*, No. 3 (March 1975), pp. 471–477.
4. A. H. Cherin and P. J. Rich, "Multigroove Embossed-Plastic Splice Connector for Joining Groups of Optical Fibers," Appl. Opt., *14*, No. 12 (December 1975), pp. 3026–3030.
5. P. W. Smith, D. L. Bisbee, D. Gloge, and D. L. Aimnock, "A Molded Plastic Technique for Connecting and Splicing Optical-Fiber Tapes and Cables," B.S.T.J., *54*, No. 6 (July-August 1975), pp. 971–984.
6. D. Gloge, P. W. Smith, D. L. Bisbee, and E. L. Chinnock, "Optical Fiber End Preparation for Low-Loss Splices," B.S.T.J., *52*, No. 9 (November 1973), pp. 1579–1588.
7. M. J. Saunders, "The Determination of Fiber Optic Splicing Fixture Groove Depths by Means of White Light Interference Fringes," unpublished work.
8. D. N. Ridgway, "Accurate Splice Loss Measurements of Long Fibers Using Loose Tube Splices," unpublished work.
9. A. H. Cherin, C. J. Aloisio, P. J. Rich, "Precision Molding of a Fiber Optic Splice Connector, a Feasibility Study," unpublished work.

THE BELL SYSTEM TECHNICAL JOURNAL
Vol. 58, No. 8, October, 1979
Printed in U.S.A.

Design of a Wideband, Constant Beamwidth, Array Microphone for Use in the Near Field

By F. PIRZ

(Manuscript received April 30, 1979)

Directional microphones have long been proposed for the removal of room reverberation. An array microphone would seem ideal for this purpose, since theoretically it can be aimed anywhere within the room. However, microphone pattern beamwidth is related to wavelength and aperture size. For a fixed-size aperture, as wavelength goes down so does beamwidth. The change in beamwidth over a decade change in wavelength would seem to be unacceptable for this application. We discuss the design of a constant beamwidth array microphone for the frequency range 300 to 3000 Hz. Because the microphone-to-talker distance is assumed to be about 3 ft while the array has a 9-ft aperture, the microphone is optimized for near field. We also discuss the use of a nonlinear optimization program for choosing the array parameters.

I. INTRODUCTION

Directional microphones have been proposed for the removal of room reverberation on the assumption that a properly aimed microphone would pick up the direct path speech energy and reject the reverberant energy. Indeed, highly directive microphones are often employed in "press conference" situations to pick up questions from an auditorium. An array microphone would seem to be an ideal replacement for the "directional" mike in such a situation since it would offer a quick automatic aiming capability and, if so designed, either multiple-speaker monitoring or the ability to correlate multiple reverberant paths from a single speaker.

Conventional array microphones, however, suffer from a number of drawbacks which must be considered. If we consider speech in the frequency range 300 to 3000 Hz, then the microphone designer must consider the decade change in frequency (and wavelength). In particular, the beamwidth of the radiation pattern is related to wavelength

and microphone aperture size (microphone dimensions). As wavelength goes down, so does beamwidth. The change in beamwidth over a decade change in wavelength would seem to be unacceptable for this application.

If we would like to employ our microphone for small conference room dereverberation, then we must also consider the near-field/far-field transition region of the microphone. Note that at 300 Hz the wavelength of sound is about 4 ft. A microphone with a two-wavelength aperture at this frequency is therefore 8 ft wide. However, most rooms have an 8 to 10 ft ceiling. As a result, speakers in such a situation are between 1 wavelength (standing) and 2 wavelengths (seated) away from a ceiling-mounted microphone. We consider a ceiling-mounted mike because of symmetry with respect to aiming the microphone and because there is always a direct path between the microphone and talker. This, of course, does not mean that it is an optimal location. We note, however, that TV studios use overhead boom mikes for sound pickup.

Finally, most array design texts concentrate on single-frequency (or narrowband) designs. Because of the near-field constraints, however, the design equations are highly nonlinear and thus difficult (or impossible) to solve analytically. As a result, some type of optimization approach must be taken to select the proper design parameters, such as element position and gain, for the microphone. We discuss this problem later. First, we discuss the microphone design problem in more detail.

II. MICROPHONE DESIGN

Microphone design, that is, the selection of position and gain for each element of an array of microphones, is *not* a simple task. Most texts on array design, e.g., Ref. 1, start out with a uniformly illuminated aperture (opening) and develop the radiation pattern from basic physical constraints. An array microphone then corresponds to a spatially (uniform) sampled aperture. The analogy to sampling theory is usually drawn at this point since, in the *far* field, the radiation pattern is the (discrete) Fourier transform of array illumination (element gains). Since we are constrained to working in the near-field/far-field transition region, the exact response r, at observation point o and wavelength λ, for an *array* of N omnidirectional microphones is:

$$r(o, \lambda) = \sum_{k=1}^{N} \frac{A(k)}{d(k)} e^{-j(2\pi/\lambda)(d(k)+\phi(k))}$$

where $d(k)$ is the distance from the kth microphone to the observation point o.

$A(k)$ is the gain of the kth microphone

$\phi(k)$ is the phase shift (delay) of the kth microphone
λ is the wavelength.

Using this equation, we have calculated the response for the array consisting of five elements uniformly spaced over the range $-\lambda_0$ to $+\lambda_0$ depicted in Fig. 1. The element gains have a triangular weighting and no phase shift. The polar response, at a distance of $10\lambda_0$, of this array is plotted on a log scale in Fig. 2 for the range $-90°$ to $+90°$. (This corresponds to measuring the response along the circle BAC.) Curve (a) is the response at $\lambda = \lambda_0$; curve (b) at $\lambda = 0.75\lambda_0$ shows that the main lobe response has narrowed appreciably. Curve (c) at $\lambda = 0.5\lambda_0$ shows a marked increase in the sidelobes. Curve (d) at $\lambda = 0.4\lambda_0$ shows spatial foldover since the element spacing is only $0.5\lambda_0$. Finally, curve (e) at $\lambda = 0.3\lambda_0$ shows severe foldover.

Figure 3 shows the polar response of this same array as a function of distance. Curves (a), (b), and (c) are for distances of $10\lambda_0$, $5\lambda_0$, and $3\lambda_0$, respectively. The flattening of the array response is obvious. Curves (d) and (e) for distances of $2\lambda_0$ and $1.5\lambda_0$ show even more severe flattening. Curve (f) for a distance of $1.1\lambda_0$ illustrates a serious problem associated with plotting the near-field response of a microphone array. Figure 1 illustrates the array configuration and two distances, $d = 10\lambda_0$ and $d = 1.1\lambda_0$, for which responses are being measured. For the circle at $d = 10\lambda_0$ and $\theta = 0°$ (point A), all elements are at least $10\lambda_0$ away from the observation, while at $\theta = \pm 90°$ (points B, C) the array elements are between $9\lambda_0$ and $11\lambda_0$ away from the observation point (a 10-percent change). However, for $d = 1.1\lambda_0$ at $\theta = 0°$ (point D), all elements are at least $1.1\lambda_0$ away while, at $\theta = \pm 90°$ (points E, F), the array elements are between $0.1\lambda_0$ and $2.1\lambda_0$ away (a 90-percent change).

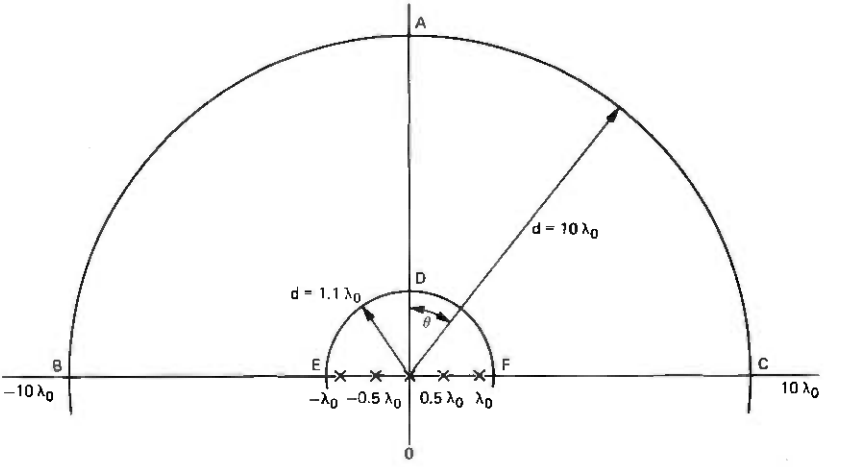

Fig. 1—Array response observation paths.

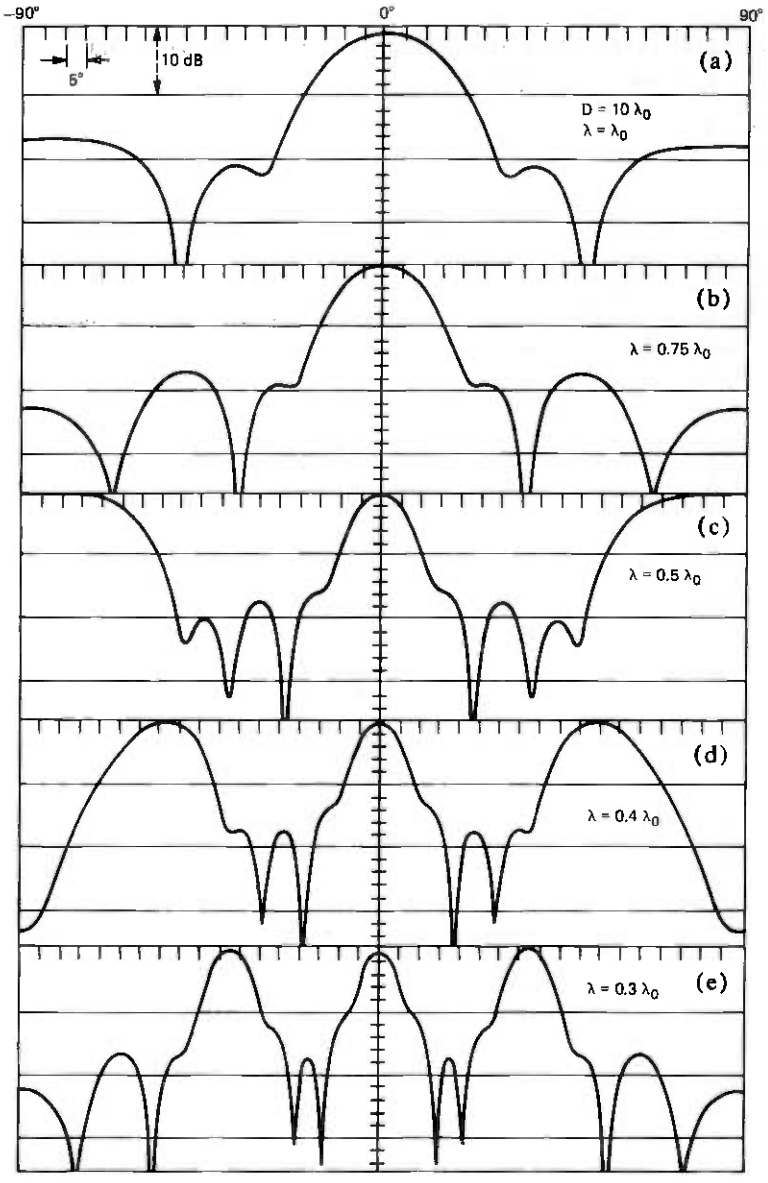

Fig. 2—Response variation with λ.

In essence, what results is a proximity effect. At $d = 1.0\lambda_0$ and $\pm 90°$, the observation point and the microphone locations coincide. The resulting response plot is useless because the A/d term in the response equation becomes infinite. Because we are most interested in room responses, we have modified the subsequent response plots to be the microphone response in a plane parallel to the microphone. As a result,

the response at ±90° falls to zero since this corresponds to an infinite distance from the array.

III. MICROPHONE DIRECTIVITY

Microphone directivity index (DI) may be defined as the ratio of the maximum microphone sensitivity at the peak of the main lobe to the

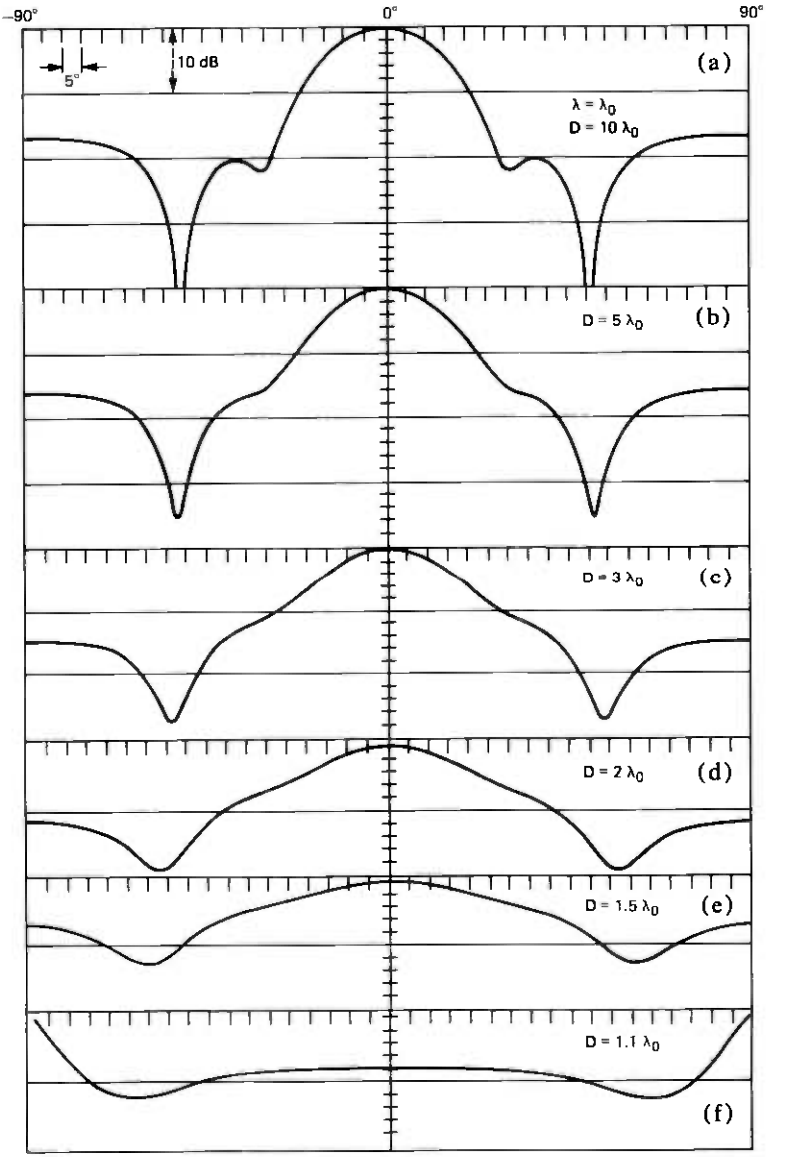

Fig. 3—Response variation with D.

sensitivity of an isotropic (uniform response in all directions) microphone with the same average sensitivity.[2] However, because we are dealing with a wideband microphone, directivity is also a function of frequency. This introduces a problem since averaging implies uniform sampling across the band which unfairly weights one band edge over the other. For comparison purposes, we have calculated directivity by averaging over both frequency and wavelength for both polar and planar response functions. The average directivity indices we have obtained range from 8.8 to 5.1. For comparison, a second-order gradient microphone has a directivity index of 7, a cardioid of 4.8, and a limacon of 6.0.[2]

IV. NONLINEAR OPTIMIZATION GOAL PROGRAMMING

As discussed previously, microphone design must be done by a nonlinear optimization program. However, in terms of nonlinear optimization, microphone design poses a problem. Typically, we begin with a desired response, for example, the ideal specifications of Fig. 4 and then try to build a microphone which has that response "*or better*." The "or better" rules out any kind of least-squares optimization technique since responses which are better (below the sidelobe requirement, for example) are counted in as part of the error term. Ignizio[3] has developed a technique which he refers to as "goal programming," which deals with this problem. In this case, when the current solution meets or exceeds the goal, the penalty function is zero. If the solution does not meet the goal, then the penalty is nonzero. The optimization program then seeks to minimize the penalty function(s) by varing the

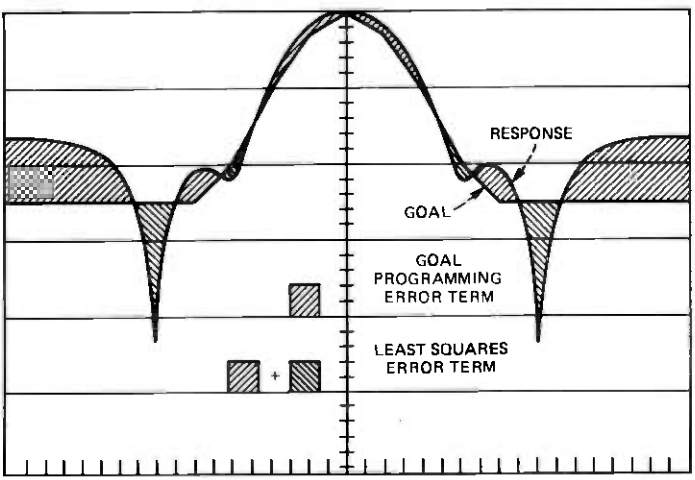

Fig. 4—Goal programming error comparison.

microphone parameters (called decision variables). For our microphone design problem, the 180-degree response field of the microphone is evaluated at 19 separate points. A penalty function is written for each point. This allows different points of the response to be weighted separately and to be constrained in different ways. The optimization program then seeks to minimize an achievement function which is a combination of each of the penalty functions.

Unlike most nonlinear optimization, goal programming does not need gradients or derivatives, and it does not need an initial valid solution. Unfortunately, like most nonlinear optimization techniques, there is no guarantee of global maximum. A version of Ignizio's optimization program was programmed for our Data General Eclipse Computer and used to optimize the microphone designs presented here. Our experience with this algorithm has been very good. It has enough flexibility with respect to the optimization goal, variable weighting, and penalty function construction to make it practical to use. Running time is linearly proportional to the number of variables, as is storage space required. Optimization of a microphone involving 20 decision variables with 57 goal points and 72 terms in the achievement function typically takes 10 to 15 minutes.

As with most optimization programs, one must carefully pose the problem. The optimization program will take advantage of any "loopholes" left in the problem statement, usually with disastrous results. When considering designs for a single frequency, the optimized result was often a superdirective design (a design with close element spacing and phase alternations between elements). Superdirectivity, unfortunately, is an extremely narrowband phenomenon and is of little interest for the intended application.

V. MICROPHONE DESIGN RESULTS

Because of the decade range of frequencies involved, an array properly sampled at the highest frequency is grossly (10:1) oversampled at the lowest frequency. In addition, the number of elements implied by such oversampling is excessive, impractical, and also unnecessary, as we shall see. As a result, we must now consider a nonuniformly sampled array (also called a thinned or random array).

The technique which we have developed to handle this problem makes use of superposition. Essentially, three arrays are designed, one for midband and one for each band edge as in Fig. 5. These three arrays are then combined (superimposed), with suitable filtering, to give a single array which covers the full frequency band. This approach is essentially similar to that taken in Refs. 4 and 5, except that the array is constrained to operate in the near field. Other approaches which are suitable only in the far field are detailed in Refs. 6 and 7.

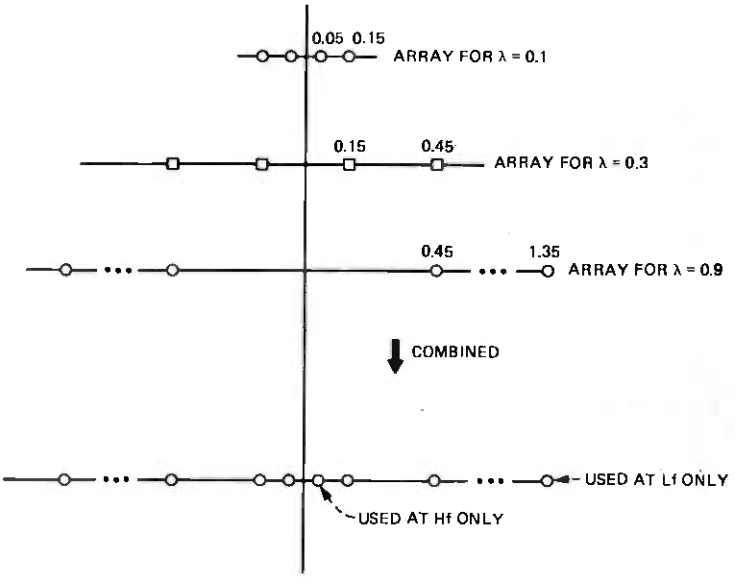

Fig. 5—Wideband array prototype.

Our first approach was to attempt to design a microphone optimized at both ends of the frequency band. However, without any frequency-dependent components in the microphone, the result was optimized for midband with very poor response at band edges. It became obvious that some frequency-dependent element would have to be introduced into the microphone design to allow the microphone *aperture* to vary with frequency. Since each microphone will need a pre-amplifier of some sort, we decided to introduce some frequency shaping into the amplifier design. A second order 12dB/octave filter was incorporated into the microphone preamplifier and the goal programming model was modified to set the cutoff frequencies accordingly. When the amplifier phase shift is ignored, the results of Fig. 6 are obtained. This design was optimized using a polar response function at a distance of $3\lambda_0$. For these designs, λ_0 corresponds to an f_0 of 300 Hz. Here the filter cutoff frequencies correspond to approximately what would be expected for the given frequency band. This figure illustrates the microphone response at the band edges and the average responses for both frequency and wavelength averaging. The set of plots on the left of the figure are polar responses, while those on the right are planar. Figure 7 illustrates the response of a microphone array designed using polar response at a distance of $1\lambda_0$. Amplifier phase shift, however, has been included in this design and the cutoff frequencies have shifted to compensate for this. Figure 8 illustrates the responses of a microphone optimized using planar response instead of polar response.

VI. DISCUSSION OF ARRAY RESULTS

Initially, a steerable array was proposed for removing room reverberation. However, the directivity factors and beamwidths attainable with the arrays we have been able to design indicate that perhaps these arrays might better be applied as fixed microphones. In this case, the directivity of the microphone would allow it to be located over a conference table, while rejecting (or reducing) room noise and reverberation from the balance of the room. An additional factor which

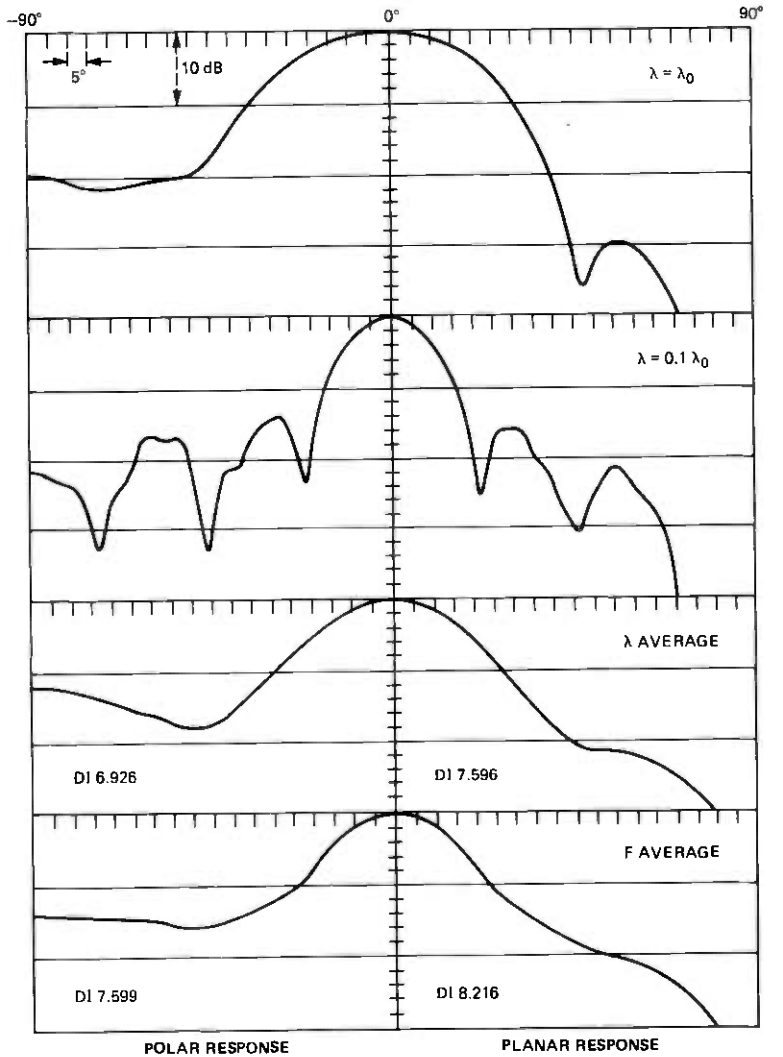

Fig. 6—Array response ignoring phase shift.

favors a fixed microphone is the cost and complexity of the hardware required to steer the array.

The 8-element linear arrays presented here imply approximately 64 elements in a two-dimensional array. A steerable array would require a phase shifter (variable delay) for each element of the array. Current CCD technologies allow the construction of fairly cheap analog delay lines (several commercial grade circuits are already available). A multibeam microphone, however, would require multiple tapped delay

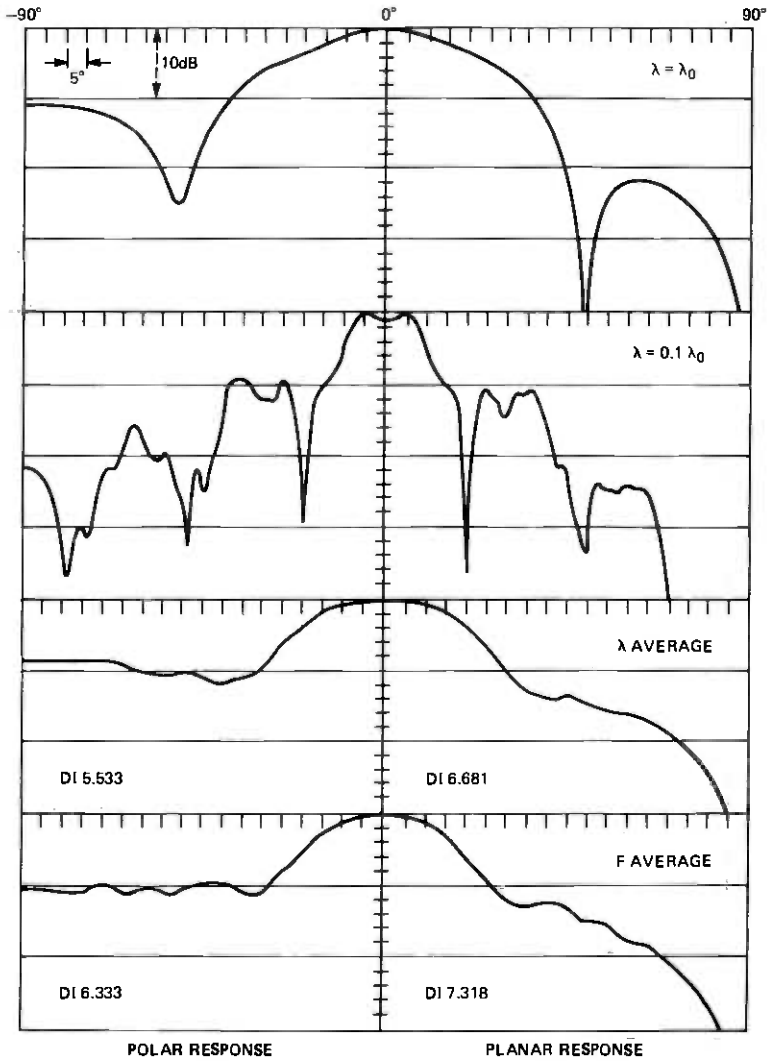

Fig. 7—Array response polar optimization.

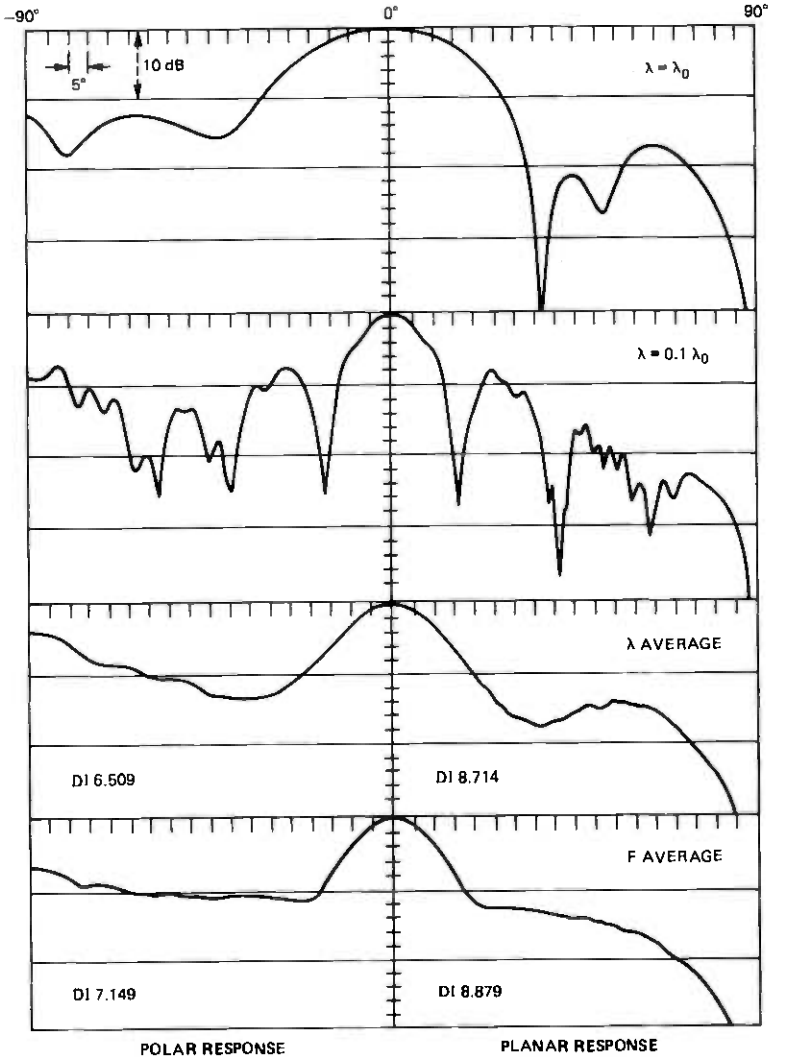

Fig. 8—Array response planar optimization.

lines which are difficult to realize in analog form. The summation and switching circuits would also be fairly complex. A multitapped digital delay line made from an A/D converter, RAM storage, and D/A converter could probably be implemented for approximately $100/channel (prototype quantities). A typical array then begins to cost almost $5000, which is enough to make it unattractive.

Since the microphone is not *significantly* directive, simple geometric constraints indicate that a microphone with perhaps four to nine beam

positions might be fabricated using analog techniques. One of these beam positions could then be chosen (dynamically perhaps) during a conference as the active speaker(s) move about in a conference room.

VII. CONCLUSION

We have shown that it is possible to design a wideband, approximately constant beamwidth array microphone for use in the near field. We conjecture that using more elements in the array would improve the beamwidth/sidelobe ratio and overall response. We have yet to attempt to steer this array design. Because of the poor sidelobe response, we do not see much prospect of pencil point focusing of this type of microphone for small room dereverberation unless, as mentioned previously, the number of elements is increased to improve response. We note, however, that the array steering mechanism then increases in complexity and may become prohibitively expensive. This work, and that cited in Refs. 4 to 7, however, indicate that an array microphone might indeed be suitable for large room (auditorium) dereverberation.

REFERENCES

1. B. D. Steinberg, *Principles of Aperture and Array System Design,* New York: John Wiley and Sons, 1976.
2. H. F. Olson, *Modern Sound Reproduction,* New York: Van Nostrand Reinhold, 1972.
3. J. P. Ignizio, *Goal Programming and Extensions,* Lexington, Mass: D. C. Heath, 1976.
4. J. C. Morris and E. Hands, "Constant-Beamwidth Arrays for Wide Frequency Bands," Acoustica, *11* (1961), pp. 341–347.
5. J. P. Smith, "Constant Beamwidth Receiving Arrays for Broad Band Sonar Systems," Acoustica, *23* (1970), pp. 21–26.
6. P. H. Rogers and A. L. Van Buren, "New Approach to a Constant Beamwidth Transducer," J. Acoust. Soc. Amer., *64,* No. 1 (July 1978), pp. 38–43.
7. J. Jarzynski and W. J. Trott, "Array Shading for a Broadband Constant Directivity Transducer," J. Acoust. Soc. Amer., *64,* No. 5 (November 1978), pp. 1266–1269.

THE BELL SYSTEM TECHNICAL JOURNAL
Vol. 58, No. 8, October 1979
Printed in U.S.A.

Fast Simultaneous Thickness Measurements of Gold and Nickel Layers on Copper Substrates

By J. R. MALDONADO and D. MAYDAN

(Manuscript received April 20, 1979)

The thickness of nickel and gold films plated on a copper substrate has been determined by measuring the intensity of various fluorescent lines excited in reflection by a 50-kV tungsten X-ray source. An exploratory system has been constructed which can simultaneously measure the thickness of the gold and nickel layers on an area of 125 × 175 μm. Thickness of gold from 0.2 μm to 5 μm and from 0.3 μm to 1.5 μm of nickel can be measured to an accuracy of ±6 percent in the gold films and ±10 percent in the nickel films in about 20 seconds, including the measurement and calculation. The equations describing the attenuation of the incident radiation, the primary and secondary excitation of fluorescence radiation in the films, and the attenuation of the fluorescence radiation in the films have been determined for the case of nickel and gold films on copper substrates and for indium and gold films on copper substrates and are solved by a computer in the system. The method could be extended to other multilayer systems.

I. INTRODUCTION

With the recent increase in the price of gold and other precious metals, new ways are being investigated to reduce the consumption of these materials. For example, replacing the uniform plating process with the selective electroplating of gold to tailor-fit the gold layer to the small mating surfaces of the contacts in connectors and integrated circuit packaging hardware will result in large savings of gold. With this new approach, monitoring the thickness of the gold and the nickel layer underneath it at relatively high degrees of accuracy and at high speed becomes an important factor in controlling the deposition process.

Today, the most common way to measure the thickness of the gold layer is to use a radioactive beta source which generates high-energy

electrons and then to monitor the backscattered electrons from the gold layer to determine its thickness. Since bright radioactive sources are not available, the system is only adequate for the thickness measurement of materials over 0.5 mm in diameter and with measurement times of 1 min or longer. In addition, the measurement is very sensitive to any change in position of the substrate material relative to the electron detector.

X-ray fluorescence has been used by many authors to determine thickness of both the nickel and gold layers.[1,2] This is done by monitoring the magnitude of the direct fluorescence from the two layers which are excited by a shorter X-ray wavelength. However, as shown in this paper, the fluorescence intensity produced by the gold saturates at gold thicknesses above 3 μm, which limits the useful range of thickness measurements to less than 3 μm. Also, the systems reported in the literature are not capable of simultaneous measurements of nickel and gold films.

We describe in this paper an X-ray fluorescence system for the simultaneous measurement of small areas of gold and nickel layers plated on copper substrates. The system, schematically shown in Fig. 1, consists of an X-ray source with a tungsten or rhenium target operating at 50 kV (less than 1 mA), a 160-eV lithium-doped silicon detector with a specially designed detector collimator and a programmable X-ray analyzer. This system allows us to display the value of the thickness of small areas (~100 μm diameter) of gold and nickel films on copper substrates in times of the order of 20 s and with an accuracy of better than 10 percent.

For the thickness measurement of a thin nickel layer deposited on a copper substrate and a thicker gold layer deposited on top of the nickel, we excite $K\alpha_{12}$ lines in the copper and nickel with the broad wavelength spectrum from the X-ray source as shown in Fig. 1. The nickel thickness is determined by the magnitude of the direct fluorescence, while the gold thickness is measured by the attenuation of the $CuK\alpha_{12}$ lines passing through the gold film. The $CuK\alpha_{12}$ lines are denoted by $CuK\alpha$ in this paper.

Experimental results obtained with the X-ray fluorescence system are presented and compared with results obtained by cross-sectioning the samples and determining the thickness by optical means. An extension to other multilayer systems is also presented.

II. DESCRIPTION OF SYSTEM

2.1 Geometry of the system

The X-ray system is shown in Fig. 1. It consists of an X-ray source illuminating the sample, an X-ray detector to detect the fluorescence radiation from the sample with a specially designed detector collimator, and associated electronics. Optical alignment of the samples is also

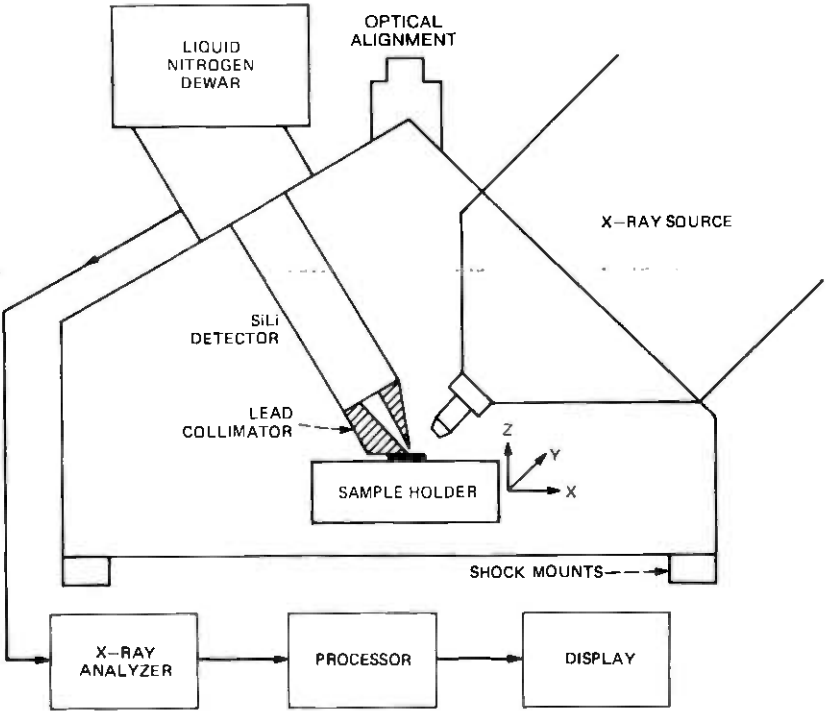

Fig. 1—X-ray system.

provided. The X-ray source incident angle (45 degrees) was chosen to minimize the interaction of the different layers due to the attenuation of the incident beam and also to allow for optical registration. The detector angle (30 degrees) (fluorescent angle measured from the normal to the surface) was chosen to minimize the attenuation of the NiKα line in the gold film and also to allow for the thickness measurement of relatively thick gold films (4 to 5 μm). If optical alignment can be obtained from the backside of the sample, the reflection angle could be reduced to 0. This will increase the thickness measuring range of the gold films and increase the counting accuracy of the nickel films.

In operation (shown in Fig. 2), the X-ray output from the tube is collimated by a dual lead collimator (shown in Fig. 2), about 2 mm in diameter (each path) and 1 cm long. The beam collimated normal to the beryllium window is used for X-ray fluorescence excitation of the sample (i.e., CuKα, NiKα, and AuLα). The second beam induces fluorescence in the lead collimator on the detector. To determine the thicknesses of the gold and nickel layers, the magnitude of the CuKα and NiKα lines from the sample are compared with the corresponding lines obtained from thick copper and nickel samples. The PbLβ line is used as a reference signal to account for variations in the X-ray flux

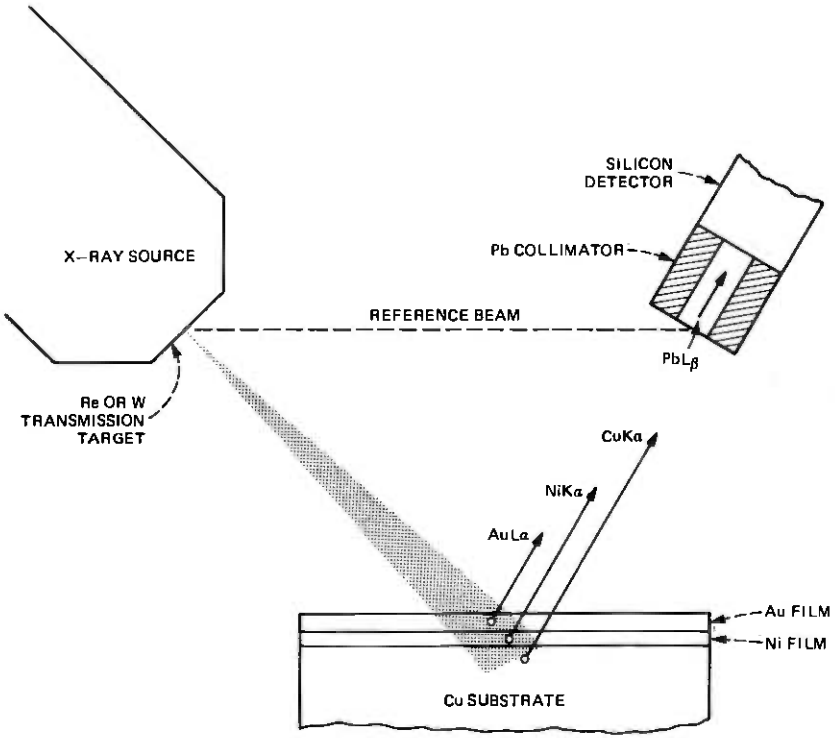

Fig. 2—Thickness measurement technique. The magnitude of the fluorescent lines from the sample (CuKα), NiKα, and AuLα, excited by the X-ray source, are measured by the silicon detector and the X-ray analyzer. The magnitude of those fluorescent lines is compared with the magnitude of the fluorescent lines obtained with thick layers of copper and nickel. The thickness of the gold and nickel layers is obtained by solving a system of two nonlinear equations with two unknowns in the computer built in the X-ray analyzer. The PbLβ line from the detector X-ray collimator is used to compensate for source intensity variations.

from the source. The presence of the PbLβ line increases the input count rate to the system. Therefore, some trade-off is needed in the magnitude of the PbLβ line and the minimum measurement time. In our present setup, the PbLβ line is not needed if the system is calibrated once a day. X-ray flux variations from one day to another are typically less than 2 percent for the counting statistics of our experiments.

2.2 X-ray source

The system X-ray source is manufactured by Watkins Johnson, with a tungsten or rhenium target capable of operating at 1 mA maximum current from 10 kV to 75 kV. The power supply regulation is better than 1 percent, and the long-term stability of the system is $\pm 3\sigma$, ($\sigma \approx (1/\sqrt{N})$, where σ is the standard deviation and N is the number of

counts in the detector. The electron beam spot size is less than 2 mm in diameter.

We have considered two kinds of X-ray sources, a reflection tube and a transmission tube. The experimental results reported here were performed with a conventional 50-kV solid tungsten target reflection tube with a side-mounted Be window. The transmission tube (schematically shown in Fig. 1), manufactured by Watkins Johnson to our specifications, consists of a 10-μm thick rhenium or tungsten dot about 3 mm in diameter deposited on a 250-μm thick beryllium foil about 1.25 cm in diameter. This geometry allows the target to be located very close to the sample (<2 cm) to maximize the X-ray flux and reduce the measuring time. However, the fluorescence excitation obtained from the transmission tube was considerably lower than the one produced by the side window tube.

2.3 X-ray detector and electronics

The X-ray detector is a conventional nitrogen-cooled, lithium-doped silicon detector (3 mm thick), manufactured by PGT (Princeton Gamma Tech). The effective detector diameter is 4 mm and the detector-to-window distance is 3 mm. In order to reduce the detector-to-sample distance, the detector nozzle diameter is about 16 mm.

After being amplified and processed by proper pileup rejection, the detector output is fed into a PGT 1000 multichannel analyzer. The analyzer has 16 kbits of memory and two floppy disks (256,000 words). The disks are used for basic programs and thickness calculations. The analyzer allows for qualitative analysis with automatic element identification. The system has the capability of performing quantitative analysis with appropriate software. If analysis of elements with $Z < 13$ is required, the system may be operated in vacuum or in a helium chamber.

2.4 Detector collimator

A typical lead collimator used on the 16-mm diameter detector nozzle is shown in Fig. 3. It consists of a truncated conical hole (in the lead piece) of about 1.7 cm long. The collimator is constructed by casting lead in an appropriate mold. This shape was chosen to maximize the detector solid angle. The smallest aperture in the cone is about 100 μm in diameter, and the largest aperture is about 3.5 mm in diameter. In operation, the sample is placed in contact with one of the surfaces of the lead piece. This surface is covered with a smooth surface (like glass), as shown in Fig. 3. The excited fluorescence from the sample is transmitted to the detector through the collimator. Therefore, the collimator serves two purposes: (i) it maximizes the fluorescence signal reaching the detector from a small area on the

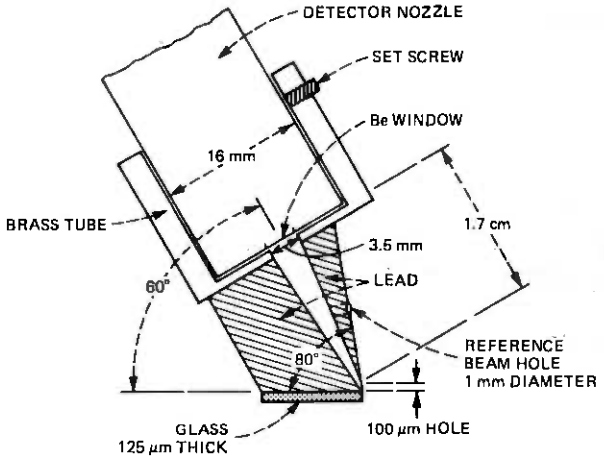

Fig. 3—Detector collimator.

sample and (*ii*) it determines the distance from sample to detector to minimize geometrical errors. The average distance from the 100-μm aperture in the collimator to the sample is about 100 μm.

2.5 Optical alignment

In our prototype system, the alignment is performed under a microscope by removing the collimator from the detector. The alignment also may be performed optically by means of a telescope (shown in Fig. 1) and an *XYZ* positioner. In this arrangement, the sample may be moved in the *XY* plane against the glass surface of the collimator by means of the *XYZ* positioner. The collimator is provided with a fiducial mark (arrow) next to the 100-μm aperture to optically align the sample relative to the mark.

III. SYSTEM CONSIDERATIONS

To study the feasibility of the X-ray fluorescence system for the fast thickness measurement of small areas of gold and nickel on copper substrates, we needed an estimate of the required X-ray flux from the source. For this purpose, we calculated the magnitude of the CuKα lines from the substrate attenuated by the gold film. The calculations are presented in Appendix A using the model shown in Fig. 4. The results are shown in Fig. 5 normalized to the tube current and solid angles σ_{in}, σ_{out} defined in Fig. 4. The calculations for the AuLα radiation are presented in Appendix B, and the results are also shown in Fig. 5. For the case of a 1-mm diameter source, placed 10 mm away from a 100-μm diameter sample, with a sample-to-detector (12 mm^2) distance of 20 mm, we get $\sigma_{in}\sigma_{out} \approx 1.2 \times 10^{-6}$. For a 3.4 μm gold film (using the

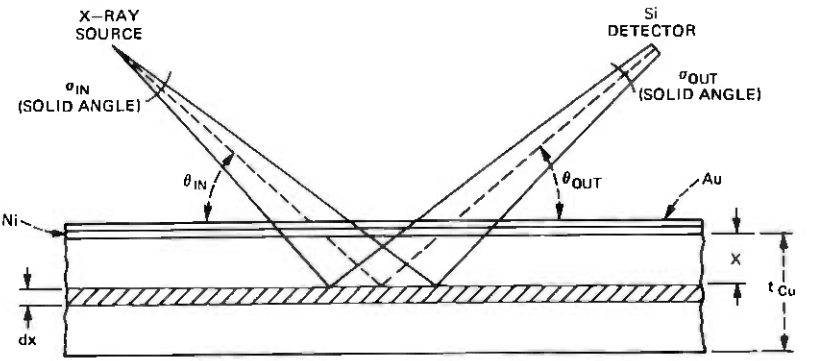

Fig. 4—Model used for calculations in the X-ray fluorescence system.

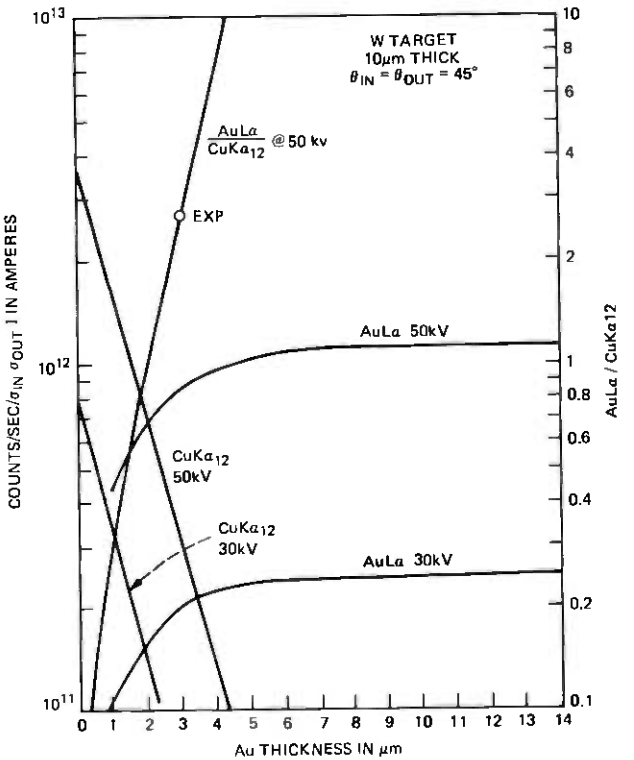

Fig. 5—Calculated counting rate/$\sigma_{in}\sigma_{out}$ I (amps) of the CuKα_{12} lines vs gold thickness at two different target voltages. The calculated counting rate/$\sigma_{in}\sigma_{out}$ I (amp) of the AuLα line vs gold thickness is also shown. The ratio of AuLα/CuKα_{12} lines is also shown in the figure. This ratio is independent of the input and output solid angles and the tube current. An experimental point is included in the figure to show the excellent agreement with the calculated value.

geometry described above), we get from Fig. 5 that a 1-mA, 50-kV tungsten tube, with a 10-μm tungsten filter, will produce about 360 counts/s of CuKα radiation at the detector. In practice (with no tungsten filter), because of the simultaneous presence of the NiK lines, the AuL lines, and the background radiation, the total count rate reaching the detector is considerably higher (a factor of 10 or more). Therefore, for a 1-mA tube current, the analyzer will have to handle count rates larger than 3500 counts/s. The programmable analyzer used in our system could process only about 3500 counts/s (6-μs time constant) with a 50-percent dead time; hence, the minimum counting time is limited by the analyzer and not by the X-ray source. To get good statistics (less than 5 percent error) in the NiKα line when measuring thin nickel films (less than 1 μm) under thick gold films (about 3 μm), it is necessary to have a counting time of about 20 s (real time, about 10 s lifetime). This performance is achieved using about 0.5 mA tube current with no tungsten filter. Shorter measuring times are possible if larger standard deviations are tolerable or when only gold films are present. In the last case, for gold films larger than 2 μm, only 1 or 3 s (real time) are needed. For thinner gold films, the statistical error in the CuKα is relatively small; however, the change in gold thickness for a given change in the counting rate is larger than for the case of thick gold films, as can be observed from Fig. 5. Therefore, for measuring thin gold films, a somewhat longer counting time is necessary if accuracies of less than 3 percent are desired. In our present system, a 5-s counting time is used for measuring single gold films larger than 0.4 μm for counting accuracies of about 5 percent.

IV. SIMULTANEOUS THICKNESS DETERMINATION OF TWO-LAYER SYSTEMS

4.1 Gold and nickel films

To minimize the interaction between the metallic layers, we have considered using a suitable filter in the source to provide a spectrum peaking at high energies (above 30 kV). However, doing this requires the penalty of having a lower fluorescence signal generated in the thin layers (in particular, the nickel layers less than 1 μm thick) when compared to the case of an unfiltered incident spectrum. The presence of the WL lines and the low energy background radiation from the X-ray source increases the NiKα fluorescence due to the high absorption of nickel at those energies. Therefore, in order to increase the accuracy of our measurements, we are presently using a reflection system with an unfiltered tungsten target capable of efficient generation of X-ray energy down to a few kilovolts. Under these conditions, the interaction between the layers can occur in two ways: (*i*) by one layer (or layers) absorbing incident radiation effective for excitation of fluorescence in

another layer underneath; or (*ii*) by secondary fluorescence (this case is always present independent of the incident spectrum) that occurs when fluorescence lines excited in one layer induce fluorescence in other layers (increasing the total fluorescent radiation from this layer).

In the case of the gold-nickel-copper system, the thickness of the top gold layer affects the fluorescence of the nickel and copper layers underneath it in the two ways mentioned above and described in detail below. The incident radiation from the X-ray tube induces L electron transitions in the gold film. The AuL lines produced in this manner are absorbed by the nickel film and the copper substrate and induce NiKα and CuKα radiation on both metal layers respectively. This secondary induced radiation adds to the excited radiation induced by the incident beam (attenuated by the gold layer) in the nickel and copper layers and, if not corrected for, gives an apparent increase in the nickel thickness. Furthermore, as mentioned before, the WLα line, from the source (very effective in exciting NiKα radiation) is reduced in amplitude by the gold layer. Therefore, as the gold thickness increases, we expect a large decrease in attenuation of the incident radiation effective to excite the NiKα line. This is because the spectrum has been filtered and the radiation available for excitation of the NiKα line now lies at higher energies and is less effective than in the case without gold where the WLα (~8.2 kV) was the predominant excitation mechanism. As mentioned above, there is also a secondary excitation effect for the CuKα line due to the gold film fluorescence and also an effect due to the gold film absorption of the incident radiation. However, the energy of the WLα, line is below the copper K absorption edge and only the continuum radiation (higher energy) contributes to the CuKα excitation. The effect on the CuKα line due to the presence of the gold film was found experimentally to be small in the range of Au thickness of interest (0 to 5 μm).

The calculation of the above interactions is very involved and will not be presented in this paper. Fortunately, the above effects tend to compensate for each other in the range of gold thicknesses below 4 μm, and can be corrected in first order by assuming that the effective absorption coefficient of gold to the NiKα line decreases linearly with the thickness of the gold layer. For thicker gold films, an exponential correction has been found adequate. For a given geometry of the system, we can write for the attenuation coefficient of gold to the NiKα line

$$\alpha_{\mathrm{NiK}_\alpha}^{\mathrm{Au}} = \alpha_1 + \alpha_2 t_{\mathrm{Au}}, \tag{1}$$

where α_1 and α_2 are determined experimentally. The magnitude of the NiKα line measured after a gold thickness t_{Au} is given by the empirical formula

$$\mathrm{NiK}\alpha = \mathrm{NiK}\alpha_\infty[1 - \exp(-\alpha_3 t_{\mathrm{Ni}})]\exp(-\alpha^{\mathrm{Au}}_{\mathrm{NiK}\alpha} t_{\mathrm{Au}}), \tag{2}$$

where $\mathrm{NiK}\alpha_\infty$ is the magnitude of the NiKα line for a thick Ni plate (>25 μm) and an α_3 and an $\alpha^{\mathrm{Au}}_{\mathrm{NiK}\alpha}$ are experimentally determined parameters.

The magnitude of the CuKα line (in a given system) attenuated by the nickel and gold layers is given by

$$\mathrm{CuK}\alpha = \mathrm{CuK}\alpha_\infty \exp(-\alpha^{\mathrm{Ni}}_{\mathrm{CuK}\alpha} t_{\mathrm{Ni}})\exp(-\alpha^{\mathrm{Au}}_{\mathrm{CuK}\alpha} t_{\mathrm{Au}}), \tag{3}$$

where $\mathrm{CuK}\alpha_\infty$ is the magnitude of the CuKα line obtained from a thick copper plate, and $\alpha^{\mathrm{Ni}}_{\mathrm{CuK}\alpha}$ and $\alpha^{\mathrm{Au}}_{\mathrm{CuK}\alpha}$ are the attenuation coefficients of nickel and gold to the CuKα line, respectively. It must be clarified at this point that $\alpha^{\mathrm{Au}}_{\mathrm{CuK}\alpha}$, $\alpha^{\mathrm{Au}}_{\mathrm{NiK}\alpha}$, and $\alpha^{\mathrm{Ni}}_{\mathrm{CuK}\alpha}$ include the attenuation of the incident X-ray beam as well as the attenuation by the gold or nickel layer of the excited fluorescent beam, and depend on the geometry of the system.

Because the NiKβ line is very close in energy to the CuKα line it is necessary to correct the measured CuKα line $\mathrm{CuK}\alpha_M$ in the following way:

$$\mathrm{CuK}\alpha = \mathrm{CuK}\alpha_M - \alpha_5 \mathrm{NiK}\alpha[1 + (\alpha^{\mathrm{Au}}_{\mathrm{NiK}\alpha} - \alpha^{\mathrm{Au}}_{\mathrm{CuK}\alpha}) t_{\mathrm{Au}}], \tag{4}$$

where α_5 is determined experimentally by measuring the number of counts in the CuKα window produced by a pure nickel sample, and knowing the ratio NiKβ/NiKα. The quantity in parenthesis corrects by the difference in absorption for the CuKα and NiKα lines in gold. Typically, $\alpha_5 \approx 0.037$ and $\alpha^{\mathrm{Au}}_{\mathrm{NiK}\alpha} - \alpha^{\mathrm{Au}}_{\mathrm{CuK}\alpha} \approx 0.08$ (average).

From eqs. (1) to (4) we can solve for the nickel and gold thicknesses:

$$t_{\mathrm{Ni}} = \frac{1}{\alpha_3} \ln\left(1 - \frac{\mathrm{NiK}\alpha}{\mathrm{NiK}\alpha_\infty} \exp \alpha^{\mathrm{Au}}_{\mathrm{NiK}\alpha} t_{\mathrm{Au}}\right)^{-1} \tag{5}$$

$$t_{\mathrm{Au}} = \frac{1}{\alpha^{\mathrm{Au}}_{\mathrm{CuK}\alpha}} \ln\left(\frac{\mathrm{CuK}\alpha_\infty \exp(-\alpha^{\mathrm{Ni}}_{\mathrm{CuK}\alpha} t_{\mathrm{Ni}})}{\mathrm{CuK}\alpha_M - \alpha_5 \mathrm{NiK}\alpha[1 + (\alpha^{\mathrm{Au}}_{\mathrm{NiK}\alpha} - \alpha^{\mathrm{Au}}_{\mathrm{CuK}\alpha}) t_{\mathrm{Au}}]}\right). \tag{6}$$

Equations (5) and (6) may be solved by successive iterations taking the initial value of $t_{\mathrm{Au}} = t_{\mathrm{AUF}}$, where t_{AUF} is the thickness of gold film* obtained by direct fluorescence:

$$t_{\mathrm{AUF}} = \frac{1}{\alpha_6} \ln\left[1 - \frac{\mathrm{AuL}\alpha}{\mathrm{AuL}\alpha_\infty}\right]^{-1}, \tag{7}$$

* Although the iteration could be started from any initial value of t_{AUF}, the value of t_{AUF} obtained from eq. (7) is very useful when measuring gold thin films less than 1 μm thick. If the value of t_{AU} [obtained by eq. (6)] $\ll t_{\mathrm{AUF}}$, the thin film is suspected of having a large pinhole density.

where $AuL\alpha_\infty$ is the magnitude of the $AuL\alpha$ line for a thick gold film (>10 μm) and α_6 is determined experimentally. In addition, by manipulating eqs. (2), (3), and (7) it is possible to obtain a system of two equations with two unknowns that involve the ratio of the fluorescent lines to the $CuK\alpha$ line. These equations are independent of the geometrical and intensity variations of the measuring apparatus.

These equations are:

$$t_{Ni} = \frac{1}{\alpha^{Ni}_{CuK\alpha}} \ln \frac{AuL\alpha_\infty}{CuK\alpha} \frac{CuK\alpha_\infty}{AuL\alpha_\infty} [1 - \exp(-\alpha_6 t_{Au})]^{-1} \times \exp(-\alpha^{Au}_{CuK\alpha} t_{Au}) \quad (5')$$

$$t_{Au} = \frac{1}{\alpha^{Au}_{CuK\alpha} - \alpha^{Au}_{NiK\alpha}} \ln \frac{NiK\alpha}{CuK\alpha} \frac{CuK\alpha_\infty}{NiK\alpha_\infty} \frac{\exp(-\alpha^{Ni}_{CuK\alpha} t_{Ni})}{1 - \exp(-\alpha_3 t_{Ni})}, \quad (6')$$

where $\alpha^{Au}_{NiK\alpha}$ is given by (1) and $CuK\alpha$ is given by eq. (4). However, the experimental results presented in this paper were not obtained using eqs. (5′) and (6′). A value for t_{AuF} can also be found by the ratio of the $AuL\alpha/CuK\alpha$ when the nickel thickness is small as shown in Fig. 3, and also by the ratio of $AuL\alpha/AuM\alpha_{12}$ for any thickness of nickel (providing a calibration curve for $AuL\alpha/AuM\alpha_{12}$ vs t_{Au} is obtained). The determination of the Au thickness by the ratio of $AuL\alpha/AuM\alpha_{12}$ could prove to be an effective technique, assuming that enough counts are obtained in the $AuM\alpha_{12}$ line for a desired measurement time. The $AuM\alpha_{12}$ is attenuated somewhat by the air between the detector and the sample. (This attenuation can be taken care of in the calibration of t_{Au} vs $AuL\alpha/AuM\alpha_{12}$). This correction may not be necessary if the full fluorescence analysis capability (detection of elements with <13) of the system are utilized by filling the sample chamber with helium or operating under vacuum. The use for the $AuL\alpha/AuM\alpha_{12}$ ratio in determining the gold thickness is essential for determining the thickness of gold-nickel and copper layers on some other substrate, as discussed below.

4.2 Measurements of other metallic layers

4.2.1 The three-layer system: gold-nickel-copper

Using the fluorescence technique, it is possible to determine the thickness of gold on nickel on copper layers (<10 μm) on unknown thickness palladium substrates. The gold thickness (t_{Au}) is first determined by the $AuL\alpha/AuM\alpha_{12}$ ratio from a previously determined dependence. The thickness of the nickel and copper layers is then determined by the direct fluorescence of those layers attenuated by the layers above.

The fluorescence $K\alpha$ radiation in a given system due to the copper layer is given by

$$\text{CuKa} = \text{CuK}\alpha_\infty[1 - \exp(-\beta t_{\text{Cu}})]\exp(-\alpha^{\text{Ni}}_{\text{CuK}\alpha} t_{\text{Ni}})\exp(-\alpha^{\text{Au}}_{\text{CuK}\alpha} t_{\text{Au}}), \quad (8)$$

where β is a parameter determined experimentally.

The magnitude of the NiKα line is given by eq. (2). Using eq. (4) to correct for the measured (CuKα_{M}) and eq. (1) for other corrections, we get a system of two equations, (2) and (8) with two unknowns, t_{Ni} and t_{Cu}. Equation (2) can be directly solved for t_{Ni}, knowing t_{Au} (from above) and eq. (8) can then be solved for t_{Cu}.

In all the above calculations we have neglected the effect of the CuKβ line on producing NiKα fluorescence. This effect is lumped in $\alpha^{\text{Au}}_{\text{NiK}\alpha}$ given in eq. (1).

4.2.2 The two-layer system: gold and indium on thick copper substrates

The thicknesses of the gold and indium layers can be obtained in two different ways: (*i*) by first determining the t_{Au} by the AuLα/AuMα ratio and then getting t_{In} by the attenuated InLα line transmitted by the gold layer or (*ii*) by using eqs. (1) to (7) with InLα substituted by NiKα and using $\alpha^{\text{In}}_{\text{CuK}\alpha}$ and $\alpha^{\text{Au}}_{\text{InL}\alpha}$ for the exponentials.

V. EXPERIMENTAL RESULTS

To determine the thickness of the gold, t_{Au}, and nickel, t_{Ni}, layers (on the copper substrates), the number of counts (photons excited by fluorescence) in selected characteristic lines of the metallic layers and substrate are measured. The magnitude of the CuKα and NiKα lines from the sample are compared with the magnitude of the CuKα and NiKα lines produced by thick metallic plates of copper and nickel. The magnitude of the AuLα line is also compared with the AuLα line produced by a thick gold plate to obtain an approximate value of the gold thickness t_{AUF}. For gold films less than 2 μm thick, the value of gold thickness t_{Au} obtained from the magnitude of the CuKα and NiKα lines when compared with t_{AUF} gives information on the physical characteristics of the gold film. If $t_{\text{AUF}} \gg t_{\text{Au}}$, the gold film may not be uniform in thickness due to pinholes or other defects.

The system calibration consists of two steps: (*i*) obtaining the values of the parameter α's defined in the last section and (*ii*) obtaining the magnitude of the characteristic lines corresponding to thick layers. For a given system geometry, the first step is done only once (when the system is set up). The second step is done as a routine check once a day (normally no changes are necessary over a period of several days). The second step could also be done only once if a reference signal (PbLβ) is utilized to compensate for variation in X-ray flux from the source.

Typical values of $\alpha^{\text{Au}}_{\text{NiK}\alpha}$, $\alpha^{\text{Au}}_{\text{CuK}\alpha}$, $\alpha^{\text{Ni}}_{\text{CuK}\alpha}$ used in eqs. (5) and (6) as measured in our system are listed in Table I. The experiments were done by placing layers of gold and nickel (of known thicknesses) on

Table I

For $\theta_{in} = \theta_{out} = 45°$
$\alpha^{Au}_{CuK\alpha} = 0.75$
$\alpha_1 = 0.84$
$\alpha^{Ni}_{CuK\alpha} = 0.15$
$\alpha_2 = 0.06$
$\alpha_3 = 4.87$
$\alpha_5 \approx 0.037$

copper or nickel substrates and comparing the magnitude of the CuKα or NiKα lines from the substrate with and without the layers. The value of α_3 was obtained from a known sample of nickel on a copper substrate for $t_{Au} = 0$. The values of α_1 and α_2 were obtained by measuring three standard samples in the range of 0.4 to 4 μm provided by T. Briggs (Western Electric), which had been previously measured by atomic absorption. For $\alpha = \alpha^{Au}_{NiK\alpha}$ (measured above) and $\alpha_2 \approx 0.06$, the three samples were measured with 5 percent of the nominal values for the gold films and within 10 percent of the nominal values for the nickel films. A more precise fit was not attempted due to the unknown tolerances of the standard samples.

The measurement time used for the standard samples was 100 s (real time). A 10-μs pulse-shaping time constant was used in the amplifier and the pileup rejector. The count rate reaching the detector was about 1000 c/s with a 0.15-mA X-ray tube beam current at 50 kV. The target-to-sample distance was about 6 cm, and the detector-to-sample distance was about 1 cm.

To determine the reliability of the thickness measurements, the following experiment was performed. We measured several lead frame samples of the shape shown in Fig. 6. Each finger (16 per sample) was measured at the tip (dashed elliptical area in Fig. 4) and the thickness of gold and nickel were recorded. The measuring spot size was about 125 $\times$ 175 μm. Subsequently, the samples were measured by R. C. Kershner and N. Panousis at Bell Laboratories, Allentown by cross sectioning. The results are shown in Table II for the gold and Table III for the nickel.

The results performed using the X-ray technique were reproducible within $\pm$2.4 percent for the gold thicknesses and $\pm$4 percent for the nickel thicknesses in a series of 10 measurements (100 s each) in a given finger. The counting statistics were estimated to be $\pm$1.2 percent for the gold thickness measurements (7000 counts in the CuKα line) and $\pm$2.6 percent for the nickel thickness measurements (1500 counts in the NiKα line). Variations of $\pm$10 percent were observed along the tip of the fingers except for Sample 730 in which, due to off-centering of the plated pattern, larger variations were observed (as shown in Table II). The absolute accuracy of the X-ray measurements is mainly

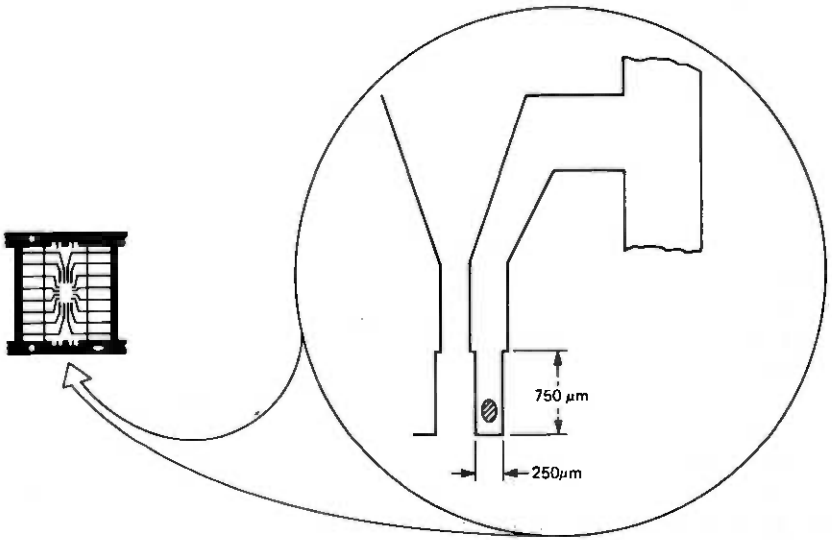

Fig. 6—Detail of lead frame. One of the fingers (leads) is magnified to show the effective area of X-ray measurement.

Table II—Au thickness (μ inches)

	Sample 730		Sample 801		Sample 822	
Lead No.	X-Ray	Cross Section	X-Ray	Cross Section	X-Ray	Cross Section
1	112.6	110.2	99.3	93.9	155.8	151.1
2	97.4	109	99.4	103	143.3	149.3
3	104.5	113.8	104.6	112.6	140.3	151.7
4	63.8–115*	116.6	99.6	113.2	151.6	162.5
5	102.3	111.4	106.5	112.0	150.4	155.3
6	69.8–115.8*	112.6	108.9	98.7	158.5	157.7
7	103.6	94.5	96.8	99.9	153.1	139.7
8	92.8	109.6	96.2	101.7	159.3	152.3
9	100.8–116.8*	106.6	98.8	104.1	152.5	150.5
10	93.5	95.1	98.9	96.3	148.3	143.9
11	102.3	111.4	99.3	102.3	156.3	153.5
12	98	116.2	103.6	99.9	155	159.5
13	102.2	107.2	99.9	101.1	154.3	152.9
14	101.6	107.8	107.1	99.9	155	146.9
15	97.2	104.2	96.9	101.1	146.5	141.5
16	107.5	104.8	97	104.2	148.9	153.5

* Uneven sample plating due to off-centering.

determined by the standard samples, the counting statistics, background corrections, and variations in system geometry. Due to the collimator design, the latter effect probably can be neglected. The scattering by the sample of the WLα line from the source (very close in energy to the CuKα line) precludes the use of background correction for the CuKα line. However, background correction for the NiKα line

Table III—Ni thickness (μ inches)

Lead No.	Sample 730		Sample 801		Sample 822	
	X-Ray	Cross Section	X-Ray	Cross Section	X-Ray	Cross Section
1	24.7	18.7	19.4	11.4	30.3	19.3
2	22.8	15.7	20.1	12.0	28.9	21.7
3	25.8	15.7	21.3	14.5	29	20.5
4	22.2	15.7	20.7	13.8	31.3	22.9
5	23.9	15.1	21.5	15.7	29.9	22.3
6	25.9	15.1	22.9	10.8	30.2	25.5
7	23.7	15.7	19.8	13.8	29.6	18.1
8	22	16.3	19.3	13.2	31.1	19.9
9	27.6	15.7	20.4	12.6	29.2	19.9
10	23.7	16.3	20.3	13.2	29.5	23.5
11	24.7	16.3	19.2	13.8	30	19.3
12	23.2	14.4	20.8	12.6	31.2	19.9
13	23.2	14.5	19.7	14.5	31.5	22.3
14	23.4	13.2	20.7	13.8	31.3	22.3
15	23.6	17.5	19.3	11.4	29.6	23.5
16	25.5	16.3	18.1	12.0	28.7	16.9

is possible, but was not used in the reliability experiments. We assume that the standard samples are within ±5 percent of the true value of gold thickness and within ±10 percent of the true value of nickel thickness. The absolute accuracy of the X-ray measurements is about ±6 percent for gold, in which background correction can be neglected, and ±11 percent for nickel, also neglecting background correction. However, lack of NiKα background correction could make the thin (<0.5 μm) nickel films appear somewhat thicker. Automatic background correction for both gold and nickel thickness determinations is presently being done without increasing the measurement time, using a rhenium target X-ray tube (the ReLα and the CuKα lines are well separated).

When we compare the results shown in Tables II and III, we must bear in mind that the X-ray results indicate an average on a small, approximately elliptical, area while the cross-sectioning results indicate an average along a cord in the ellipse. Therefore, we do not expect complete agreement unless the films are uniform in the measured area. This was not always the case, since variations in thickness of ±10 percent were observed along a given fingertip. These variations together with the accuracy of the measurements could show a spread in gold thicknesses of ±12 percent and certainly an even larger spread for the nickel thicknesses. The cross-sectioning results shown in Table II are claimed to be within ±5 percent of the true value. From Table II we observe that the maximum discrepancy between the two measuring techniques in any finger (not considering Sample 730, already discussed) was about 12 percent in Lead No. 4 of Sample 801. This result agrees very well with the estimated 6-percent accuracy of the X-ray

technique. The excellent agreement is substantiated by the fact that the correlation coefficient for both techniques (gold measurement) is 0.96, taking the higher values with asterisk in Sample 730. The correlation coefficient was calculated comparing the three samples (48 measurements in each technique). The accuracy of the nickel thicknesses obtained by cross-sectioning was claimed to be ±50 percent. Therefore, very good agreement is not expected in Table III. However, we observe from the table that both techniques indicate that Sample 801 has the thinnest nickel film and Sample 822 has the thickest. The correlation coefficient for the nickel film measurements is about 0.9.

VI. CONCLUSIONS

In this paper, we demonstrated the capabilities of monitoring the thickness of small areas of gold and nickel thin films deposited on copper substrates, in time less than 20 s. The accuracy of the system depends on the measuring time and also on the accuracy of the standard samples used to calibrate the system. One possible source of error is the variation in distances among the sample, the detector, and the X-ray source. This has been minimized by the design of a special lead collimator to fix the geometry of the system. The collimator also maximizes the detector solid angle relative to the sample to decrease the measuring time. (This variation could also be eliminated as described above by utilizing the ratios of the fluorescent lines.)

Shorter measurement times can be obtained either by using a pulsed X-ray source to decrease system dead time or by using a faster X-ray analyzer. Increasing the spot size probably would also be worthwhile in order to obtain a more meaningful average on a given sample due to nonuniformity of metallization. Finally, the system described in this paper also has the capability of chemical qualitative analysis.

VII. ACKNOWLEDGMENTS

The authors wish to thank G. A. Coquin and D. R. Herriott for many helpful discussions, C. J. Schmidt for constructing the detector collimator and technical assitance, W. Flood and C. Steidel for providing the lead frame samples. T. Briggs* of Western Electric (Allentown) for providing the standard samples, and R. Kershner and N. Panousis for the cross-section measurements.

---

* T. Briggs has built a thickness measuring production system based on the prototype described in this paper. The system is presently being used at the Western Electric facility in Allentown, Pa., for monitoring lead frames used in packaging integrated circuits.

APPENDIX A

$CuK\alpha_{12}$ Fluorescence Counting Rate in the Reflection System

The $CuK\alpha_{12}$ fluorescence in the reflection system can be obtained using Fig. 4. The incident X-rays from the source subtending a solid angle σ_{in} are partially absorbed by the gold and nickel films and then by the copper substrate. At any depth x, these X-rays excite isotropic fluorescent $K\alpha_{12}$ radiation from an element of volume of thickness dx equal to

$$dN_{CuK\alpha} = 1.66 \times 10^{12}\sigma_{in}\sigma_{out} I\, dx \int_{8.3}^{V_0} \sin\theta_{in} \frac{\mu_{Cu}\rho_{Cu}}{\exp(-\mu_w\rho_w t_w)} \times \left(\frac{V_0}{V} - 1\right)\exp[-(\mu_{Cu}\rho_{Cu}\csc\theta_{in} + \mu_{Cu}^{CuK\alpha}\rho_{Cu}\csc\theta_{out})] \times \exp[-(\mu_{Ni}\rho_{Ni}\csc\theta_{in} + \mu_{Ni}^{CuK\alpha}\rho_{Ni}\csc\theta_{out})t_{Ni})] \times \exp[-(\mu_{Au}\rho_{Au}\csc\theta_{in} + \mu_{Au}^{CuK\alpha}\rho_{Ni}\csc\theta_{out})t_{Au}]\, dV, \quad (9)$$

where σ_{out} is the detector solid angle, σ_{in} and σ_{out} are defined in Fig. 4, and the mass absorption coefficients of the different materials to the $CuK\alpha_{12}$ radiation have been considered. The expression given by Kramers[3] for the continuum radiation from a tungsten target has been used in the calculations.

For source-to-sample and sample-to-detector distances, large relative to the copper substrate effective thickness (~30 μm), we can write for the total $CuK\alpha_{12}$ radiation reaching the detector:

$$N_{CuK\alpha_{12}} = 1.66 \times 10^{12}\sigma_{in}\sigma_{out} I \times \int_{8.3}^{V_0} \frac{\mu_{Cu}\rho_{Cu}(V_0/V)\exp(-\mu_w\rho_w t_w)}{\sin\theta_{in}(\mu_{Cu}\rho_{Cu}\csc\theta_{in} + \mu_{Cu}^{CuK\alpha}\rho_{Cu}\csc\theta_{out})} \times(1 - \exp[-(\mu_{Cu}\rho_{Cu}\csc\theta_{in} + \mu_{Cu}^{CuK\alpha}\rho_{Cu}\csc\theta_{out})t_{Cu}]) \times \exp[(\mu_{Ni}\rho_{Ni}\csc\theta_{in} + \mu_{Ni}^{CuK\alpha}\rho_{Ni}\csc\theta_{out})t_{Ni}] \times \exp[-(\mu_{Au}\rho_{Au}\csc\theta_{in} + \mu_{Au}^{CuK\alpha}\rho_{Ni}\csc\theta_{out})t_{Au}]\, dV, \quad (10)$$

where the × integration through the copper substrate was already performed. The results obtained from eq. (9) are presented in Fig. 5 for two different cases.

APPENDIX B

Calculation of the Direct AuLα Fluorescence

The model used for the following calculations is based on Fig. 4 with the copper substrate substituted by the gold film and by eliminating

any additional films. Integrating through the gold thickness, the AuLα fluorescence counting rate is given by

$$N_{\mathrm{AuL}\alpha} = 4.7 \times 10^{11} B \int_{11.9}^{V_0} \frac{(V_0/V - 1)}{B/V^{2.7} + 0.275(\sin\theta_{\mathrm{in}}/\sin\theta_{\mathrm{out}})}$$
$$\times\left(1 - \exp\left[-\left(\frac{B \csc\theta_{\mathrm{in}}}{V^{2.7}} + 0.275 \csc\theta_{\mathrm{out}}\right)t_{\mathrm{Au}}\right]\right)$$
$$\times \frac{1}{V^{2.7}} \exp(-380 t_w/V^{2.65})\, dV,$$

where a W target of thickness $t_w(\mu\mathrm{m})$ is assumed and where B is a parameter which defines μ_{Au} between the different L absorption edges. $B = 297.9$ for $11.9 \leq V < 13.7$, $B = 410$ for $13.7 \leq V < 14.3$, and $B = 570.4$ for $14.3 \leq V \leq V_0$. The results are shown in Fig. 5 of the text.

REFERENCES

1. H. A. Liebhafsky, et al., *X-Ray Absorption and Emission in Analytical Chemistry*, New York: John Wiley & Sons, 1960.
2. R. H. Zimmerman, "Industrial Applications of X-Ray Methods for Measuring Plating Thickness," Advances in X-Ray Analysis, *4*, 1961, p. 335.
3. H. A. Kramers, Phi. Mag., *46*, 1923, p. 836.

THE BELL SYSTEM TECHNICAL JOURNAL
Vol. 58, No. 8, October, 1979
Printed in U.S.A.

The Nature and Use of Limit Cycles in Determining the Behavior of Certain Semideterminate Systems

by S. V. AHAMED

(Manuscript received May 3, 1979)

For some well-known systems such as speech encoders or digital filters, the excursions of the input are so dramatic and so loosely correlated that the system performance itself appears indeterminate. For these systems we present a technique of determining the system behavior by feeding a set of coherent frequency signals. For the analog inputs of any such system, we derive these inputs from coherent frequency synthesizers all synchronized to a common signaling frequency. For digital inputs into the system, we derive these inputs from a single master clock and set of logic functions to yield the desired bit patterns at different input ports. We present experimental evidence of the existence and utilization of these limit cycles for systems with some initial knowledge about the configuration and interconnections of components. The techniques presented here do not apply to systems for which complete initial ignorance is asserted.

I. INTRODUCTION

In the context of this paper, a limit cycle is defined as the periodic output into which the behavior of a system is forced by controlling one or several periodic inputs. The conditions which lead to an operation under a limit cycle vary from system to system. A perfectly linear system may exhibit a level-insensitive, limit-cycle condition whenever the input frequencies bear integral relationship(s) with respect to each other. A highly nonlinear system may exhibit several level-sensitive limit-cycle operations for each integral relationship(s) between the input signal frequencies. General techniques for using these limit cycles to evaluate and categorize system behaviors are presented. However, it is up to the ingenuity of the experimentalist to use the techniques to obtain the information sought about the system.

The coherence of the input signals is the fundamental concept behind the generation of limit cycles. For example, consider a network with several input ports. A set of input signals to the system would not produce a periodic response unless the inputs were mutually coherent, as well as individually periodic. The availability of stable frequency synthesizers and jitter-free digital signal generators has an immense effect on the stability of limit cycles and thus upon the design of experiments for evaluating the system behavior. In a sense, the technique is an extension of the single-input, single-output analysis which probes the system by changing the frequency and amplitude of the input signal. With multiport systems, the concept is expanded by using *coherent, periodic, and jitter-free* signals at the inputs. Phase jitter of analog signals and timing jitters of digital signals have detrimental effects on the stability of the limit cycles.

The determination of the behavior of semideterminate systems is often sought by exciting it with a given input signal and measuring the output response. Such techniques are potentially made difficult by variations in the initial state of the system when excited and the brevity of the measurement duration. The more suitable technique would be to excite the system in such a manner that a periodic response is generated. Furthermore, if a variety of input excitation exists which generate a variety of periodic responses, several aspects of system behavior can be probed. The basic condition for the generation of such periodic responses is that all input signals to the system be coherent. The condition of coherence is often difficult to achieve in real systems since random effects typically occur within the system. The random effects which cause variations in the functions performed by the system components are generally negligible. However, the additive random signals due to noise generation, etc. are usually not negligible and prevent fully coherent system signals.

Many systems exhibit the phenomenon of limit-cycle* behavior, however. Limit-cycle behavior is basically generation of a periodic output response with the application of a given set of periodic input signals despite the random, aperiodic noise effects. The limit-cycle behavior therefore allows coherent periodic input signals to be used to generate periodic output responses in a real system contaminated by random effects. The excitation of a limit cycle requires that a specified and well-controlled set of inputs be provided to the system. A somewhat stronger definition of limit-cycle behavior is used here to allow characterization of the overall system in terms of the behavior of

* Limit cycles generally degrade the system performance and for this reason they have been routinely eliminated, suppressed, or controlled (see the IEEE Trans. on Circuits and Systems, *CAS 24*, No. 6 (June 1977), p. 291 or 300). However, under specific conditions they provide an insight into the behavior of complex systems.

individual components. In particular, a stable limit cycle is defined as the condition in which the terminal voltages and currents for each component of the system are periodic, when random noise and circuit element parameter variations are included. Limit-cycle hopping occurs when the random effects are sufficient to disrupt a given limit cycle and trigger a new limit cycle with the same set of coherent signals applied. Limit-cycle hopping may occur since there may be more than one stable limit cycle associated with a given set of coherent input signals.

The discussion below characterizes some properties of limit-cycle behavior and presents examples of the use of limit cycles in determining the behavior of systems compatible with such an approach. In presenting limit cycles as a potential probe of system behavior, an important consideration is the variety of limit cycles which can be excited upon variation of the input signals. Examples of changes in the system inputs which may lead to different limit cycles are presented.

The most common method of visual and experimental observation of the system behavior is by synchronizing the oscilloscopic sweep with the frequency of input variation into the system. However, for a multi-input system consisting of both digital and analog inputs, the principle may be extended by ascertaining that the periodic repetition of all the inputs is derived from a common source frequency. Many such standard common source frequencies (e.g., Cesium clock, 64-kHz and 8-kHz standard signals, or any one of the overall Bell System synchronization[1] network frequencies at central offices) are available within the telephone network.

The nonlinearities within the system generally cause the system behavior to be level-sensitive after the synchronization of inputs has been achieved. However, if hysteresis and jump effects are tentatively ignored, then a finite set of input levels may often be achieved,* which will force perfectly repetitive behavior from the system. The number of components and the interaction of the nonlinearity of the various components also influence the level at which the system would reach a "limit cycle."

II. CHARACTERISTICS OF A LIMIT CYCLE

2.1 Modality of the limit cycle

When a set of coherent frequencies are present at the input to a system, then its reaction would tend, for certain parameter values, to

* In some "systems," limit cycle will never be achieved. For instance, take the case of an unbounded system or the case where the input is open-circuited and the output is connected to a source of arbitrary frequency or a case where the system has an infinite memory with variable initial conditions.

stabilize itself repeatedly during that minimum duration which can accommodate an integral number of cycles of each input frequency. For instance, when a linear delta modulator has a clock frequency of 24 kHz and the audio frequency (generated coherently from the 24 kHz) is 1.8 kHz, then the binary pattern generated would be perfectly repetitive every 1⅔ ms, thereby constituting three of 1.8-kHz cycles and 40 of 24-kHz cycles, and so on. Further, an oscilloscopic sweep should be able to display the voltages and currents at each component of the encoder and decoder as a stationary pattern. The nonlinearity of the adaptive delta modulation (ADM) introduces another dimension into the problem. Whereas the binary patterns, voltages, and currents, may be stable for selected values of the audio frequency input to a delta modulator without any memory effects, a further restriction of voltage levels for a limit cycle occurs for an adaptive delta modulator, because of the multiple weighted memory effects from the past bits. These tend to alter the final values of the currents and voltages of each of the components of the encoder and decoder from their initial values exactly 1⅔ ms earlier. Hence, the stability of the limit cycle, by definition, is that the voltages and currents for each component of the system do not violate the boundary condition every 1⅔ ms, or some integral multiple, which constitutes the duration of a limit cycle. Section A1 in the appendix describes the ADM codec operation[2] and Section A2 discusses the generation and experimental existence of such limit cycles for the ADM codecs.

The relative phases of the inputs also influence the existence of a stable limit cycle. When three coherent inputs A, B, and C, are forced at the inputs of a system, then the boundary conditions for various values of the phase relations between A, B, and C, would all be different. Such a condition influences the input levels for which the system would reach a limit cycle, especially if the former has nonlinear feedback. Under these conditions, the phase relations between the inputs offer another parameter to control the stability of the limit cycle if it is difficult to achieve by level adjustment alone.

2.2 Advantages of operation under limit cycle conditions

When the performance of a system and its components must be critically evaluated, then the limit cycle functioning presents a repeated picture of all the parameters within the system. Further, since a large number of limit cycles can be generated, the observer can obtain the parameters under a diversity of conditions, thus having an opportunity to "freeze" the performance of the components by synchronizing the inputs. Such a "frozen" picture would depict the component performance under a given set of conditions which would otherwise exist only as transients. (See Section A3 in the appendix.)

During early developmental steps of a system, these limit cycles offer an invaluable tool in critically deriving the component values and ascertaining their accurate performance.

These limit cycles can be used to characterize the system performance and the component values. Further, when uncertainty of performance* has to be eliminated, the inputs may be synchronized to study the effect on performance. The concept applies to both linear and nonlinear systems. For hybrid systems, both coherent analog and digital inputs may be derived from frequency synthesizers which also trigger pulse generators. While testing the coherence of a system in the time domain, the limit cycle still offers a means of validating the correct functioning. Coherent inputs under specific conditions produce a coherent output from determinate systems. This principle has been exploited to test the interfacing of a minicomputer from an ADM voice encoder. The computer clock, the ADM clock, and the audio frequency input are coherently derived with respect to a predefined frequency synthesizer. The received binary data within the memory must form a repetitious pattern repeating at the limit cycle frequency. When the sequence is permitted to accumulate over several seconds or minutes, the memory core locations at which the binary pattern repeats yields any malfunctioning of the interfacing. In addition, the exact input conditions which caused the error can be traced by the break in the limit cycle. This principle is further explained and utilized in Section A4 in the appendix.

III. STABILIZATION OF AN n INPUT SYSTEM

3.1 Analog system

Consider the n inputs into a system to be at $f_1, f_2, \cdots f_n$ Hz. The limit cycle would have a duration of t seconds, which is the lowest common multiple of $t_1, t_2 \cdots t_n$ seconds at the respective frequencies of $f_1, f_2, \ldots f_n$ Hz. If the frequencies are adjusted to have no phase jitter with respect to one another, then the initial boundary conditions at the start of the limit cycle are such as to lead to identical final boundary conditions at the conclusion of the limit cycle. Unless this criterion is satisfied, there is no limit cycle every t seconds. However, it is sometimes possible to meet these boundary conditions every $2t$, $3t$ seconds, etc. Under these circumstances, the limit cycle would form not at the lowest common multiple of $t_1, t_2 \ldots t_n$, but at its multiple values. When the number of inputs and the complexity increases, then

* We have successfully used this principle (Ref. 3) to eliminate the idle channel noise (which becomes worse as the clock rate diminishes) of an ADM decoder by forcing a bit pattern of 0101 ···, 00110011, 01001101, etc. (derived from the master clock) during silence periods.

it becomes more and more frequent to see the limit cycle* itself hopping from one period to another (say, from $2t$ to $3t$ seconds and so on). Stabilization of an n input system thus becomes progressively more difficult as n increases considerably.

When the wave shapes of various inputs are not sinusoidal, the response of the system contains transient or higher frequency effects. The overall criterion, even though identical to the one described earlier, is influenced by multiple n' frequency effects† superimposed by n'' sinusoidal responses. Under these conditions of mixed inputs, the existence of the stability is not evident, especially in the presence of intrinsically nonlinear feedback effects within the system. However, for experimental investigation, the control parameters (i.e., the levels of inputs and the phase relationships), if judiciously used, may lead to a stable limit cycle at t or multiple t second periods.

3.2 Digital systems

The n digital input signals may be coherently derived from a single master clock and a series of n logic circuits. When the input patterns repeat, an input cycle is created even though the bit values could vary in any order within this input cycle. The n inputs so derived would correspond to the n inputs of analog systems and the entire discussion of the periodicity and stability of the limit cycle applies for digital systems as well.

However, since far greater transients are imposed upon the system unless it is a perfect digital system, the system is unlikely to achieve the limit cycle within the lowest period t. Once the digital system is functioning perfectly synchronously, out of transients, it must achieve its limit cycle within the period t, and this test may be critically employed to test the overall functioning of the system and to localize any malfunctions. Hybrid systems, on the other hand, face all the uncertainties that a perfectly analog system would face with nonsinusoidal inputs, and the input flexibility available for the analog system does not exist for the n digital input hybrid system. However, the experimentalist does have a control of the bit patterns within the input cycle, and it may be controlled to yield a limit cycle. This principle may be extended to study the transient behavior of a system. For instance, when the transient response of an ADM compander is to be determined, a data pattern of a sequence of 0's or 1's followed by a sequence of 0 to 1 (which is coherent with the clock frequency) excites

* The existence of these "quasi-limit cycles" is analogous to the existence of instantaneous frequency. These quasi-limit cycles occur when the stability of two or more limit cycles becomes equally likely.

† n' is the number of the nonsinusoidal inputs and $n'' = n - n'$.

the decoder. The audio frequency output (or the voltage at the output capacitor) contains the nature and extent of the transient response when the binary data changes from a sequence of 0 and 1 to a long sequence of 0's or 1's, and vice versa. The details are presented in Section A4 of the appendix.

IV. DEGREE OF CHARACTERIZATION AND NUMBER OF INTERMEDIATE POINTS

Multi-input systems are generally too complex to have the overall system performance analyzed by a single output study. Hence, a series of intermediate points can be selected to determine the characteristics of the elements constituting the system. Under limit cycle conditions, the propagation of the input at each port is influenced by the character of the input at all the other ports by a determined amount and at a repeated interval.

If the effect of the inputs is also experimentally determined (by studying the intermediate points limit-cycle conditions), then the behavior of each element can be uniquely described to make up for the overall system performance. Hence, the choice of intermediate points and the study of the circuits and voltages at these points is critical in determining an overall system performance. For instance, if the characterization of an ADM codec[2] is necessary, the decoder, consisting of a four-bit shift register, a compander circuit, a current generator, a polarity selector, and an integrator capacitor, can be modeled by (*i*) forcing a series of synchronous binary bit patterns at the input and by (*ii*) recording the following:

(*i*) Compander functioning (to relate the shift register pattern and compander action).

(*ii*) The compander capacitor voltage (to relate the compander function with the extent of the change in compander capacitor voltage).

(*iii*) The generated step current (to relate the compander capacitor voltage and the size of the current).

(*iv*) The integrator capacitor voltage (to relate the change in audio frequency output and the size of the step current).

If it is not already known that the polarity reverses with the binary bit, it would also be necessary to record the polarity selector function. These principles, used together under various limit-cycle conditions, have led to the development of an ADM decoder model.

V. CONCLUSIONS

Limit cycles are useful in (*i*) characterizing a system function in a time domain, (*ii*) "freezing" the transient response of systems and their components especially if there are two or more inputs, and (*iii*) debugging and testing a multi-input system operation.

System coherence is the fundamental concept behind the technique of generating and stabilizing limit cycles.

Inputs are most easily obtained by synchronous frequency synthesizers and/or triggered pulse generators for the analog, hybrid, and/or digital systems. The method has proven satisfactory for a complex ADM system and can be valuable for other coherently excited systems. A judicious choice of intermediate points is necessary to characterize a system and, when extreme nonlinearities are present, a study under a series of limit cycles also becomes essential. For completely digital systems, the pulse generators and word generators assume the role of frequency synthesizers. However, the master clock is the most essential component to prevent any drift in the pulse generators which completely destroys the stability of the limit cycle.

VI. ACKNOWLEDGMENTS

The author appreciates the opportunity of having discussed the contents of this paper with H. Seidel and I. W. Sandberg. Some suggestions and comments of both the gentlemen are incorporated here. The comments and suggestions by S. K. Tewksbury were most welcome in the final preparation of the paper.

APPENDIX

A1. ADM CODEC DESCRIPTION

Adaptive delta modulation (ADM) decoders are D to A converters in which digital data are translated to an analog or an audio signal. Under ideal conditions, the signal from the decoder closely approximates the analog or audio signal originally used at the encoder to generate the digital stream of data. Decoders consist of three main components: (*i*) the compander, (*ii*) the polarity selector, and (*iii*) the integrator. The compander function controls the current step size which directly accumulates or depletes the charge on the integrator capacitor. The polarity selector controls the charge or depletion of the integrator capacitor; charging it if the last bit was a one, and depleting it if the last bit was a zero. The action of the compander is generally accomplished by controlling the voltage on another capacitor (step-size capacitor). The attack time constant for syllabic companding is about 3 ms, and the decay time is about 9 ms. The history of the received bits dictates the functioning of the compander, forcing a charge on the step-size capacitor (thus increasing the step size) if the last four bits were identical. In the absence of any companding, the step size of incremental current on to the integrator capaciter decays to about $\frac{1}{200}$ of the maximum current step size. The change of step size is quite nonlinear, changing dramatically when the step size is low, and absolutely saturating as the step size approaches the 46-dB range.

The encoder has a comparator in addition to the decoder. The decoder voltage and the incoming voltage are continuously compared, and the output of the comparator (0 or 1) is forced back into the decoder and also constitutes the digital stream from the encoder. The encoder-decoder pair is called the codec, and the characteristics of this device are examined by the limit cycle techniques in this paper.

A2. ADM ENCODER CHARACTERIZATION WITH SINUSOIDAL INPUT

In this configuration, the system is hybrid with audio input (which is obtained from a frequency synthesizer tuned to the master clock at 1 mHz) and digital clock input (derived from a triggered pulse generator also synchronized to the same master clock). The ADM encoder is a nonlinear device in which the step size can vary within a range of 46 dB. Hence, the stability of the limit cycle critically depends on the value of the input voltage. Limit cycles, even though possible for any time period encompassing integral cycles of audio frequency and clock frequency, were obtained readily at 240, 480, 720, 1000, 1200, 1500, 1800, 2000, 2400, 2700, 3000-Hz audio frequency and at 18-kHz or 24-kHz clock frequency. Two examples of the limit cycle are shown in Figs. 1a and 1b. In Fig. 1a, the 240-Hz cycle is shown with an 18-kHz clock. The period of the limit cycle is 12.5 ms spanning three 240-Hz cycles and 225 18-kHz cycles. The binary bits pattern is generated $b\ \bar{b}\ b'\ \bar{b}\ b\ b''$,*

where $b = 0000100001000100100010101010101001000100$ (= 38 bits)
$b' = 000111000001110011100011001110111011$ (= 36 bits)
and $b'' = \bar{b}'1$ (= 37 bits).

The entire number of these bits totals 225, corresponding to one bit generated by the encoder every clock cycle. The lower trace indicating the output from the codec exhibits a fairly satisfactory 240-Hz wave shape generated at its output.

In Fig. 1b, when the audio frequency is at 2700 Hz and the clock frequency is at 24 kHz, the performance of the codec is evident from the lowermost trace. Here the codec is incapable of regenerating a satisfactory 2700-Hz signal at the output. The limit cycle is generated every ⅓ ms to span 9 cycles at 2700 Hz and 80 cycles at 24 kHz. The bit pattern can be denoted as

$$(b\ \bar{b}\ b\ \bar{b}'\ b\ \bar{b}'\ b'\ \bar{b}\ b\ \bar{b}\ b'\ \bar{b}'\ b\ \bar{b}\ b'\ \bar{b}'\ b'\ \bar{b}),$$

where b is equal to 1111 and $b' = 11111$. This is a perfectly balanced example of b and $\bar{b}$; b′ and $\bar{b}'$. The total number of bits amount to 80, covering 9 cycles of input frequency.

---

* $\bar{b}$ represents the complement of the block b.

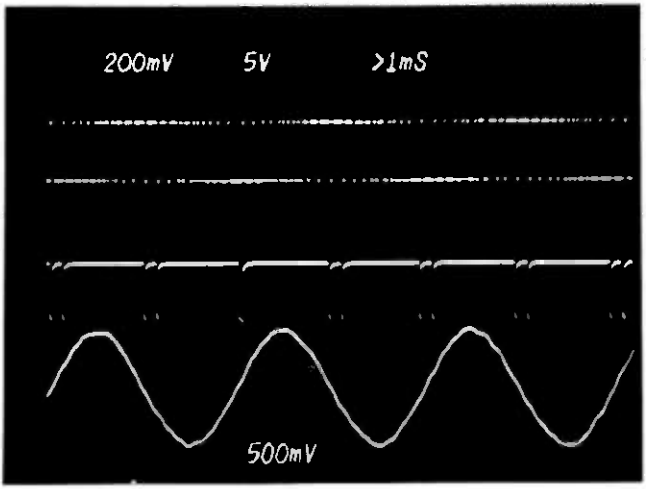

(a)

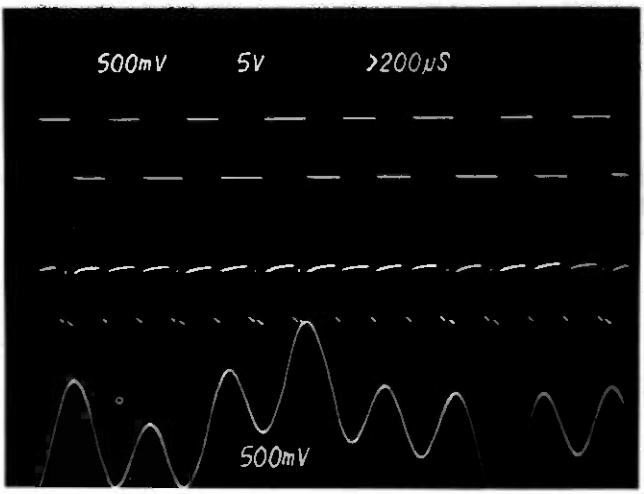

(b)

Fig. 1—Generation of encoder limit cycles. Top trace: Binary data. Middle trace: Compander action. Lower trace: Output of the ADM decoder. (a) Limit cycle obtained by 240 Hz at the AF input and 18 kHz at the clock frequency input into a *SLC*®-40 encoder. (b) Limit cycle obtained by 2700 Hz at the AF input and 24 kHz at the clock frequency input into a *SLC*-40 encoder.

In other cases where the relation between audio frequency input and the clock rate is a lower integer number such as (8 or 10), the binary repeat patterns are simpler and generally far more stable than the examples presented.

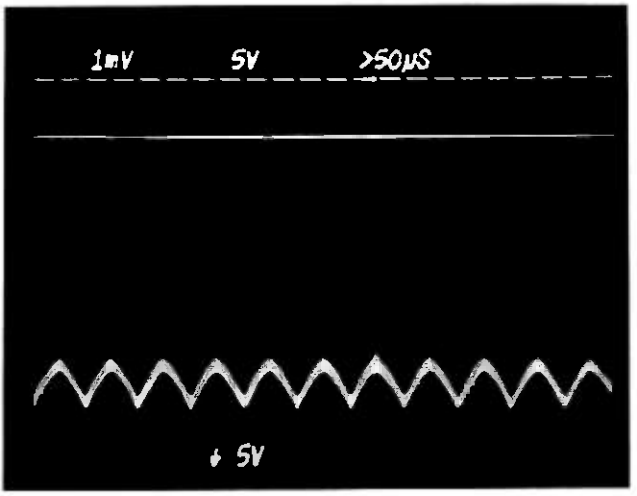

(a)

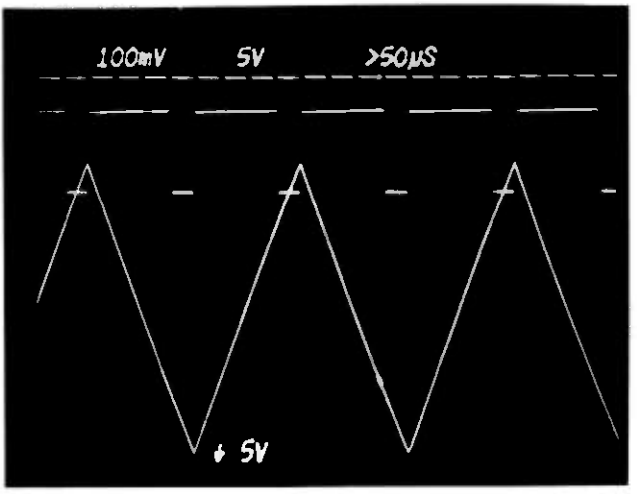

(b)

Fig. 2—Generation of decoder limit cycles. (a) Integrator voltage (lower trace) from a *SLC*®-40 decoder for a 0101 ··· sequence of coherent data input. (b) Integrator voltage from the decoder for a 00001111 ··· sequence of coherent data input. (*Continued*)

A3. ADM DECODER CHARACTERIZATION

When the clock and the binary bit pattern are synchronized, the operation of the decoder can be made perfectly repetitive. In the three sections of this appendix, three such models are presented (*i*) characterization with (0101, 00110011, etc.) inputs (to study the stable step

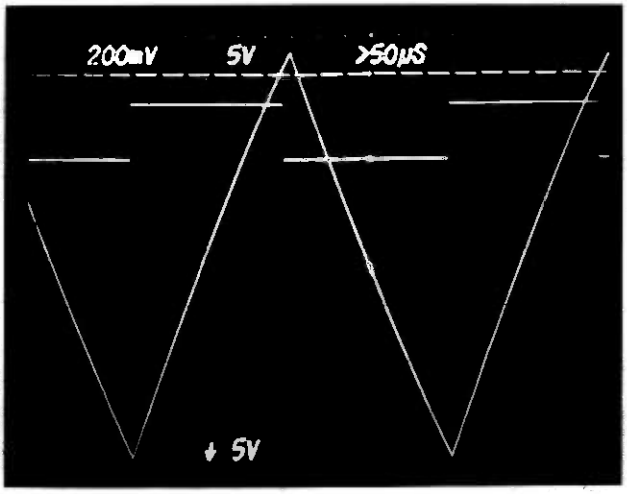

(c)

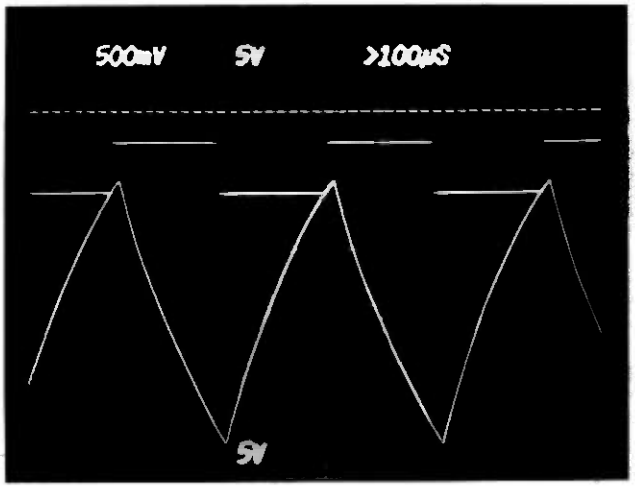

(d)

Fig. 2 (*continued*)—(c) Integrator voltage for a 111111000000 ··· sequence of coherent data input to the decoder. (d) Integrator voltage for a 1111111100000000 ··· sequence of binary input data.

sizes at different frequencies), (*ii*) characterization with (010101 ··· 00001111 00001111 ···) inputs (to study the decay and build-up of step sizes) and (*iii*) characterization with (0000 ··· or 1111 ···) ··· 010101 ···) input (to study growth and decay to the maximum step size).

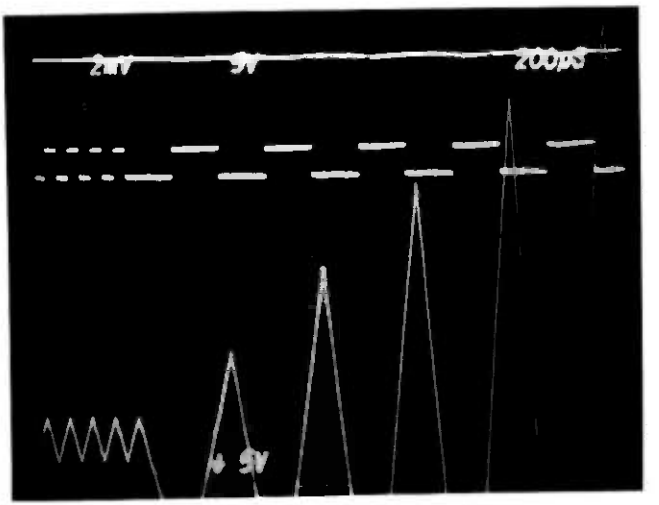

(a)

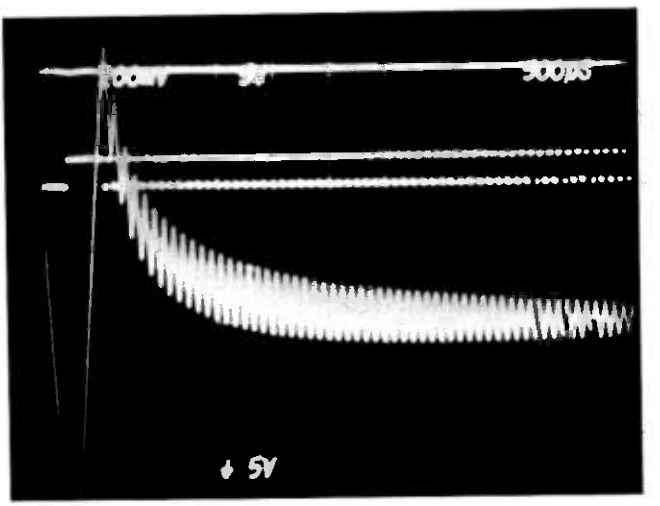

(b)

Fig. 3.—(a) Growth of step size at the decoder integrator capacitor by a sequence of 0101 ··· 00001111 ··· data. Limit cycle is generated by accommodating the 0101 sequence in 64 cycles of the master clock and 00001111 sequence within the 64 clock cycles of the master ADM clock. The periodicity of the limit cycle is 128 master clock cycles. (b) Decay of step size at the decoder integrator voltage by a sequence of 0101 ··· 01000000011111111 ··· binary data. The 0101 sequence is lodged in 256 master clock cycles at 24 kHz and 0000000011111111 sequence within the next 256 cycles. The limit cycle repeats every $10\frac{2}{3}$ ms.

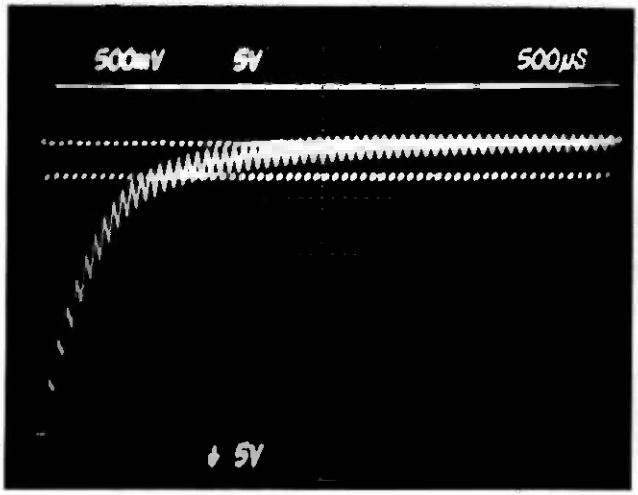

(a)

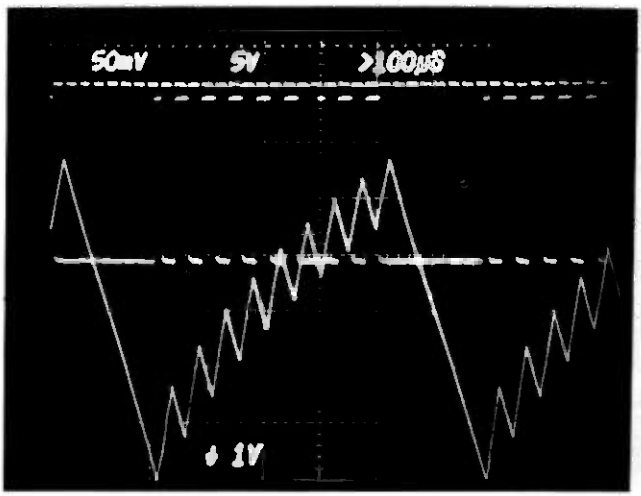

(b)

Fig. 4—(a) Decay of integrator voltage from high values. The system is forced into a limit cycle by a string of 256 zeros and by a string of 0101 ··· for the next 256 clock cycles. The periodicity of the entire limit cycle is 10⅔ ms at 24-kHz master clock. (b) Limit cycle generated by a sequence of 0000010101010101010101 (repeat) from a 24-kHz clock showing the change in step size of the decoder at medium ranges of integrator voltage. Three synthesizers were used in synchronization to generate the more complicated coherent bit patterns.

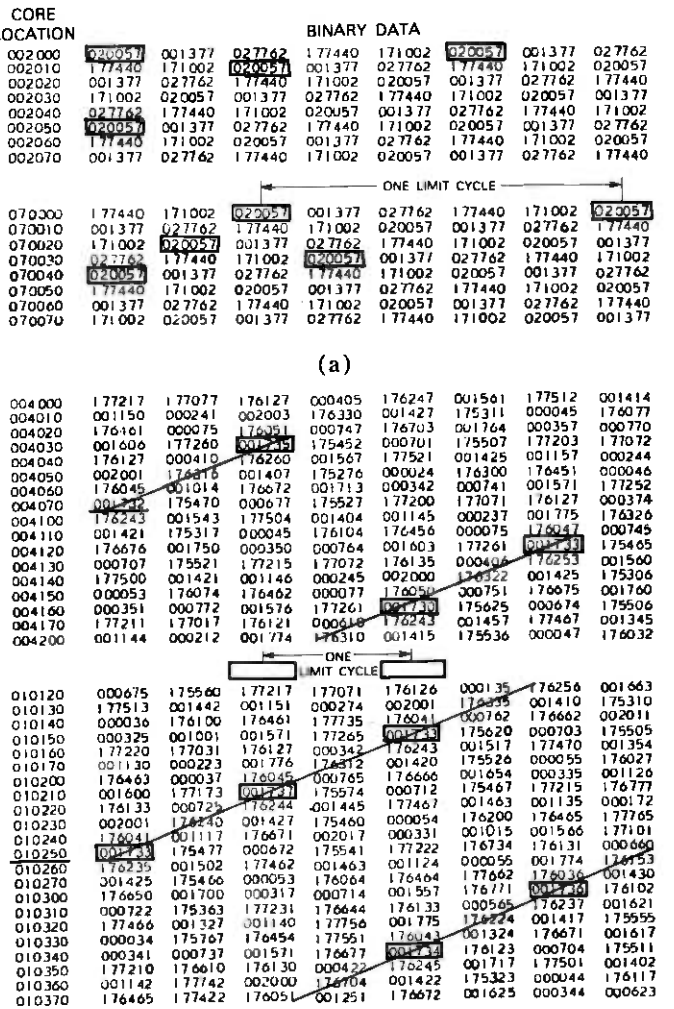

Fig. 5—(a) Limit cycle generated in the stored data from the ADM encoder for the interface testing. Note that location (70040_8 to 2000_8) is a perfect multiple of 5 confirming that the intermediate locations have also received the ADM data from the interface correctly. (b) Limit cycle generated by the stored analog-to-digital converter interface testing. Note that corresponding points on a repeating sine wave as they are scanned by the A to D converter occupy corresponding locations in the computer core, thus implying a properly functioning interface.

A.3.1. Stable step size characterization

Typical voltages at the integrator of the decoder are shown in a sequence of oscillograms, Figs. 2a through 2d. The input is generated by a series of simple logic circuits but activated by the same master clock feeding into the decoder.

A.3.2. Growth and decay of step sizes

When a sequence of 0101 ··· is interleaved with a series of 00001111 ··· (or any sequence during which the compander is repeatedly activated), then the step-size build-up may be studied in any desired detail. If the time constant for the build-up and decay are not known, then results offer an exact method to experimentally determine their exact values. Typical oscillograms are presented in Figs. 3a and 3b.

A.3.3. Growth and decay up to the maximum step size

Maximum step size of the decoder can be generated by a long sequence of zeros or ones. When such a sequence is interleaved with a sequence of 0101, the transient phenomenon of the build-up or decay can be rendered cyclic. This leads to the calculation of the maximum step size and its response to the compander circuit parameters (such as the compander capacitor voltage, the changing registers, etc.). Typical oscillograms are shown in Figs. 4a and 4b, and a series of such oscillograms have been used to characterize the decoder model used for additional work.

A4. MINICOMPUTER INTERFACE TESTING

When the input of the encoder is stored in a minicomputer, it is essential to check the validity of interface effectively. Such a test can be performed by forcing the encoder into a limit cycle operation yielding known bit patterns repeatedly. When the same clock is also used to shift and store data into the core (and then into a disk storage by subjugating the computer clock to the ADM clock), then these patterns lead to a series of binary stored words. Figs. 5a and 5b show two such examples for testing the ADM interface and the ADC (analog to digital) interface. In Fig. 5a, the bit pattern generated leads to a sequence of binary words:

100177 003772 077650 175200 124007

in the computer core (and also on the disk), when the audio frequency input and the clock frequency input are 800 Hz and 24 kHz. The same input into an ADC converter (at the input and output of the codec, odd and even word count; see Fig. 5b) leads to a sequence where every 30th word repeats (within the accuracy of A to D conversion feasible with the interface).

REFERENCES

1. J. F. Oberst, "Keeping Balance System Frequency on the Beam," Bell Laboratories Record, *52* No. 3 (March 1974), pp. 84–89.
2. S. J. Brolin and G. E. Harrington, "The SLC-40 Digital Carrier Subscriber System," IEEE Intercon Conference Record, 1975, *81*, pp. 1–5.
3. S. V. Ahamed, "Idle Channel Noise Suppression by Block Relaxation of Binary ADM-Encoded Speech," B.S.T.J., *57*, No. 5 (May–June 1978), pp. 1699–1706.

THE BELL SYSTEM TECHNICAL JOURNAL
Vol. 58, No. 8, October 1979
Printed in U.S.A.

A Characterization of the Invariance of Positivity for Functional Differential Equations

By I. W. SANDBERG

(Manuscript received April 4, 1979)

For systems of functional differential equations that can take into account finite or infinite delays, a complete characterization is given of the invariance of positivity in the sense that all solution components are positive whenever the initial condition function is positive. A related result concerning a comparison of the solutions of pairs of initial value problems is also given. One application of the results described concerns a model for synchronizing geographically separated oscillators and another is in the area of economics.

I. INTRODUCTION

Consider a system of functional differential equations of the form

$$\dot{x} = f(t, x_t), \qquad t \geq t_0, \qquad x_{t_0} = \phi, \tag{1}$$

in which x is a real n-vector valued function of t, $\dot{x}$ denotes dx/dt, ϕ is an initial condition function, and x_t denotes the function defined by $x_t(s) = x(t + s)$ for $s \leq 0$.* (When $f(t, x_t)$ depends only on t and $x_t(0)$, (1) reduces to a system of ordinary differential equations.)

The main purpose of this paper is to give a solution to the problem of determining conditions under which (under certain typically very reasonable conditions on f), $x(t)$ of (1) has components that are all positive for $t \geq t_0$ whenever ϕ is positive in, for example, the sense that $\phi(s)$ has positive components for $s \leq 0$. The problem arises in connection with the mathematical modeling and analysis of economic processes, and it comes up in several other areas as well. (An example concerning the synchronization of geographically separated oscillators is described in Section 2.6.) In some instances, the invariance of positivity in the sense described above is crucial, in that the lack of

* For background material concerning equations of the type (1), see, for example, Refs. 1 and 2.

positivity of a component of $x(t)$ for some t and positive ϕ means that the associated model is inappropriate.

Our main result, Theorem 1 of Section II, is concerned with the case in which f is continuous and locally Lipschitz. It provides an explicit and useful condition under which positivity is invariant, and it also asserts that positivity is invariant if and only if (1) preserves nonnegativity in the sense that $x(t)$ has nonnegative components for $t \geq t_0$ whenever ϕ is nonnegative.

The nonnegativity-preservation problem has been considered in Refs. 3, 4, and 5, and the relationship between Theorem 1 and the earlier material is indicated in Section 2.3.

A corollary of Theorem 1 is as follows. Suppose that (1) is a system of *ordinary* differential equations, and that f is continuous and satisfies a global Lipschitz condition (in the usual sense). Let $g(t, x)$ denote $f(t, x_t)$. Then positivity is invariant for (1), by which we mean invariant for each starting point t_0, if and only if for each i, $g_i(t_0, v) \geq 0$ for each t_0 and each real n-vector v such that $v_i = 0$ and $v_j \geq 0$ for $j \neq i$. Notice that for the special case in which $f(t, x_t) = Ax$, where A is an $n \times n$ matrix of real constants, our condition is equivalent to the requirement that the off-diagonal elements of A are nonnegative. The corresponding proposition concerning nonnegativity preservation for this case is well known.[6] Of some interest is the fact that the corollary described above becomes false if the Lipschitz hypothesis is replaced with the assumption that (1) has exactly one solution for each initial condition (see Section 2.3).

A result related to Theorem 1 that provides a necessary and sufficient condition for the invariance of positivity, or of nonnegativity, of the difference of the solutions of a pair of equations of the type (1) is given in Section 2.4. Specific applications of that result, as well as of Theorem 1, are described in Section 2.6.

II. CHARACTERIZATION OF THE INVARIANCE OF POSITIVITY

2.1 Preliminaries

We use the following notation and definitions. With n an arbitrary positive integer, R^n denotes the set of real n-vectors $v = (v_1, v_2, \cdots, v_n)$, $R^n_+ = \{v \in R^n: v_i \geq 0 \text{ for each } i\}$, and $|v| = \max_i |v_i|$ for $v \in R^n$. For u and v in R^n, the inequality $u \geq v$ ($u > v$) means that $u_i \geq v_i$ ($u_i > v_i$) for each i. The zero n-vector of R^n is denoted by θ.

We denote by C the Banach space of bounded continuous functions from $(-\infty, 0]$ to R^n, with norm given by

$$|w| = \sup_{t \in (-\infty, 0]} |w(t)|$$

for all $w \in C$.

The symbol T denotes any real interval of the form $[\alpha, \infty)$, (α, ∞), or $(-\infty, \infty)$, and t_0 is an element of T. For each $t \in T$ and each bounded continuous function w from $(-\infty, t]$ to R^n, w_t denotes the element of C defined by $w_t(s) = w(t + s)$ for $s \leq 0$.

Throughout Section II, f in (1) denotes a mapping of $T \times C$ into R^n. We say that f is *continuous in t* if $f(t, w_t)$ is a continuous function of t for $t \geq t_0$ whenever $t_0 \in T$ and w is a bounded continuous mapping of $(-\infty, \infty)$ into R^n, and we say that f is *locally Lipschitz* if for each $t_0 \in T$, each $\gamma \in [t_0, \infty)$, and each compact set B in R^n, there is a constant $\rho(t_0, \gamma, B)$ such that $|f(t, u) - f(t, v)| \leq \rho(t_0, \gamma, B)|u - v|$ for each $t \in [t_0, \gamma]$ and each u and v in C such that the range of u, and also of v, is contained in B.

A *solution* of (1) through a given $(t_0, \phi) \in T \times C$ means a continuous R^n-valued function x that is defined on $(-\infty, \infty)$, is differentiable on (t_0, ∞), and is such that (1) is satisfied (with the understanding that at $t = t_0$, $\dot{x}$ denotes the right-hand derivative).* As in the case of ordinary differential equations, if f is continuous in t and satisfies a uniform Lipschitz condition in the sense that f satisfies a local Lipschitz condition with $\rho(t_0, \gamma, B)$ independent of B, for each $(t_0, \phi) \in T \times C$ there is a unique solution of (1) through (t_0, ϕ) (see p. 409 of Ref. 2).

In the next section, we refer to the following hypothesis.

H.1: *There is a solution x of* (1) *through each* $(t_0, \phi) \in T \times C$, *and f is locally Lipschitz as well as continuous in t.* (*In particular, each solution of* (1) *is unique.*)

2.2 Our principal result

Under the assumption that H.1 holds, consider the following properties and condition.

Property 1 (*Invariance of Positivity, Version* 1): *For each* $(t_0, \phi) \in T \times C$ *such that* $\phi(0) > \theta$ *and* $\phi(s) \in R^n_+$ *for* $s \leq 0$, *we have* $x(t) > \theta$ *for* $t \geq t_0$.

Property 2 (*Invariance of Positivity, Version* 2): *For each* $(t_0, \phi) \in T \times C$ *such that* $\phi(s) > \theta$ *for* $s \leq 0$, *we have* $x(t) > \theta$ *for* $t \geq t_0$.

Property 3 (*Invariance of Nonnegativity*): *We have* $x(t) \geq \theta$ *for* $t \geq t_0$ *whenever* $(t_0, \phi) \in T \times C$ *with* $\phi(s) \in R^n_+$ *for* $s \leq 0$.

Condition 1: *For each i,* $f_i(t_0, \phi) \geq 0$ *whenever* $(t_0, \phi) \in T \times C$ *with* $\phi(s) \in R^n_+$ *for* $s \leq 0$ *and* $\phi_i(0) = 0$.

Theorem 1: *Let H.*1 *be satisfied. Then the following four statements are equivalent: Property* 1 *holds, Property* 2 *holds, Property* 3 *holds, and Condition* 1 *is met.*

---

* It will become clear that our development can be extended at once to cover the case in which a solution need be defined on only an interval of the form $(-\infty, \beta)$ with $\beta > t_0$.

Proof: We first show that Property 3 and Condition 1 are equivalent.

Suppose that Condition 1 is satisfied, that $(t_0, \phi) \in T \times C$ is given, with $\phi(s) \in R^n_+$ for $s \leq 0$, and that $x(t) \geq \theta$ for $t \geq t_0$ is violated. Then there is a $t' > t_0$ and an index ℓ such that $x_\ell(t') < 0$. Since f is continuous in t and locally Lipschitz, the Bellman-Grownwall Lemma[7] and Theorem 3 of Ref. 2 can be used to show that, given any $\tau > t'$, there are an $\epsilon > 0$ and an R^n-valued function w defined on $(-\infty, \tau]$, and differentiable on (t_0, τ), such that $\dot{w}_i = f_i(t, w_t) + \epsilon$, $t \in [t_0, \tau)$, $i = 1, 2, \cdots, n$, with $w_{t_0} = \phi$ *and* $w_\ell(t') < 0$.* Let $I = \{i: w_i(t) < 0 \text{ for some } t \in (t_0, \tau)\}$, and for each $i \in I$, let $t_i = \inf\{t \in (t_0, \tau): w_i(t) < 0\}$. Choose k so that $t_k = \min\{t_i: i \in I\}$. We have $w_k(t_k) = 0$, $\dot{w}_k(t_k) \leq 0$, and $w_{t_k}(s) \in R^n_+$ for $s \leq 0$. Thus, $f_k(t_k, w_{t_k}) + \epsilon \leq 0$, which contradicts Condition 1. Therefore, we have Property 3 when Condition 1 is met. On the other hand, if Condition 1 is not satisfied, there is an index ℓ and a $(t_0, \phi) \in T \times C$ with $\phi(s) \in R^n_+$ for $s \leq 0$ and $\phi_\ell(0) = 0$ such that $f_\ell(t_0, \phi) < 0$. Since there is a solution x through (t_0, ϕ), and it clearly satisfies $x_\ell(t) < 0$ for $(t - t_0)$ positive and sufficiently small, we see that Property 3 implies that Condition 1 is met. This proves the equivalence of Property 3 and Condition 1.

It is clear that Property 1 implies Property 2. To see that Condition 1 is satisfied when Property 2 holds, suppose once more that Condition 1 is not met. Then, as in the paragraph above, there is a $(t_0, \phi) \in T \times C$ with $\phi(s) \in R^n_+$ for $s \leq 0$ such that x satisfies $x_\ell(t') < 0$ for some ℓ and $t' > t_0$. By H.1 and Lemma 2 of Ref. 2 (which is a result concerning the continuous dependence of the solution on the initial data), there is a $(t_0, \tilde{\phi}) \in T \times C$ such that $\tilde{\phi}(s) > \theta$ for $s \leq 0$ and such that the corresponding solution $\tilde{x}$ meets $\tilde{x}_\ell(t') < 0$. Therefore, Condition 1 is satisfied when Property 2 holds. To complete the proof of the theorem, we now show that Property 3 implies Property 1.

Assume that Property 3 holds and that Property 1 does not hold. Then there is a $(t_0, \phi) \in T \times C$ and a corresponding solution x such that $\phi(0) > \theta$, $\phi(s) \in R^n_+$ for $s \leq 0$, $x(t) \in R^n_+$ *for* $t \geq t_0$, and $x_\ell(t') = 0$ for some ℓ and $t' > t_0$. We assume without loss of generality that $t' = \inf\{t > t_0: x_i(t) = 0 \text{ for some } i\}$. Thus, $x(t) > \theta$ for $t \in [t_0, t')$.

Let

$$B = \{v \in R^n_+: v_i \leq \sup_{t \in (-\infty, t']} |x(t)|, i = 1, 2, \cdots, n\}.$$

From $x_\ell(t') = 0$ and the observation that

$$\int_{t''}^{t'} \frac{\dot{x}_\ell(s)}{x_\ell(s)}\, ds = \ln[x_\ell(t)] - \ln[x_\ell(t'')],\ t \in [t'', t')$$

* At $t = t_0$, the unique solution with which Theorem 3 of Ref. 2 is concerned has a right-hand derivative equal to the value of the functional that corresponds here to f. (See the proof of Theorem 2 of Ref. 2.)

for any $t'' \in (t_0, t')$, we see that $\dot{x}_\ell(t)\,[x_\ell(t)]^{-1}$ is not bounded from below on (t_0, t'). Let $\sigma \in (t_0, t')$ be chosen so that $\dot{x}_\ell(\sigma) + \rho(t_0, t', B)\, x_\ell(\sigma) < 0$, in which ρ is the Lipschitz constant in Section 2.1.

Define $w(\sigma) \in C$ by $[w(\sigma)]_\ell(s) = \max[0, (x_\sigma)_\ell(s) - (x_\sigma)_\ell(0)]$ for $s \leq 0$, and $[w(\sigma)]_i(s) = (x_\sigma)_i(s)$ for $s \leq 0$ and $i \neq \ell$. It can be verified that $w(\sigma)(s) \in B$ for $s \leq 0$, and that $|x_\sigma - w(\sigma)| \leq x_\ell(\sigma)$.

Therefore,

$$\begin{aligned} f_\ell[\sigma, w(\sigma)] &= \dot{x}_\ell(\sigma) - f_\ell(\sigma, x_\sigma) + f_\ell[\sigma, w(\sigma)] \\ &\leq \dot{x}_\ell(\sigma) + \rho(t_0, t', B)\,|x_\sigma - w(\sigma)| \\ &\leq \dot{x}_\ell(\sigma) + \rho(t_0, t', B)\, x_\ell(\sigma). \end{aligned}$$

We have $f_\ell[\sigma, w(\sigma)] < 0$, $(\sigma, w(\sigma)) \in T \times C$, $w(\sigma)(s) \in R^n_+$ for $s \leq 0$, and $[w(\sigma)]_\ell(0) = 0$, which, in view of the equivalence of Condition 1 and Property 3, contradicts our assumption that Property 3 holds. Thus Property 3 implies Property 1, which completes the proof of Theorem 1.

2.3 Notes

The Condition 1-implies-Property 3 assertion of the theorem becomes false if the hypothesis that f is locally Lipschitz is dropped and Property 3 is modified in the natural way so that it concerns *all* solutions that correspond to the indicated type of initial condition.[4]

The following example shows that the theorem becomes false if the Lipschitz hypothesis is replaced with the assumption that (1) has at most one solution for each $(t_0, \phi) \in T \times C$. Let $n = 1$, and let f be defined for all t by $f(t, x_t) = -(x(t))^{1/2}$ for $x(t) \geq 0$, and $f(t, x_t) = 0$ for $x(t) < 0$. Observe that f is continuous, and that a solution (in the usual sense) of $\dot{x} = f(t, x_t)$ for $t \geq 0$, $x(0) = x^0$, is given by $x(t) = x^0$ for $t \geq 0$ if $x^0 \leq 0$, and $x(t) = ((x^0)^{1/2} - \tfrac{1}{2}t)^2$ for $t \in [0, 2(x^0)^{1/2}]$ with $x(t) = 0$ for $t > 2(x^0)^{1/2}$ if $x^0 > 0$. It can be verified that there are no other solutions, even though f is not locally Lipschitz. While here $x(t)$ is nonnegative for $t \geq 0$ whenever $x^0 \geq 0$, it is obviously not true that $x(t)$ is positive for all $t \geq 0$ whenever x^0 is positive.

Essentially, the fact that Condition 1 and Property 3 are equivalent for ordinary differential equations is proved in Ref. 4, and in Ref. 5 (and in the setting provided by the results in Ref. 2) that result is extended to cover the more general case. At the time Ref. 4 was written, this writer was unaware of Ref. 3, which contains a theorem (proved in a very different way) from which the result in Ref. 4 can be obtained. Our proof of the equivalence of Condition 1 and Property 3 is basically the same as the proof in Ref. 4 for the ordinary differential equations case. We did not omit the proof mainly because a modification of it is referred to in the next section. Also, for the case in which

(1) takes into account only finite delays (i.e., for equations of "retarded" type), a direct variation of the proof, using the continuous dependence result in, for example, Ref. 1, p. 41, shows that Condition 1 and Property 3 are equivalent without the Lipschitz hypothesis, provided that (1) has exactly one solution for each $(t_0, \phi) \in T \times C$.

Our proof of Theorem 1 shows also that, when *H*.1 is met, Condition 1 is necessary and sufficient that positivity is invariant in the sense that Property 3 holds *and* we have $x_l(t) > 0$ for $t \geq t_0$ whenever $(t_0, \phi) \in T \times C$ is such that $\phi(s) \in R^n_+$ for $s \leq 0$ and the index l is such that $\phi_l(0) > 0$.

2.4 The comparison theorem

The proof of Theorem 1 can be modified to establish a corresponding theorem concerning a comparison of the solutions of two initial value problems. To describe that result, let g be a function from $T \times C$ into R^n, and consider together with (1) the equation

$$\dot{y} = g(t, y_t), \qquad t \geq t_0, \qquad y_{t_0} = \psi, \tag{2}$$

as well as the following hypothesis, properties, and condition.

H.2: *For each* $(t_0, \phi) \in T \times C$, (1) *has a solution* x, *and similarly, for each* $(t_0, \psi) \in T \times C$, (2) *has a solution* y. *The mappings* f *and* g *are continuous in* t, *and at least one of the mappings* f *or* g *is locally Lipschitz.*

Property 4: *For each* $(t_0, \phi, \psi) \in T \times C \times C$ *such that* $\phi(0) > \psi(0)$ *and* $\phi(s) \geq \psi(s)$ *for* $s \leq 0$, *we have* $x(t) > y(t)$ *for* $t \geq t_0$ (*i.e., we have* $x(t) > y(t)$ *for* $t \geq t_0$ *for any solution* x *of* (1) *through* (t_0, ϕ) *and any solution* y *of* (2) *through* (t_0, ψ)).

Property 5: *For each* $(t_0, \phi, \psi) \in T \times C \times C$ *such that* $\phi(s) > \psi(s)$ *for* $s \leq 0$, *we have* $x(t) > y(t)$ *for* $t \geq t_0$.

Property 6: *We have* $x(t) \geq y(t)$ *for* $t \geq t_0$ *whenever* $(t_0, \phi, \psi) \in T \times C \times C$ *such that* $\phi(s) \geq \psi(s)$ *for* $s \leq 0$.

Condition 2: *For each* i, $f_i(t_0, \phi) \geq g_i(t_0, \psi)$ *whenever* $(t_0, \phi, \psi) \in T \times C \times C$ *with* $\phi_i(0) = \psi_i(0)$ *and* $\phi(s) \geq \psi(s)$ *for* $s \leq 0$.

Our result is the following.

Theorem 2: *If H*.2 *is met, then Property* 4, *Property* 5, *Property* 6, *and Condition* 2 *are equivalent to one another.*

Proof: The proof is similar to the one given of Theorem 1. In fact, straightforward modifications show that Property 6 and Condition 2 are equivalent, and that Property 5 implies Condition 2. Since it is clear that Property 4 implies Property 5, it therefore suffices to use the equivalence of Condition 2 and Property 6 to prove that Property 6 implies Property 4. We do that as follows.

Assume that Property 6 holds, but that Property 4 fails to hold. Thus there are $(t_0, \phi, \psi) \in T \times C \times C$, a number $t' > t_0$, and an index ℓ such that $\phi(0) > \psi(0)$, $\phi(s) \geq \psi(s)$ for $s \leq 0$, $x_\ell(t') = y_\ell(t')$, and $x(t) > y(t)$ for $t \in [t_0, t')$. Let

$$B = \{v \in R^n: |v| \leq \sup_{t \in (-\infty, t']} [\max (|x(t)|, |y(t)|)]\}.$$

Assume for the moment that f is locally Lipschitz. Using the fact that $[\dot{x}_\ell(t) - \dot{y}_\ell(t)][x_\ell(t) - y_\ell(t)]^{-1}$ is not bounded from below on (t_0, t') (see the proof of Theorem 1), choose $\sigma \in (t_0, t')$ so that $\dot{x}_\ell(\sigma) - \dot{y}_\ell(\sigma) + \rho(t_0, t', B)[x_\ell(\sigma) - y_\ell(\sigma)] < 0$.

Define $u(\sigma) \in C$ by the conditions $[u(\sigma)]_\ell(s) = \max[(y_\sigma)_\ell(s), (x_\sigma)_\ell(s) - (x_\sigma)_\ell(0) + (y_\sigma)_\ell(0)]$, $s \leq 0$, and $[u(\sigma)]_i(s) = (x_\sigma)_i(s)$, $s \leq 0$, $i \neq \ell$. We have $[u(\sigma)]_\ell(0) = (y_\sigma)_\ell(0)$, and $y_\sigma(s) \leq u(\sigma)(s) \leq x_\sigma(s)$ for $s \leq 0$. In particular, $u(\sigma)(s) \in B$ for $s \leq 0$. Also, if $(x_\sigma)_\ell(s) - (x_\sigma)_\ell(0) + (y_\sigma)_\ell(0) \geq (y_\sigma)_\ell(s)$, then $(x_\sigma)_\ell(s) - [u(\sigma)]_\ell(s) = (x_\sigma)_\ell(0) - (y_\sigma)_\ell(0)$. On the other hand, if $(x_\sigma)_\ell(s) - (x_\sigma)_\ell(0) + (y_\sigma)_\ell(0) < (y_\sigma)_\ell(s)$, then $(x_\sigma)_\ell(s) - (y_\sigma)_\ell(s) < (x_\sigma)_\ell(0) - (y_\sigma)_\ell(0)$. Consequently, $|x_\sigma - u(\sigma)| \leq (x_\sigma)_\ell(0) - (y_\sigma)_\ell(0)$. Therefore,

$$f_\ell[\sigma, u(\sigma)] - g_\ell(\sigma, y_\sigma) = \dot{x}_\ell(\sigma) - \dot{y}_\ell(\sigma) + f_\ell[\sigma, u(\sigma)] - f_\ell(\sigma, x_\sigma)$$

$$\leq \dot{x}_\ell(\sigma) - \dot{y}_\ell(\sigma) + \rho(t_0, t', B)[x_\ell(\sigma) - y_\ell(\sigma)],$$

which shows that $f_\ell[\sigma, u(\sigma)] - g_\ell(\sigma, y_\sigma) < 0$. This contradicts Condition 2 and hence Property 6. A similar contradiction can be obtained when g rather than f is locally Lipschitz. (In the analogous argument, the function $v(\sigma) \in C$ that plays the role of $u(\sigma)$ is defined by $[v(\sigma)]_\ell(s) = \min[(x_\sigma)_\ell(s), (y_\sigma)_\ell(s) - (y_\sigma)_\ell(0) + (x_\sigma)_\ell(0)]$ for $s \leq 0$, and $[v(\sigma)]_i(s) = (y_\sigma)_i(s)$ for $s \leq 0$ and $i \neq \ell$.) This shows that Property 6 implies Property 4, and it completes the proof.

2.5 Comments

Since Property 6 does not hold when $f = g$ and (1) has more than one solution through some $(t_0, \phi) \in T \times C$, we see that the Condition 2-implies-Property 6 part* of Theorem 2 becomes false if the hypothesis that at least one of the functions f or g is locally Lipschitz is omitted. The example given in Section 2.3 shows that the theorem becomes false even if the hypothesis is replaced with the assumption that (1) and (2) have at most one solution for each $(t_0, \phi) \in T \times C$ and each $(t_0, \psi) \in T \times C$, respectively. On the other hand, the equivalence of Condition 2 and Property 6 holds for equations of retarded type when the Lipschitz hypothesis is replaced with the assumption of uniqueness of solutions for at least one of the equations (1) and (2).†

* For ordinary differential equations with $f = g$, this part of Theorem 2 is along the lines of a well-known result (Ref. 8).

† See the corresponding comment in Section 2.3.

The proof of Theorem 2 described in the preceding section can be used to verify that C in Theorem 2 can be replaced with the set of continuous bounded functions from $(-\infty, 0]$ to D, where D is any open rectangular interval of R^n, provided that by a solution of (1) or (2) is meant a solution whose values are contained in D for $t \geq t_0$. (In this connection, note that $u(\sigma)$ of the proof of Theorem 2 satisfies $u(\sigma)(s) \in D$ for $s \leq 0$ whenever $D \subset R^n$ is a rectangular interval and both $x_\sigma(s)$ and $y_\sigma(s)$ are contained in D for $s \leq 0$.) Of course, the case in which $D = \{v \in R^n: v > \theta\}$ is of particular interest.

2.6 Applications

There are many applications of Theorems 1 and 2. As a simple example for the purpose of illustration, consider the delay-differential equations

$$\dot{x}_i(t) = \sum_{\substack{j=1 \\ j \neq i}}^{n} h_{ij}(t)[x_j(t - \tau_{ij}) - x_i(t)], \; t \geq 0$$

$$i = 1, 2, \cdots, n, \quad (3)$$

which arise[9] in the study of models of systems for synchronizing geographically separated oscillators. In (3), each τ_{ij} is a nonnegative constant, each h_{ij} is nonnegative, continuous, and bounded on $[0, \infty)$, $x_i(t)$ denotes the frequency of the ith oscillator, and the h_{ij} can depend on x as well as on certain fixed nonlinear functions. Under certain reasonable hypotheses concerning the h_{ij} (see Ref. 9), given a continuous $x(t)$ for $t \in \tau$, where $\tau = [-\max_{j \neq i} \tau_{ij}, 0]$, there is a constant ρ such that for each i, $x_i(t) \to \rho$ as $t \to \infty$. Assume here that there is such a ρ for each initial-condition function.

Theorem 1 shows that each $x_i(t)$ in (3) is positive for $t \geq 0$ whenever $x(t) > \theta$ for $t \in \tau$.* (The nature of the dependence of the h_{ij} on x is not of consequence at this point. If it were not true that $x(t) > \theta$ for $t \geq 0$ whenever $x(t) > \theta$ for $t \in \tau$, we would have a contradiction to the theorem.) Assuming now that the h_{ij} are independent of x, it follows from Theorem 2 that, for example, ρ is either increased or unchanged when $x(t)$ for $t \in \tau$ is replaced with any continuous $\tilde{x}(t)$ for which $\tilde{x}(t) \geq x(t)$ for $t \in \tau$.

Two related observations concern the equations

$$\dot{x}_i(t) = -b_{i0}[x_i(t)] + \sum_{\substack{j=1 \\ j \neq i}}^{n} b_{ij}[x_j(t - \tau_{ij})] + u_i(t), \; t \geq 0$$

$$i = 1, 2, \cdots, n \quad (4)$$

* This proposition is a special case of Lemma 1 of Ref. 9 whose proof is very different.

of a model of a compartmental system with delays,[10] in which the b_{i0} and the b_{ij} for $i \neq j$ are locally Lipschitz monotone-nondecreasing functions such that $b_{i0}(0) = b_{ij}(0) = 0$, each u_i is continuous and satisfies $u_i(t) \geq 0$ for $t \geq 0$, and, as in the preceding example, the τ_{ij} are nonnegative constants. In (4), $x_i(t)$ denotes the amount of material in the ith compartment.

From Theorem 2, we see that if x^a is a solution of (4) corresponding to $(u_1, u_2, \cdots, u_n) = u^a$ and $x(t) = x^a(t)$ for $t \in \tau$, where again $\tau = [-\max_{i,j} \tau_{ij}, 0]$, and similarly with regard to x^b and u^b, then we have $x^a(t) \geq (>)\ x^b(t)$ for $t \geq 0$ when $u^a(t) \geq u^b(t)$ for $t \geq 0$ and $x^a(t) \geq (>)\ x^b(t)$ for $t \in \tau$. The "$\geq$ part" of this proposition was given in Ref. 10. From Theorem 1, it is clear that we have $x(t) > \theta$ for $t \geq 0$ whenever $x(t) > \theta$ for $t \in \tau$, which does not seem to have been proved earlier, even for the case in which $\tau_{ij} = 0$ for all $i \neq j$.*

Consider now the case in which f in (1) is given by $f_i(t, x_t) = h_i(x_t)$ for each i, where each h_i is a functional on C with the property that $h_i(u) \geq h_i(v)$ for all u and v in C such that $u_i(s) = v_i(s)$ and $u(s) \geq v(s)$ for $s \leq 0$. Functions f of this form are generalizations of time-invariant quasimonotone (or Wazewski-type) functions[11] which are of interest in several areas, including economics. In economics applications, the $x_i(t)$ often denote prices (see, for example, Refs. 12 and 13). Observe that (4) is of the form considered here when the u_i are independent of t.

Assuming that H.1 is met, Theorem 1 provides the following simple necessary and sufficient condition for the invariance of positivity in the sense of Property 1 or Property 2.

For each i, $h_i(w) \geq 0$ for each w in C such that $w_i(0) = 0$, $w_i(s) \geq 0$ for $s \leq 0$, and $w_j(s) = 0$ for $s \leq 0$ and $j \neq i$.

REFERENCES

1. J. Hale, *Theory of Functional Differential Equations*, New York: Springer Verlag, 1977.
2. R. D. Driver, "Existence and Stability of Solutions of a Delay Differential System," Arch. Rational Mech. Anal., *10* (1962), pp. 401–426.
3. M. Nagumo, "Über die Lage der Integralkurven gewöhnlicher Differentialgleichungen," Proc. Phys.-Math. Soc. Japan, Ser. 3, *24* (1942), pp. 550–559.
4. I. W. Sandberg, "A Nonnegativity-Preservation Property Associated with Certain Systems of Nonlinear Differential Equations," Proc. Int. Conf. Syst. Man. Cyber., Dallas, Texas, 1974, pp. 230–233.
5. G. Seifert, "Positively Invariant Closed Sets for Systems of Delay Differential Equations," J. Differential Equations, *22* (1976), pp. 292–304.
6. R. Bellman, *Introduction to Matrix Analysis*, New York: McGraw-Hill, 1970, p. 176.
7. V. V. Nemytskii and V. V. Stepanov, *Qualitative Theory of Differential Equations*, Princeton; Princeton U. Press, 1960.
8. V. Lakshmikantham and S. Leela, *Differential and Integral Inequalities*, Vol. I, New York: Academic Press, 1969, pp. 28–29.

* The monotonicity of the b_{i0} and b_{ij} is not needed for this result. It suffices that $b_{ij}(\alpha) \geq 0$ for $\alpha > 0$ and $i \neq j$.

9. I. W. Sandberg, "Some Properties of a Nonlinear Model of a System for Synchronizing Digital Transmission Networks," B.S.T.J., *48*, No. 9 (November 1969), pp. 2975–2997.
10. R. M. Lewis and B. D. O. Anderson, "Insensitivity of a Class of Non-linear Compartmental Systems to the Introduction of Arbitrary Time Delays," Preprint, February 1979.
11. A. N. Michel and R. K. Miller, *Qualitative Analysis of Large Scale Dynamical Systems*, New York: Academic Press, 1977, p. 59.
12. K. J. Arrow and L. Hurwicz, "Competitive Stability Under Weak Gross Substitutability: The 'Euclidean Distance' Approach," Internat. Econ. Rev., *1* (1960), pp. 38–49.
13. J. G. Kemeny and J. L. Snell, *Mathematical Models in the Social Sciences*, Cambridge, Mass.; MIT Press, 1972, pp. 37–38.

Contributors to This Issue

Syed V. Ahamed, B.E., 1957, University of Mysore; M.E., 1958, Indian Institute of Science; Ph.D., 1962, University of Manchester, U.K.; Post-Doctoral Research Fellow, 1963, University of Delaware; Assistant Professor, 1964, University of Colorado; M.B. A. (Economics), 1978, New York University; Bell Laboratories, 1966—. At Bell Laboratories, Mr. Ahamed has worked in computer-aided engineering analysis and design of electromagnetic components, designed and implemented minicomputer software and hardware interfacing, applied algebraic analysis to the design of domain circuits, and investigated computer aids to the design of bubble circuits. He has investigated new varacter designs for microwave power in the C-band and developed hardware and software interfacing for audio frequency codecs. Beginning in 1975, he optimized codec designs, encoding techniques, and speech-encoded data storage and manipulation by minicomputers. Since 1977, he has been simulating the overall performance of the loop plant while carrying bidirectional digital data in the range of 56 to 324 kbaud.

Jont B. Allen B.S. (E.E.), 1966, University of Illinois; M.S., 1968, Ph.D., 1970, University of Pennsylvania; Bell Laboratories, 1970—. Mr. Allen is presently working in the areas of cochlear modeling, small room acoustics, dereverberation of speech signals, and digital signal processing. His main efforts have been directed toward cochlear mathematical modeling, the problem of removing room reverberation from recorded speech signals by digital signal processing, and modeling the psychophysical effects of room reverberation.

Charles J. Aloisio, Jr., B. S. (E.E.), 1965, Newark College of Engineering; M.S., 1968, Ph.D. (Eng.), 1970, School of Aeronautics and Engineering Sciences, Purdue University; Bell Laboratories, 1952—. At Bell Laboratories, Mr. Aloisio has been investigating the mechanical and electrical characteristics of plastics and the relationship between

processing and the resulting properties of plastics. He is currently supervisor of the Plastics Engineering and Characterization Group.

Ray R. Cammons, A.A. (Mechanical Engineering), Southern Technical Institute; Certified Apprenticeship, Aircraft Tooling, Lockheed Aircraft Corp; Western Electric, 1972–1977; Bell Laboratories, 1977—. Mr. Cammons has had experience in plastic compounding and wire and cable extrusion, and currently is working in injection molding and mold design.

Allen H. Cherin, B.E.E., 1961, City College of New York; M.S.E.E., 1965, University of Vermont; Ph.D. (E.E.), 1971, University of Pennsylvania; Bell Laboratories, 1965–. Mr. Cherin is engaged in studies associated with the characterization, splicing, and packaging of optical fibers. Member, IEEE, OSA.

Fan R. K. Chung, B.S., 1970, National Taiwan University; Ph.D., 1974, University of Pennsylvania; Bell Laboratories, 1974—. Mrs. Chung's current interests include combinatorics, graph theory, and the analysis of algorithms. She is presently investigating various problems in the theory of switching networks.

Juan R. Maldonado, Doctor in Ciencias Fisico Matematicas, 1961, University of Havana, Cuba; Ph.D., Experimental Solid State Physics, 1968, University of Maryland; CMQ-TV, Havana, Cuba, 1957–61; University of Havana, 1960–61; University of Maryland, 1962–68; Bell Laboratories, 1968—. Mr. Maldonado was engaged at CMQ-TV with television transmitters and video equipment. He was an instructor in the E.E. and Physics Departments at the University of Havana, and was supervisor of the electronics facilities of the Physics Department and a Research Assistant at the University of Maryland. He has worked with ferroelectric ceramic electro-optic and display devices, liquid crystals, X-ray fluorescence systems, and X-ray lithography at Bell Laboratories. Member, AIP, IEEE, SPIE, AAAS, Sigma Xi, and Sigma Pi Sigma.

Dan Maydan, B.Sc. (E.E.), 1957, and M.Sc. (E.E.), 1962, Israel Institute of Technology; Ph.D. (Physics), 1965, Edinburgh University; Bell Laboratories, 1967—. Mr. Maydan has worked on acousto-optical interaction for modulating laser beams. He currently supervises a group working on X-ray lithography for the fabrication of VLSI devices and dry processing techniques. Senior Member, IEEE.

Frank C. Pirz, B.S.E.E., 1968, Polytechnic Institute of Brooklyn; M.S.E.E., 1972, M.S. Computer Science, 1972, University of Massachusetts; Bell Laboratories, 1972—. Mr. Pirz is currently involved in real-time signal processing software and hardware development in the Acoustics Research department.

Montel V. Pursley, B.S.E.E., 1960, M.S.E.E., 1967, Newark College of Engineering; Bell Laboratories, 1953—. Mr. Pursley is currently involved in processing and analysis of line-of-sight microwave radio propagation data. His earlier Bell Laboratories experience included work on single-sideband long-haul radio systems, phased array radars, and oxide coated cathodes. Member, Tau Beta Pi.

Lawrence R. Rabiner, S.B. and S.M., 1964, Ph.D. (electrical engineering), 1967, Massachusetts Institute of Technology; Bell Laboratories, 1962—. From 1962 through 1964, Mr. Rabiner participated in the cooperative plan in electrical engineering at Bell Laboratories. He worked on digital circuitry, military communications problems, and problems in binaural hearing. Presently, he is engaged in research on speech communications and digital signal processing techniques. He is coauthor of *Theory and Application of Digital Signal Processing* (Prentice-Hall, 1975) and *Digital Processing of Speech Signals* (Prentice-Hall, 1978). Former President, IEEE G-ASSP Ad Com; former Associate Editor, G-ASSP Transactions; former member, Technical Committee on Speech Communication of the Acoustical Society. Member, G-ASSP Technical Committee of the Acoustical Society. Member, G-ASSP Technical Committee on Speech Communication, IEEE Proceedings Editorial Board, Eta Kappa Nu, Sigma Xi, Tau Beta Pi. Fellow, Acoustical Society of America and IEEE.

Philip J. Rich, B.S., 1972, University of Illinois, M.S. (Physics), 1974, Georgia Institute of Technology, Bell Laboratories, 1974–. Mr. Rich is currently engaged in studies related to the characterization and splicing of optical fibers. Member, OSA.

Aaron E. Rosenberg, S.B (E.E) and S.M. (E.E.), 1960, Massachusetts Institute of Technology; Ph.D. (E.E.), 1964, University of Pennsylvania; Bell Laboratories, 1964—. Mr. Rosenberg is presently engaged in studies of systems for man-machine communication-by-voice in the Acoustics Research Department at Bell Laboratories. Member, Eta Kappa Nu, Tau Beta Pi, Sigma Xi; fellow, Acoustical Society of America; member IEEE and IEEE Acoustics, Speech, and Signal Processing Group Technical Committee on Speech Processing.

Irwin W. Sandberg, B.E.E., 1955, M.E.E., 1956, and D.E.E., 1958, Polytechnic Institute of Brooklyn; Bell Laboratories, 1958—. Mr. Sandberg has been concerned with analysis of radar systems for military defense, synthesis and analysis of active and time-varying networks, several fundamental studies of properties of nonlinear systems, and with some problems in communication theory and numerical analysis. His more recent interests include macroeconomics and the economic theory of large corporations. Fellow and member, IEEE; member, American Association for the Advancement of Science, Eta Kappa Nu, Sigma Xi, and Tau Beta Pi.

Carolyn E. Schmidt, B.S. (Mathematics), 1974, Lafayette College; Bell Laboratories, 1974—. Miss Schmidt is a member of the Acoustic Research Department and is currently involved in work on speech communications. Member, Phi Beta Kappa.

Arvids Vigants, B.E.E., 1956, City College of New York; M.S. (E.E.), 1957, Eng. Sc.D. (E.E.), 1962, Columbia University; Bell Laboratories, 1962—. Mr. Vigants has worked on various electromagnetic wave propagation topics and is currently working on problems in line-of-sight microwave propagation and microwave radio systems. Member, Eta Kappa Nu, Tau Beta Pi, Sigma Xi, URSI/USNC Commission F, IEEE.

THE BELL SYSTEM TECHNICAL JOURNAL
Vol. 58, No. 8, October 1979
Printed in U.S.A.

Papers by Bell Laboratories Authors

BIOLOGY

Occurrence of Glottal Stops in Fluent Speech. N. Umeda, J. Acoust. Soc. Amer., *64*, No. 1 (July 1978), pp. 88–94.

On Perceptual Analyzers Underlying Visual Texture Discrimination—Part I. T. Caelli and B. Julesz, Biol. Cybern., *28*, No. 3 (1978), pp. 167–75.

Acoustic Determinants of Phrase Boundary Perception. L. A. Streeter, J. Acoust. Soc. Amer., *64* (1978), pp. 1582–1592.

CHEMISTRY

The Absolute Sense of Pyroelectric P3 and Piezoelectric D33 Coefficients in Lanthanum Acid 10 Date Heptahydrate. S. C. Abrahams and J. L. Bernstein, Solid State Commun., *27* (September 1978), pp. 973–6.

Block Copolymer Theory. 5. Spherical Domains. E. Helfand and Z. R. Wasserman, Macromolecules, *11* (September-October 1978), pp. 960–6.

Brownian Dynamics Study of Transitions in a Polymer Chain of Bistable Oscillators. E. Helfand, J. Chem. Phys., *69* (Aug. 1, 1978), pp. 1010–18.

Chain Dynamics of Poly (But-1-ENE) from Carbon-13 Nuclear Magnetic Relaxation Measurements. F. C. Schilling, R. E. Cais, and F. A. Bovey, Macromolecules, *11* (March/April 1978), pp. 325–8.

Degradation of Hydrogen-Absorbing Rare Earth Intermetallics by Cycling. R. L. Cohen, K. W. West, and K. H. J. Buschow, Solid State Commun. *25* (1978), pp. 293–5.

Effect of Stereosequence on Carbon-13 Spin-Lattice Relaxation Time for Poly (Vinyl Chloride). F. C. Schilling, Macromolecules *11* (Nov./Dec. 1978), p. 1290.

The Electronic Structure and Conductivity of Tetrathiotatracent, Tetrathionaphthalene and Tetraselenotetradene Studied by ESCA. J. Riga, J. Verbist, F. Wudl, A. Kruger, J. Chem. Phys., *69* (1978), p. 3221.

The Optical Absorption Spectrum of Fluid Sulfur Up to Supercritical Conditions. G. Weser, F. Hensel, and W. W. Warren, Ber Bunsenges Phys. Chem., *82* (1978), pp. 589–94.

A Positive Photoresist: The Photochemical Wolfe Rearrangement. F. B. Brammell, R. E. Zaojura, C. Paley, and S. R. Fahrenholtz, J. Chem. Ed., *55* (June 1978), pp. 403–5.

The Preparation of Some Monophenyltetrathiafulvalenes and P-Vinyl-phenyltetrathiafulvalene and Its Polymerization. M. L. Kaplan, R. C. Haddon, F. Wudl, and E. D. Feit, J. Org. Chem., *43* (1978), p. 4642.

Proposed Experiment to Estimate the Mixing Free Energy of Polymers. E. Helfand, Macromolecules, *11* (July/August 1978), pp. 682–5.

Pyroelectric Lanthanum Acid Iodate Heptahydrate Crystal Structure of the Transition Metal Iodates. S. C. Abrahams and J. L. Bernstein, J. Chem. Phys., *69* (September 15, 1978), pp. 2505–13.

The Sizes and Shapes of Those Giant Molecules. A. E. Tonelli, Chemistry, *51* (1978), pp. 11–13.

Synthesis of Ammonium Cyanate and Urea From Nitrous Oxide Over Platinum Osmium Ruthium and Copper-Nickel Catalysts. D. J. Freed, F. J. Voorhoeve, and L. E. Trimble, J. Cata., *53* (1978), pp. 251–9.

Synthesis of Isocyanic Acid From Nitrous Oxide Over Palladium and Iridium Catalysts. F. J. Voorhoeve and L. E. Trimble, Science, *202* (November 3, 1978), pp. 525–6.

COMPUTING

Computerized Tomography: The New Medical X-Ray Technology. L. A. Shepp and J. B. Kruskal, Amer. Math, *85*, No. 6 (1978), pp. 420–39.

Design and Implementation of the S System for Interactive Data Analysis. R. A. Becker and R. McGill, Proc. Comput. Software Appl. Conf., Nov. 1978, pp 226–29.

ECONOMICS

A Model of Cooperative Games with Binding Commitments. R. W. Rosenthal, in *Game Theory and Political Science*, P. Ordeshook, ed., New York: N.Y.U. Press, 1978, pp. 97–111.

Related Market Conditions and Interindustrial Mergers: Comment. M. K. Perry, Amer. Econ. Rev., *68* (March 1978), pp. 221–4.

Supportable Cost Functions for the Multiproduct Firm. W. W. Sharkey and L. G. Telser, J. of Economic Theory, *18* (1978), pp. 23–37.

Vertical Integration: The Monopsony Case. M. K. Perry, Amer. Econ. Rev., *68* (September 1978), pp. 561–70.

ELECTRICAL AND ELECTRONIC ENGINEERING

Charge-Coupled Devices: Technology and Applications. A. Gersho, IEEE Trans. Acous. Speech and Signal Processing (April 1978), p. 178.

Charge Routing Networks. B. Gopinath and A. Gersho, Proc. IEEE Circuit System Int. Symp. (1978), pp. 734–9.

Depolarization of 19 and 28 GHz Earth-Space Signals by Ice Particles. D. C. Cox, H. W. Arnold and H. H. Hoffman, Radio Science, *13*, No. 3 (May/June 1978), pp. 511–7.

Double Phase Matching Function. D. F. Nelson, J. Opt. Soc. Amer., *68* (December 1978), pp. 1780–1.

The Effects of Large Interference in Digitally Implemented Adaptive Echo Cancellers. R. D. Gitlin and S. B. Weinstein, IEEE Trans. Commun., *26*, No. 6 (June 1978), pp. 833–39.

Electrooptic Nonlinear Fabry-Perot Devices. P. W. Smith, E. M. Turner and P. J. Maloney, IEEE J. Quantum Electron. *14*, No. 3 (March 1978), pp 207–212.

Empirical Calculation of Microwave Rain Attenuation Distribution on Earth Satellite Paths. S. H. Lin, IEEE Proc. Electron Aerosp. Sys. Conv. (September 1978), *78* (CH 1354-4 AES), pp. 372–8.

Evaluation of Adaptive Speech Coders Under Noisy Channel Conditions. C. Scagliola, Proc. Inter. Conf. Commun. (June 1978), pp. 8.1.1–8.1.5.

Generation of Intense Subnanosecond Pulses 0.58–0.60 Micron with a Flashlamp Pumped Dye Laser. T. J. Negran and A. M. Glass, Appl. Opt., *17* (Sept. 1978), pp. 2812–16.

The Hagelin Cipher Machine (M-209) Reconstruction of the Internal Settings. R. Morris, Cryptologia, *2*, No. 2 (July 1978), pp. 267–89.

Heat Capacity of Europium Sulfide Near the Ferromagnetic Transition. A. Kornblitt, G. Ahler and E. Buehler, Phys. Rev. B, *17*, No. 1 (January 1978), pp. 282–92.

A High Capacity Satellite Utilizing Fixed and Scanning Spot Antenna Beams. D. O. Reudink and Y. S. Yeh, Proc. of the 8th Eur. Microwave Conf., 1978.

High Efficiency Solar Cells Based on Indium Phosphide. J. L. Shay, S. Wagner, K. J. Bachmann and E. Buehler, Proc. Soc. Photo-Opt. Instrum. Eng., *114* (August 1977), pp 16–19.

Integrated Bistable Optical Devices. P. W. Smith, I. F. Kaminow, P. J. Maloney and L. W. Stultz, Appl. Phys. Lett., *33*, No. 1 (July 1, 1978), pp. 24–6.

Integrated Electrooptic Nonlinear Fabry-Perot Devices. P. W. Smith, I. F. Kaminow, P. J. Maloney and L. W. Stultz, Proc. Integr. Guid. Wave Opt. Top. Meet., January 1977, p. FUB 2/1-4.

An Introduction to the Use of Digital Signal Processing for TOM/FDM Conversion. S. L. Freeny, Proc. IEEE Commun. Int. Conf., 1978, pp 39.1/1-7.

A Phase Adaptive Structure for Echo Cancellation. R. D. Gitlin and J. S. Thompson, IEEE Trans. Commun., *26*, No. 8 (August 1978), pp. 1211–20.

A Phased Array for a 12/14 GHz Toma Transponder. D. C. Reudink, Y. S. Yeh and A. S. Acampora, Proc. Electron. Aerosp. Sys. Conf. (EASCON) (1978), p. 417–24.

PNPN Optical Detectors and Light-Emitting Diodes. J. A. Copeland and A. G. Dentai, Proc. Intern. Electron. Device Conf. (1977), p. 580–1/A-B.

Polarization Characteristics of Non-Circular Core Single Mode Fibers. V. Ramaswamy, W. G. French, and R. D. Standley, Appl. Opt., *17*, No. 18 (September 1978), pp. 3014–7.

A Rapid Scan Area Coverage Satellite. D. O. Reudink and Y. S. Yeh, AIAA 7th Comm. Satell. Sys. Conf., San Diego (April 1978), pp. 137–45.

Real-Time Extraction of Bubble Chamber Tracks Using A Single Vidicon. J. O. Limb, E. G. Bowen, and C. E. Roos, Nucl. Instrum. Methods, *153* (1978), pp 383–8.

Scanning Properties of a 7-Meter Offset Cassegrainian Antenna. T. S. Chu and R. M. England, Proc. Antenna Propag. Int. Symp. (August 1978), pp 259–62.

Semiconductor Laser Self-Pulsing Due to Deep Level Traps. J. A. Copeland, Electron. Lett., *14* (December 1978), pp. 809–10.

Signal to Noise Ratio Degradation Due to Cross Polarization Interference Cancellation in Narrow Band or Nondispersive Radio Channels. N. Amitay, Nat. Telecommun. Conf. Rec. (1977), pp. 38:5/1-5.

Single Polarization Optical Fiber: Exposed Cladding Techniques. V. Ramaswamy, I. P. Kaminow, P. Kaiser and W. G. French, Appl. Phys. Lett., *33*, No. 9 (November 1978), pp. 814–6.

Some Properties of Palladium Photocathodes Used in the Electron Image Projection System (ELIPS). W. R. Sinclair, L. H. Lin, P. K. Gallagher and R. A. Fastnacht, Electrochem. Soc., *125* (1978), pp. 950–2.

Spatial Differentiation as an Auditory "Second Filter" Assessment on a Nonlinear Model of the Basilar Membrane. J. L. Hall, J. Acoust. Soc. Amer., *61* (February 1977), p. 520.

Spotbeams Promise Satellite Communications Breakthrough. D. O. Reudink. IEEE Spectrum (September 1978), pp. 36–42.

Subharmonically Pumped Millimeter Wave Mixtures. E. R. Carlson, M. V. Schneider and T. F. McMaster, IEEE Trans. Microwave Theory Tech., *26* (October 1978), pp. 706–15.

Subpicosecond Pulse Generation in a Synchronously Mode-Locked CW Rhodamine 6G Dye Laser. R. K. Jain and C. P. Ausschnitt, Opt. Lett. 2, No. 5 (May 1978), pp. 117–9.

Threshold Dependence on Active Layer Thickness in Indium Gallium Arsenide Phosphide Indium Phosphide DH Lasers. R. E. Nahory and M. A. Pollack, Electron. Lett., *14* (1978), pp. 727–9.

Tunable Optical Waveguide Directional Coupler Filter. R. C. Alferness and R. V. Schmidt, Appl. Phys. Lett., *33* (July 1978), pp. 161–3.

Video Transmission Tests Performed on Lightwave IF Entrance Links. A. Albanese and H. F. Lenzing, J. Soc. Motion Picture Telev., *87*, No. 12 (December 1978), pp. 821–4.

GENERAL MATHEMATICS AND STATISTICS

Asymptotic Theory of Least Absolute Error Regression. R. Koenker and G. Bassett, J. Amer. Statis. Assoc., *73* (1978), pp. 618–22.

Bounds for Binary Codes of Length Less than 25. M. R. Best, A. E. Brouwer, F. J. MacWilliams, A. M. Odlyzko and N. J. A. Sloane, IEEE Trans. Inform. Theory, *23* (1978), pp. 81–93.

A Definition of Conditional Mutual Information for Arbitrary Ensembles. A. D. Wyner, Inform. Contr., *38*, No. 1 (July 1978), pp. 51–9.

Enumeration of Power Sums Modulo A Prime. A. M. Odlyzko and R. P. Stanley, J. Number Theory, *10*, pp. 263–72.

On Graphs Which Contain All Small Trees. F. R. K. Chung and R. L. Graham, J. Comb. Theory, Ser. B, *24*, No. 1 (February 1978), pp. 1–23.

Maximal Prefix-Synchronized Codes. A. M. Odlyzko and L. J. Guibas, SIAM J. Appl. Math., *35* (1978), pp. 401–8.

Nonnegative Digit Sets in Positional Number Systems. A. M. Odlyzko, Proc. London Mathematical Soc., *3* (1978), p. 37.

A Note on Linear Models of Mutual Deterrence. I. W. Sandberg, J. Peace Science, Spring 1978, pp. 259–260.

Optimal Multistage Switching Networks. F. R. K. Chung, IEEE Trans. Commun., *26*, No. 8 (August 1978), pp. 1282–7.

Orthogonal Bases for Two Subspaces With All Mutual Angles Acute. S. Guthmann and L. A. Shepp, Indiana Math. J., *27*, No. 1 (1978) pp. 79–90.

On the Partitions of Graphs Into Trees. F. R. K. Chung, Discrete Math., *23* (1978), pp 23–30.

A Problem on Hook Lengths. J. E. Herman and F. R. K. Chung, Discrete Math., *20* (1977), pp. 33–40.

The Rate Distortion Function for Source Coding with Side Information at the Decoder—II: General Sources. A. E. Wyner, Inform. Contr., *38*, No. 1 (July 1978), pp. 60–80.

Realizing a Weak Solution on a Probability Space. V. E. Benes, Stochastic Process. Appl., *7* (1978), pp. 205–25.

A Theorem Concerning Properties of an Arms Race Model. I. W. Sandberg, IEEE Trans Syst. Man. Cybern., *8*, No. 1 (January 1978), pp. 29–31.

Two Results Concerning Multicoloring. V. Chvatal, M. R. Garey, D. S. Johnson, Ann. Math., *2* (1978), pp. 151–4.

MECHANICAL AND CIVIL ENGINEERING

Apparatus for High Resolution Surface Tension Measurements. J. H. Magerlein and T. M. Sanders, Rev. Sci. Inst., *49* (1978), p. 94.

Experiments in the Automation of Visual Inspection. J. F. Jarvis, Proc. JACC, *1* (October 1978), pp. 307–13.

Flow between a Stationary and a Rotating Disk with Suction. L. O. Wilson and N. L. Schryer, J. Fluid Mech., *85* (3), No. 3 (April 1978), pp. 479–98.

A Method for Automating the Visual Inspection of Printed Wiring Boards. J. F. Jarvis, Computer Graph Image Proc., *6* (1977), pp. 452–84.

MATERIALS SCIENCE

Amorphous Metal Films by Getter-Sputtering at 25K. J. J. Hauser, R. J. Schutz, and W. M. Augustyniak, Phys. Rev. B, *18*, No. 8 (October 1978).

Analysis of Nonlinear Stress Relaxation in Polymeric Glasses. S. Matsuoka, S. S. Bearder, H. E. Kern, Polymer Eng. Sci., *18*, No. 4 (1978), pp. 1074–80.

Bubble Properties of Garnet Films Prepared From Molybdate Fluxes. W. A. Bonner, R. C. LeCraw, R. D. Pierce, and L. G Van Uitert, J. Appl. Phys., *49*, No. 3 (March 1978), pp. 1871–2.

Characterization of a Nonlinear Cochlear Model By Wide Band Stimuli. J. L. Hall, J. Acoust. Soc. Amer., *64* (1978), p. 5133.

Classical Trajectory Calculations of the Dissociation of Hydrogen on Copper (111) The Effect of Surface Roughness. A. Gelb and M. J. Cardillo, Surf. Sci., *75* (July 1978), pp. 199–214.

Compatibility and Physical Properties of Blends of Poly(Vinyl Chloride) and PB3041, A Polymeric Plasticizer. H. E. Bair, D. Williams, T. K. Kwei, and F. J. Padden, Polym. Preprints, *19*, No. 1 (March 1978), pp. 143–8.

The Concept of Frustration in Spin Glasses. P. W. Anderson, J. Less Common Metals, *62* (1978) p. 291.

Consideration of Processing Conditions on the Properties of Solid Polymers. S. Matsuoka, Polymer Eng. Sci., *18*, No. 4 (1978) pp. 264–7.

Correlation Between Elastic Constants and Flow Behavior in Metallic Glasses. H. S. Chen, J. Appl. Phys., *49*, No. 1 (Jan 1978), pp. 462–3.

A Coulometric Analysis of Iron (II) In Ferrites Using Chlorine. P. K. Gallagher, Amer, Ceram. Soc. Bull., *57* (June 1978), pp. 578–8.

CuCl: More Facts Generate More Thoughts on High Temperature Copper Chloride Superconductivity. J. A. Wilson, Phil. Mag. B, *38* (1978), pp. 427–44.

Defects in Indium Phosphide Homoepitaxial Layers. S. Mahajan, K. J. Bachmann, D. Brasen, and E. Buehler, J. Appl. Phys., *49*, No. 1 (January 1978), pp. 245–8.

Diffusion in a Palladium Copper-Silicon Metallic Glass. H. S. Chen, L. C. Kermerling, J. M. Poate, and W. L. Brown, Appl. Phys. Lett., *32*, No. 8 (April 1978), pp. 461–3.

Electric Micropositioning With Ferroelastic-Ferroelectrics. R. A. Lemons and L. A. Coldren, Rev. Sci. Instrum., *29*, No. 12 (December 1978), pp. 1650–2.

On the Diffusion of Excess Vacancies to Free Surfaces and Voids in Thin Films. J. R. Lloyd and S. Nakahara, J. Electrochem. Soc., *125* (1978), p. 2037.

An Electroluminescence in Thin Film Zinc Selenide Manganese. J. Shah and A. E. DiGiovanni, Appl. Phys. Lett., *33* (1978), p. 995.

The Evidence of Structural Relaxation as the Origin of Curie Temperature Aging in Metallic Glass. H. S. Chen, J. Appl. Phys. *49*, No. 8 (August 1978), pp. 4595–7.

Examination of Aluminum Copper Films During Anodic Oxidation—Part I, Corrosion Studies. H. H. Strehblow and C. J. Doherty, J. Electrchem. Soc., *125*, No. 1 (1978), pp. 30–3.

The Growth of Indium-Rich Bulk Single Crystals of Gallium Indium (1-x) Phosphide(y) Arsenide (1-y) Via The Gradient Freeze Method. K. J. Bachmann, F. A. Thiel, and S. D. Ferris, J. Crys. Growth, *43*, No. 6 (July 1978), pp. 752–5.

The History and Present Status of Synthetic Diamond, Part I. K. Nassau and J. Nassau, Lapidary J., *32* (1978), pp. 79–96.

The History and Present Status of Synthetic Diamond, Part II. K. Nassau and J. Nassau, Lapidary J., *32* (1978), pp. 490–508.

The Influence of Structural Relaxation on the Density and Youngs Modulus of Metallic Glasses. H. S. Chen, J. Appl. Phys. *49*, No. 6 (June 1978), pp. 3289–91.

On Interpreting a Quantity in the Burton, Prim and Slichter Equation as a Diffusion Boundary Layer Thickness. L. O. Wilson, J. Cryst. Growth, *44*, No. 2 (September 1978), pp. 247–50.

Investigation of the Reactions of Silicon Chloride and Dioxide at Elevated Temperatures by Infrared Spectroscopy. D. L. Wood, J. B. MacChesney, and J. P. Luong, J. Mater. Sc., *13*, No. 8 (August 1978), pp. 1761–8.

Linear Defects Observed in Nickel Electrodeposits. S. Nakahara, J. Electrochem. Soc., *125* (1978), p. 1050.

A New Look at the Burton, Prim and Slichter Model of Segregation During Crystal Growth from the Melt. L. O. Wilson, J. Cryst. Growth, *44*, No. 4 (November 1978), pp. 371–6.

Nonisothermal Reaction Analysis. P. K. Gallagher, Ceramic Abst. *57*, No. 9 (1978) p. 255.

Origin of Coercivity in a Chromium-Cobalt-Iron Alloy (Chrominoup). S. Mahajan, E. M. Gyorgy, R. C. Sherwood, S. Jin, S. Nakahara, D. Brasen, M. Eibschutz, Appl. Phys. Lett., *32*, No. 10 (May 1978), pp. 688–90.

The Origin of Color in Minerals. K. Nassau, Amer. Mineral, *63*, No. 3–4 (Mar/Apr 1978), pp. 219–29.

Plasma Assisted Etching Techniques for Pattern Delineation. C. M. Melliar-Smith and C. J. Mogab, in *Thin Film Processes*, New York: Academic Press, 1978; pp. 497–556.

Preparation of P-Type Indium Phosphate Films By Close Space Vapor Transport. L. Goldstein and S. Wagner, Mater. Res. Bull., *13*, No. 1 (1978), pp. 1455–60.

Report on the 5th International Conference on Crystal Growth, Boston July '77. K. Nassau, Mater. Rec. Bull. *13* (1978) pp. 251–6.

A Room Temperature Interdiffusion Study in a Gold Thin Film Couple. J. R. Lloyd and S. Nakahara, Thin Solid Films, *54* (1978) p. 207.

The Sputter and S-Gun Magnetrons. D. B. Fraser, in *Thin Films Process*, New York: Academic Press, 1978.

Stable Room Temperature Light Emission from Metal-Insulator-Metal Junctions. P. K. Jain, S. Wagner, and D. H. Olson, Appl. Phys. Lett., *32*, No. 1 (1978), pp. 62–4.

The State of Tin in Tin-Anodized Aluminum. R. L. Cohen, G. L. Miller, and K. W. West, Phys. Rev. Lett., *41*, No. 6 (August 1978), pp. 381–4.

Survey of Chemical Strippers for Silicones. F. X. Ventrice, Plast. Eng., *24* (April 1978), pp. 608–9.

Thermal Expansion of Zinc Oxide. H. M. O'Bryan, L. G. VanUtert, E. D. Kolb, and G. Zydzik, J. Amer. Ceram. Soc., *61*, No. 5–6 (May/June 1978), p. 269.

Thermally Assisted Flash Annealing of Silicon and Germanium. R. L. Cohen, J. S. Williams, L. C. Feldman, and K. W. West, Appl. Phys. Lett., *33* (1978), pp. 751–3.

Thermodynamic Properties of Surface Steps. J. D. Weeks and G. H. Gilmer, J. Cryst. Growth, *43*, No. 3 (April 1978), pp. 385–7.

Dynamics of Crystal Growth. J. D. Weeks and G. H. Gilmer, Phys. Rev. Lett., *40* (1978), pp. 733–6.

Topochemical Reactions of Rutile Related Structures with Lithium. D. W. Murphy, F. J. DiSalvo, J. N. Carides, and J. V. Waszczak, Mater. Res. Bull., *13*, No. 12 (1978) pp. 1395–1402.

Transformation-Induced Microstructures in Cobalt-Iron Alloys. S. Mahajan and D. Brasen, Phys. Met. Trans. A, *9A* (December 1978), pp. 1817–24.

Validity of the Energy and Entropy Interfacial Tension Models Examined in View of the Stability of Metallic Glasses. H. S. Chen, Mater. Res. Bull., *13* (1978) pp. 737–41.

Water Sorption of Polycarbonate and its Effect on the Polymer's Dielectric Behavior. H. E. Bair, G. E. Johnson, R. Merriweather, J. Appl. Phys., *49* (October 1978), pp. 4976–84.

PHYSICS

Angle Resolved Photoemission From Surfaces and Adsorbates. N. V. Smith, J. Appl. Phys., *39*, No. 4 (1978) pp. 157–61.

Angular Dependence of the In 4D and Selenium 3D Core Level Photoemission From Indium Selenium. D. Norman, D. P. Woodruff, N. V. Smith, M. Traum, and H. H. Farrell, Phys. Rev. B, *18* (1978), p. 6789.

Angular Dependent Photoemission. N. V. Smith in *Photoemission in Solids I*, M. Cardona and L. Ley (eds.), Vol 26, Heidelberg: Springer-Verlag, 1978, p. 237.

Anisotropy in the Magnetic Susceptibility of Tantalum Selenide. J. L. Benchinol, F. T. Hedgoock, and F. J. DiSalvo, Solid State Commun., *25* (1978), pp. 677–78.

Annealing Studies of Beryllium-Doped Gallium Arsenide Grown by Molecular Beam Epitaxy. W. V. McLevige, K. X. Vaidyanathan, B. G. Streetman, J. Comas, M. Ilegems, and L. Plew, Appl. Phys. Lett., *33* (1978), pp. 127.

Anomalous Behavior in the Low Temperature Properties of Uranium Palladium (3). K. Andres, D. Davidov, P. Dernier, F. Hsu, W. A. Reed, and G. J. Nieuwenhuys, Solid State Commun., *28* (1978), p. 405.

Arbitrary Doping Profiles in Antimony Doped Silicon MBE. J. Bean, Appl. Phys. Lett., *33*, No. 7 (1978), pp. 654–6.

Balanced Bridge Modulator Switch Using Titanium Diffused Lithium Niobium Trioxide Strip Waveguides. V. Ramaswamy, M. D. Divino, and R. D. Standley, Appl. Phys. Lett., *32*, No. 10 (May 1978) pp. 644–6.

Bandgap vs. Composition and Demonstration of Vegard's Law for Indium (1-x) Gallium (x) Arsenic (y) Phosphorus (1-y) Lattice-Matched to Indium Phosphide. R. E. Nahory, M. A. Pollack, W. D. Johnston, and R. L. Barns, Appl. Phys. Lett., *33* (1978) pp. 659–61.

Capacitance Spectroscopy of Degraded GaAsP Light Emitting Diodes. B. Tell and C. Van Opdorp, J. Appl. Phys., *49* (1978), pp. 2973–7.

Comparison of a Time-of-Flight System with an Electrostatic Analyzer in Low Energy Ion Scattering. T. M. Buck, G. H. Wheatley, G. L. Miller, D. A. H. Robinson, and Y. S. Chen, Nucl. Instrum. Methods, *149* (1978), pp. 591–4.

Compton Profile Studies of Amorphous and Single Crystal Silicon Dioxide. M. Rosenberg, F. Martino, W. A. Reed, and P. Eisenberger, Phys. Rev. B, *18* (1978), p. 844.

Contribution of the Conformational Specific Heat of Polymer Chains to the Specific Heat Difference Between Liquid and Glass. R. J. Roe and A. E. Tonelli, Macromolecules, *11* (1978), pp. 114–7.

Corrections for Scattering in X-Ray Fluorescence Experiments. H. D. Keith and T. C. Loomis, X-Ray Spectrum, *7* (1978) pp. 217–24.

Deep Level Capacitance Spectroscopy in Nitrogen Doped VPE Gallium Phosphide. B. Tell and F. P. J. Kuijpers, J. Appl. Phys., *49* (1978) pp. 5938–43.

Dependence of Oxygen Diffusion in Epitaxial YIG: Calcium on Defect Concentration. E. M. Gyorgy, R. C. LeCraw, S. L. Blank, R. D. Pierce, and D. W. Johnson. J. Appl. Phys., *49*, No. 2 (March 1978), pp. 1885–7.

Detection of Atomic Hydrogen and Deuterium by Resonant Three-Photon Ionization. G. C. Bjorklund, C. P. Ausschnitt, R. R. Freeman, and R. H. Storz, Appl. Phys. Lett., *33*, No. 1 (July 1978), pp. 54–6.

Diamagnetic Structure of Rubidium in Intense Magnetic Fields. N. P. Economou, R. R. Freeman, and P. F. Liao, Phys. Rev. A, *18* (December 1978), p. 2506.

Direct Calculation of Wannier Functions, Silicon Valance Bands. E. O. Kane and A. B. Kane, Phys. Rev. B, *17*, No. 6 (March 1978), pp. 2691–704.

Directional Photoemission From Two-Dimensional Systems. N. V. Smith and P. K. Larsen in *Photoemission and Electronic Structure of Surfaces*, New York: John Wiley, 1978, p. 409.

Dynamic Stark Tuned FIR Laser in Rubidium. T. Y. Chang, T. C. Damen, W. T. Nguyen, J. D. McGee, and T. J. Bridges, Appl. Phys. Lett., *32*, No. 10 (May 1978).

Effect of Electron-Phonon Scattering on Charge Density Wave Phase Transitions. D. J. Huntley, F. J. DiSalvo, and T. M. Rice, J. Phys., *11* (1978) pp. 767–70.

The Effect of Parallel Magnetic Field on Interband Transition in Two-Dimensional Systems. P. M. Platzman and B. I. Halperin, Phys. Rev. B., *18* (1978), pp. 226.

The Effect of Surfaces and Nonuniform Fields in Electroreflectance: Application to Germanium. R. DelSole, D. E. Aspenes, Phys. Rev. B., *17* (1978) pp. 3310–17.

Effects of Atomic Order in α and β Phase AgCd Alloys and Reduced by X-Ray Photo-electron Spectroscopy. G. Crecelius and G. K. Wertheim, Phys. Rev. B, *18*, No. 12 (December 1978), pp. 6525–30.

Effects of Magnetic Fields on Four Wave Mixing Processes in Atomic Vapors. N. P. Economou, R. R. Freeman, G. C. Bjorklund, Optics Lett., *3* (December 1978) pp. 209–11.

Electric Dipolar Echoes in Glasses. L. Bernard, L. Piche, G. Schumaker, J. Joffrin, and J. E. Graebner, J. Phys. Lett., *39* (May 1978), pp. 126.

Electrochromic Cells Based on Phosphotungstic Acid. B. Tell and S. Wagner, Appl. Phys. Lett., *33* (1978), pp. 837–38.

Electrochromism in Anodic Iridium Oxide Films. S. Gottesfeld, J. McIntyre, G. Beni, and J. L. Shay, Appl. Phys. Lett., *33*, No. 2 (July 1978) pp. 208–10.

Electrochromism in Lithium (X) Tungsten Trioxide. S. K. Mohapatra, J. Electrochem. Soc., *125*, No. 2 (February 1978), pp. 284–8.

Electrochromism of Anodic Iridium Oxide Films on Transparent Substrates. J. L. Shay, G. Beni, and L. M. Schiavone, Appl. Phys. Lett., *33* (1978) p. 942.

Electron Collisional Laser in Lead (+) Populated by Recombination. W. T. Silfvast, L. H. Szeio, and D. R. Wood, Appl. Phys. Lett., *33* (1978) p. 936.

Electroreflectance and Ellipsometry of Silicon From 3 to 6 EV. A. Daunois and D. E. Aspenes, Phys. Rev. B, *18* (1978), pp. 1824–39.

Elliptic Polarization of Balmer Radiation From Low Energy Grazing Incidence Collisions of Hydrogen Ions on Surfaces. N. H. Tolk, J. C. Tully, J. S. Kraus, W. Heiland, and S. H. Neff, Phys. Rev. Lett., *41* (August 1978), pp. 643–6.

EMF Measurements on Electrochromic Amorphous Lithium Tungstate Films. S. K. Mohapatra and S. Wagner, J. Electrochem. Soc., *125* (October 1978), pp. 1603–4.

Epitaxial Laser Crystallization of Thin Film Amorphous Silicon. J. C. Bean, H. J. Leamy, J. M. Poate, G. A. Rozgonyi, J. S. Williams, T. T. Sheng, and G. K. Celler, Appl. Phys. Lett., *33*, No. 3 (1978), pp. 227–30.

Extended X-Ray Absorption Fine Structure of Surface Atoms on Single Crystal Substrates: Iodine Adsorbed on Silver (III). P. H. Citrin, P. Eisenberger, and R. C. Hewitt, Phys. Rev. Lett., *41*, No. 5 (July 1978), pp. 309–12.

Germanium-Tin Barrier Josephson Tunnel Junctions. E. L. Hu, L. D. Jackel, A. R. Strand, R. W. Epworth, R. F. Lucey, C. A. Zogg, and E. Gornick, Appl. Phys. Lett., *32*, No. 9 (May 1978), pp. 584–6.

Hardness and Bonding in A15 Superconducting Compounds. G. Y. Chin, J. H. Wernick, T. H. Geballe, S. Mahajan, and S. Nakahara, Appl. Phys. Lett., *33*, No. 1 (July 1978), pp. 103–5.

Heating of Cathode Surfaces Caused by Glow Discharges and Minimum Conditions Necessary for Catastrophic Bridging. J. R. Pharney, 5th Intern. Conf. on Gas Discharges, *165* (September 1978), pp. 285–8.

Heterostructure Lasers—Part B: Materials and Operating Characteristics. H. C. Casey and M. B. Panish, New York: Academic Press, 1978.

High Efficiency Indium (1-x) Gallium (x) Arsenide (y) Phosphide (1-y)/Indium Phosphide Photodetectors with Selective Wavelength Response Between 0.9 and 1.7 Microns. M. A. Washington, R. E. Nahory, M. A. Pollack, and E. D. Beebe, Appl. Phys. Lett., *33* (November 1978), pp. 854–6.

Hot Electrons and Photons Under High Intensity Photoexcitation of Semiconductors. J. Shah, Solid State Electron., *21* (1978) p. 43.

Hyperfine Enhanced Nuclear Magnetic Cooling. K. Andres, Cryogenics, *1* (1978), pp. 473–7.

Hyperfine Enhanced Nuclear Magnetic Cooling in Praseodymium Beryllium (13). K. Andres and S. Darack, J. de Phys. (Paris) *C-6:* No. 2 (1978) pp. 1157–8.

An Indium Gallium Arsenide Detector for the 1.0 to 1.7 Micron Wavelength Range. K. J. Bachmann and J. L. Shay, Appl. Phys. Lett., *32*, No. 7 (April 1978), pp. 446–8.

Influence of Noncircular Core on the Polarization Performance of Single Mode Fibers. V. Ramaswamy and W. G. French, Electron. Lett., *14*, No. 5 (March 1978), pp. 143–4.

Infrared Absorption and Scattering by Electron-Hole Droplets in Germanium. J. H. Rose, H. B. Shore, and T. M. Rice, Phys. Rev. B, *17* (1978), p. 752.

Initial Permeability and Intrinsic Magnetic Properties of Polycrystalline Manganese Zinc Ferrites. B. Hoekstra, E. M. Gyorgy, P. K. Gallagher, D. W. Johnson, G. Zydzik, and L. G. VanUitert, J. Appl. Phys., *49* (September 1978), p. 4902.

Integrated Multijunction Gallium Arsenide Photodetector with a High Output Voltage. M. Ilegems, B. Schweartz, L. A. Koszi, and R. C. Miller, Appl. Phys. Lett., *33* (1978), p. 629.

An Introduction to the Physics of Ferroelectrics. P. C. Lissaide, Ferroelectrics, *17* (1978) pp. 583–4.

Landau-Levels—Electron Lifetimes Nitrogen-Indium Antimonide. W. Muller, E. Gornik, T. Y. Chang, and T. J. Bridges, Phys. Rev. Lett., *40*, No. 17 (April 1978), pp. 1151–4.

Liquid Phase Epitaxial Indium (1-x) Gallium (x) Arsenide (y) Phosphorus (1-y) Lattice-Matched to (100) Indium Phosphorus Over the Complete Wavelength Range 0.93 Less Than or Equal to Gamma Less Than or Equal to 1.66 Microns. M. A. Pollack, R. E. Nahory, D. E. Winter, and A. A. Ballman, Appl. Phys. Lett., *33*, No. 4 (August 1978), pp. 314–6.

Low Energy Ion Scattering (LEIS) for Composition and Structure Analysis of the Outer Surface. M. H. Brongersma and T. M. Buck, Nuc. Inst. and Methods, *149* (1978), pp. 569–75.

Magnetic Field Quantum Beats in Two-Photon Free Induction Decay. N. P. Economou and P. F. Liao, Opt. Lett., *3* (November 1978), p. 172.

Magnetic Order and Giant Negative Magnetoresistance in the Intermediate Valance Compound Tantalum Selenide. K. Andres, W. M. Walsh, S. Darack, L. W. Rupp, and L. D. Longinotti, Solid State Commun., *27* (1978), pp. 825–8.

Manganese-55 Silicon-29 NMR in the Helically Ordered State of Manganese Silicon (X). K. Motoya, H. Yasuoka, Y. Nakamura, V. Jaccarino, and J. H. Webnick, J. Phys. Soc. Jap., *44*, No. 3 (March 1978), pp. 833–91.

Many-Body Effect on Level Broadening and Cyclotron Resonance in Two-Dimensional Systems Under Strong Magnetic Fields. H. Fukuyama, Y. Kuramoto, and P. M. Platzman, Surf. Sci. *73* (1978), p. 491.

Measurement of K-Shell Fluorescence Yield and K/Alpha-Beta Intensity Ratio for Nickel. H. D. Keith and T. C. Loomis, X-Ray Spectrom., *7* (1978), pp. 225–40.

A Miniature Electrostatic Lens for Forming MEV Millibeams. W. M. Augustyniak, D. Betteridge, and W. L. Brown, Nucl. Instrum. Methods, *149* (1978), pp. 669–73.

Molecular Cooling and Thermal Balance of Dense Interstellar Clouds. P. F. Goldsmith and W. D. Langer, Astrophys. J., *222*, No. 3 (June 1978), pp. 881–895.

Monte Carlo Test of Theories for the Planar Model, the F Model and Related Systems. W. J. Shugard, J. D. Weeks, and G. H. Gilmer, Phys. Rev. Lett., *41* (November 1978), 1399–402.

Nanosecond Time Resolved Raman Spectra of Photolyzed Carboxyhemoglobin. K. B. Lyons, J. M. Friedman, and P. A. Fleury, Nature, *275*, No. 5680, pp. 565-6.

A New Resonant Ellipsometric Technique for Characterizing the Interface Between Gallium Arsenide and its Plasma Grown Oxide. J. B. Theeten, D. E. Aspene, and R. P. H. Chang, J. Appl. Phys., *49* (1978), pp. 6097-6102.

A New Self-Consistent Green's Function Approach to the Electronic Structure of Localized Defects. G. A. Baraff and M. Schluter, Phys. Rev. Lett., *2* (1978), pp. 892-5.

A New Inter-Impurity Recombination in Gallium Phosphide Revised Values for Acceptor Binding Energies. M. O. Sturge, A. T. Vink, and F. J. M. Kuijpers, Appl. Phys. Lett., *32*, No. 1 (Jan 1978), pp. 49-51.

Nonlinear Instability of Electromagnetic Drift Waves. K. Mina and A. Hasegawa, Phys. Fluids, *21*, No. 1 (1978), pp. 81-6.

Nonlinear Optical Measurements in the Excitonic Region of Cadmium Sulfide at 4.2K. J. L. Jackle and H. Mahr, Phys. Rev. B, *17*, No. 8 (1978), pp. 3387-400.

Nonlinear Wave Effects in Laboratory Plasmas. M. Porkolab and R. P. H. Chang, Rev. Mod. Phys., *50* (1978), p. 745.

Nuclear Resonance Excitation by Synchrotron Radiation. R. L. Cohen, G. L. Miller and K. W. West, Phys. Rev. Lett., *41*, No. 6 (August 1978), pp. 381-4.

Observation of Focusing of Neutral Atoms by the Dipole Forces of Resonance Radiation Pressures. J. E. Bjorkholm, R. R. Freeman, A. Ashkin, and D. B. Pearson, Phys. Rev. Lett., *41*, No. 20 (November 1978), pp. 1361-4.

Observation of Phase Separation in a Chromium Cobalt-Iron Alloy (Chromindur) by Mossbauer Effect. M. Eibschutz, G. Y. Chin, S. Jin, and D. Brasen, Appl. Phys. Lett., *33* (1978), p. 362.

PSYCHOLOGY

The Attention Operating Characteristic: Examples From Visual Search. G. Sperling and M. J. Melchner, Science, *202* (October 20, 1978), pp. 315-318.

Distortion Criteria of the Human Viewer. J. O. Limb, Nat. Telecomm. Conf. Rec., 1977 (621.38/N275).

On Identifying Detectors. J. Krauskopf in *Visual Psychophysics and Physiology*, J. C. Armington, J. Krauskopf, and B. R. Wooter (eds.), New York: Academic Press, 1978, pp. 283-295.

Experiments on Temporal Aspects of Keyboard Entry. S. Sternberg, R. L. Knoll, and C. E. Wright in *Getting it Together: Research and Applications in Human Factors*, J. P. Duncanson (ed.), Santa Monica: Human Factors Society, 1978, pp. 29-50.

Future Prospects in Language and Communication for the Congenitally Deaf. G. Sperling, in *The Development of Deaf Children*, L. Liben (ed.), New York: Academic Press, 1978, pp. 103-114.

Hearing Words Without Words—Prosodic Cues for Word Perception. L. H. Nakatani and J. A. Schaffer, J. Acoust. Soc. Amer., *63*, No. 1 (January 1978), pp. 234-245.

The Latency and Duration of Rapid Movement Sequences: Comparisons of Speech and Typewriting. S. Sternberg, S. Monsell, R. L. Knoll, and C. E. Wright, in *Information Processing in Motor Control and Learning*, G. E. Stelmach (ed.), New York: Academic Press, 1978, pp. 117-152.

A New Program of Research on Interpersonal Communication: Laboratory Facility and Some Early Results. P. D. Bricher and M. Wish, Conf. Record, Nat. Telecommun. Conf., 1978, Paper 34.3.

Pitch Changes During Attempted Deception. L. A. Streeter, R. M. Krauss, V. Geller, C. Olson, and W. Apple, J. Personality and Social Psychology, *35* (1977), pp. 345-350.

Recency, Immediate Recognition Memory, and Reaction Time. S. Monsell, Cog. Psychol., *10* (1978), pp. 465-501.

Visual Search, Visual Attention, and the Attention Operating Characteristic. G. Sperling and M. J. Melchner, in *Attention and Performance VII*, J. Reguin (ed.), Hillsdale, N.J.: Erlbaum, 1978, pp. 675-686.

SYSTEMS ENGINEERING AND OPERATIONS RESEARCH

Automatic Trouble Analysis System. J. R. Lyons, Proc. Electron. Nat. Conf, *32* (October 1978), pp. 314-317.

A Continuous Presence Video Conference System. E. F. Brown, J. O. Limb, and B. Prasada, Nat. Telecommun. Conf. Rec., *3* (December 3-6, 1978), pp. 34.1.1-34.1.4.

Experimental Speakerphone System for Teleconferencing. J. E. West, D. J. MacLean, J. R. Nelson, and J. L. Flanagan, J. Acoust. Soc. Amer., *64* (1978), pp. 1561–1565.

A Flexible Experimental Digital Switching Office. R. W. Lucky, Proc. Digit. Commun./Digit Trans. Switch Local Network Int. Sem., March 1978, pp. A4/1-4.

An Intelligent Network Processor for a Digital Central Office. H. G. Alles, Proc. Digital Commun/Digit Trans. Switch Local Network Int. Sem. (March 1978), pp. A5/1-6.

A Microprocessor-Based, Programmable Laboratory Equipment Controller and Data Acquisition System. D. W. Taylor, Rev. Sci. Instrum., *49*, No. 11 (November 1978), pp. 1551–1556.

Selection of Microform Readers and Reader Printers. C. H. Robertshaw, J. Microgr., *12*, No. 2 (Nov-Dec 1978), pp. 70–72.